Artificial Activation of *APETALA1* using Recombinant Proteins and Cell Penetrating Peptides

A thesis submitted to Imperial College London in candidature for the degree of Doctor of Philosophy in Chemical Biology

William David Leonard Brierley Joyce

Department of Chemistry

Faculty of Natural Sciences

Imperial College London

Exhibition Road, South Kensington, London

March 2019

In Loving Memory of Grandma and Grandad

Patricia Joyce (6th September 1933 – 26th December 2014)

&

Philip Joyce (27th February 1930 – 12th December 2017)

Declaration of Originality

I hereby declare that the work presented in this thesis is from my own original research conducted in the laboratories at Imperial College London in South Kensington, between October 2015 and October 2018. The contributions from others through collaboration are clearly stated within the text. Conclusions derived from both the published and unpublished work of others are properly referenced.

William Joyce

March 2019

Copyright Declaration

The copyright of this thesis rests with the author. Unless otherwise indicated, its contents are licensed under a Creative Commons Attribution-Non Commercial 4.0 International Licence (CC BY-NC). Under this licence, you may copy and redistribute the material in any medium or format. You may also create and distribute modified versions of the work. This is on the condition that: you credit the author and do not use it, or any derivative works, for a commercial purpose. When reusing or sharing this work, ensure you make the licence terms clear to others by naming the licence and linking to the licence text. Where a work has been adapted, you should indicate that the work has been changed and describe those changes. Please seek permission from the copyright holder for uses of this work that are not included in this licence or permitted under UK Copyright Law.

Acknowledgements

I thank my supervisors Colin Turnbull, Ed Tate and Xiaodong Zhang for their guidance and support throughout my PhD, for the encouragement to grow the project and to take the scientific routes which have enabled me to present a wholesome and satisfying story – I am very grateful and thank you for this opportunity. I am also grateful to the EPSRC and Grantham Institute for Climate Change for funding my studentship.

I thank students whom have worked alongside me during the project and in particular Laure Fourquet for her dedication as an excellent support student during both her undergraduate project and as a summer intern. I thank Rosa Lopez-Cobollo for her help and practical guidance in the laboratory, Javaid Iqbal for his technical assistance in plant culturing and Ciaran Mckeown for his kind support and training in protein purifications.

I thank friends whom have helped me along the way and in particular Max Hodges, Chris Waite, Sean Linsdall, Alex Quinn and notably Amira Burshan for her kindness and support. Most of all, particular recognition goes to my family and for their love over the last 25 years, without which the completion of this PhD would not have been possible. I thank my mother, Gwen, father David, sister Emily and Edward Cook for their unwavering support and for everything they have done for me. In addition, I thank my Grandma, Pat, and Grandad, Philip, for their love and support, and interest in my endeavours - I am sad that you were not able to see this to the end. Grandad it was you who first encouraged me to take this on!

Abstract

This thesis reports a novel method for the artificial activation of reproductive development in Arabidopsis. In this way, reproductive development was triggered by an exogenous delivery of the recombinant florigen protein, Flowering Locus T (FT), at the shoot apical meristem in order to artificially activate Apetala 1 (AP1), the major floral homeotic gene. This was assessed by large phenotyping experiments after protein treatment. In addition, a transgenic reporter was created, using the promoter of AP1 and GFP to assess the artificial activation of AP1.

Furthermore, this thesis reports the action of cell penetrating peptide uptake (namely R9, Tat, TP10 and pVEC) into plant tissue. An in-depth investigation into R9 uptake revealed mechanistic details in particular the initial interaction of R9 with the cell wall to create a high local peptide concentration in proximity to the membrane. Further studies reported the successful uptake of R9 into mesophyll cell culture, protoplasts and apical meristems, including the development of a novel quantitative assessment for R9 uptake into root tips.

Tool development notably included the covalent attachment of R9 and Tat to FT and Sortagging, a novel labelling method enabling the fluorescent tracking of proteins *in planta* using confocal microscopy. Superior uptake was reported for FT-Tat over FT-R9 in cell culture and FT-Tat uptake was reported in the shoot apical meristem. This is the first example of covalent CPP-mediated delivery of a functional protein to the apical tissue.

This study reports progress en route to developing a universal tool for flowering time control in agriculture. It is the first reported example of an exogenous macromolecular treatment with a recorded biological effect *in planta* and as such is a novel approach to target and control AP1 expression.

Abbreviations

µM	Micromolar
35S	Cauliflower mosaic virus promoter
Ala, A	Alanine
A_{280}	Absorbance at 280 nm
aa	Amino acid
ABA	Abscisic acid
ADH	Alcohol dehydrogenase
AG	AGAMOUS
Agl1	Agrobacterium strain
AGL24	AGAMOUS-LIKE 24
AP1	APETALA1
AP2	APETALA2
AP3	APETALA3
APS	Ammonium persulphate
Arg, R	Arginine
ATC	CENTRORADIALIS homologue
ATP	Adenosine triphosphate
β-Gal	Beta Galactosidase
BF	Brightfield
BFT	BROTHER OF FT AND TFL1
BME	β-Mercaptoethanol
BSA	Bovine Serum Albumin
BY-2	Bright Yellow - 2 tobacco cells
bZIP	Basic leucine zipper
C	Central Zone
˚C	Degrees Celsius
c.f.	Conferatur
CAL	CAULIFLOWER
C-Box	GACGTC DNA binding motif
CK2	CAESIN KINASE II
CLV	CLAVATA
CO	CONSTANS
Col-0	Columbia-0
CPK33	CALCIUM DEPENDENT PROTEIN KINASE 33
CPK6	CALCIUM DEPENDENT PROTEIN KINASE 6
CPNT	CPP derived from Brome mosaic virus
CPP	Cell Penetrating Peptide
CRISPR Cas-9	DNA modification technology
CRY1	CRYPTOCHROME1
CRY2	CRYPTOCHROME2
CTAB	Cetyltrimethylammonium bromide
Da	Dalton
DCM	Dichloromethane
ddH2O	Double distilled water
DIC	Dicyclohexylcarbodiimide
DMF	Dimethylformamide
DMSO	Dimethylsulphoxide
DNA	Deoxyribonucleic acid
dNTP	Deoxyribonucleotide triphosphate
DSF	Differential scanning fluorimetry
dsRNA	Double-stranded ribonucleic acid
DTT	Dithiothreitol

ε_{280}	Molar extinction coefficient at 280 nm
E. Coli	Escherichia coli
EDT	1,2-ethanedithiol
EDTA	ethylenediaminetetraacetic acid
EIPA	5-(N-Ethyl-N-isopropyl)amiloride
EMSA	Electrophoretic Mobility Shift Assay
eq.	Molar equivalent
Et_2O	Diethyl ether
EtOH	Ethanol
FAC	Florigen Activation Complex
FCA	4-Amino-1-(beta-D-arabinofuranosyl)-5-fluoro-2(1H)-pyrimidinone
FIC	Florigen Inhibition Complex
FLC	FLOWERING LOCUS C
fm	Floral meristem
Fmoc	Fluorenylmethyloxycarbonyl
FPLC	Fast Protein Liquid Chromatography
FRI	FRIGIDA
FT	FLOWERING LOCUS T
FUL	FRUITFULL
GA	Gibberellic acid
gDNA	Genomic DNA
GF14	14-3-3 Protein (Rice)
GFP	Green Fluorescent Protein
GI	GIGANTEA
Glu, E	Glutamic Acid
Gly, G	Glycine
GUS	B-Glucuronidase
H	Histone
HBTU	Hexafluorophosphate Benzotriazole Tetramethyl Uronium
Hd3a	Heading Date 3a
HDA5	Histone Deacetylase 5
HEPES	4-(2-hydroxyethyl)-1-piperazineethanesulfonic acid
His, H	Histidine
HIV	Human Immunodeficiency Virus
HoBt	Hydroxybenzotriazole
HRP	Horseradish peroxidase
HyD	High Definition Detector
IPTG	Isopropyl β-D-1-thiogalactopyranoside
Kan	Kanamycin
λ	Wavelength
L1	Layer 1
L2	Layer 2
L3	Layer 3
LacUV5	Promoter from E. coli Lac Operon
LB	Lysogeny Broth
LC	Liquid chromatography
LCMS	Liquid chromatography-mass spectrometry
LD	Long-day
Leu, L	Leucine
LFY	LEAFY
LP	Leaf primordia
M	Molar
MADS-box	DNA binding motif
MeOH	Methanol

MES	2-(N-morpholino)ethanesulfonic acid
Met, M	Methionine
MFT	MOTHER OF FT AND TFL1
mg	Milligram
min	Minute
mL	Millilitre
mM	Millimolar
mol	Molarity
MOPS	3-(N-morpholino)propanesulfonic acid
Mr	Molecular mass
mRNA	Messenger RNA
MS	Mass spectrometry
MW	Molecular weight
MWCO	Molecular weight cut-off
ng	Nanogram
NHS	N-Hydroxysuccinimide
OC	Organising centre
OD_{600}	Optical density at 600 nm
OsFD1	Rice FD homologue
OsMADS15	Rice AP1 homologue
P	Peripheral zone
p	Promoter
PAGE	Poly-acrylamide-gel-electrophoresis
PCR	Polymerase chain reaction
PEBP	Phosphatidyl-ethanolamine-binding-protein
pET-28b	Protein Expression vector
pH	Relative acidity scale
PHYA	PHYTOCHROME A
PHYB	PHYTOCHROME B
PI	PISTILLATA
pI	Isoelectric point
PIF4	PHYTOCHROME INTERACTING FACTOR 4
PP2A	PROTEIN PHOSPHATASE 2A-2
Pro, P	Proline
R	Rib zone
r.p.m.	Revolutions per minute
RCF	Relative centrifugal force
RFP	Red Fluorescent Protein
RNA	Ribonucleic acid
RT	Room temperature
SAM	Shoot apical meristem
SD	Short-day
SDS	Sodium dodecyl sulphate
PAGE	Polyacrylamide gel electrophoresis
SEC	Size exclusion chromatography
SEP	SEPALLATA
Ser, S	Serine
SMZ	SCHLAFMUTZE
SOC1	SUPPRESSOR OF OVEREXPRESSION OF CONSTANS 1
SPL	SQUAMOSA PROMOTER BINDING PROTEIN-LIKE
SPPS	Solid phase peptide synthesis
SVP	SHORT VEGETATIVE PHASE
T_1	First generation transgenic plant
T_2	Second generation transgenic plant

T-6-P	Trehalose-6-phosphate
TAIR	The Arabidopsis Information Resource
TBST	Tris-buffered saline tween
TEM1	TEMPRANILLO1
TEMED	N,N,N′,N′-Tetramethylethylenediamine
TEV	Tobacco Etch Virus
TFA	Trifluoroacetic acid
TFL1	TERMINAL FLOWER 1
Thr, T	Threonine
TIS	Triisopropylsilane
tm	Transition meristem
TOE	TARGET OF EAT1
TPS1	TREHALOSE-6-PHOSPHATE SYNTHASE1
Tris	Tris(hydroxymethyl)aminomethane
Trp, W	Tryptophan
TSF	TWIN SISTER OF FT
Tyr, Y	Tyrosine
UV	Ultraviolet radiation
UFO	UNUSUAL FLORAL ORGANS
v/v	Volume ratio
VIN3	VERNALISATION INSENSITIVE 3
VRN1	REDUCED VERNALISATION RESPONSE 1
VRN2	REDUCED VERNALISATION RESPONSE 2
WT	Wild type
WUS	WUSCHEL
X	Magnification multiple
YFP	Yellow Fluorescent Protein

Table of Contents

Chapter 1 - Introduction

1.1 Global Food Security 17
1.2 Model Organism – Arabidopsis and Flowering 19
1.3 Flowering Time Signals Integrate through Flowering Locus T 20
1.3.1 Photoperiodism 20
1.3.2 Flowering Locus T 22
1.3.3 PEBP Protein Family 23
1.3.3.1 FT Homologues – Floral Activators 23
1.3.3.2 FT Homologue – TFL1 24
1.3.3.3 FT Orthologues in Sugar beet 27
1.3.4 Flowering Locus D 28
1.3.5 Florigen Activation Complex 28
1.3.5.1 FAC and FIC Action 30
1.3.6 FLC and the Repression of FT 31
1.3.6.1 FLC and Vernalisation 31
1.3.6.2 FLC and Autonomous Regulation 33
1.3.7 Trehalose-6-Phosphate 33
1.3.8 microRNA – miR156 and miR172 34
1.4 Apical Meristem Development – Apetala 1 Action 36
1.4.1 ABC Model for Floral Organ Development 36
1.4.2 APETALA 1 37
1.4.3 Maintenance of the Shoot Apical Meristem 38
1.4.4 Apical Meristem Differentiation 40
1.4.4.1 Meristem Identity Genes - LEAFY 41
1.5 Entry of Macromolecules Inside the Cell 42
1.5.1 Barriers to Entry 42
1.5.1.1 Plant Cell Membrane 42
1.5.1.2 Plant Cell Wall 42
1.5.2 Uptake across the Membrane 44
1.5.2.1 Small Molecule Transport 44
1.5.2.2 Endocytosis 44
1.5.3 Cell Penetrating Peptides 46
1.5.3.1 Cell Penetrating Peptide *in Planta* 48
1.5.3.2 CPP Mediated Protein Transduction Studies *in Planta* 50
1.6 Project Objectives 52

Chapter 2 – Materials and Methods

2.1 Solid Phase Peptide Synthesis 54
2.1.1 Automated Backbone Coupling Reactions 54
2.1.2 N-Terminal Modification – 5-Carboxytetramethylrhodamine Coupling 54
2.2 Cloning 56
2.2.1 Site Directed Mutagenesis (*FT-Tat and FT-R9 Construction; TEV Site Insertion)* 56
2.2.2 Gibson Assembly (*FT-GFP Construction)* 57
2.3 Protein Expression and Purification 58
2.3.1 Transformation 58
2.3.2 Induction 58
2.3.3 Cell Harvesting and Sonication 58
2.3.4 Protein Buffer Compositions 59
2.3.5 Ion Exchange Chromatography Protocol 60
2.3.6 Nickel Affinity Chromatography Protocol 60
2.3.7 His-tag Removal using Thrombin 60
2.3.8 Size Exclusion Chromatography 61
2.3.9 Other Proteins 61
2.3.10 SDS-PAGE Preparation 61
2.4 Western Blot Protocol 63

2.5 Sortagging 64
2.6 Plant Culture 66
2.6.1 Sterile Root Tip Growth 66
2.6.2 Callus and Cell Culture Formation 67
2.6.2.1 Callus Culture 67
2.6.2.2 Cell Culture 67
2.6.3 Protoplast Isolation 67
2.7 Delivery and Uptake Methodologies 68
2.7.1 Uptake in Model Systems 68
2.7.1.1 CPP Uptake Study in Root Tips 68
2.7.1.2 CPP Uptake Study in Cell Culture 68
2.7.1.3 Uptake of Sortagged Proteins into Callus Culture 70
2.7.2 Uptake of Protein into Whole Organism 70
2.7.2.1 Protein Infiltration and Extraction Method from Leaf 70
2.7.2.2 Apical Meristem Dissection 71
2.7.2.3 Microinjection 71
2.8 pAP1::GFP Molecular Reported Construction 72
2.8.1 DNA Extraction from Plants 72
2.8.2 TOPO Cloning 72
2.8.3 LR Reaction 73
2.8.4 Agrobacterium Transformation 73
2.8.5 Floral Dip Protocol 73
2.9 Confocal Microscopy 75
2.9.1 Acquisition Parameters 75
2.9.2 Propidium Iodide Root Tips Staining 76

Chapter 3– Assessment of CPP Internalisation in Plant Tissue
3.1 Introduction 77
3.2 Experimental Aims for the Chapter 79
3.3 Results 80
3.3.1 SPPS of Tat, TP10 and pVEC 80
3.3.2 Assessment of R9, Tat, pVEC and TP10 Uptake 82
3.3.2.1 Uptake into Root Tips 82
3.3.2.2 Uptake into Root Tips – Assessment with Propidium Iodide 85
3.3.3 Further Assessment of R9 Uptake 88
3.3.3.1 Assessment of R9 Uptake into Arabidopsis Leaf Cell Culture 88
3.3.3.2 R9 Incubation with Protoplasts 93
3.3.3.3 R9 Quantitative Uptake Assessment 94
3.3.3.4 R9 Uptake into the Shoot Apical Meristem 102
3.4 Discussion 106
3.4.1 Analysis of R9 Uptake 107
3.4.1.1 Quantitative Assessment of R9 Uptake 108
3.4.1.2 R9 Shoot Apical Meristem Delivery 109
3.4.2 The Effect of The Cell Wall on Uptake 109
3.4.3 Poly Arginine Uptake Mechanism in Plants 110
3.4.4 Bespoke Plant CPPs 114
3.5 Conclusion 116

Chapter 4 – Tools to Assess Cellular Delivery using Tat and R9
4.1 Introduction 118
4.2 Experimental Aims for the Chapter 120
4.3 Results 121
4.3.1 Purifications for FT, FT-Tat and FT-R9 121
4.3.1.1 FT Purification 122
4.3.1.2 FT-Tat and FT-R9 Purifications 124
4.3.2 Development of Fluorescent Protein Tools 128

4.3.2.1 FT-GFP Cloning and Purification 128
4.3.2.2 Fluorescent Labelling of FT by Sortase Trans-Peptidation Reactions 130
4.3.3 Assessment of FT, FT-Tat and FT-R9 Uptake in Cells 137
4.3.3.1 Covalent CPP Mediated Cellular Delivery with FT, FT-Tat & FT-R9 137
4.3.3.2 Assessment of Non-Covalent Protein Delivery of FT-GFP via R9 141
4.4 Discussion 144
4.4.1 Fluorescent Labelling of FT 144
4.4.2 Covalent Delivery of Cargo 147
4.4.3 Non-Covalent Delivery of Cargo 149
4.5 Conclusion 150

Chapter 5 – Assessment of Exogenous FT Delivery and Biological Action

5.1 Introduction 153
5.2 Experimental Aims for the Chapter 155
5.3 Results - Part 1 156
5.3.1 Routes of Entry for Recombinant FT 156
5.3.1.1 Stomatal Openings on the Underside of the Leaf 156
5.3.1.2 Microinjection 162
5.3.1.3 Direct SAM Infiltration 168
5.3.1.4 Review of Available Delivery Routes 172
5.4 Results – Part 2 173
5.4.1 Phenotypic Assessment 173
5.4.1.1 Flowering Time Results – Treatment at 45 Days Old 173
5.4.1.2 Additional FT Treatments, 25 Days, 32 Days, Summary 178
5.4.2 Molecular Readout 181
5.5 Discussion 186
5.5.1 Examples of Recombinant Protein Use as a Therapeutic 186
5.5.2 Apical Meristem Development 187
5.5.3 Floral Reversion Phenotype 188
5.5.4 Exogenous Control of Flowering Time 189
5.5.5 Further Studies in Different Organisms 192
5.6 Conclusion 194

Chapter 6 – Concluding Remarks

6.1 Summary 196
6.2 Future Perspectives 198
6.2.1 R9 Uptake Could Guide Electrotrophic Response in Plant Growth 198
6.2.2 Further Flowering Time Experiments 198
6.2.3 Optimising the Exogenous Treatment Technology 199
6.2.4 A Universal Treatment Across Species 199
6.2.5 Commercial Possibilities for FT Protein Therapy 200

Index of Figures

Figure 1 – Rapeseed (*Brassica napus*) crop flowering profiles……..……..…18
Figure 2 – Circadian control of CO transcription during photoperiodism……20
Figure 3 – FT is activated in the photoperiod pathway through CO……21
Figure 4 – The crystal structures of TFL1 and FT……..26
Figure 5 – The Florigen Activation Complex reported in rice……...29
Figure 6 – Chromatin modification in FLC activation……32
Figure 7 – Interactors in the floral activation pathway……...35
Figure 8 – The ABC model and spatial patterning of floral homeotic genes……..37
Figure 9 – Regions and layers of cells in the SAM……39
Figure 10 - Four stages of apical meristem development after floral developmental cues..……40
Figure 11 – The composition of the primary plant cell wall……43
Figure 12 – A summary of cellular entry mechanisms……46
Figure 13 – Schematic showing the SPPS chemical workflow……..…80
Figure 14 – Analytical assessment of peptide purity and characterisation using LCMS……81
Figure 15 – Setup for confocal microscopy experiments of Arabidopsis root tips……..82
Figure 16 – 20-minute incubations of CPPs with Arabidopsis root tips……83
Figure 17 - 6-hour incubations of CPPs with Arabidopsis root tips……...…84
Figure 18 – 6-hour CPP incubations with propidium iodide staining……..……87
Figure 19 – Arabidopsis cell culture confocal images for incubations with R9 after both 20 minutes and 6 hours……89
Figure 20 – Arabidopsis cell culture nucleation……..……...…90
Figure 21 – 20-minute incubation of R9 with cell culture – line intensity assessment……91
Figure 22 – 6-hour incubation of R9 with cell culture – line intensity assessment……...…92
Figure 23 – Confocal Images of protoplasts before and after R9 uptake……93
Figure 24 - A representation of the computational assessment of R9 uptake in root tips……..…96
Figure 25 – Control and 6-hour uptake acquisitions for R9 into Wave131 root tips……97
Figure 26 – Computational cell type assignment for control and 6-hour uptake incubations for R9 into WAVE131 root tips……..…98
Figure 27 – Control incubations – cumulative cellular uptake assessment……..99
Figure 28 – 6-hour R9 incubations – cumulative cellular uptake assessment……100
Figure 29 – Apical meristem incubations with TAMRA-R9……...103
Figure 30 – Proposed uptake mechanism for R9 and Tat into plant cells……..113
Figure 31 – Introduction of Tat and R9 sequences at the C-terminus of FT……..121
Figure 32 – FT purification with His-tag cleavage……..123
Figure 33 – FT-Tat and FT-R9 SEC traces following nickel affinity chromatography……..125
Figure 34– Purification properties for FT, FT-Tat and FT-R9……126
Figure 35 – FT-GFP construction using Gibson Assembly……...…12
Figure 36 – 2-step purification of FT-GFP……...123
Figure 37 – N-terminal Sortagging schematic for FT……..…125
Figure 38a – Introduction of sterically available N-terminal glycines for Sortagging……..……127
Figure 38b –Purification of protein constructs with introduced TEV sites……128
Figure 39 – Sortagging of FT, FT-Tat, FT-R9 and TFL1……...129
Figure 40a – Incubation of Sortagged FT with callus culture cells……132
Figure 40b – Incubation of Sortagged FT-Tat with callus culture cells……..…133
Figure 40c – Incubation of Sortagged FT-R9 with callus culture cells……..…134
Figure 41 – Non-covalent FT-GFP delivery to Arabidopsis cells with TAMRA-R9…..……136
Figure 42 – Surface lysine and cysteine protein labelling probes……140
Figure 43 – Stomatal protein delivery via pressurised syringe……..…150
Figure 44 – FT-GFP Infiltration inside the leaf via stomatal entry……151
Figure 45 – The direction of movement of FT-GFP inside the leaf after infiltration……..……152
Figure 46 – Further assessment of FT-GFP inside the leaf……..…153
Figure 47 – FT, FT-Tat and FT-R9 infiltration into Col-0 leaves……..…155
Figure 48 – Microinjection schematic of FT into the sieve elements……..…156
Figure 49 – Microscopy images of the phloem and xylem in sugar beet……158

Figure 50 – Microinjection of FT-GFP into sugar beet phloem……159
Figure 51 – Direct protein delivery to the SAM...……160
Figure 52 – FT-Tat incubation with the SAM……161
Figure 53 – FT-Tat incubation with the SAM – further examples……163
Figure 54- Experimental design for FT and FT-Tat treatment for 45-day old plants……167
Figure 55a- 45-day old treatment, summary & unique partial induction phenotype……168
Figure 55b – Repeat of 45-day old FT treatment, summary and unique partial induction phenotype……171
Figure 56 – Additional exogenous FT protein treatments……172
Figure 57a – pAP1:GFP::Col-0 molecular reporter design……175
Figure 57b – Activation of AP1 via FT in complex with the 14-3-3 dimer and FD dimer (FAC)…...175
Figure 57c – AP1 Sequence, 2000 base pairs used in the pAP1::GFP in Col-0 design……...175
Figure 58 – Assessment of pAP1:GFP::Col-0 function in the apical tissue……176
Figure 59 – Additional assessment of pAP1:GFP::Col-0 GFP expression……177
Figure 60 – Regions and cellular layers in the differentiating apical meristem……179
Figure 61 - Example of other species for exogenous protein treatment……184

List of Tables

Table 1 – FT homologues, the pocket residue and the external loop……..27
Table 2 – CPP sequence designs……48
Table 3 – Independent CPP action reported in plant systems……..….50
Table 4 – Examples of covalent and non-covalent protein transduction in the plant sciences literature……....51
Table 5 – PCR cycling conditions……...56
Table 6 – Primers used for site-directed mutagenesis……..……..57
Table 7 – Primers used for FT-GFP construction……...57
Table 8 – Protein buffers used in purification and application assays…….…….59
Table 9 – SDS-PAGE gel composition…….……62
Table 10 – Composition of Western blotting buffers…….……63
Table 11 – Sortase reaction buffer composition……..……..…….64
Table 12 – Compositions and preparation requirements of essential plant growth and regeneration media…….……66
Table 13 – Composition of infiltration and extraction buffer for protein leaf infiltration……..…70
Table 14 – Primers used in the construction of pAP1::GFP:Col-0……..…73
Table 15 – Confocal microscopy settings for the detection of fluorophores…… 76
Table 16 - Cellular uptake assessment summary……..……...…101

List of Text Inserts

Text Insert 1 – Attached to *Figure 32*……124
Text Insert 2 – Attached to *Figure 36*……129
Text Insert 3 – Attached to *Figure 38a*…….……133
Text Insert 4 – A summary of exogenous protein delivery routes……172

1. Introduction

1.1 – Global Food Security

Global food production hinges on the widespread reliable flowering times of important cropping species because successful flowering predetermines harvest timings and yields. Principally, the worldwide availability of annual harvest stocks from important flowering crops, including grain and other staples such as fruits, is essential to feed a global population approaching 8 billion people [1, 2]. The global economy relies on both the availability and price of grain (from flowering plants) because it affects baseline values across commodity markets and the prices of many everyday consumer products. In this way, the annual supply of grain from flowering crops is essential to maintain a stable global economy.

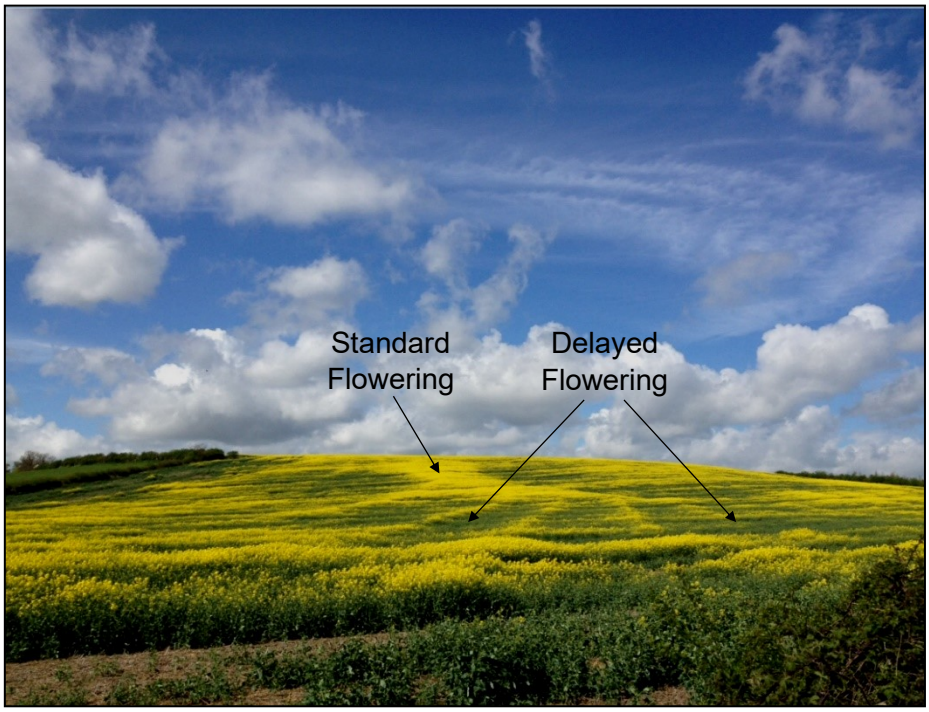
Erratic seasonal weather patterns caused by the onset of global warming, are affecting growing conditions for flowering crops [3]. Moreover, the effect of permanent climate change, will cause widespread disruption, shifting plant growth cycles. Namely, plant responses to the change in growing temperatures will have a negative impact on yields [4, 5]. In addition, extreme weather occurrences will result in a higher incidence of drought and flooding, causing crop failures and ultimately rendering certain geographical regions unusable for agriculture [6].

It is clear that research into the artificial control of flowering time is essential in order to improve yields to sustain an increasing global population and also mitigate the adverse effects to growing conditions caused by the onset of climate change. The work in this thesis investigates the possibility of a macromolecular therapy that could be used to artificially activate flowering.

(1) Ideal Rapeseed Canopy Bloom



(2) Partial Rapeseed Canopy Bloom



(2) Also used in MRes Thesis [7]

Figure 1 – Rapeseed (*Brassica napus*) crop flowering profiles. The flowering canopy recorded in early May, in Rutland, England. **(1)** Successful flowering across the canopy is essential for pollination, subsequent seed formation and yield determination. **(2)** Flowering canopy is not uniform, with areas of delayed flowering. Harvest timing occurs 12 weeks after flowering, as such delayed flowering regions will mature later which will disrupt the harvest as the ripening of the whole crop will occur at different times.

1.2 - Model Organism – Arabidopsis and Flowering

Arabidopsis thaliana, otherwise known as mouse-ear or thale cress has a fully sequenced genome and has become an established model for plant biology, including reproductive development [8]. It was popularised in research due to its ease of handling, small size, short growth cycle and phylogenetic positioning with close relatives in agronomically important cropping species across the Brassicaceae family, including oilseed rape, cabbage, broccoli, mustard, cauliflower, kale, horseradish and turnips [9]. Close genetic links with important cropping species make it an excellent model to study reproductive development as numerous homologues exist, indeed also across a wider branch of angiosperms, with many conserved pathways [9]. Arabidopsis is a facultative long-day plant and under long-day growth conditions, the macroscopic appearance of buds is within 4 weeks, full floral phenotype at 5 weeks and seed formation from 6 weeks in healthy plants – ideal for academic experiments [10, 11].

A successful floral transition is essential to ensure successful reproduction and this is especially important for monocarpic plants, including Arabidopsis, which only have one opportunity to flower. Flowering is characterised by a significant irreversible developmental change at the apex where the production of leaf primordia is replaced by developing floral primordia. The purpose of flowering (sexual reproduction) is to produce a plentiful number of seeds which are photosynthate sinks; this photosynthate accumulation is essential for the successful forthcoming germination of seeds [12, 13]. A healthy plant therefore only proceeds to flowering once sufficient photosynthate has been accumulated and is beyond its juvenile stage [13]. Many plants respond to environmental cues such as temperature and photoperiod and are tuned to flower ideally when advantageous environmental conditions will enable successful seed production [13]. In principle, under standard growth conditions, this enables the completion of the lifecycle and seed production before the onset of disadvantageous cold environmental temperatures.

1.3 – Flowering Time Signals Integrate through Flowering Locus T

1.3.1 - Photoperiodism

Photoperiodism is categorised by three main types of response; long-day plants flower once the photoperiod extends beyond a threshold, short-day plants when photoperiod drops below the threshold, and day-neutral plants which are unaffected by photoperiod changes [14]. Arabidopsis is a facultative long-day plant and photoperiod is detected in the leaf, resulting in a mobile protein stimulus, called florigen, which travels to the apex and co-ordinates the plant's flowering time response [14, 15].

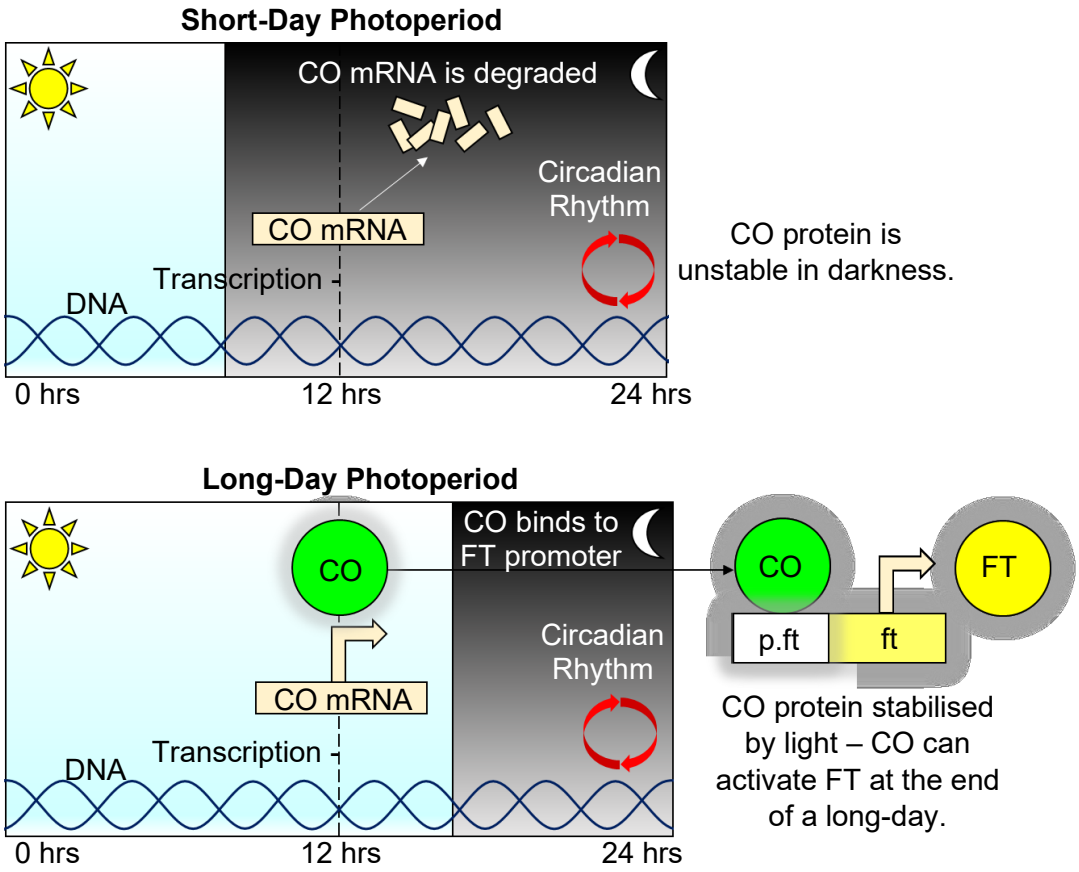


Figure 2 – Circadian control of CO transcription during photoperiodism. The circadian rhythm is entrained to a 24-hour cycle and CO mRNA is transcribed 12 hours after dawn, however it is degraded in the darkness. This means that CO protein is present only during long-day photoperiods which directly correlates with FT expression. This is the basis for photoperiod regulation of flowering.

The internal circadian clock is entrained to a 24-hour cycle and CONSTANS (CO) mRNA transcription occurs, 12 hours after dawn [16]. CO protein is degraded during darkness - and light is required for CO stabilisation [17]. In this way, a peak in CO protein is observed only at the end of a long-day and this will coincide with the annual pattern of increasing day-length in the spring when light levels pass this threshold [18]. CO encodes a transcription factor which binds to a cis-element within the FT promoter, activating FT transcription [19]. FT protein then translocates to the apex and this is the basis for photoperiodic regulation [15].

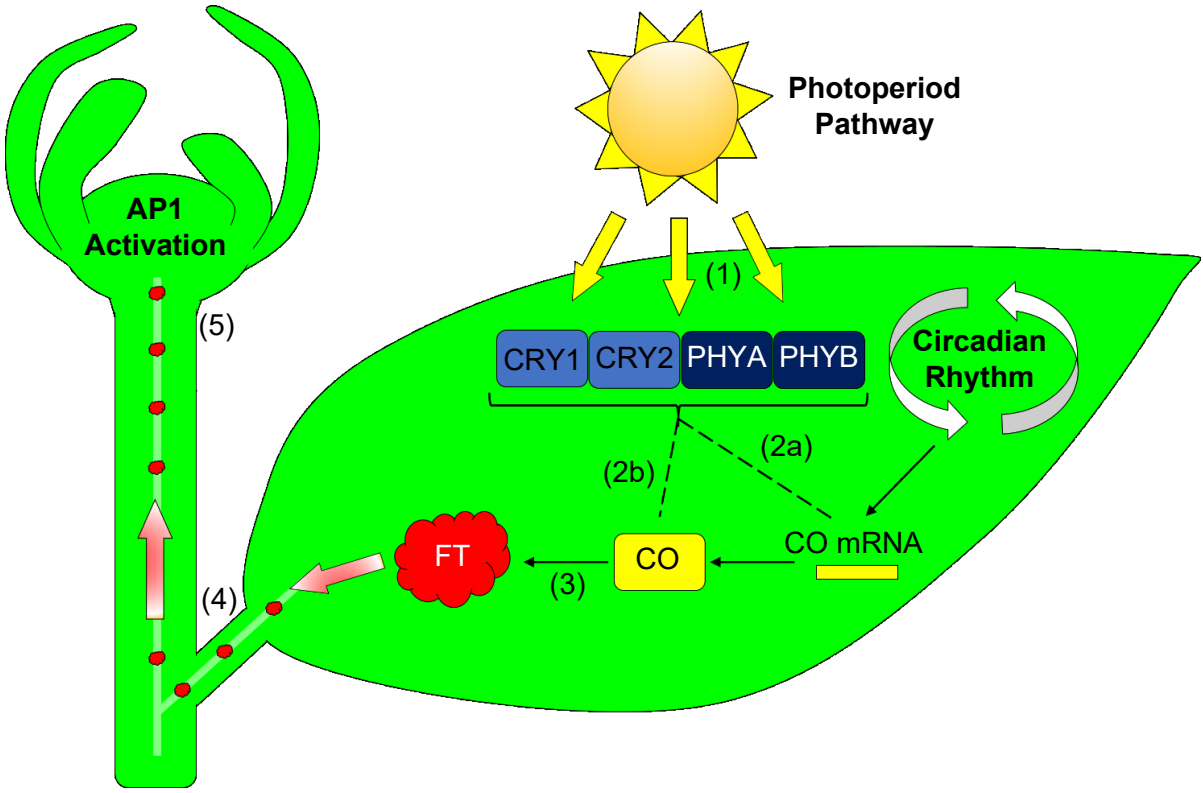


Figure 3 – FT is activated in the photoperiod pathway through CO. (1) Cryptochromes (CRY1 and CRY2) and Phytochromes (PHYA and PHYB) detect the presence of light in the leaf. **(2a)** CO mRNA is downregulated by PHYB and upregulated by PHYA and CRY2. CO mRNA is circadian controlled and a peak occurs 12 hours after dawn. **(2b)** PHYB, CRY1 and CRY2 stabilise CO protein whereas PHYB causes targeted ubiquitination. **(3)** CO activates FT through promoter binding – this is the foremost activation mechanism of FT. **(4)** FT translocates to the shoot apical meristem via the phloem. **(5)** FT activates AP1 causing the shoot apical meristem to transition to an inflorescence meristem.

Phytochromes (PHYA and PHYB) and cryptochromes (CRY1 and CRY2) are photoreceptors in the leaf which detect ambient light levels and affect the presence of CO at both the mRNA and protein level [20, 21]. CO mRNA transcription is downregulated by PHYB and upregulated by PHYA and CRY2 in order to co-ordinate the daily cycle which includes a peak in CO mRNA approximately 12 hours after dawn [21]. The circadian rhythm is entrained by photoreceptors which respond to incident light wavelengths and strengths. They are essential to keep the plant under a tight 24-hour cycle. In addition, CO protein stabilisation is by PHYA (responding to far-red light), CRY1 and CRY2 (both responding to blue and UV light); PHYB however has an antagonistic effect and causes CO degradation through targeted ubiquitination [20], [21]. The balance between photoreceptor responses is important for CO regulation and ensures an mRNA peak 12 hours after dawn - protein is either degraded or stabilised depending on the presence of light at the end of the day for long-day plants [16].

1.3.2 – Flowering Locus T

In flowering time, the photoperiod detection and response organs are spatially decoupled meaning that a long-distance signal is required to initiate the response, this was postulated in the 1930s and remained elusive until the discovery of a long-distance signal in 2007 which was the small and mobile protein, FT [15]. FT integrates the complicated network of detection signals within the leaf, translocates to the apex via the phloem, where it activates the meristem identity genes *LEAFY* (*LFY*) (via SOC1) and in particular, *AP1,* causing differentiation of the apical cells to form an inflorescence meristem [22]. The role of FT in flowering response is widespread across species and homologues exist across angiosperms - it is considered a universal florigen signal [23]. The identity of florigen had remained a mystery until experimental claims proposed that FT mRNA was able to travel to the apex to initiate floral induction [24]. This evidence was quickly retracted and the true identify of florigen revealed as the FT protein in a landmark discovery; at the same time, this was also corroborated in rice with the analogous discovery of HEADING DATE 3A (Hd3a), an FT homologue [15, 25].

FT is an instrumental signalling molecule whose downstream effects cause major and irreversible developmental changes to the plant and as such its regulation is key to ensuring timely and successful flowering. The foremost mechanism for FT activation occurs via CO in the companion cells [19]. Other partners also contribute to FT activation, namely, GIGANTEA (GI) binds to the *FT* promoter, in addition, PHYTOCHROME INTERACTING FACTOR 4 (PIF4) and CRYPTOCHROME 2/ CRYPTOCHROME-INTERACTING bHLH complex (CRY2/CIB) both activate *FT* through promoter binding and this is reviewed by Pin *et al.* [26-29]. Conversely, a number of partners repress *FT* through promoter binding and these include FLOWERING LOCUS C (FLC) through both the autonomous and vernalisation pathways, SCHLAFMUTZ (SMZ) and TEMPRANILLO 1 (TEM1) also reviewed by Pin *et al.* [29-32]. FT integrates a number of pathways in the leaf and its transcription is tightly controlled by both positive and negative regulators; in this way, transcription only occurs at the point of positive inductive conditions [22].

1.3.3 - PEBP Protein Family

1.3.3.1 – FT Homologues - Floral Activators

FT belongs to the phosphatidylethanolamine-binding protein (PEBP) family and is conserved across kingdoms, indeed sharing similarity with the human Raf kinase inhibitor protein (RKIP) [33]. 6 members of this family are present in Arabidopsis of which FT plays the major role in floral induction. TWIN SISTER OF FT (TSF) is both mobile and able to induce flowering, travelling from the leaf to the shoot apex, its role is however inferior to induction by FT [34, 35]. TSF shares the closest similarity to FT (82% sequence conservation) and is activated via CO, repressed by FLC and likewise expressed in the companion cells [34]. Overexpression accelerates flowering and TSF acts independently of FT as a secondary florigen signal [34]. Both the mobility and stability of FT is higher than for TSF, and whilst FT is graft transmissible, this is not apparent during TSF movement studies [15, 35]. The region between L28-G98 in FT

enhances chimeric TSF mobility, including graft transmission and as such is inferred important for FT protein mobility [35]. The overexpression of MOTHER OF FT AND TFL1 (MFT) showed a slight acceleration of flowering however knockout mutants did not show any observable changes in either flowering time or meristem identity showing that MFT is not an essential floral stimulus [36, 37]. The floral inductive effects of MFT are limited and actually its main function is in seed germination through ABA signalling [37].

1.3.3.2 - FT Homologue –TFL1

TERMINAL FLOWER 1 (TFL1) is a closely related homologue of FT, within the PEBP protein family, and they share almost 60% sequence similarity [33, 38]. TFL1 however curiously functions antagonistically to FT, repressing the conversion to floral transition, and their different roles within floral development lead to TFL1 categorisation as a meristem identity gene whereas FT is a floral integrator gene [39, 40]. This fascinating juxtaposition is explained by subtle differences existing within the sequences of these two proteins. Both FT (175 amino acids) and TFL1 (177 amino acids) are comprised of four exons, and an exon swapping experiment showed that chimeras about the 4th exon exhibited opposite activity when FT was replaced with this exon from TFL1 [33]. The reverse swap into TFL1 however showed little effect [33]. Indeed, the 4th exon is where the greatest variation exists between the two sequences and codes for an external loop (containing 14 residues) which is involved in both 14-3-3 association and hypothesised to play an important role in DNA binding [33, 41]. The external loop is likely to play an important role in the different functions however details of the exact molecular nature remain unknown [33]. Crystal structures were solved by Ahn *et al.* and the external loop displays significant variation in both sequence and conformation between FT and TFL1 [33]. In particular, a hydrogen bond forms between this and the ligand binding pocket in TFL1, which is not observed in FT [33].

The functional similarity between FT and TFL1 is high, signified by interchanging a single residue at the ligand binding pocket which is enough to switch the activity of these two proteins [38]. Importantly, the amino acid exchange is reciprocal and in an *tfl1;ft* double null mutant background, 35S::TFL1(H88Y) accelerated flowering, likewise, 35S::FT(Y85H) resembled TFL1 action [38]. It is important to note however, that the effects, although characteristic, are weaker than constitutive overexpression of the other partner, and FT(Y85H) only caused terminal flower formation whereas TFL1(H88Y) weakly accelerated the flowering phenotype [38]. Whilst this finding is significant towards explaining their opposite functions, it also implies that other functioning domains within FT and TFL1 are responsible to completely explicate their opposing activities [38], [42]. This also corroborates the evidence presented for chimeras about the 4th exon – whilst opposite phenotypes are observed, they are not as strong in resembling the other protein [33].

For completion, the remaining two members of the PEBP family are BROTHER OF FT AND TFL1 (BFT) and CENTRORADIALIS homologue (ATC), and both are floral repressors [43, 44]. 35S::BFT displayed delayed flowering, with a spatial patterning in the meristem and repressed *AP1* and *LFY*, hindering inflorescence meristem transition [43]. ATC is a long-distance floral inhibitor expressed in the vasculature, and is graft transmissible [44]. It interacts with FD in the apex, repressing *AP1*, to prevent inflorescence development [44].

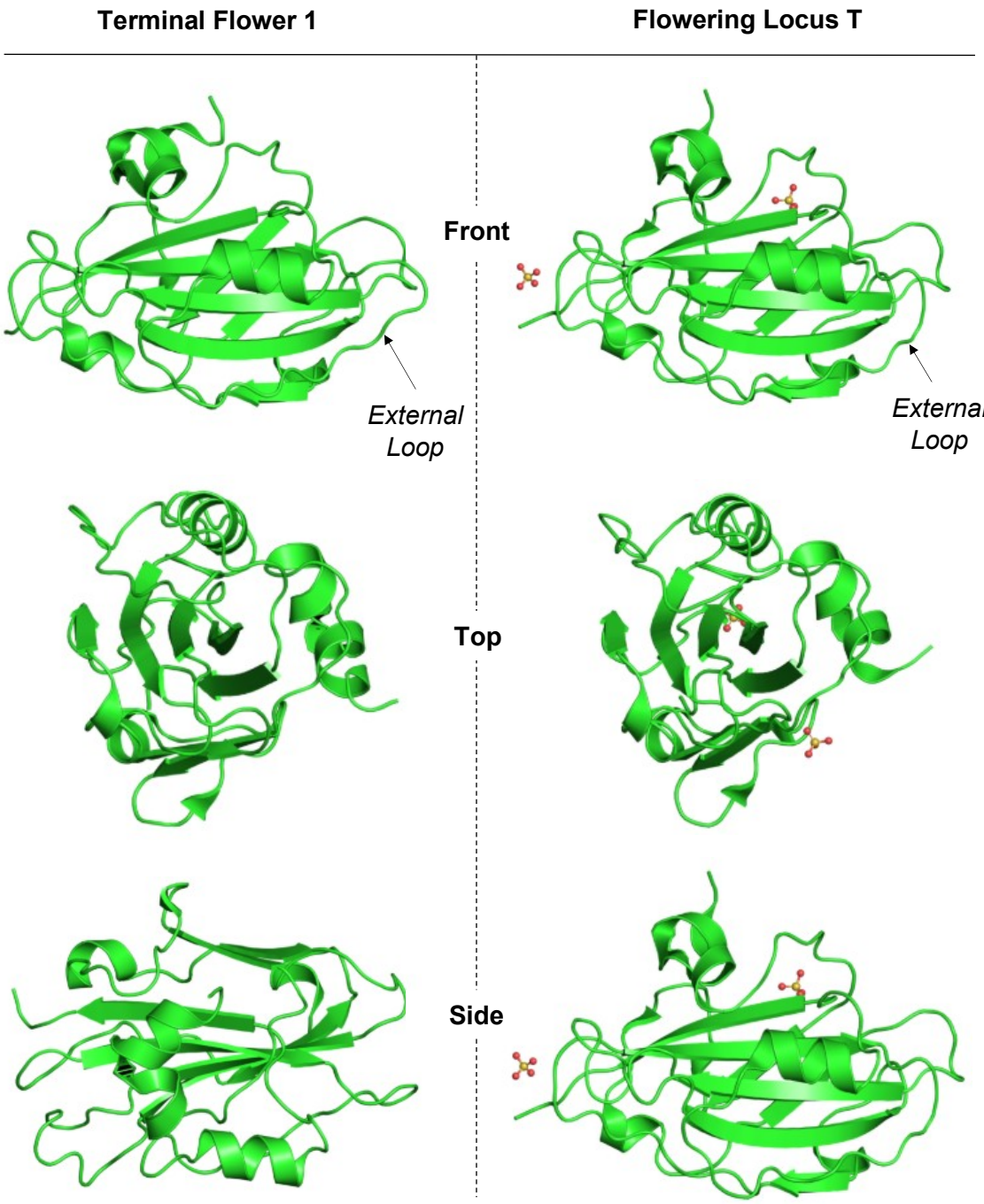


Figure 4 – The crystal structures of TFL1 and FT. These are taken from the *European Crystal Structure Database*. They show the close structural similarity between the two homologues. The external loop is where the two structures differ most in sequence identity and this is illustrated in the figure. The crystal structures of TFL1 and FT were solved by Ahn et al. [33].

1.3.3.3 - FT Orthologs in Sugar Beet

A fascinating situation arises in sugar beet where the floral transition is under the control of two FT paralogues [45]. BvFT2 is a floral activator whereas BvFT1 is a repressor, however bearing resemblance to the FT-like clade, rather than to TFL1 [45]. Cultivated sugar beet has been designed without the dominant bolting B allele and plants are able to dodge flowering in the first year; as such they bolt and produce seeds in the second year after a strong vernalisation response and the subsequent increasing photoperiod [45].

In addition, cloning the *BvFT1* floral repressor into Arabidopsis delayed flowering [45]. This result is especially curious as an FT-like protein from sugar beet is able to delay flowering in Arabidopsis [45]. Both emphasising the universality of FT orthologues and depicting how the subtle differences in sequence caused this reversal in flowering time response. This selective natural example compliments the chimeric work of both Hanzawa *et al.* and Ahn *et al.* [33, 38, 45]. In addition, the accompanying result is observed when *BvFT2* is cloned into Arabidopsis showing accelerated flowering [45].

Table 1 - FT homologues, the pocket residue and the external loop. FT, TSF and MFT are floral activators in Arabidopsis. FT and TSF share 82% sequence conservation and the external loop is identical except for 1 residue. The external loops of BvFT1 and BvFT2 are identical except for 3 residues. The external loop of TFL1 is significantly different from FT and TSF, likely conferring their opposite activity *in vivo*. The characteristic tyrosine at the ligand binding pocket in FT is also present in BvFT1 and BvFT2.

Protein	Pocket Residue	Sequence of External Loop
FT	-Y-	-LGRQTVY-APGWRQN-
TSF	-Y-	-LGRQTVY-APGWRQQ-
MFT	-W-	-SPVGLMVQQPPSRDN-
BvFT1	-Y-	-LGRQTV**N**AP**Q**-**Q**RQN-
BvFT2	-Y-	-LGRQTV**Y**AP**G**-**W**RQN-
TFL1	-H-	-KQRVIFPNIP-SRDH-
BFT	-Y-	-RGRQAVKAAPETREC-
ATC	-H-	-TRRGSVVSVPSYRDQ-

Tyrosine is present at residue 85 for both BvFT1 and BvFT2, which is the characteristic amino acid for FT shown by Hanzawa *et al.* at the ligand binding pocket (Y85H displays TFL1-like function) [38, 45]. Indeed, the antagonistic functions of BvFT1 and BvFT2 are narrowed down to three residues within the 14 amino acid section of the external loop, cited in Arabidopsis as playing a major role in the opposing functions of FT and TFL1 [33, 45]. All bar three residues are conserved in this section, and interchange followed by transgenic expression yields a remarkable switch in function for BvFT1 and BvFT2 [45]. The emergence of BvFT1 as a floral repressor was likely through mutation at these three distinct positions [45].

1.3.4 - Flowering Locus D

FD is expressed in the meristem where it interacts with FT to promote flowering [46]. The expression of FD is not circadian nor affected by light levels, and as such it is not a limiting factor in the photoperiod response [46]. It resides in the apex awaiting interaction from FT to co-ordinate the downstream flowering response. *AP1* is a major target of the FD-FT complex, other downstream targets also include *FRUITFULL* (*FUL*) and *SUPPRESSOR OF OVEREXPRESSION OF CONSTANS 1* (*SOC1*), controlling meristem identity [46, 47]. FD is a bZIP transcription factor, which binds to a C-box (GACGTC motif) in the *AP1* promoter; it acts in a complex called the Florigen Activation Complex (FAC) along with FT and 14-3-3 protein partners [46, 48].

1.3.5 – Florigen Activation Complex

Whilst FT is the mobile signalling molecule, it does not contain any classical DNA binding domains and as such, must function in tandem with bZIP transcription factor FD [46, 49]. Abe *et al.* showed the interaction between FD and FT in yeast cells however this was not observed for the analogous system in rice, where homologues Hd3a and OsFD1 (FD homologue) showed no interaction *in vitro* [46, 48]. Hd3a and OsFD1 interaction is mediated by GF14c, a 14-3-3 protein which bridges the complex [48]. This enables stable complex formation and the

trimeric complex, which is observed across species, is called the Florigen Activation Complex (FAC) [48, 50-52]. FAC comprises two FT monomers at opposite ends of the bridging 14-3-3 dimer, with an interstitial FD dimer bound to the positively charged 14-3-3 cleft [48]. 14-3-3 proteins are pervasive in plant molecular processes and exist as a class of 14 proteins in Arabidopsis, with redundancy amongst members, and the ability to share functions [53].

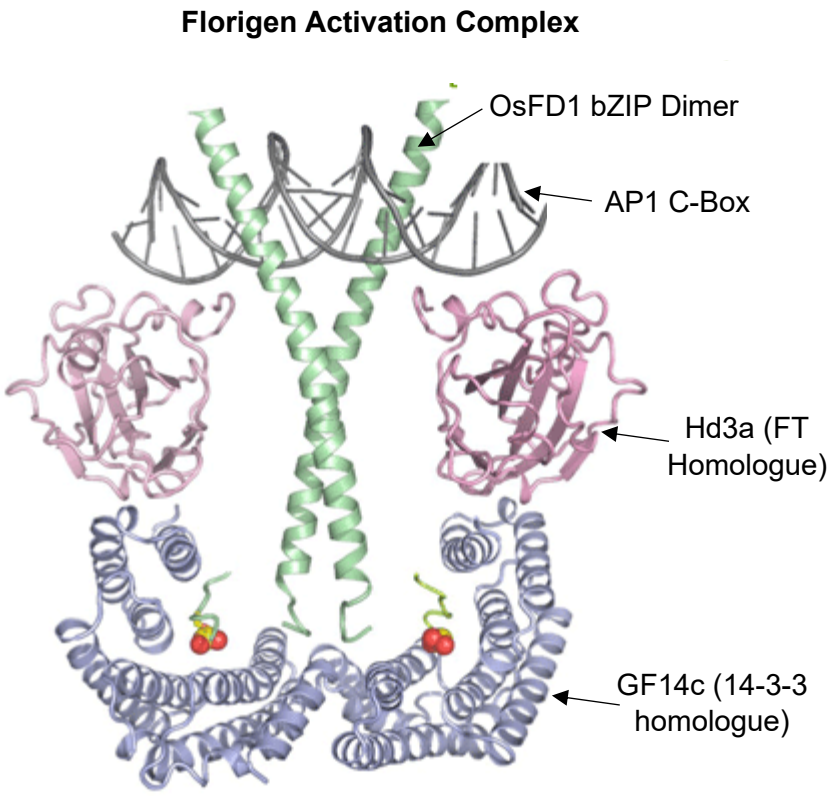


Figure 5 – The Florigen Activation Complex reported in rice. The crystal structure above is taken from Taoka et al. [48] . It reports the Florigen Activation Complex (FAC) which was solved for OsFD1, Hd3a and GF14c, which are the rice homologues of FD, FT and 14-3-3 respectively. The complex was reported to bind to a C-box (GACGTC motif) within the AP1 promoter. FAC is universal and is reported across species.

Taoka *et al.* solved a 2.4-Å crystal structure for FAC in rice [48]. OsFD1 must be phosphorylated at S192 in order to interact with the ligand binding cleft in GF14c, indeed Abe *et al.* expected to observe the phosphorylation of FD at T282 in the wild type Arabidopsis sequence [46, 48]. Full length OsFD1 contains unstructured N-terminal regions and as such is not stable *in vitro*,

instead, a 9 amino acid OsFD1 C-terminal phosphorylated peptide was used in the crystal structure, which bound to the GF14c cleft [46] . In Arabidopsis, two calcium dependent kinases (CPK6 and CPK33), expressed in the SAM, were reported to phosphorylate FD at position T282 and interestingly, delayed flowering was observed after CPK33 knockout [54]. This implies that phosphorylation of FD is essential for floral activation, most likely by enabling interaction with 14-3-3 in the FAC complex [54]. The interaction of FAC with the *AP1* promoter is centred about a C-box, indeed gel-shift with a 22-base pair section including the C-box is not observed when GF14c is absent from the rice FAC complex [48]. In addition, whilst previously noted that FT does not contain any characteristic DNA interaction surfaces, Hd3a in the rice FAC complex may however interact with DNA [48]. The morphology of the complex created by the W-shaped 14-3-3 dimer appeared to enable Hd3a to form a contact with the DNA as OsFD1 interacts with the C-box [48].

1.3.5.1 – FAC and FIC Action

The corresponding complex with TFL1 is termed the Florigen Inhibition Complex (FIC); a potential difference in DNA anchoring between FT and TFL1, in both FAC and FIC, at the *AP1* promoter could help to explain the opposite actions of both FT and TFL1 at the molecular level [7, 41]. The current understanding is that 14-3-3 is present in the cytoplasm of apical cells and FD in the nucleus [55]. FT arrives as a signal in response to inductive conditions, and binds to 14-3-3; this proto-complex traffics to the nucleus where it interacts with FD followed by transcriptional activation at the promoter of *AP1* [55]. 14-3-3 proteins have previously been reported with transport abilities, enabling trafficking of partners to the nucleus [56]. FT and TFL1 characterise the opposite actions of FAC and FIC as such the subtle differences between homologues FT and TFL1 are likely to explain differential anchoring at the DNA [42]. In addition, a hypothesis is that FIC might anchor at the C-box with higher affinity, thus preventing transcription by blocking FAC, however currently there is no published evidence in support of this. A surge in FT availability in the SAM after floral inductive conditions may

enable FAC to outcompete for the same site, and as a positive regulator – enable *AP1* transcription. Differential anchoring at the DNA could potentially lead to TFL1 in FIC sterically blocking the C-box, whereas the binding of FAC could occur at farther regions enabling a conformational change in the promoter to activate the transcription of *AP1*. Further experimentation is required to fully elucidate the molecular mechanisms of FAC and FIC to explain their antagonistic actions.

1.3.6 – FLC and the Repression of FT

1.3.6.1 – FLC and Vernalisation

The MADS-box protein FLC acts through the vernalisation pathway to avert flowering [57]. Vernalisation is a flowering time pathway where an inductive cold period prepares a plant for flowering, the response is either obligate, facultative or insusceptible thus not requiring cold treatment to flower [58]. FLC is the major component of the vernalisation pathway activated by FRIGIDA (FRI), the precise molecular details of FRI are unknown but it causes the trimethylation of lysine-4 at histone H3 [59, 60]. *FLC* encodes a MADS-box transcription factor which represses the expression of major flowering time genes including FT and as such must be repressed itself for flowering to proceed [61]. Whilst Arabidopsis is a winter annual with a facultative cold requirement, Columbia ecotype only has a slight vernalisation response with low basal levels of FLC because Columbia ecotype lacks FRI function thus FLC is minimally active [62]. In contrast, a plant with an obligate (*c.f.* facultative) vernalisation requirement will not allow flowering to proceed until a perceived cold period has passed [58].

In cold requiring lines (*c.f.* Columbia ecotype), during vegetative periods FLC is active in preventing the floral transition by inhibiting *FT*, *SOC1* and *FD* [61]. During this period *FLC* chromatin resides in an open conformation and *FLC* is active [57]. Epigenetic regulation represses FLC in response to the extended cold period, causing chromatin remodelling in particular involving histone H3 at the *FLC* locus [63]. Firstly, VERNALISATION INSENSITIVE

3 (VIN3) causes deacetylation of H3 histone at lysine-9 and lysine-14 stopping FLC transcription and then further action by REDUCED VERNALISATION RESPONSE 1 (VRN1) and REDUCED VERNALISATION RESPONSE 2 (VRN2) to di-methylate lysine-9 and lysine-27 at H3 histone caps the residues preventing unsolicited acetylation which could reactivate the gene [62-65]. The action of VIN3 together with VRN1 and VRN2 close the histone structure to form a stable conformation thus repressing *FLC* and this continues as the plant re-enters warmer growing conditions [62-65].

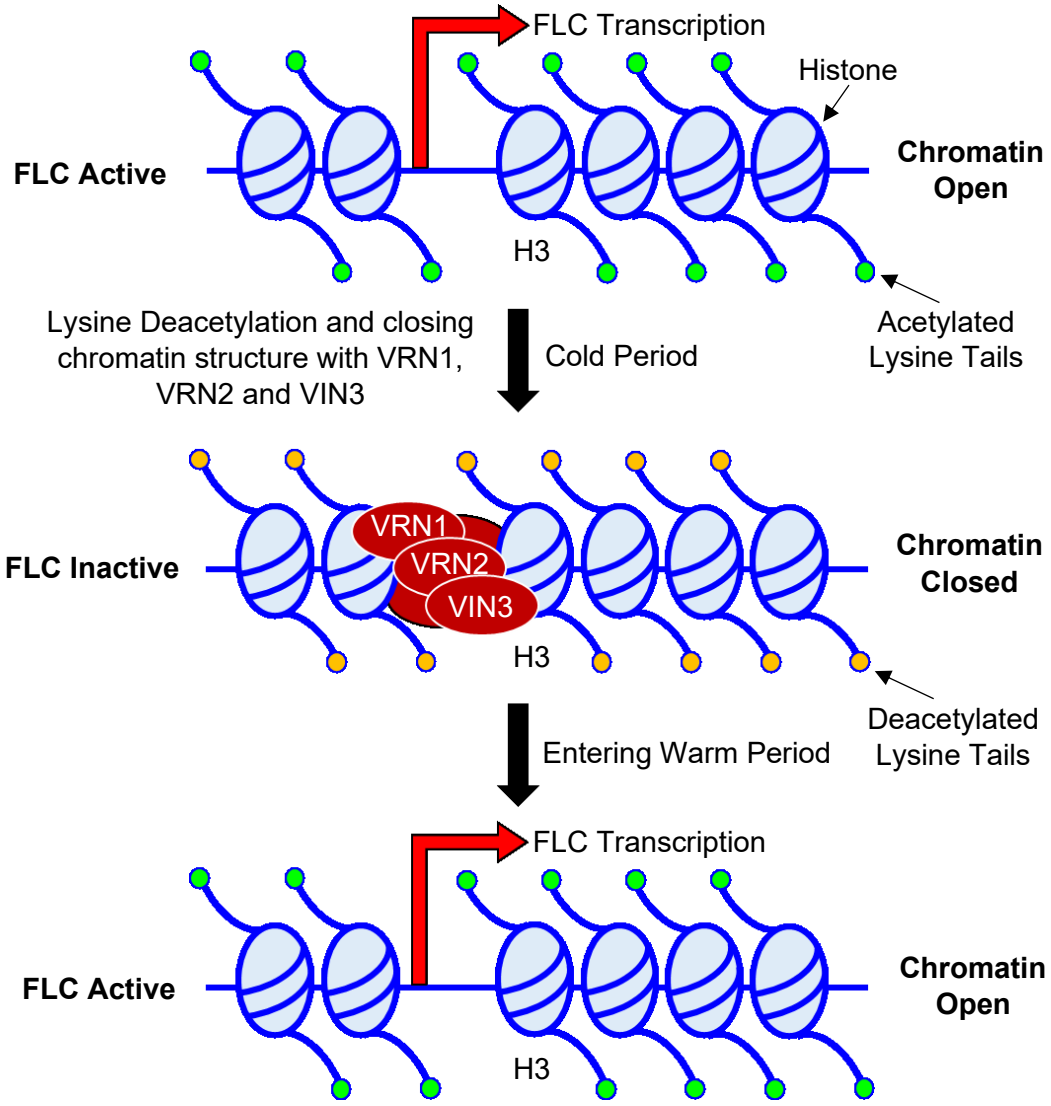


Figure 6 – Chromatin modification in FLC activation. Epigenetic regulation at the FLC locus activates the gene. FLC is active when the chromatin is in an open conformation, VRN1, VRN2 and VIN3 close the histone structure and acetylation of lysine tails causes FLC to become inactive. FLC is activated again once the plant enters warmer goring conditions, with an open histone conformation.

1.3.6.2 – FLC and Autonomous Regulation

FLC plays an important part in the autonomous flowering response which occurs independently from inductive environmental conditions, when it is in the plant's interest to flower as a matter of course – to proceed to seed development [66]. Autonomous regulation of *FLC* differs from the mechanism set-out above for vernalisation and focuses on RNA processing, post-translational modification of FLC in addition to the epigenetic regulation of chromatin [67]. Post-translational modification involves both kinase CASEIN KINASE 2 (CK2) and phosphatase activity PROTEIN PHOSPHATASE 2A (PP2A) and whilst it is unclear how this affects FLC abundance, it is likely to affect protein stability and functionality [68, 69]. Chromatin modification occurs through deacetylation and demethylation of histones; for example, *hda5* encodes a histone deacetylase and *FLD* encodes a histone demethylase involved in autonomous epigenetic *FLC* repression [70]. RNA processing at *FLC* occurs by polyadenylation of RNA at the 3'-end rendering it void by RNA binding proteins such as FLOWERING CONTROL LOCUS A (FCA) [71].

1.3.7 – Trehalose-6-Phosphate

Photosynthate accumulation affects flowering time and in particular the levels of trehalose-6-phosphate (T-6-P) [72]. TREHALOSE-6-PHOSPHATE SYNTHASE 1 (TPS1) synthesises T-6-P from glucose-6-phosphate and uridine diphosphate, and T-6-P acts as a carbohydrate indicator for flowering time readiness; loss of function of TPS1 severely delays flowering time [72, 73]. T-6-P accumulation is not confined to the leaves and as such is detected in both the leaves and the apical meristem with causal effect; importantly the recognition of T-6-P is crucial as in cases when substituted high levels of sucrose are present, the same acceleration of flowering time is not caused, meaning that T-6-P is used as an internal marker instead of sucrose [72].

T-6-P follows the same circadian pattern where daily maxima are observed in sync with FT expression at the end of the day and accordingly T-6-P activates FT within the photoperiod pathway [72]. In the SAM, T-6-P acts independently of FT to promote flowering, activating SQUAMOSA PROMOTER BINDING PROTEIN-LIKE 3 (SPL3), which activates flowering time proteins AP1, LFY and FUL [72, 74]. This enables the plant to coincide high photosynthate accumulation with floral transition to ensure reproductive success and the resultant seed production; T-6-P acts through both the photoperiod and age-dependent pathways, independently [72].

1.3.8 - microRNAs – miR156 and miR172

The function of microRNAs is RNA cleavage and translational suppression (including epigenetic effects) and consequently disruption of gene expression [75]. They are small RNA sequences of between 18-24 nucleotides and play an important role in the age-related flowering pathway in Arabidopsis and in particular, miR156 and miR172 play a prominent role [75, 76]. miR156 levels drop as the plant age increases [74]. miR156 is a direct suppressor of *SPL* gene expression which activates *FT*, *SOC1* and *AGAMOUS-LIKE 24* (*AGL24)*; flowering is as such accelerated due to reduced miR156 levels [74]. In contrast, high levels of miR172 accelerates flowering which acts downstream of miR156, it acts to repress genes such as *APETALA 2* (*AP2*), *SMZ* and *TARGET OF EARLY ACTIVATION TAGGED 1* (*TOE1*) which means that *AP1*, *LFY* and *FUL* are no longer repressed, thus causing an acceleration of flowering [77]. Older plant age and higher levels of photosynthate reduce the levels of miR156 which in turn through *SQUAMOSA PROMOTER BINDING PROTEIN-LIKE* (*SPL)* expression increases miR172; this characterises the main facets of this age dependent flowering time pathway [75, 78].

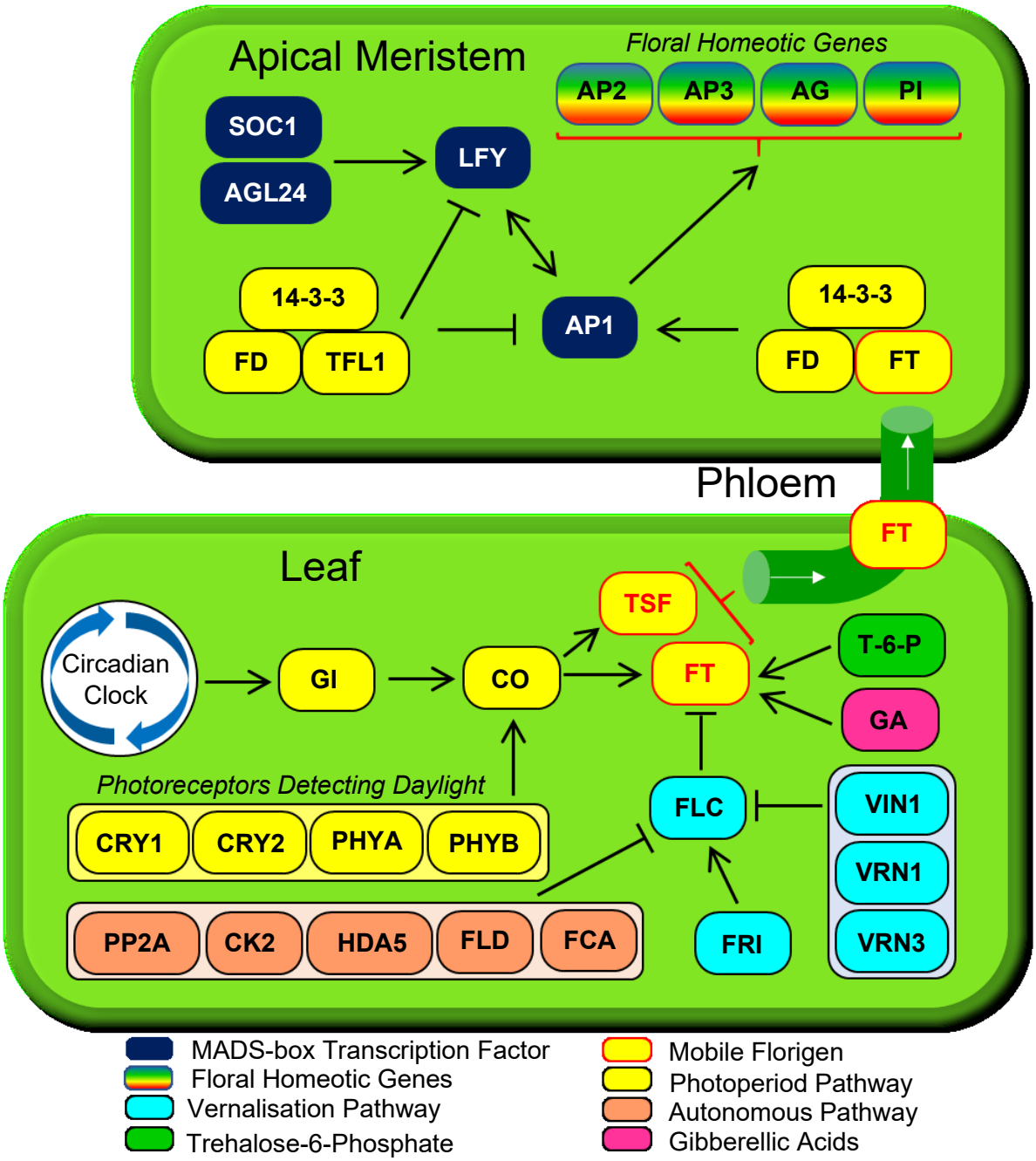


Figure 7 – Interactors in the floral activation pathway. The regulation of flowering time is controlled by 4 main pathways – photoperiod, vernalisation, autonomous pathways and gibberellins. Trehalose-6-phosphate from photosynthesis accumulation also activates flowering. The signal detection in the leaf integrates through mobile florigen, namely FT. MADS-box genes are important for meristem developmental regulation. Floral homeotic genes activate floral morphogenesis via the ABC model. AP1 plays a cross-over role between meristem regulation and as a floral homeotic gene activating sepal formation.

1.4 – Apical Meristem Development – Apetala 1 Action

1.4.1 – ABC Model for Floral Organ Development

The ABC model is a well-established principle for floral organ development and details how three classes of genes specify the four floral organs. Organs form sequentially and concentrically at the apex, firstly with the expression of *Class A* genes specifying sepal development [79]. The *Class A+B* combination specifies the petal, *Class B+C* the stamen and *Class C* genes the carpel [79]. A curious list of mutants lacking in particular floral identity genes display phenotypes lacking in those organs. For example, the double mutant lacking functional *B* and *C* genes only displays sepals; mutations to *A* and *B* genes causes solely stamen formation [79]. Indeed, when complete knockout of *A*, *B* and *C* genes is achieved, leaf structures develop at the apex [79].

SEPALLATA 1-3 genes are also expressed in the floral meristem and are required, in tandem with the homeotic genes to cause developmental changes [80]. The spatial location of gene expression is important for floral primordia formation. *AP1*, specifying sepal development, is expressed at the peripheral meristem region and *C* genes encoding the carpel, in the centre, with interstitial *Class B* expression. This creates combinations of *A+B* and *B+C* in the corresponding regions leading to the concentric whorl formation of organ primordia [80]. *C* genes are expressed last as floral bud development reaches completion, another important function of *Class C* genes is to curtail stem cell production as proliferation is no longer required [81]. This is achieved by repressing *WUSCHEL* (*WUS*) which regulates undifferentiated cells in the organising centre [81]. Floral organ identity genes are detailed in *Figure 4* below.

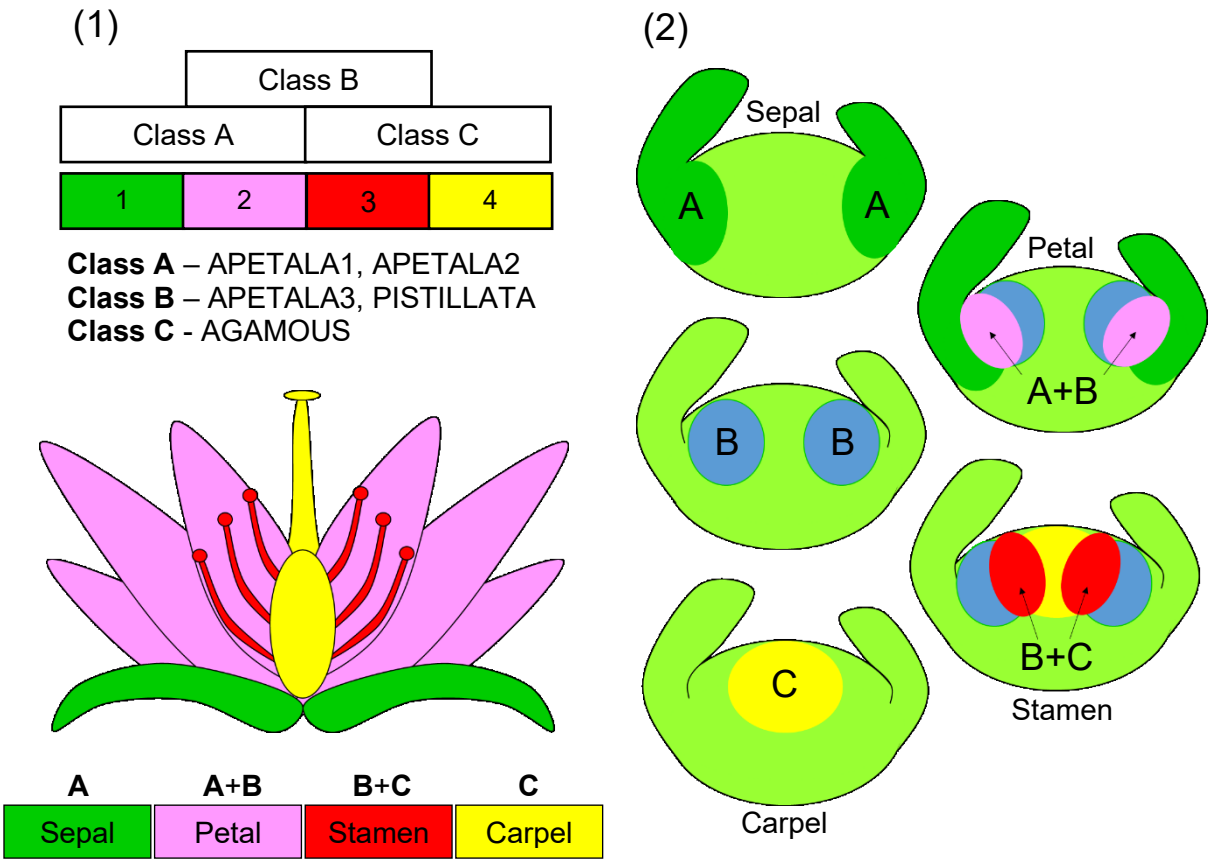


Figure 8 – The ABC model and spatial patterning of floral homeotic genes. **(1)** The ABC model details the formation of the floral organs – sepal, petal, stamen and carpel, from three classes of homeotic genes and their combinations. Examples of *Class A*, *B* and *C* genes are given. **(2)** The homeotic genes are expressed at specific locations in the meristem, the *Class A* genes are expressed on the periphery and *Class C* genes in the centre; the overlap of expression patterning results in the petal (*A+B*) and stamen (*B+C*) formation.

1.4.2 – APETALA 1

AP1 gene expression causes meristem identity change, beginning the shift from indeterminate to determinate fate [82]. *AP1* encodes a MADS-box transcription factor of roughly 30 kDa and primarily specifies sepal development in the first whorl and when in combination with *Class B* genes – the petal [83]. Localisation data of *AP1* mRNA via *in situ* hybridisation is reported in the early inflorescence meristem, and this concentrates in the petal and sepal as mature floral development stages are reached; AP1-GFP fusion protein data also follows this pattern [83, 84]. In loss of function *AP1* mutants, sepal formation is replaced by leafy structures protruding from

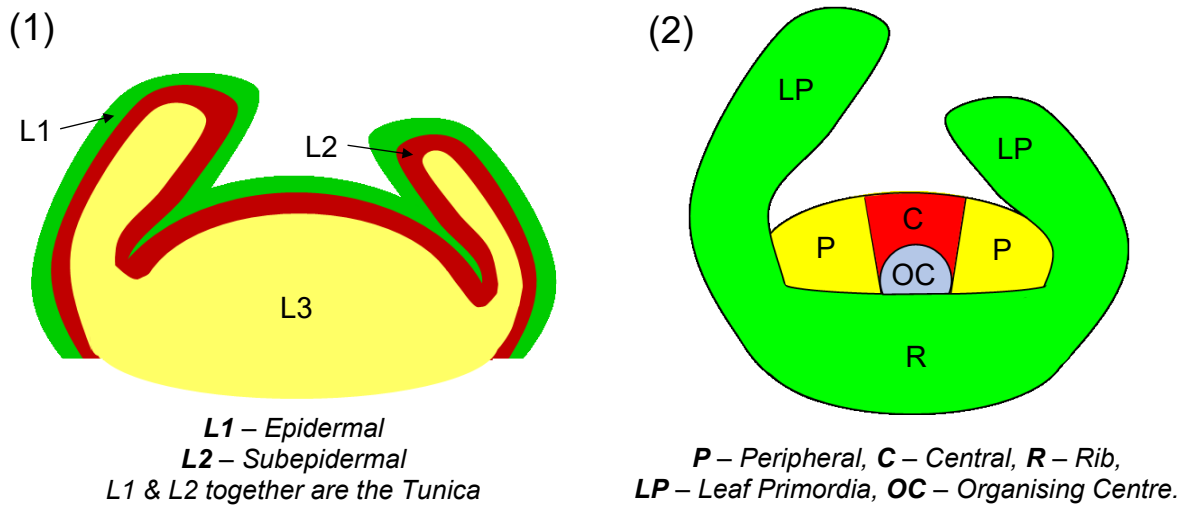
the inflorescence meristem and additionally petal formation is not observed [85]. *AP1*, as a *Class A* gene however, is not involved in stamen or carpel development and as such its localisation is not observed in these organs during floral maturation [83]. *CAULIFLOWER* (*CAL*) is a paralog of *AP1* and *35S::AP1* exhibits early flowering [83, 86]. In the absence of *AP1*, its paralog *CAL and LEAFY (LFY)*, formation of floral organs is not observed [86, 87].

1.4.3 – Maintenance of the Shoot Apical Meristem

The apical meristem has a high rate of cellular division and is distinct from other tissue around it in a number of ways. It is a unique structure and is the dividing centre at the tip of the plant responsible for the development of above ground tissue [88]. The meristem structure contains three distinct layers of cells, the epidermal L1 and subepidermal L2 layers are one cell thick and L3 comprises the interior cells underneath [89]. Distinction between these regions is apparent by the direction of cell division [89]. Anticlinal cell division takes place in the tunica layers (L1 and L2) parallel to the meristem surface, whereas L3 cell division occurs in all directions contributing to the internal cells of the structure [89].

The meristem is also characterised by regions with different rates of cell division [90]. Organ primordia form at the peripheral zone where the rate of cell division is highest, the central zone supplies cells to the differentiating periphery and the rib zone located at the bottom of the meristem which contributes to developing tissue in the stem [90]. Stem cells reside in the central zone of the SAM with a cluster of around 35 undifferentiated cells [91]. The organising centre consists of approximately 10 cells located in L3 and provides undifferentiated cells to the stem cell niche in the central zone and delivers daughter cells to the rib zone which become pluripotent [91]. The organising centre is the expression site for WUS [91].

WUS is a homeodomain transcription factor which maintains the undifferentiated nature of the stem cell niche in the central zone, acting as a signal, characterised by its spatial expression



L1 *– Epidermal*
L2 *– Subepidermal*
L1 & L2 together are the Tunica

P *– Peripheral,* ***C*** *– Central,* ***R*** *– Rib,*
LP *– Leaf Primordia,* ***OC*** *– Organising Centre.*

Figure 9 – Regions and layers of cells in the SAM. **(1)** The apical meristem is arranged in layers of cells based on directional cell division. The anticlinal cell division of L1 and L2 is in contrast to L3 where cells divide in all directions. **(2)** The SAM is divided into the *Peripheral*, *Central* and *Rib* zones. The *Organising Centre* is the stem cell niche just below the central zone. *Leaf Primordia* are also shown.

pattern, and this enables the meristem to retain its indeterminate state [92, 93]. WUS expressed in the organising centre is essential to maintain the supply of stem cells to the central zone [94]. In *WUS* mutants, a lack of stem cells in the central zone causes the meristem to cease activity and it reforms at leaf axils and this continues through a cycle of formation and rapid cessation [95].

CLAVATA-1 (CLV1) and CLAVATA-2 (CLV2) form a receptor for the extracellular mobile signalling peptide CLAVATA-3 (CLV3) expressed at the top of the central zone. *CLAVATA* (*CLV*) genes are essential in maintaining the meristem within normal growth limits and their repression causes cell division to increase [96]. They act by repressing WUS and the CLV-WUS negative feedback loop [96]. In this way, the high expression of WUS is countered by increasing CLV expression which in turn represses WUS [96]. The function of WUS, is to maintain the supply of stem cells to the central zone, and so WUS repression prevents excessive growth of the meristem and an abnormal supply of cells to the central and thus adjacently supplied regions [92]. The WUS-CLV feedback loop enables the meristem to retain

both its stem cell niche whilst also enabling the steady proliferation of pluripotent cells to the peripheral regions to form leaf primordia and the rib region for growth of the stem [97].

1.4.4 – Apical Meristem Differentiation

During vegetative growth, the meristem retains its flat dome structure [98]. Once the meristem responds to signals for floral development, the dome structure becomes pronounced as an inflorescence meristem [98]. Indeterminate inflorescence in Arabidopsis causes a number of determinate floral meristems to develop as a raceme which are floral clusters subtended at equal distances from the main stem until the inflorescence meristem finally forms a terminal flower completing the transition [99]. During meristem differentiation, AGAMOUS (AG) represses WUS through a feedback loop enabling differentiation and the determinate formation of floral organs [81].

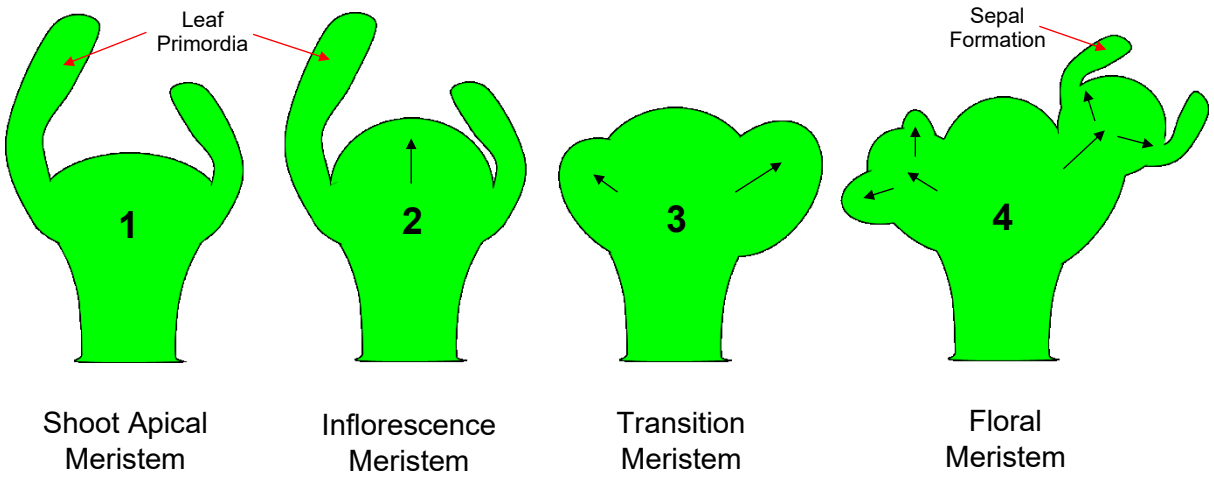


Figure 10 – Four stages of apical meristem development after floral developmental cues. After floral induction and activation of AP1, the apical meristem undergoes changes in preparation for flowering and these are categorised in four stages above and the arrows show direction of cellular differentiation. **(1) shoot apical meristem** - is observed during the vegetative stages, **(2) inflorescence meristem** - the dome enlarges after AP1 activation, **(3) transition meristem** - floral primordia begin to form at the periphery instead of leaf primordia, **(4) floral meristem** - floral organs begin to develop starting with the sepal.

Floral meristems form at the periphery of the inflorescence meristem as new determinate structures whilst the inflorescence meristem cycles on, producing further floral meristems [98]. The commercial crop, cauliflower, exploits this transition through the formation of inflorescence instead of floral meristems which in turn yield further inflorescence meristems [100]. This leads to the entire apical region developing as a mass of indeterminate inflorescence meristem structures [100].

1.4.4.1 – Meristem Identity Genes - LEAFY

LFY is a floral meristem identity gene, expressed in the emerging primordia. It encodes a transcription factor which causes the primordia at the inflorescence meristem to commit to flowering [101]. Essentially the action of LFY is the basis for determinate floral meristem formation [102]. LFY activates *AP1,* beginning the cascade of developmental changes through the homeotic genes outlined in the ABC model [102]. LFY along with TFL1 and AP1 are floral meristem identity genes with unique functions controlling meristem development. LFY and AP1 both activate whereas TFL1 represses floral development [39].

1.5 – Entry of Macromolecules inside the Cell

1.5.1 – Barriers to Entry

1.5.1.1 - Plant Cell Membrane

The fluid mosaic model depicts the organisation of the phospholipid bilayer, and the lateral movement that occurs throughout the domain [103]. Primarily the bilayer is comprised of phospholipids which have a polar head which orientates outwards towards the extracellular aqueous environment and a lipophilic tail which points inwards creating a hydrophobic membrane core. This alignment essentially means that the membrane is impermeable to molecules which aren't lipid soluble.

1.5.1.2 - Plant Cell Wall

Water availability depends on many environmental factors beyond the organism's control (*e.g.* drought stress and flood tolerance). The cell wall function is to mediate against potential damage from water stress and during hypertonic environments, the cell wall is able to withstand large positive pressures [104]. Additionally, when high external water potential is present, the cell is protected from bursting. Turgour is attained when the vacuole and cytosol fill and the osmotic pressures causes the cell to become turgid against the cell wall maintaining a high level of structural integrity across the plant.

The cell wall is primarily made of cellulosic microfibrils which are formed from bundles of polysaccharide, with hemicellulose and pectin also contributing to the structure [105]. Importantly, the cell wall does not form an impermeable barrier around the cell enabling the passage of small molecules and proteins through the matrix with a threshold size limit around 60 kDa [106]. The lamella is the outermost layer which forms the interface with adjacent cells, around the primary layer [107].

Linear β-1,4-glucan (cellulose) is the major component of the primary cell wall, present as rigid structural microfibrils [107]. It is synthesised at the cell membrane by cellulose synthases ready for integration into the structure [105]. Hemicelluloses are linked by hydrogen bonds and tethers join the cellulose microfibrils which are fixed in the pectin framework; xyloglucan is the most prevalent hemicellulose [108]. Xylans, mannans and glucomannans are also hemicelluloses present in the primary cell wall [107].

Pectins connect microfibrils, they are soluble (*c.f.* microfibrils) and as such can be synthesised inside the cell at the Golgi and reach the extracellular matrix via exocytosis [107]. Pectins are subdivided into rhamnogalacturonan I and II, xylogalacturonan and homogalacturonan groups, as well as adding structure, they are important for connecting end-to-end cells at the lamellae zone [107, 109, 110].

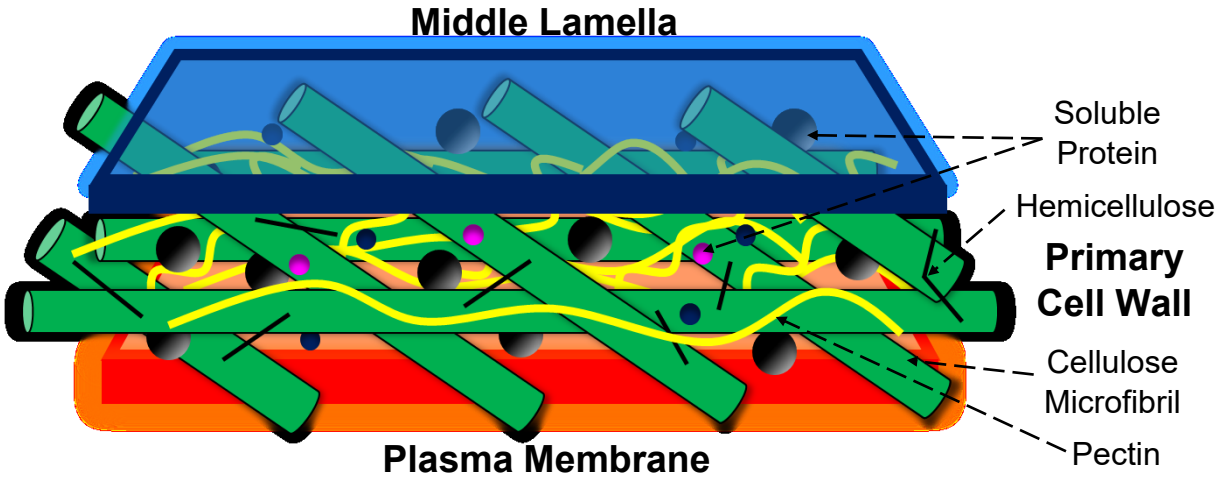


Figure 11 – The composition of the primary plant cell wall. Redesigned from M. Sticklen *et al.* [111]. The structure is porous and is a lattice of cellulose microfibrils joined together by soluble pectins and tethered by hemicelluloses. Microfibrils form the main structural integrity component of the cell wall.

1.5.2 – Uptake across the Membrane

1.5.2.1 – Small Molecule Transport

Ion transport channels in the membrane allow the passage of ions through the hydrophobic core of the phospholipid bilayer. The uptake of larger water-soluble molecules such as glucose and sucrose enter either via active transport or facilitated diffusion [112]. Active transport requires an input of energy to transport ions to an area of high concentration from an area of low concentration against the concentration gradient [112]. The unhindered passage of lipid soluble molecules is possible by simple diffusion and the process of osmosis specifically details the passage of water molecules from areas of high water potential to areas of low water potential across the membrane. The passage of larger molecules inside the cell is receptor mediated, involving chiral recognition motifs on the cellular surface – for example for membrane transport of larger macromolecules and proteins [112].

1.5.2.2 - Endocytosis

There is a distinction between passage across the membrane and actual membrane uptake which involves the formation of vesicles. Endocytosis is the broad term classifying uptake across the membrane where vesicles containing cargo form through an invagination process [113], 113. There are four main subset mechanisms for this process which are given in *Figure 7*. Broadly, endocytosis either acts via clathrin and is receptor mediated or is one of three other forms - caveolae, pinocytosis (macropinocytosis) or phagocytosis [113], 114, [114]. In short, clathrin mediated endocytosis firstly requires clathrin to be recruited to the plasma membrane and a clathrin coated pit forms around the material to be internalised [113, 115]. A clathrin lattice is constructed enabling the vesicle to form and once pinching by dynamin and adapter proteins is complete, clathrin dissociates and cargo is trafficked inside the cell for vesicular sorting [113], 113.

Macropinocytosis is a constituent type of pinocytosis which acts through the formation of a wave crest outside the cell membrane (*c.f.* the invagination process), and the vesicle seals whereby its contents are enveloped inside the cell [116], [114]. Actin rearrangement in the membrane enables the formation of the macropinosomes [114].

Phagocytosis marks internalisation at a cellular level, whereby the whole cell envelops foreign particles or other damaged cellular material and debris [117]. Phagocytosis is an essential component within immune response in humans whereby specific cells (phagocytes and macrophages) engulf pathogens into phagosomes and the contents are then subsequently degraded [117]. Whilst phagocytosis is an early evolutionary process it occurred after the animal kingdom's divergence from plants and phagocytosis does not occur in plants because the structural framework of the cell wall does not allow this cellular entry mode [118].

Caveolae is a mammalian process, and involves a protein called caveolin which binds to the cholesterol in the membrane forming inverted assemblies in the membrane [119]. Again, contents are trafficked for endosomal release or lysosomal degradation [119]. Potocytosis involves caveolae however in this case, vesicular release is straight into the cytosol [120].

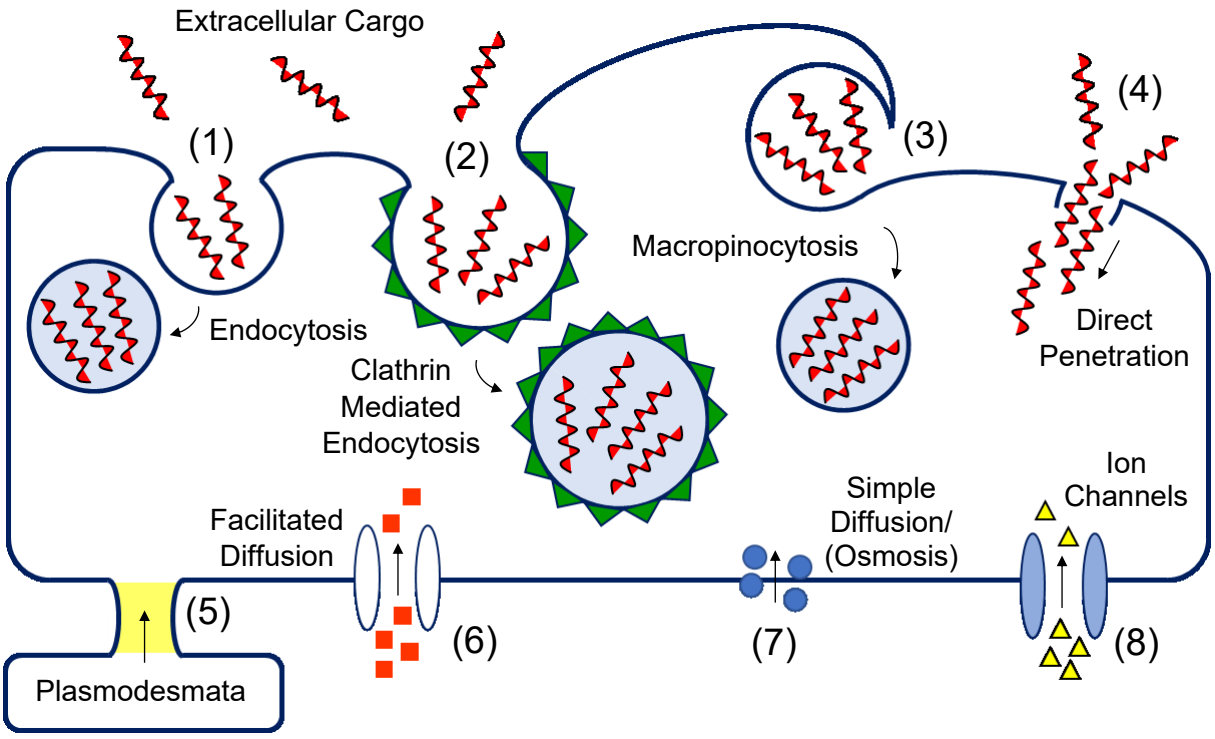


Figure 12 – A summary of cellular entry mechanisms. The widespread processes of cellular internalisation are detailed above. Endocytosis is categorised by receptor mediation acting through a clathrin mechanism or independently as pinocytosis, caveolae or phagocytosis. Processes by which cell penetrating peptide uptake has been reported include **(1)** endocytosis, **(2)** clathrin mediated endocytosis, **(3)** macropinocytosis and **(4)** direct penetration. **(5)** Plasmodesmata is a mechanism which plant cells use to transport micromaterial between cells. **(6)** Facilitated diffusion requires carrier proteins to deliver large molecules such as sugars, **(7)** simple diffusion enables lipid soluble molecules to pass (osmosis is the specific term for water movement) and **(8)** ion channels enable transport of charged ions across the membrane.

1.5.3 – Cell Penetrating Peptides

An important discovery, made independently by two separate laboratories in 1988, was that the Transactivator of Transcription protein was able to directly enter cells through the plasma membrane, forming the active component of the HIV-1 virus [121, 122]. The minimal domain responsible for enabling protein transduction inside cells was a 13 amino acid cationic and arginine rich sequence which also comprised a nuclear localisation signal [123]. This was further refined to 9 residues and hereby called Tat (RKKRRQRRR) [124]. Since then the field of cell penetrating peptides has expanded and a large number of peptide sequences have

been reported that have an ability to cross the plasma membrane in an energy independent manner [125].

CPP sequences are short with only primary structure, typically between 8 and 30 residues in length [126]. Both sequence length and amino acid composition is important for their mode of action with the latter leading to CPP classification into three categories – cationic, amphipathic and hydrophobic peptide sequences [127]. Histidine, lysine and arginine are positively charged amino acids constituting cationic sequences, the most effective residue is arginine which has greatest penetrating capacity [128]. Indeed, Tat is a naturally occurring CPP, rich in arginine residues and R9 is a synthetic mimetic both of which are highly cited as successful sequences [128]. Amphipathic sequences contain a mixture of cationic and hydrophobic residues in key positions which enables interaction with the hydrophobic lipid tail core during entry which is not possible for cationic sequences [127]. Examples include pVEC and TP10 investigated in this work [129, 130]. Hydrophobic sequences have niche applications and are not cited in investigations into plant tissue uptake, due most probably to the hydrated cell wall which would act as a further barrier for a hydrophobic CPP [127].

Different uptake mechanisms for CPP action are reported and these vary based on sequence and peptide concentration; in addition, factors such as whether the CPP is transporting cargo and the nature of the cargo influence uptake [131]. CPPs are either designed for a specific system in an organism or are broadly cited as having universal action. The uptake mechanisms broadly involve either endocytic entry or direct penetration [131].

For amphipathic CPPs, evidence for inverted micelle formation as an entry mechanism is supported and this firstly involves interaction of cationic residues with the negatively charged membrane surface, the hydrophobic residues then interact with the hydrophobic lipid tails enabling the inverted micellular formation and entry inside the cell [131]. Direct membrane penetration is cited for cationic CPPs such as Tat and R9, operating about the pH gradient

that exists across the membrane and involving the fatty acid composition in the membrane [132]. Transient pores are created across the membrane as peptides spontaneously infuse in an energy independent manner [132]. Endocytic entry methods are likely to occur when cargo is covalently tethered to the CPP. Macropinocytosis is cited in plant cells as a likely route for the non-covalent entry of cargos through the formation of macropinosomes [133]. Endocytic entry methods are also cited at low CPP concentration [131].

Table 2 – CPP sequence designs. R9, Tat, TP10 and pVEC CPP sequences are investigated in this thesis and are listed with their characteristics, origins and derivations.

CPP	Length	M_r	Type	Ref
Cationic				
Tat – RKKRRQRRR The minimal domain from the transactivator of transcription protein, a transcription factor part of the active viral mechanism expressed by the human immunodeficiency virus.	9	1340	Cationic, Naturally Derived	[121]
R9 – RRRRRRRRR A synthetic sequence comprised of 9 arginine residues. It is derived from the already arginine rich Tat sequence.	9	1424	Cationic, Synthetic	[134]
Amphipathic				
pVEC –LLILRRRIRKQAHAHSK pVEC is an 18-amino acid peptide from the murine vascular endothelial-cadherin protein.	17	2097	Amphipathic, Naturally derived	[129]
TP10 –AGYLLGKINLKALAALAKKIL TP10 is a shortened part of the Transportan sequence. Transportan is a hybrid sequence with a C-terminus derived from wasp venom mastoparan connected to a C-terminal domain from the neuropeptide galanin.	21	2183	Amphipathic, Fusion, Truncated, Naturally Derived	[130]

1.5.3.1 – Cell Penetrating Peptides *in Planta*

Whilst the Tat CPP was reported in 1988, the first reported example of a cell penetrating peptide application in plant systems was reported significantly later in 2004, and involved the delivery of dsRNA for gene silencing in tobacco suspension cells using a cationic peptide comprising of 12 contiguous arginines [135]. Since this early report a steady stream of research has shown the potential uses and applications of CPPs in plant systems, with the most recent paper in 2018 reporting screening methods to optimise CPP properties for different plant

systems [136]. Whilst the mammalian literature is teeming with examples of CPP applications, the evidence in plant science is limited to 20 published studies to date and in this way the field is incomplete leaving novel areas available for further exploration. Whilst a universal mechanism for membrane transduction is cited for certain sequences, plant systems do present major structural differences, notably, the cell wall which is an additional obstacle for cellular entry [132]. It is possible to present a complete summary of reported isolated independent CPP action, without considering macromolecular cargo transduction, and this is given in *Table 1* above.

Table 2 below, depicts the wide range of peptides that have been studied. The scope of research is however limited to protoplasts and suspension cell culture with the exception of Chugh *et al.* whose work sought to investigate root tips and leaf bases in triticale and epidermal cells in onions [137]. Tobacco is the most studied organism with 4 examples and interestingly the recent hybrid crop triticale, has been used twice as a model organism to test CPP action [137, 138]. It is clear from *Table 1* that there is a difficulty in comparing results across studies because of the different model systems used and, in this way, it is not possible to determine which CPP sequences are most effective. For example, the successful absorption of pVEC into a tobacco protoplast cannot be compared with Transportan penetration into triticale leaf bases [137, 139].

Table 3 – Independent CPP action reported in plant systems. The articles are summarised according to organism, cell type and CPP used.

Author	Year	Cell Type	Organism	Peptides	Ref
Mäe *et al.*	2005	Leaf protoplasts Bowes human melanoma	Tobacco Human	Transportan TP10 Penetratin pVEC S-pVEC	[139]
Chugh *et al.*	2007	Mesophyll protoplasts	Triticale	Tat Tat_2, M-Tat	[138]
Chugh *et al.*	2008	Mesophyll cells Root tips Leaf bases Epidermal cells	Triticale Onion	pVEC Transportan S-pVEC	[140]
Mizuno *et al.*	2009	Tobacco suspension cells	Tobacco	R4 R8 R12	[141]
Eggenberger *et al.*	2011	Suspension cells (BY-2)	Tobacco	BP100	[142]
Eggenberger *et al.*	2017	Suspension cells (BY-2)	Tobacco	BP100	[143]

M-Tat – Mutated Tat, S-pVEC – Scrambled pVEC.

1.5.3.2 – CPP Mediated Protein Transduction Studies *in Planta*

A small subsection of examples exists in the plant systems for both covalent and non-covalent CPP mediated protein transduction (a complete list of nine examples is presented in *Table 2* below). Intrinsically fluorescent proteins are used as cargo including GFP and RFP (*and derivatives*) in seven studies. In two other examples, cargos are chosen with the specific intention of recording a visual output, detectable with microscopy, using GUS enzymatic staining [140, 144]. An example does exist detailing the delivery of BSA and alcohol dehydrogenase, however the choice of CPP is unusual, using the peptides $(BP100)_2K_8$ and $BP100(KH)_9$ which are adaptations of the plant based BP100 CPP in both monomeric and dimeric form along with added lysine residues [145].

It is clear that the field is limited to a small number of cargo proteins bearing intrinsic fluorescence. Functional GUS and β-Gal have been delivered and an output has been recorded with successful GUS staining [140, 144]. Examples of larger proteins including GUS (68.3 kDa), β-Gal (116.3 kDa), BSA (66 kDa) and Alcohol dehydrogenase (150 kDa) have been delivered but the remainder are under 30 kDa and these are reported in *Table 3*. This

is encouraging as FT has a molecular weight of 21 kDa and a similar size range suggests this technique might be extrapolated to FT cellular delivery. Importantly, the cited examples are all hypothetical cargo, and aside from GUS and β-Gal, are included to yield a fluorescent readout showing uptake. No reported attempts however have been made to deliver a functional protein such as FT.

Table 4 - Examples of covalent and non-covalent protein transduction in the plant sciences literature. Some articles report a combination of covalent and non-covalent protein transduction and this is reported as CPP used, cargo delivered, strategy (covalent or noncovalent) and system.

Author	Year	CPPs	Cargo	Strategy	System	Ref
Chang *et al.*	2005	R9 & Tat	GFP RFP	Covalent	Onion Root Tips Tomato Root Tips Onion Epidermal Cells	[146]
Wang *et al.*	2006	R9 & Tat	GFP RFP mTomato mCherry mOrange	Non-Covalent	Onion Root Tips	[147]
Chang *et al.*	2007	R9 & Tat	β-Gal GFP RFP	Non-Covalent	Corn Root Tips Onion Root Tips Onion Epidermal Cells	[133]
Chugh *et al.*	2008	Tat, Tat_2, pVEC & Transportan	GUS	Non-Covalent	Wheat Immature Embryos	[140]
Chugh *et al.*	2009	Tat, Tat_2, pVEC & Transportan	GUS	Non-Covalent	Triticale Microspores	[144]
Lu *et al.*	2010	R9	GFP	Covalent	Onion Root Tips	[148]
			dTomato mCherry RFP	Non-Covalent		
Qi *et al.*	2011	CPNT	GFP	Covalent	Barley Protoplasts Arabidopsis Roots Tobacco Cell Culture	[149]
				Non-Covalent		
Bilichak *et al.*	2015	Penetratin, Transportan, R9 & MAP	mCherry	Covalent	Wheat Microspores	[150]
		R9		Non-Covalent		
Ng *et al.*	2016	$(BP100)_2K_8$ $BP100(KH)_9$	BSA ADH Citrine	Non-Covalent	Arabidopsis Leaves	[145]

1.6 – Project Objectives

The investigation presented in this thesis is divided into three distinct areas including (1) an investigation into cell penetrating peptide uptake in Arabidopsis; (2) tool development linking cell penetrating peptides to FT as a facilitation tool for cellular entry and finally (3) the artificial activation of flowering using recombinant FT. The investigation into these three topics is presented as individual results chapters within this thesis including a list of sub-objectives for each topic which are broadly detailed below.

(1) Cell Penetrating Peptide Uptake in Arabidopsis

- Consider the action of both cationic and amphipathic sequences, in this way, study Tat, R9, pVEC and TP10 sequences *in planta*.
- Use confocal microscopy to record the uptake of Tat, R9, pVEC and TP10 in different plant tissue types to evaluate their advantages and disadvantages.

(2) Tool Development for Recombinant FT

- Design FT clones incorporating a covalent CPP into the FT sequence and set up recombinant protein purifications.
- Design approaches to fluorescently label recombinant proteins so that they can be tracked *in vivo*.
- Assess covalent and non-covalent protein transduction of FT facilitated by CPPs.

(3) Artificial Activation of Flowering

- Consider the available routes to deliver recombinant FT inside the plant following the endogenous route that FT takes from site of expression to action.
- Develop a phenotypic screen for recombinant FT floral activation.

- Develop a molecular readout through a transgenic reporter to assess whether AP1 is activated by recombinant FT.

2. Materials and Methods

2.1 - Solid Phase Peptide Synthesis

2.1.1 - Automated Backbone Coupling Reactions

20 μmol of Tentagel rink amide resin was swelled in DMF in a fritted vessel before Fmoc deprotection with piperidine (20% v/v DMF). Amino acids (5 eq.) were dissolved in NMP to attain a 0.5 M solution, and activated with HBTU (4.25 eq.) and NMM (10 eq.) in DMF, with shaking for 40 minutes before the first coupling step. The resin was washed with DCM and DMF before the activated amino acids were added through sequential coupling in the automated procedure. Fmoc Deprotection with piperidine (20% v/v DMF) followed the final coupling reaction and washing with DMF, DCM, MeOH and Et_2O followed before capping with Ac_2O (5% v/v DMF). Anchored peptide on resin was dried under vacuum.

2.1.2 - N-Terminal Modification - 5-Carboxytetramethylrhodamine Coupling

Activation of TAMRA (1.5 eq.) by DIC (1.7 eq.) and HOBt (1.5 eq.), dissolved in DMF with piperidine (20% v/v DMF), followed deprotection of the anchored peptide (1 eq. – calculated from Tentagel rink amide resin loading capacity of 0.24 $mmolg^{-1}$). The reaction was agitated for 30 mins and washed with piperidine (20% v/v DMF). Anchored labelled peptide was washed extensively with DMF, DCM, MeOH and Et_2O and dried under vacuum overnight. TFA, DTT, TIS and H_2O (92.5%, 2.5% 2.5%, 2.5% v/v/v/v) cocktail cleaved labelled peptide during agitation for 3 hours. Precipitation with ice cold MeOH, centrifugation and isolation of crude sediment were followed by two further washes. The pellet was dissolved in MeOH (50% v/v H_2O) and submitted for LCMS preparative purification with a MeOH/H_2O (5-95%) gradient. Clean fractions were pooled and dried under vacuum, and pure peptide lyophilised using a freeze-dryer. An analytical LCMS run gave the molecular ion splitting pattern and the purity

from the UV absorbance trace. Yield and peptide concentration were determined using the Beer-Lambert law with final dissolution in H_2O for a stock concentration of 1 M peptide, (5-carboxytetramethylrhodamine: ε = 86,000 λ = 556 nm). Storage of the peptide was at -20℃ in the dark until use.

2.2 - Cloning

FT was kindly provided by David Charles in a pET-28b (*Novagen*) plasmid, the expression sequence contains a His-tag, is under the T7 promoter and the vector confers kanamycin resistance – FT sequence is given in *Figure 26* in *Chapter 4*. FT-Tat and FT-R9 sequences were created by the insertion of Tat (RKKRRQRRR) and R9 (RRRRRRRRR) sequences into the C-terminus of FT in the pET-28b vector, adjacently behind the stop codon, by site directed mutagenic insertions. Furthermore, in additional clones, thrombin sites were replaced by TEV sites by insertion-substitution reactions and FT-GFP was created by the Gibson Assembly technique. PCR reaction cycling conditions are given below for Q5 (*New England BioLabs*) and Dream Taq (*ThermoFischer Scientific*); Q5 is used for cloning where high fidelity is required, Dream Taq for sequence verification.

Table 5 – PCR cycling conditions. These are reported for Q5 (*New England BioLabs*) and Dream Taq (*ThermoFischer Scientific*) from the manufactures' instructions.

		Thermostable Polymerase			
		Q5		Dream Taq	
Stage	№ of Cycles	Parameters		Parameters	
		Temperature	Time	Temperature	Time
Initial Denaturation	1	98 ℃	30 sec	95 ℃	180 sec
Denaturation Annealing Extension	25	98 ℃ T_A-72 ℃ 72 ℃	10 sec 30 sec gradient 30 sec (per kb)	95 ℃ T_A-72 ℃ 72 ℃	30 sec 30 sec gradient 60 sec (per kb)
Final Extension	1	72 ℃	120 sec	72 ℃	600 sec
Holding	~	4 ℃	~	4 ℃	~

500 ng genomic DNA template, or 500 pg plasmid DNA template used. Reaction volumes in 25 µL and final concentration - 500 nM of primers, 200 nM dNTPs. Polymerase and reaction buffer added according to the manufacturer's instructions.

2.2.1 - Site Directed Mutagenesis *(FT-Tat and FT-R9 Construction; TEV Site Insertion)*

Q5 Site Directed Mutagenesis kit (*New England BioLabs*) was used to insert the R9 and Tat sequences at the C-terminus of FT. Q5 High Fidelity Master Mix (1 unit) (*New England BioLabs*) was used with forward (0.5 µM) and reverse (0.5 µM) primers and plasmid template (500 pg) in 25 µL reaction volumes. The protocol (detailed in *Table 4*) was followed for a Q5

reaction. Kinase, Ligase and Dpn1 mixture was added to the PCR product and incubated for 5 minutes at room temperature before transformation via heat shock with NEB-5-alpha competent cells according to the NEB protocol

Table 6 – Primers used for site-directed mutagenesis. They Include the insertion of R9 and Tat into the FT sequence and the insertion of a TEV site into the FT and FT-Tat sequences (the same primers are used for this N-terminal insertion).

Primer Name	Sequence
FT-Tat - Forward Primer	TCAACGTCGTCGTTAGCTCGAGCACCACCAC
FT-Tat – Reverse Primer	CGGCGTTTCTTGCGAAGTCTTCTTCCTCCGCAG
FT-R9 - Forward Primer	TCGTCGTCGTCGTTAGCTCGAGCACCACCAC
FT-R9 - Reverse Primer	CGACGACGACGACGAAGTCTTCTTCCTCCGCAG
FT-(TEV) & FT-Tat-(TEV) – Forward Primer	TTTTCAGGGCCATATGTCTATAAATATAAGAGACCCTCTTATAGTA AGCAGAGTTGTTGGAGAC
FT-(TEV) & FT-Tat-(TEV) – Reverse Primer	TACAGGTTTTCCGGCACCAGGCCGCTGCT

2.2.2 - Gibson Assembly *(FT-GFP Construction)*

FT in a pET-28b vector underwent restriction digestion with Mfe1 (*NEB*) and XhoI (*NEB*). Forward and reverse primers, listed below were used to extract GFP (pT7 RBS B0034 sfGFP in pSB1C3 vector) using the Q5 PCR protocol above. Fragments were joined using the Gibson Assembly kit (*New England BioLabs*), including a 5'-3' exonuclease, DNA polymerase and DNA ligase. Component fragment concentrations were calculated according to sequence length and incubated in an ABI Veriti Thermal Cycler (*ThermoFischer*) for 15 minutes at 50℃ and after completion, vector transformation into NEB-5-alpha cells was via heat shock.

Table 7 – Primers used for FT-GFP construction. Primers extracted GFP from pSB1C3 vector, including a short G-S linker and removal of the stop codon. They were designed for the later re-assembly of GFP with FT. Primers were designed with the assistance of collaborator, Alex Nash.

Primer Name	Sequence
FT-GFP - Forward Primer	CAGTTTTCTACAATTGTCAGAGGGAGAGTGGCTGCGGAGGAAGAAGACTTGGCTCTGGCAGCGGCA GCATGCGTAAAGGCGAAGAG
FT-GFP – Reverse Primer	TGGATGAACTGTACAAATGATGAGCACCACCACCACCACCACTGAGAT

2.3 - Protein Expression and Purification

The following protocols (2.3.1-2.3.9) are modified from the original FT and TFL1 purifications presented in David Charles' thesis.

In this work, FT, FT-Tat, FT-R9, FT-GFP and TFL1 sequences are in the pET-28b vector.

2.3.1 – Transformation

Bacterial transformation was conducted with 50 ng of pET-28b plasmid containing the gene of interest and added to 50 µL of BL21-Gold (DE3) (*Agilent*) *E. coli* which are both chemically competent and suitable for electroporation transformations; following gentle agitation, cells were incubated on ice for 30 minutes, Cells were transformed by heat shock at 42℃ for 30 seconds before returning to ice for 5 minutes, SOC outgrowth media was added and cells incubated for 60 minutes at 37℃ with shaking at 220 r.p.m.. Cells were grown for 16 hours at 37℃ on LB agar plates under kanamycin (50 µg/ mL) selection.

2.3.2 - Induction

50 mL of LB media with antibiotic was inoculated with a single discrete colony and incubated at 37℃ for 16 hours with shaking at 180 r.p.m.. 10 mL from the starter culture was used to inoculate 1 L of LB media (in a 2 L growth flask). 3 L were grown in total for each purification initially at 37℃ with shaking at 180 r.p.m.. Induction with 0.5 mM IPTG was applied when the O.D. reached 0.7 after approximately 4.5 hours of growth and cells were grown for a further 16 hours at 22℃ with shaking at 180 r.p.m..

2.3.3 – Cell Harvesting and Sonication

Cells were harvested via centrifugation at 4000 r.p.m. for 20 minutes using a Fiberlite F10S-4x1000 LEX rotor (*ThermoFischer Scientific*) before resuspension of the pellet in 40 mL of lysis buffer – this is the first purification buffer with PMSF (0.15 mg/ mL) and EDTA-free

Protease Cocktail Inhibitor Tablet (*Sigma Aldrich*) added. Cell disruption was conducted on ice for 8 minutes with 2 second pulses at an amplitude of 60% and soluble protein was collected in the supernatant after centrifugation at 13,500 r.p.m. using a Fiberlite F21-8x50y rotor. The lysate supernatant was loaded into a Superloop column (*GE Healthcare*) and submitted for initial purification using an FPLC (*ÄKTA, GE Healthcare*) either via ion exchange chromatography (FT-R9 and FT-Tat) or via nickel affinity chromatography (FT, FT-GFP and TFL1). The final purification was via size exclusion chromatography (SEC) with a potential His-tag cleavage step included prior to SEC.

2.3.4 – Protein Purification Buffer Compositions

Table 8 – Protein buffers used in purification and application assays. Buffer compositions used in this study as taken from previous purifications by David Charles and adapted for application in this work [41].

	Buffer Name	Composition	Purification
(1)	Nickel Affinity Wash	50 mM imidazole, 50 mM potassium orthophosphate, 2 mM β-mercaptoethanol, pH = 6.8	FT, FT-GFP TFL1
(2)	Nickel Affinity Elution	500 mM imidazole, 50 mM potassium orthophosphate, 2 mM β-mercaptoethanol, pH = 6.8	FT, FT-GFP TFL1
(3)	Ion Exchange Wash	50 mM potassium chloride, 50 mM potassium orthophosphate, 1mM dithiothreitol, pH = 6.8	FT-R9, FT-Tat
(4)	Ion Exchange Elution	1 M potassium chloride, 50 mM potassium orthophosphate, 1 mM dithiothreitol, pH = 6.8	FT-R9, FT-Tat
(5)	Gel Filtration, Dialysis & Application	50 mM potassium chloride, 200 mM potassium orthophosphate, 1 mM dithiothreitol, pH = 6.8	FT, FT-GFP, FT-R9, FT-Tat, TFL1
Reducing agents are not required for the purification of TFL1 due to the omission of cysteine residues in the TFL1 primary sequence.			

2.3.5 - Cation Exchange Chromatography Protocol

A 5 mL HiTrap™ (*GE Heathcare*) column on an FPLC (*ÄKTA, GE Healthcare*) was equilibrated with 25 mL of Ion Exchange Wash buffer before lysate was loaded onto the column and washed until the UV measurement reached baseline. A gradient of 1% increase of elution buffer / minute over 40 minutes was conducted and held for 15 minutes, this was sufficient to remove surface bound *E. coli* proteins. A gradient of 1% increase per minute for a further 60 minutes was conducted and held for a further 15 minutes – and during this gradient, FT-R9 and FT-Tat eluted from the column. The gradient was dropped to 0% and the column washed with 25 mL of wash buffer. Fractions were assessed by SDS-PAGE and pooled for further purification. Ion exchange purifications for FT-R9 and FT-Tat are discussed in *Figure 29* in *Chapter 4* along with the purification UV chromatograms and expected protein elution timings.

2.3.6 - Nickel Affinity Chromatography Protocol

A 5 mL HisTrap™ (*GE Healthcare*) column was equilibrated on an FPLC (*ÄKTA, GE Healthcare*) with 25 mL of Nickel Affinity Wash buffer before lysate was loaded onto the column and washed until the UV absorbance measurement reached baseline. A stepped gradient was employed at 10% intervals, and 40% is sufficient to elute surface bound *E. coli* impurity fractions. His-tagged protein eluted between 60-100% stepped gradients of elution buffer. The gradient was dropped to 0% and the column equilibrated before samples were pooled and assessed by SDS-PAGE and fractions containing protein were immediately transferred to dialysis conditions for 16 hours at 4℃ to remove the imidazole.

2.3.7 - His-tag Removal Using Thrombin

20 units of Thrombin (*Sigma Aldrich*) were added to the reaction under dialysis conditions for an incubation period of 3 hours. SDS-PAGE confirmed cleavage completion and the reaction was quenched by passing back through the nickel column. Surface histidine residues require

a 50 mM imidazole presence in the buffer for cleaved protein elution and UV details the fractions containing protein on an FPLC (*ÄKTA, GE Healthcare*). A final 100% stepped gradient caused the elution of thrombin protease from the column, followed by a 25 mL re-equilibration for the column at 0% elution gradient.

2.3.8 - Size Exclusion Chromatography

Before size exclusion chromatography on an FPLC (*ÄKTA, GE Healthcare*), protein samples were concentrated to 1 mL volumes, and placed into a 2 mL superloop ready for loading onto the SEC column. Either a Superdex-75 (SD-75) (*GE Healthcare*) or a Superdex-200 (SD-200) (*GE Healthcare*) were used for FT, FT-R9, FT-Tat and TFL1 purifications; the SD-200 column was used exclusively for FT-GFP purification. The column was loaded using the drop-flow method and equilibrated at 0.5 mL/ min for a volume of 140 mL, the sample was loaded onto the column through the injection valve and elution traces were recorded in *Chapter 4*, to compliment this protocol. The column was washed with water and stored in 20% ethanol (v/v ddH_2O).

2.3.9 - Other Proteins

FT-(TEV) and FT-Tat-(TEV) were purified in an analogous fashion to FT and FT-Tat. 14-3-3 Nu was purified using Nickel Affinity and Size Exclusion Chromatography as detailed by David Charles' PhD thesis [41].

2.3.10 - SDS-PAGE Preparation

Gels comprising a resolving and stacking component were cast in a cassette as detailed in *Table 8* and polymerised after the addition of TEMED (*Sigma Aldrich*). The resolving gel was poured first comprising 75% of the total gel height. Isopropanol was added to level the top of the gel and then removed and washed with ddH_2O after polymerisation. The stacking component was then poured and a well-comb added whilst the gel set.

Table 9 – SDS-PAGE gel composition. Components are reported for both stacking and resolving gel components for a 10% bis-acrylamide resolving gel. This protocol is taken from the Cold Spring Harbor online resource [151].

Component	Reagent	Volumes
Stacking Gel	ddH_2O	6.1 mL
	Tris-HCl (1.5 M, pH = 6.8),	2.5 mL
	10% SDS (w/v ddH_2O)	100 µL
	30% bis-acrylamide (Bio-Rad)	1.3 mL
	10% APS (w/v ddH_2O)	100 µL
	TEMED	10 µL
Resolving Gel	ddH_2O	4.1 mL
	Tris-HCl (1.5 M, pH = 8.8),	2.5 mL
	10% SDS (w/v ddH_2O)	100 µL
	40% bis-acrylamide (Bio-Rad)	3.3 mL
	10% APS (w/v ddH_2O)	32 µL
	TEMED	10 µL
Cold Spring Harbor Protocol		

5 µL Laemmli 4X SDS-loading buffer (*Bio-Rad*) was added to 15 µL of protein sample, then the sample was heated at 95℃ for 3-5 minutes. SDS-PAGE gel sample wells were pre-flushed and 15 µL of sample was loaded into each well. PageRuler™ pre-stained protein ladder (*ThermoFischer Scientific*) was used.

Gels were run for 45 minutes at 180 V in MOPS running buffer (10.46 g MOPS, 6.06 g Tris-HCl, 1 g SDS, 0.3 g EDTA in 1 L ddH_2O) and stained with Coomassie Blue (50% Ethanol, 8% Acetic acid (v/v/v in ddH_2O), Brilliant Blue R-205 (*ThermoFischer Scientific*)) for 5 minutes after microwaving for 30 seconds. Gels were de-stained overnight in 5% ethanol, 6% acetic acid (v/v/v in ddH_2O).

2.4 - Western Blot Protocol

Methanol was used to clean all containers before the Western blotting procedure. A standard procedure for Western blotting was conducted after SDS-PAGE, firstly requiring transfer onto a PVDF membrane in Transfer Buffer using an iBlot© Gel Transfer Device (*ThermoFischer*). The membrane was washed in TBST and then blocking solution was added and incubation proceeded for 1 hour. His-tag monoclonal antibody HRP conjugate (*ThermoFischer*) was added in a 1:50,000 dilution and the membrane then incubated for 16 hours at 4℃. The membrane was washed 4 times with TBST and then developed via chemiluminescence using the luminol/ enhancer solution in stabile peroxidase buffer provided as a SuperSignal™ West Femto Maximum Sensitivity Substrate (*ThermoFischer*).

Table 10 – Composition of Western blotting buffers.

Name	Composition
Transfer Buffer	25 mM Tris-HCl 190 mM glycine Methanol (20% v/v)
TBST	50 mM Tris-HCl 150 mM NaCl Tween 20 (1% v/v) pH = 7.5 (with HCl)
Blocking Solution	5 g Albumin 100 mL TBST

2.5 - Sortagging

Sortagging has recently been adopted as a biochemical tool to label proteins with chemical probes, including fluorophores (in this case TAMRA) and the technique utilises a TAMRA peptide recognition motif, Sortase enzyme, and a sterically available glycine on the target protein [152]. Sortagging buffer must contain calcium (optimum concentration 10 mM calcium chloride) as a requisite for Sortase activity [152]. Initial purification of FT is in phosphate buffer (50 mM KH_2PO_4), however, calcium precipitates in phosphate buffer. FT must undergo buffer exchange into the Sortase Reaction Buffer by microdialysis, to remove the phosphate in order to achieve suitable reaction conditions.

Table 11 – Sortase reaction buffer composition. This is reported in Thiele *et al.* [152].

	Name	Composition	Source
(4)	Sortase Reaction Buffer	50 mM Tris-hydrochloride, 150 mM Sodium Chloride, 10 mM Calcium Chloride, 1 mM dithiothreitol, pH = 7.5	Thiele *et al.*[152]

The protocol by Thiele *et al.* states a range from 0.5-1 mM peptide, 10-50 μM protein and 20-150 μM Sortase in Sortase Reaction Buffer leaving for a 5-hour incubation period [152]. The reaction was optimised for this work, and high Sortase activity meant that 1 μM concentration was sufficient; 50 μM target protein and 500 μM peptide were used for an overnight incubation period. Microdialysis then removed an excess of peptide returning reaction into a phosphate buffer and quenching Sortase activity. A small Superdex gravity flow column removed any contaminant Sortase, whilst concentration is low, Sortase-acyl intermediate retains fluorescent activity which can affect confocal microscopy assay results. FT, FT-Tat, FT-R9 and TFL1 were labelled in this way.

SDS-Page (15% acrylamide) and in-gel fluorescence using a Typhoon FLA 9500 Imager (*GE Healthcare*) showed band shift after labelling and associated fluorescence of transpeptidation

products (TAMRA-labelled FT, FT-Tat, FT-R9 and TFL1). In-gel fluorescence revealed shifts before Coomassie staining (according to *2.3.10*).

2.6 - Plant Culture

Col-0 (N1092) and ft-10 mutants (N9869) were received from the Nottingham Stock Centre and pUBQ10::WAVE131:YFP were a gift from the Sena Laboratory. ft-10 was used in phenotyping experiments and pUBQ10::WAVE131:YFP in uptake studies; unless otherwise stated, Col-0 is used in all other experiments [153]. Core culturing techniques, including sterile growth, callus and cell culture formation are essential in this work and the table below gives the details for the core media preparations.

Table 12 – Compositions and preparation requirements of essential plant growth and regeneration media. This includes ½ MS Media, callus culture media, cell culture media, protoplast W1 solution and W5 solution.

	Buffer Name	Composition	Additional
(1)	½ MS Media	2.15 g MS Salts (Sigma) 10 g Sucrose 0.5 g MES 2.5 g Phytagel	Adjust to pH = 5.7 with KOH Fill to 1 L with ddH_2O Autoclave Media Sterilely pour plates and leave media to set
(2)	Callus Culture Media	4.3 g MS Salts (Sigma) 30 g Sucrose 5 g Agar 500 µL Naphthalene Acetic Acid 50 µL of 1 mg/ mL kinetin	Adjust to pH = 5.7 with KOH Fill to 1 L with ddH_2O Autoclave Media Sterilely pour plates and leave media to set
(3)	Cell Culture Media	*Callus Culture media composition without agar*	Autoclave media in 100 mL flasks
(4)	Protoplast W1 Solution	500 mM Mannitol 20 mM KCl 4 mM MES 10 mM $CaCl_2$ 0.15 g Cellulase R-10 (Duchefa) 0.45 g Macerozyme R-10 (Duchefa)	Total volume is 30 mL with ddH_2O Preheat for 15 minutes at 50 ℃ before addition of cellulase and macerozyme.
(5)	Protoplast W5 Solution	150 mM NaCl 125 mM $CaCl_2$ 5 mM KCl 5 mM Glucose 1.5 mM MES	Total volume is 30 mL with ddH_2O

2.6.1 - Sterile Root Tip Growth

Col-0 (Columbia) ecotype and pUBQ10::WAVE131:YFP (Wave131) seeds were sterilised and grown on ½ Murashige & Skoog Media. Approximately 100 seeds in a microcentrifuge tube were washed with 1 mL 70% ethanol (v/v in ddH_2O), before rinsing with ddH_2O and washing with 10% bleach (sodium hypochlorite) (v/v ddH_2O) *(Brenntag UK*) for 3 minutes. Seeds were

washed a further 6 times, with aspiration and then sown individually on ½ MS media and stratified for 48 hours at 4 ℃. Plates were erected upright for 5 days enabling vertical seedling growth on the surface of the media at 120 $\mu mol.m^{-2}.s^{-1}$ lighting for cycles of 16 hours of light and 8 hours of darkness.

2.6.2 - Callus and Cell Culture Formation

Callus was initiated from Col-0 leaves and the resultant cell culture formed.

2.6.2.1 - Callus Culture

Plants were grown under sterile conditions as detailed in *2.6.1* however 8 plants were grown per plate, this time, in a horizontal orientation and until large cauline leaves formed. Leaves were excised into thin strips with a sharp razor blade under sterile conditions and placed onto callus culture plates (detailed in *Table 11*) and kept in the dark for 1 week. Initially, callus was grown under 80 $\mu mol.m^{-2}.s^{-1}$ lighting until established, then transferred to 120 $\mu mol.m^{-2}.s^{-1}$. Callus was grown under cycles of 16 hours of light and 8 hours of darkness and healthy callus sub-cultured every 8 weeks.

2.6.2.2 - Cell Culture

Cell culture media comprised of callus culture media without agar and was liquid. Friable healthy callus was transferred to 100 mL of liquid medium and grown with shaking at 80 r.p.m. at 100 $\mu mol.m^{-2}.s^{-1}$. Once confluence was reached, subculture occured every 14 days.

2.6.3 - Protoplast Isolation

Cauline leaves were harvested from 4-week old healthy plants and excised into strips before incubating in W1 solution, enzymatic digestion occurred for 3 hours in the dark under vacuum. Gentle agitation at 50 r.p.m. for 20 min helped to release the protoplasts before filtering to remove undigested residue. 2 mL of W5 solution was added to the filtered protoplast solution,

followed by centrifugation at 70 g for 10 min. The protoplasts form at the interface and were carefully removed, washed with W5 and underwent centrifugation at 50 g for 10 min before final resuspension in W5 with 4% BSA and stored at 4˚C. Careful handling was essential as protoplasts are fragile and the cell membrane easily ruptured. This protocol was adapted by the method set out for tobacco protoplast isolation by Lelivelt *et al.* [154].

2.7 – Delivery and Uptake Methodologies

This is divided into two components – on the one hand, the delivery of CPPs and proteins into model systems including root tips, callus culture, cell culture. On the other hand, the delivery of protein into the whole Arabidopsis organism at entry points including the shoot apical meristem, the leaf and microinjection into the stem.

2.7.1 – Uptake in Model Systems

2.7.1.1 - CPP Uptake Study in Root Tips

The protocol for ½ MS Media is given in *Table 11* above. A thin 2 mm film of ½ MS Media was poured onto a square growth plate with uniform depth and allowed to dry. 20 µL of 50 µM peptide solution was infused into a 1.5 cm x 1.5 cm box on the phytagel plate and 3 Arabidopsis seedlings (either Col-0 or pUBQ10::WAVE131:YFP) were aligned with the root tip in this box and left to incubate for either 20 minutes or 6 hours according to the experimental timescale. Seedlings were washed thoroughly to remove any unbound peptide, mounted in water onto a microscope slide (*VWR*) and situated ready for confocal imaging.

2.7.1.2 - CPP Uptake Study in Cell Culture

CPP was added to 500 µL of cell culture taken from confluence from the protocol detailing cell culture formation in *2.6.2.2* to make a 5 µM final peptide solution. Incubations were carried out according to the experimental timescales. Centrifugation was at 2000 r.p.m. for 1 min and with removal of the supernatant to recover cells and resuspension in cell culture media (*Table 11*). Three washes were conducted with cell culture media to remove unbound peptide. Cells were resuspended in a minimum volume and mounted onto a microscope slide (*VWR*) ready for confocal imaging.

2.7.1.3 – Uptake of Sortagged Proteins into Callus Culture

The same protocol was followed for uptake of R9 peptide into cell culture in **2.7.1.2**.

2.7.2 – Uptake of Protein into Whole Organism

2.7.2.1 - Protein Infiltration and Extraction Method from Leaf

A 1 mL Injekt®-F Luer Solo syringe (*Braun - ISO 7886-1*) with a displacement spike was filled with 50 µL of protein solution. It was important to use this type of syringe as only a small infiltration volume was used and this prevented loss of protein through residual solution remaining in the syringe tip after infiltration. Protein was diluted to 150 µM with infiltration buffer that included protease inhibitors (EDTA-free protease inhibitor cocktail tablet (*Sigma Aldrich*), and PMSF), and the syringe was charged with 50 µL of solution ready to infiltrate on the underside of the leaf of 4-week old Col-0 plants (which had been watered the previous evening).

Table 13 – Composition of infiltration and extraction buffer for protein leaf infiltration.

Buffer Name	Composition
Leaf Infiltration and Extraction Buffer	50 mM potassium orthophosphate 200 mM potassium chloride 1 mM dithiothreitol 5 µM PMSF 1 EDTA-free protease cocktail inhibitor tablet final volume – 50 mL

Leaves were harvested after the specified time-course (0, 24 and 48 hours) and washed thoroughly with water to ensure that residual protein did not remain on the underside of the leaf surface after infiltration. Flash freezing with $N_{2(l)}$ and grinding of the sample in a pestle and mortar followed. The sample was collected in a microcentrifugation tube and 50 µL of extraction buffer was added. Samples underwent centrifugation at 13,000 r.p.m for 30 minutes

before the supernatant was removed and subjected to both SDS-PAGE and Western blot Analysis.

2.7.2.2 - Apical Meristem Dissection

Col-0 plants were grown under short-day conditions in soil for 4 weeks, to ensure that the apical meristem remained undifferentiated. Leaves and roots were removed with a razor blade, a thin cross-sectional shaving was taken containing the SAM, and mounted in water. A standard light microscope was used to assess sample quality before confocal microscopy imaging. High sample quality was essential, and many samples were assessed before suitable quality was reached for confocal imaging due to the challenging preparation technique.

2.7.2.3 - Microinjection

The microinjection needle was opened at the tip via micro-impact with a cover slip (*VWR*) and filled with 20 µL of protein solution before attaching to a Narashige Micromanipulator (*Nikon*). The sugar beet sample was clamped into position in a horizontal orientation and the injection pressure and application were controlled using a FemtoJet Express (*Eppendorf*). Microscopic observation showed successful targeting of the vasculature cells. Sugar beet stem samples were sliced into thin cross-sections and then placed on a microscope slide (*VWR*) for confocal imaging.

2.8 - pAP1::GFP in Col-0 Molecular Reporter Construction

2.8.1 - DNA Extraction from Plants

700 µL of CTAB buffer ((CTAB (2% w/v) (*Sigma Aldrich*), 1.4 M NaCl, β-mercaptoethanol (0.2% v/v), 20 mM EDTA, 100 mM Tris-HCl, pH = 8) was preheated at 60℃ and added to freshly ground, flash frozen (with $N_{2(l)}$) plant material for a 2-hour incubation. 700 µL of chloroform (95% v/v isoamylalcohol) was added with agitation for 10 minutes followed by centrifugation at 12,000 r.p.m. for 20 minutes. The supernatant was removed and RNAse (*Invitrogen*) (20 µg/ mL) added followed by a 30-minute incubation at 37℃. The DNA was precipitated using cold isopropanol (400 µL) and 3 M NaOAc (70 µL) at -20℃, overnight. Centrifugation at 12,000 r.p.m. for 10 minutes formed the DNA pellet which was washed with ethanol (70% v/v ddH_2O), and removed following subsequent centrifugation and then dried. DNA was resuspended in TE buffer and the concentration measured using a nanodrop. This protocol was adapted from Doyle *et al.* [155].

2.8.2 - TOPO Cloning

Template Arabidopsis gDNA was used from the extraction procedure and PCR was conducted using the protocol for Q5 yielding a blunt ended product. A Klenow Fragment (*New England BioLabs*) was used to A-tail DNA with dATP (0.1 mM final concentration) in an ABI Veriti Thermal Cycler (*ThermoFischer*) for 30 minutes. This enabled simple ligation into the pCR8 vector within 20 minutes and then transformation into One Shot™ TOP10 chemically competent *E. coli* cells (*ThermoFischer*) following the standard transformation protocol under spectinomycin selection. The conventional GW1 and GW2 and the M13 forward and M13 reverse primers were used to check the accuracy of the insert through sequencing. The pCR8 vector is an entry vector used for the subsequent LR reaction.

Table 14 – Primers used in the construction of pAP1::GFP in Col-0. Primers for extraction of 2000 base pair AP1 promoter, and analytical primers to analyse orientation of the construct and successful TOPO cloning and LR reaction product before agrobacterium transformation.

Primer Name	Sequence
pAP1-2kbp – Forward Primer	ACAAGTTTGTACAAAAAAAAAAGGGATATTTAATGGGAA
pAP1-2kbp - Reverse Primer	ACCACTTTGTACAAGAATTTTGATCCTTTTTTAAGAAAC
GW1 Primer	GTTGCAACAAATTGATGAGCAATGC
GW2 Primer	GTTGCAACAAATTGATGAGCAATTA
M13 – Forward Primer	GTAAAACGACGGCCAG
M13 – Reverse Primer	GTCATAGCTGTTTCCTG

2.8.3 – LR Reaction

The pAP1-2kbp insert in the pCR8 vector was transferred to the pGWB4 destination vector via a recombination reaction. 150 ng of entry vector and destination vector were mixed with LR Clonase™ (*Invitrogen*) for 60 minutes and then quenched with Proteinase K (*Invitrogen*) for 10 minutes at 37℃. This was followed according to the protocol by Invitrogen in the TA TOPO Cloning Kit for Gateway cloning reactions.

2.8.4 – Agrobacterium Transformation

Chemically competent *Agl1* strain of agrobacterium was prepared. A 100 µL aliquot was thawed on ice and 100 ng of destination vector added and retained on ice for 30 minutes before flash freezing with $N_{2(l)}$. After 1 minute the aliquot was thawed at 37℃ and 600 µL of LB media added followed by incubation for 4 hours. Centrifugation at 3000 RCF for 3 minutes yielded a pellet which was resuspended in 200 µL of LB before streaking onto agar plates under kanamycin (50 µg/mL), hygromycin (100 µg/mL) and rifampicin (100 µg/ mL) antibiotic selection and incubated at 28℃ for 72 hours.

2.8.5 – Floral Dip Protocol

A 10 mL starter culture under antibiotic selection was inoculated with a single agrobacterium colony and grown overnight at 28℃ with shaking at 200 r.p.m.. A subsequent 400 mL culture was grown to an O.D. of 1.5 before harvesting via centrifugation at 6000 r.p.m. for 6 minutes

and resuspension in infiltration buffer (0.654 g MS, 15 g sucrose, 90 µL Silwet L-77 (*PhytoTechnologies Laboratory*) in 300 mL ddH_2O). Flowering plants at the correct developmental stage (before silique formation), were dipped into the solution and held for 5 minutes and then covered for 16 hours. Subsequent seeds were harvested and the generation occured through T_1 and T_2 stages to achieve a homozygous line through antibiotic selection.

2.9 - Confocal Microscopy

It is essential to pilot settings before each confocal microscopy experiment in order to determine the most appropriate operational and post-processing parameters to record the data-set. Once these have been determined then they are consistently applied throughout the experiment to each sample acquisition in order to ensure that confocal image results are comparable across the data-set. The two primary operational settings are, laser excitation wavelength and emission detection range which affect the type of detected fluorescence. When more than one fluorophore is present in the sample (including chlorophyll autofluorescence), these two settings ensure that channel overlap between fluorophores is minimised, and that each detection window can be attributed to a particular fluorophore in the sample to record mutually exclusive and representative confocal imaging data.

In this work, the primary fluorescence detected was TAMRA (from labelled peptides and proteins) and GFP (from protein and also constitutive GFP from the pAP1::GFP reporter). Multichannel images include YFP and propidium iodide in combination with TAMRA as cell boundary markers. In chlorophyll containing tissue, autofluorescence was also detected in combination with GFP and TAMRA. The importance of piloting settings empirically ensured that channel overlap was minimised and the acquisition settings used are detailed in *Table 14* below. Confocal microscopy results were processed using open-source ImageJ software.

2.9.1 - Acquisition Parameters

In this work an upright Leica SP5 laser scanning confocal microscope (Leica Microsystems) was used with a total magnification range of 630 times. Either a 63X Oil or a 10X dry objective was used with a consistent pinhole aperture (decimal Airy unit multiple) for each dataset. Fluorescence was recorded using HyD detectors.

Table 15 – Confocal microscopy settings for the detection of fluorophores. Settings are presented for detecting the fluorophores, TAMRA and GFP, and the secondary fluorophores in the images - PI, YFP and chlorophyll autofluorescence. The application of the different combinations (1)-(5) is detailed as well.

Combination*	Laser	Fluorophore 1	Detection Window 1	Fluorophore 2	Detection Window 2
(1)	543 nm	*TAMRA*	560-650 nm		
(2)	543 nm	*TAMRA*	550-570 nm	*PI*	730-750 nm
(3)	514 nm	*TAMRA*	525-560 nm	*YFP*	620-750 nm
(4)	543 nm	*TAMRA*	560-648 nm	*Chlorophyll*	657-733 nm
(5)	488 nm	*GFP*	506-553 nm	*Chlorophyll*	657-733 nm
HyD Leica Detectors recorded fluorescence					

***Application of Acquisition Settings in Confocal Microscopy Experiments**

(1) Uptake of TAMRA labelled peptides into root tips & Cell Culture. Assessment of Sortagged FT, FT-Tat and FT-R9 proteins into callus culture.
(2) Uptake of TAMRA-peptides into root tips with the inclusion of PI cell wall marker.
(3) Uptake of TAMRA-peptides into WAVE131 root tips, utilising YFP as a cell boundary marker. This was used for quantitative uptake assessment.
(4) Uptake of Sortagged protein and TAMRA-peptides into the shoot apical meristem tissue.
(5) Assessment of GFP expression in pAP1::GFP reporter in the shoot apical meristem & assessment of Non-covalent delivery of FT-GFP into callus culture.

2.9.2 - Propidium Iodide Root Tip Staining

After peptide incubation, root tips were stained in 10 µg/mL of propidium iodide (*Sigma Aldrich*)

for 3 minutes before washing with water and mounted ready for imaging.

3. Results 1 - Assessment of Cell Penetrating Peptide Internalisation in Plant Tissue

3.1 - Introduction

Cellular delivery and uptake of biomolecules is an important concept for druggable targets in both medicine and plant sciences. In particular, recent efforts have been made to investigate the use of macromolecules, such as proteins, as potential therapeutics in medicine [156]. This concept has not been fully investigated in plant sciences and as such it is possible to detail a complete list of the CPP studies, both in isolation and reporting cargo transduction – these are given in *Tables 1* and *2* in (Sections *1.5.3.1* and *1.5.3.2*). The phospholipid bilayer is classically considered an impermeable barrier to large macromolecules including peptides and proteins without the assistance of specific receptor mediated entry. The field of cell penetrating peptides (CPPs) has developed as a way to overcome the impermeable barrier around the cell, and to facilitate cargo delivery including proteins across the cell membrane [125, 157].

Many CPPs have been reported with exotic origins and different properties [127]. CPPs are either cationic in nature containing a high proportion of arginine residues, amphipathic with both hydrophilic and hydrophobic residues or fully hydrophobic (which is unusual) [127]. Many sequences have natural origins and their design has been influenced by the natural function of the parent system where the active domain is shown to help penetrate tissue membranes. Sequence length seldom exceeds 30 amino acids [158].

This research studied uptake action of the 4 CPPs: Tat, R9, pVEC and TP10. This complement of sequences was chosen with different properties in order to investigate whether they give rise to different uptake behaviours in plant tissues. Tat and R9 are cationic, whereas pVEC and TP10 are amphipathic; R9 is synthetic whereas the other 3 sequences have natural origins, and these are detailed in *Table 1* in *Section 1.5.3.* [121, 129, 130, 134].

The main aim of this chapter was to investigate the action of different CPPs in the context of reported evidence within the plant literature and determine which display advantageous uptake properties. Although this chapter focuses on CPP action alone, a wider consideration when studying the uptake properties of CPPs is whether they could be used to deliver FT inside cells to artificially activate AP1 and other FAC targets and this broader context is of consideration when analysing the experimental results.

3.2 – Experimental Aims for the Chapter

1) Independently assess CPP action under a single controlled system, using Arabidopsis as a model organism and develop assays to study CPP behaviour.
2) Compare the Action of R9, Tat, TP10 and pVEC and determine if their different physiochemical characteristics give rise to different uptake behaviours and compare results to evidence reported in the literature.
3) Define what is meant by a successful sequence and determine the different uptake behaviours of the sequences.
4) Assess peptide uptake behaviour over time course experiments – determine uptake properties after an initial 20-minute incubation and after 6 hours.
5) Quantify CPP uptake - using Matlab to quantitatively define uptake in root tips.
6) Assess CPP action under different cellular hierarchies and structures.
7) Highlight areas of novelty where CPP action has not been investigated, in this way, investigate peptide uptake into the shoot apical meristem.

3.3 - Results

3.3.1 – SPPS of Tat, TP10 and pVEC.

Figure 8 reports solid phase peptide synthesis used to construct Tat, TP10, and pVEC sequences; accordingly, Fmoc deprotecting strategy was used to couple the residues from a C to N terminal direction. A final deprotection step exposed the N-terminal amine which was activated and coupled to the TAMRA carboxy-rhodamine fluorophore. TAMRA was selected as importantly, it displays strong fluorescence in a spectral region that can be resolved against background chlorophyll autofluorescence and GFP fluorescence.

Sequences were universally deprotected from the support resin and after chemical purification, they underwent an LCMS preparative run. A final analytical LCMS assessment revealed retention time and peptide purity as shown in *Figure 9*.

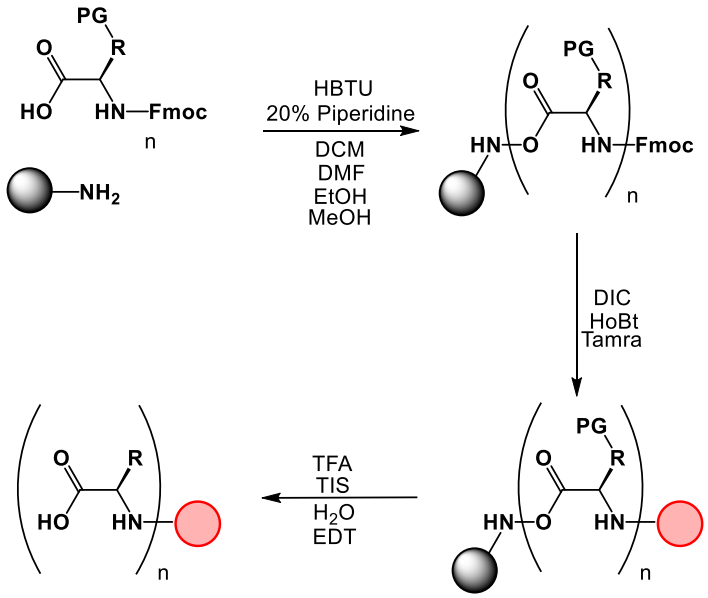
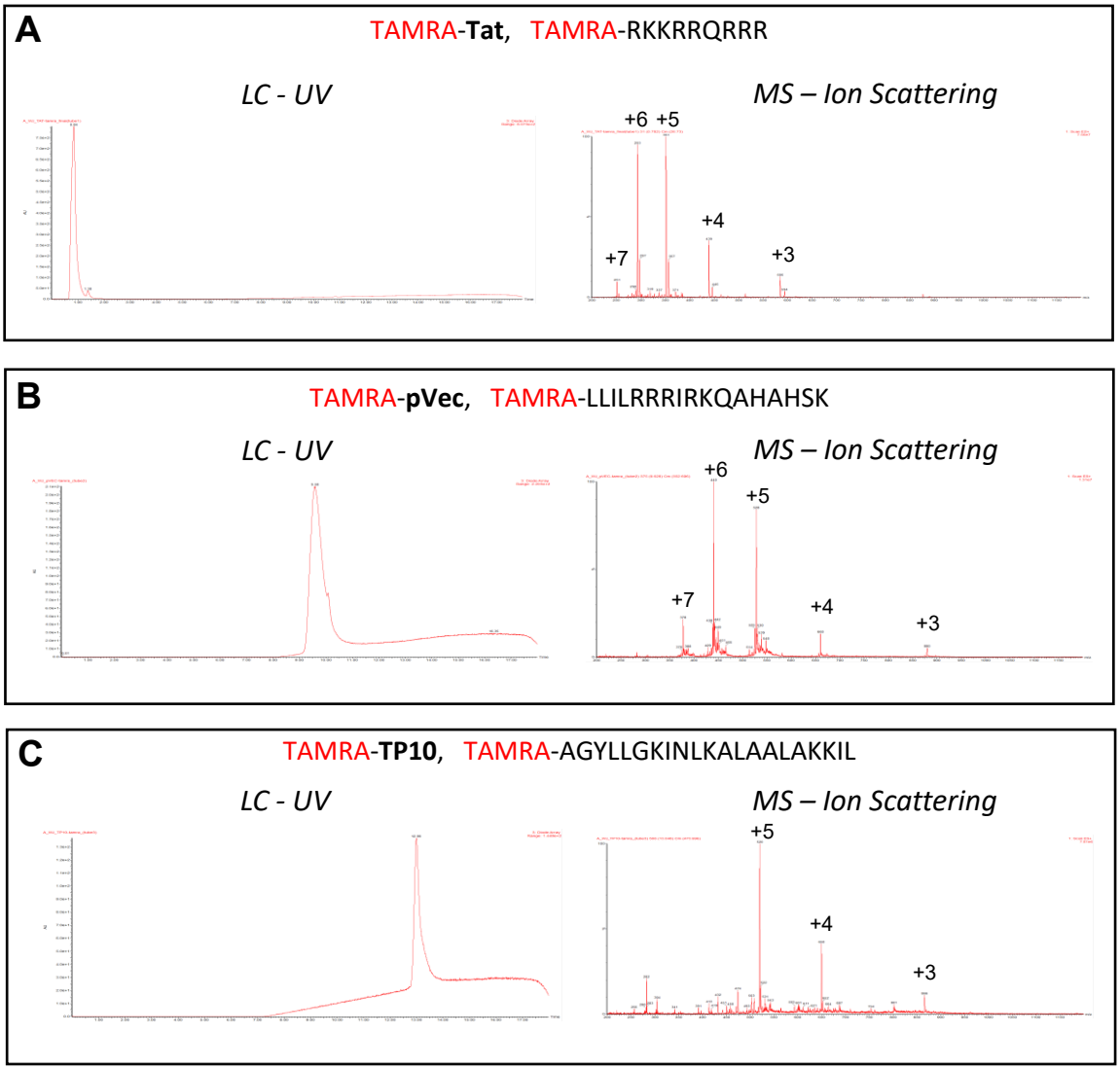


Figure 13 - Schematic showing the SPPS chemical workflow. This includes the coupling of a TAMRA fluorophore (depicted above by the red circle), the rink amide resin is depicted by a black circle.



Molecular Ion Splitting					
Tat		pVEC		TP10	
Ion	M_r	Ion	M_r	Ion	M_r
+1	-	+1	-	+1	-
+2	-	+2	-	+2	-
+3	585	+3	880	+3	866
+4	439	+4	660	+4	650
+5	351	+5	528	+5	520
+6	293	+6	440	+6	-
+7	251	+7	378	+7	-
M_r in gmol^{-1}					

Figure 14 – Analytical assessment of peptide purity and characterisation using LCMS. Characterisation is shown for **(A)** TAMRA-Tat, **(B)** TAMRA-pVEC and **(C)** TAMRA-TP10. Molecular ion splitting corresponded to the peaks in the MS ion scattering spectra above.

¶ TAMRA labelled R9 was purchased from Cambridge Peptides.

3.3.2 – Assessment of R9, Tat, pVEC and TP10 Uptake

3.3.2.1 – Uptake into Root Tips

The Arabidopsis root tip was used as a model to assess uptake of the four CPPs. 5-day old plants were grown under sterile conditions. The root was subjected to a standardised peptide treatment for an incubation period, washed and then mounted on a microscope slide ready for confocal imaging. Confocal microscopy allowed optical sectioning of the sample and the symmetry of the root tip was as such that the longitudinal centre of the organ can be found and therefore standardised comparative images were recorded. The centre of the root is marked by two quiescent centre cells and these are observed in the brightfield channel.

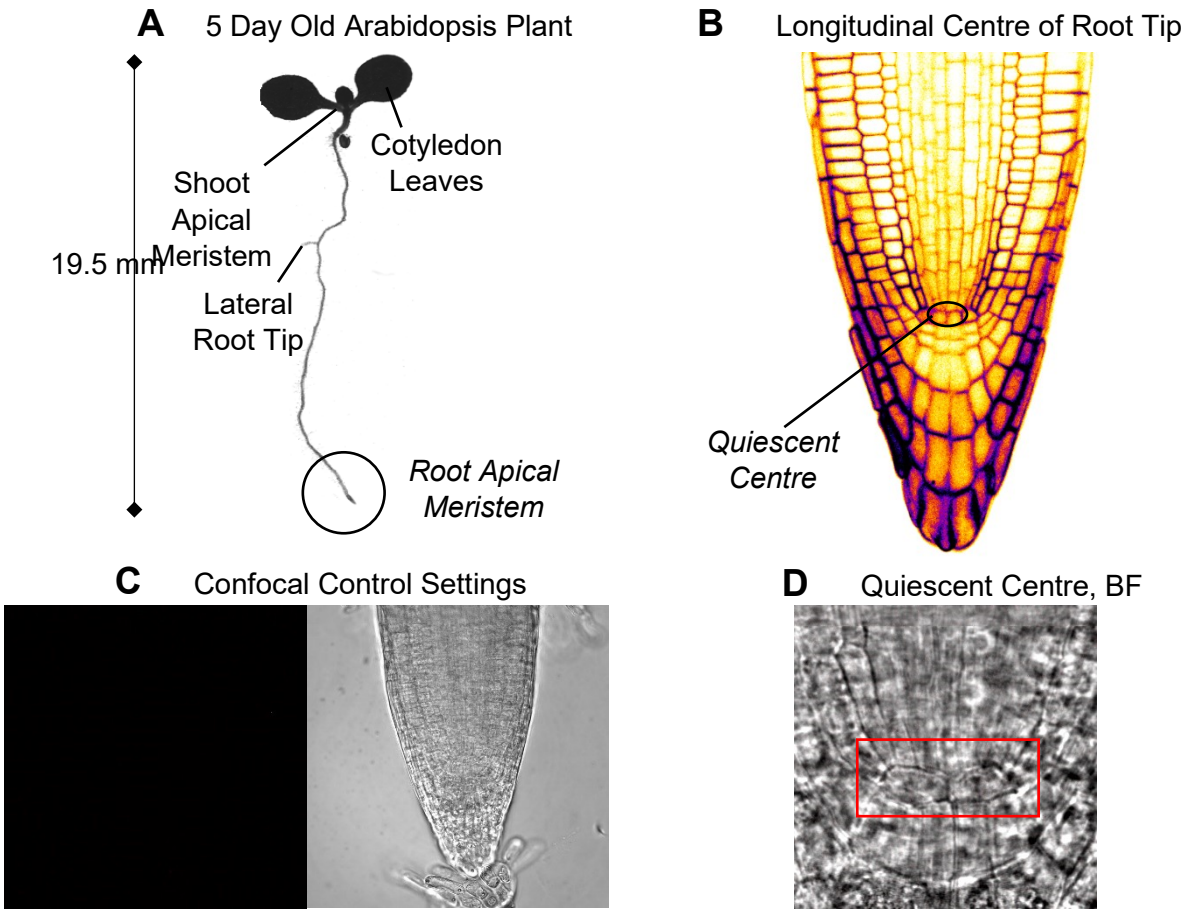


Figure 15 – Setup for confocal microscopy experiments of Arabidopsis root tips. **(A)**, Brightfield tile scan of a 5-day old Arabidopsis root; **(B)**, the longitudinal centre of a root tip showed the quiescent centre; **(C)**, control experiment: a root tip incubated in water showing no fluorescence in the TAMRA channel; **(D)**, the quiescent centre recorded from the brightfield channel.

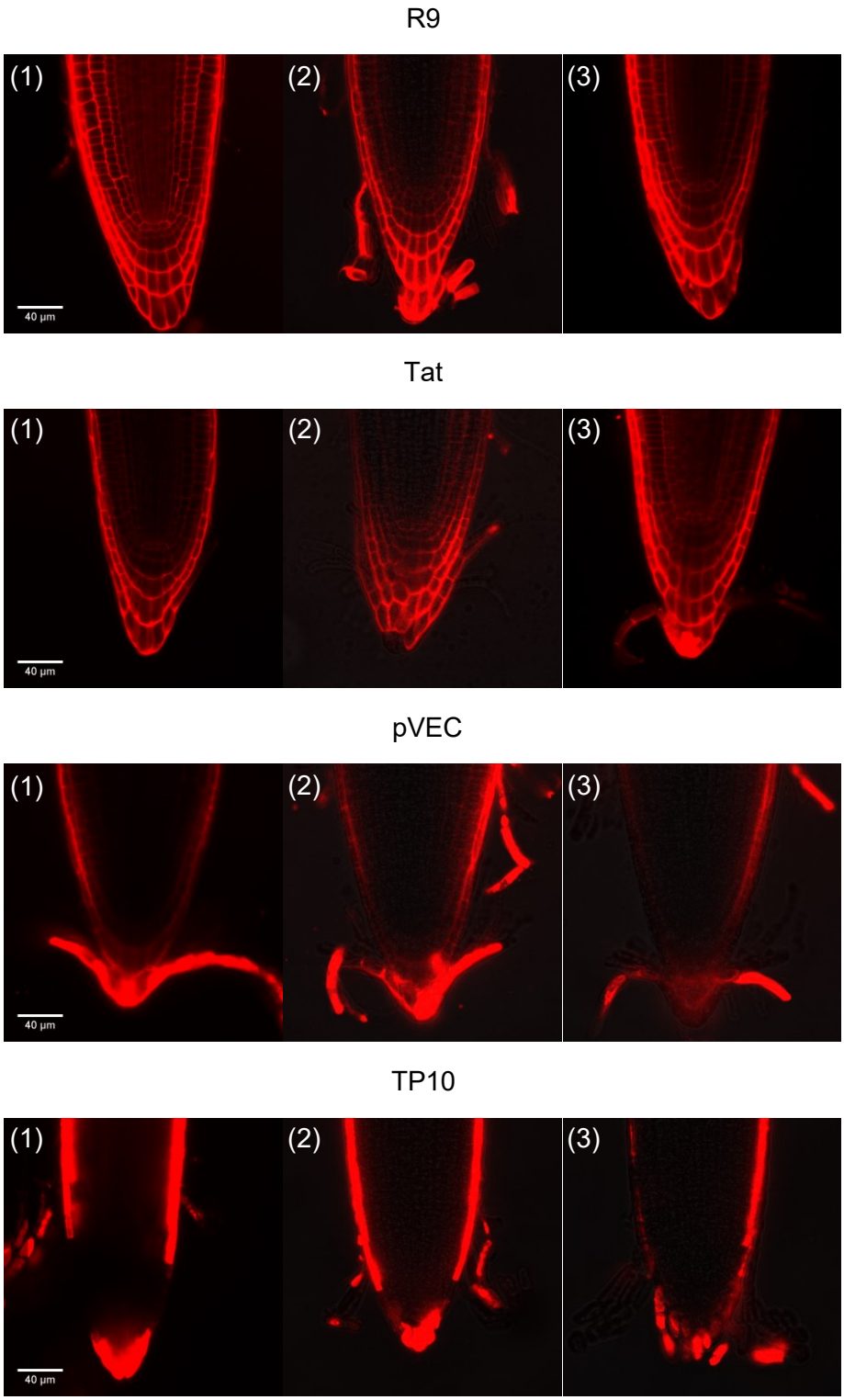


Figure 16 – 20-minute incubations of CPPs with Arabidopsis root tips. Roots were incubated with R9, Tat, TP10 and pVEC, and the images are presented in triplicate. TAMRA fluorescence was recorded showing the uptake profile of the peptides.

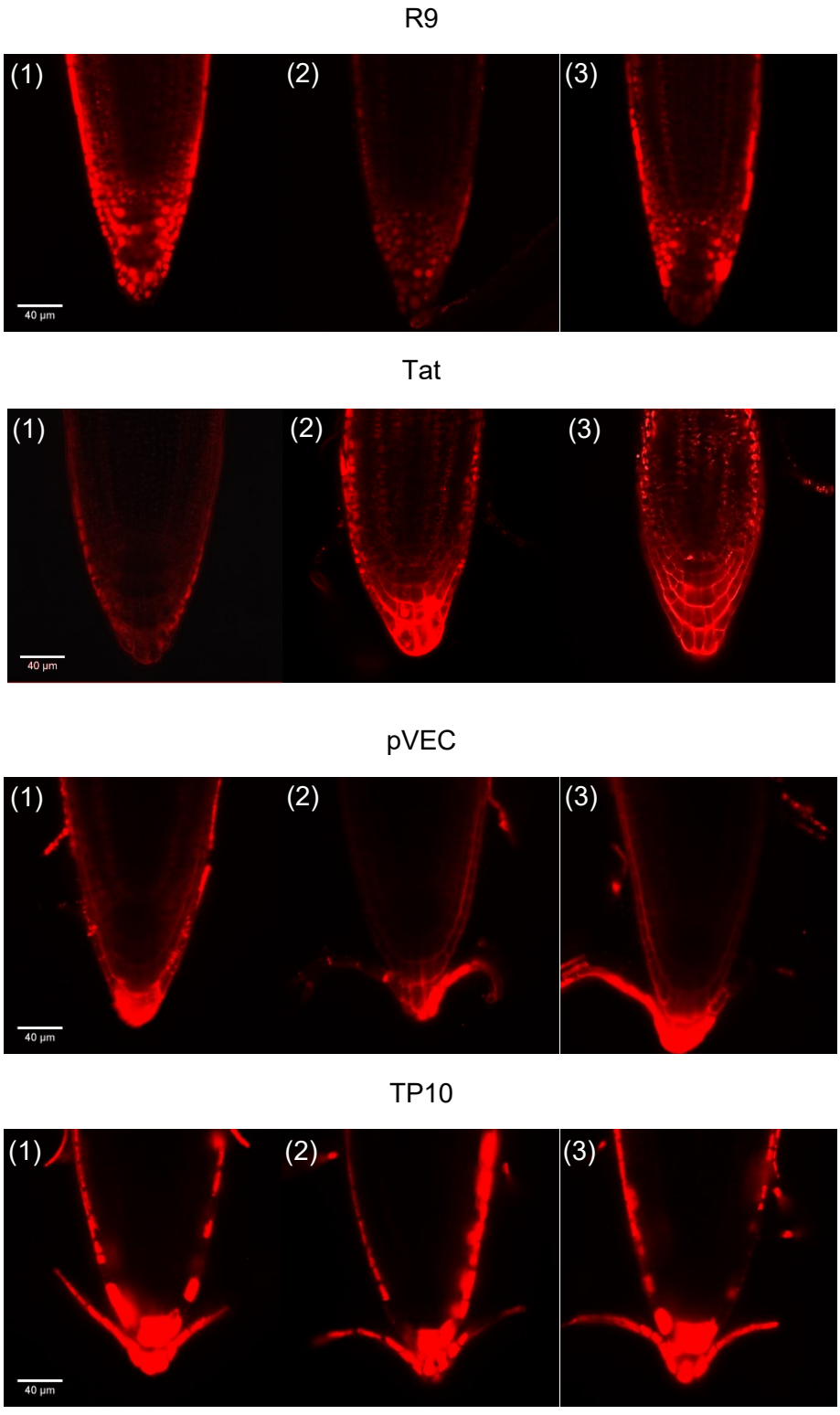


Figure 17– 6-hour incubations of CPPs with Arabidopsis root tips. Root tips incubated for 6 hours with R9, Tat, TP10 and pVEC following the same experimental setup as for the images recorded in *Figure 11* but for a longer incubation time.

Results recorded for both 20-minute and 6-hour peptide root tip incubations showed a clear difference between the cationic R9 and Tat when compared to the amphipathic pVEC and TP10 uptake profiles. After 20 minutes the cationic sequences entered the root tip and diffused around the cells - both R9 and Tat displayed matching uptake profiles. They accrued around the cells perhaps through interaction with the negatively charged components in the cell wall [141, 159].

In contrast, the TP10 and pVEC sequences both filled the outer cells of the root cap after 20 minutes, and this was particularly pronounced for TP10. TP10 and pVEC were unable to enter the inside of the root, and no fluorescence was observed around the inner cells. A clear difference in spatial accumulation was observed between the cationic R9 and Tat sequences and the amphipathic TP10 and pVEC sequences after 20 minutes.

Likewise, confocal imaging after 6-hour incubations showed the accumulation of R9 and Tat in a pattern which indicated intracellular localisation. In contrast pVEC and TP10 remained on the outermost cells. The images showed that R9 and Tat were able to enter cells after 6 hours and pVEC and TP10 were only able to fill the outer cells of the root cap inferring a clear activity difference between cationic and amphipathic sequences as shown by their different uptake profiles.

3.3.2.2 – Uptake into Root Tips – Assessment with Propidium Iodide

A propidium iodide (PI) cell wall stain confirmed the conclusions drawn in *Figures 11* and *12* that R9 and Tat were located inside the cells of the root tip. PI was included in the incubations and the detection settings optimised to reduce channel overlap. The 6-hour incubations were repeated and peptide localisation observed. PI is classically presented in a red channel so the peptide localisation in this case is presented in green in *Figure 13*.

PI is a fluorescent cell wall stain and was used to determine cellular outlines in the root tip and aided visualisation of the quiescent centre. The PI channel enabled visualisation of the peptide location within the root tip. PI confirmed that the cationic sequences were localised inside the cells with similar uptake profiles observed for both R9 and Tat. In contrast, the pVEC and TP10 sequences remained on the outer root cap after 6 hours and co-localisation of both fluorophores was observed by a colour change to yellow; both these amphipathic sequences showed similar behaviour when accumulating on the root cap cells.

Importantly, PI is a cellular viability indicator, and if a cell membrane was compromised, the cell would fill with PI. In the results in *Figure 13*, PI stain filled the root cap cells following the uptake and localisation of pVEC and TP10 into the root tip. This showed that pVEC and TP10 uptake caused membrane damage. In *Figure 13*, this outcome was most severe for the pVEC incubation as the PI stain was not able to clearly label the cells inside the root as was the case for the other 3 incubations, and perhaps the damaged outer cells which were consequently filled with PI did not allow any further stain to pass through. For the cationic R9 and Tat incubations, a conventional PI staining was recorded and this showed that localisation of peptide inside cells was achieved without damaging the cell membranes.

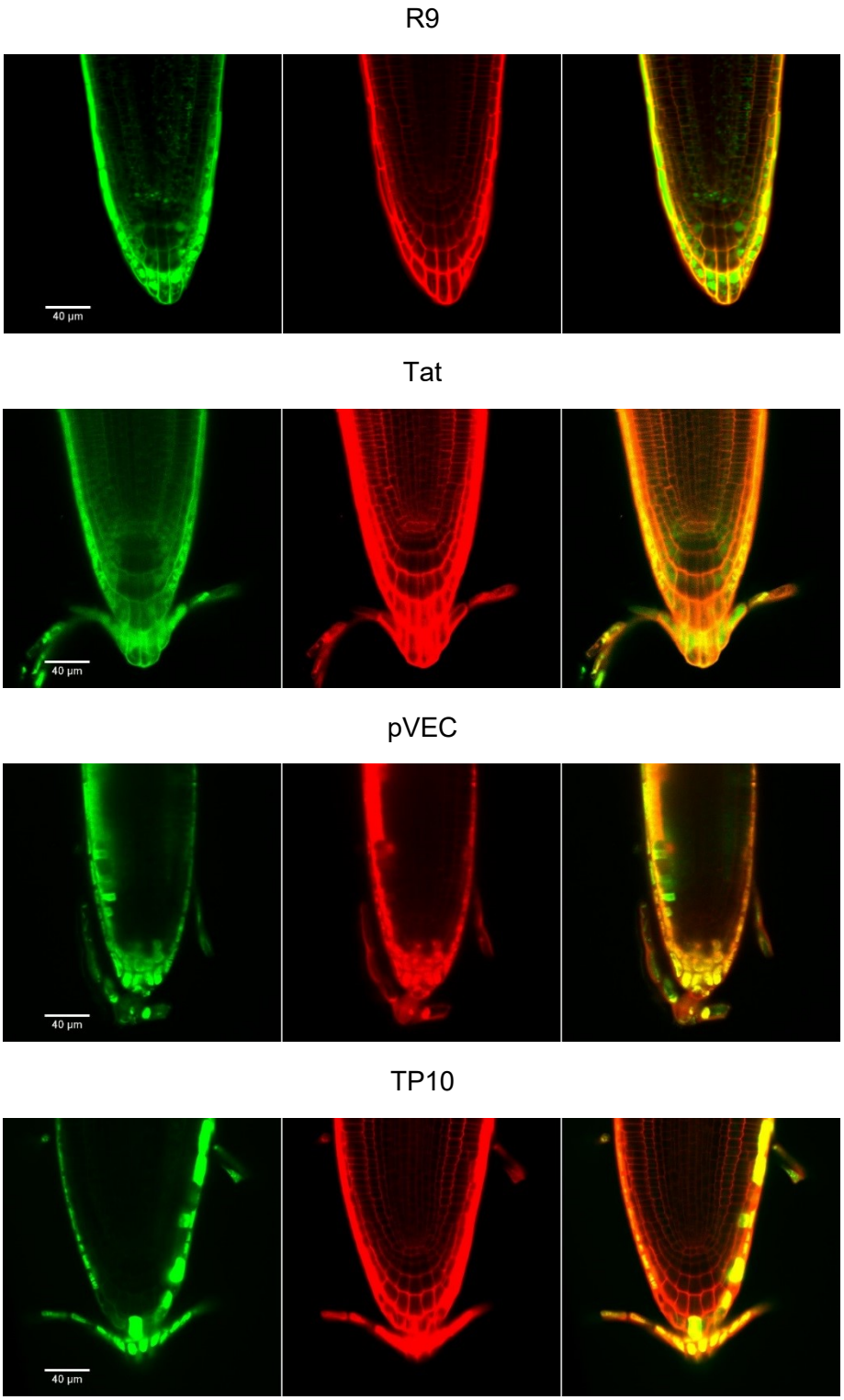


Figure 18 – 6-hour CPP incubations with propidium iodide staining. The composite images present PI in red and CPP in green. The merged channel presented co-localisation of the two fluorophores, this appears yellow where fluorescent channel overlap occurs.

3.3.3 – Further Assessment of R9 Uptake

3.3.3.1 – Assessment of R9 Uptake into Arabidopsis Leaf Cell Culture

It is clear from section *3.3.2* that the uptake of R9 was successful in root tips and as such a logical progression was to test its action in other cell types. An Arabidopsis cell culture was initiated from callus derived from leaf tissue and used as a model to assess uptake of R9 into cells.

Cells were incubated with R9 for both 20 minutes and 6 hours, then washed and mounted ready for confocal imagining. The same pattern was observed for the root tip incubations. *Figure 14* clearly showed that R9 accumulated around cells after 20 minutes and was then located inside cells after 6 hours. It is clear that R9 was interacting with the cell boundary, and this interaction could have been between the positively charged arginine and the negative components in the saccharide cell wall as R9 remained attached after extensive washings; these negatively charged cell wall elements could have been pectins, carboxyl and hydroxyl groups and embedded proteins [141, 159, 160]. At least 6 repeats were observed for both the 20-minute and 6-hour incubations presented below.

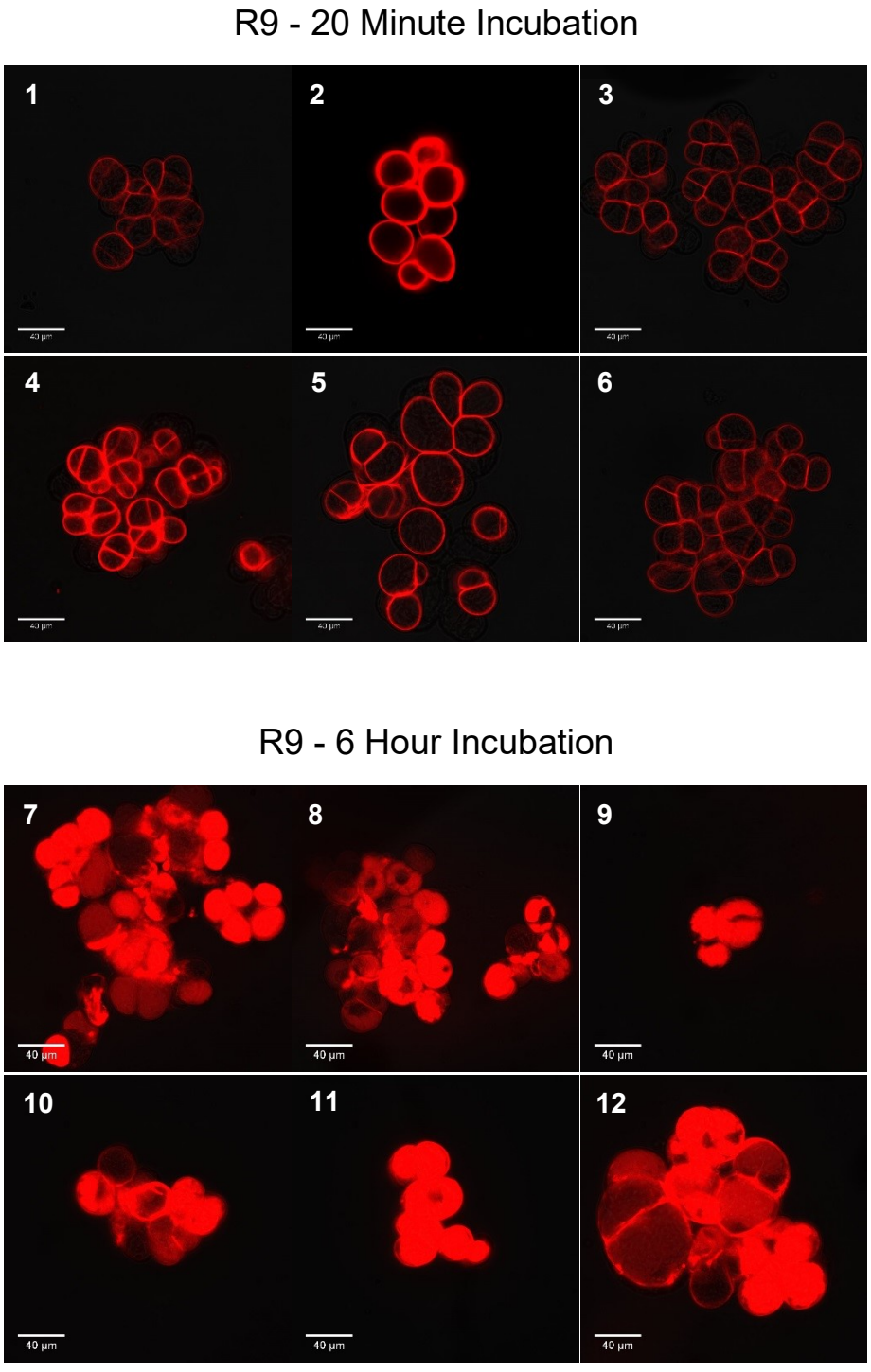


Figure 19 – Arabidopsis cell culture confocal images for incubations with R9 after both 20 minutes and 6 hours. Peptide was attached to the cellular boundary after washing for the 20-minute incubations and was internalised inside the cells after 6 hours. 6 images are presented for each incubation condition. Magnification is consistent across images.

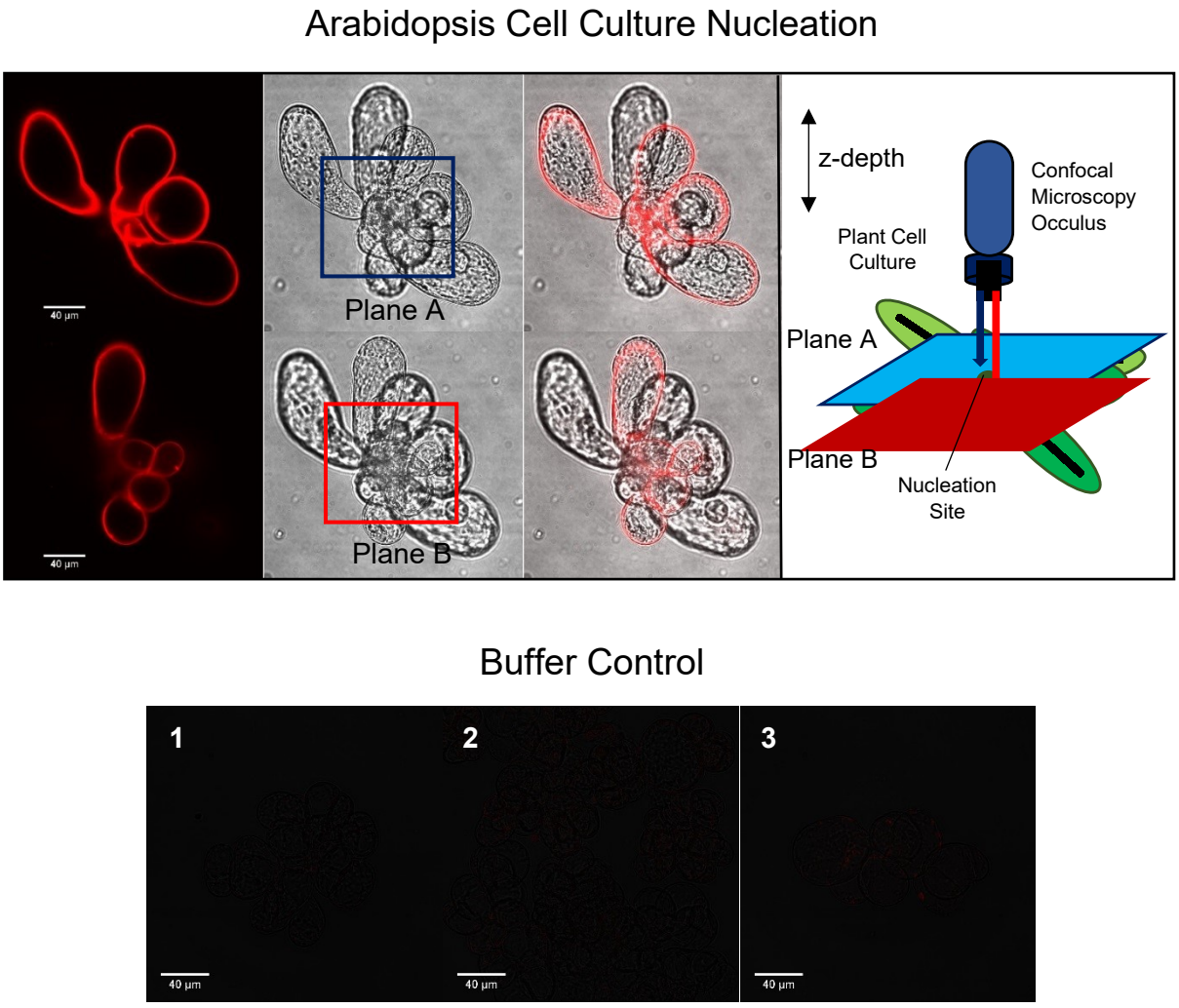


Figure 20 – Arabidopsis cell culture nucleation. The Arabidopsis cell culture nucleation diagram showed the cell culture nucleating from a central point and the cell growing in either a lower or upper plane. This was clearly depicted in the brightfield channel. The merged channel showed that as the plane reached focus in the brightfield channel, the cellular boundary overlapped with peptide location in the TAMRA channel. The buffer control ***(1)-(3)*** showed that under the confocal settings used during acquisitions there was no observed background autofluorescence.

The buffer control shows that the fluorescence signal was attributed to TAMRA-R9. In addition, *Figure 15* clearly shows how Arabidopsis cell cultures nucleate from a central point (*c.f.* chain structures from BY-2 tobacco cells) [141]. Confocal microscopy records optical sections of a sample so there are 2 available results, either a higher plane or a lower plane in the images and this is clear from the brightfield channel overlay in *Figure 15* above.

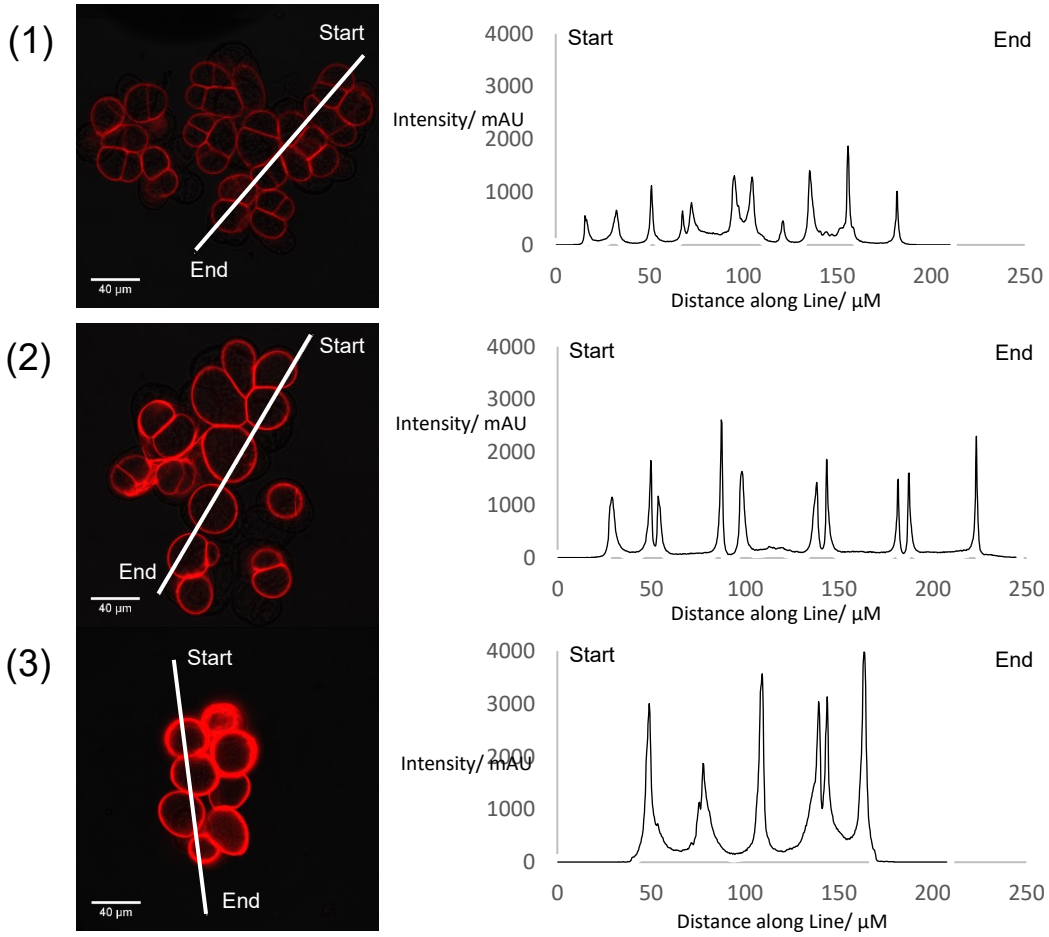


Figure 21 – 20-minute incubation of R9 with cell culture – line intensity assessment. Images were recorded under the same confocal and post processing settings to allow direct quantitative comparison between images and with the 6-hour incubation.

ImageJ intensity assessment analysis was conducted to determine and confirm R9 localisation. The sharp spikes in absorption intensity after the 20-minute incubation corresponded to R9 at the cellular boundaries. Interestingly, the larger the batch of cells in a cluster, the smaller the fluorescence recorded at the cellular boundary. For size, (1) > (2) > (3) and this was indicated by localised fluorescence intensity at cellular boundaries where (1) < (2) < (3), illustrated by the trend in peak heights.

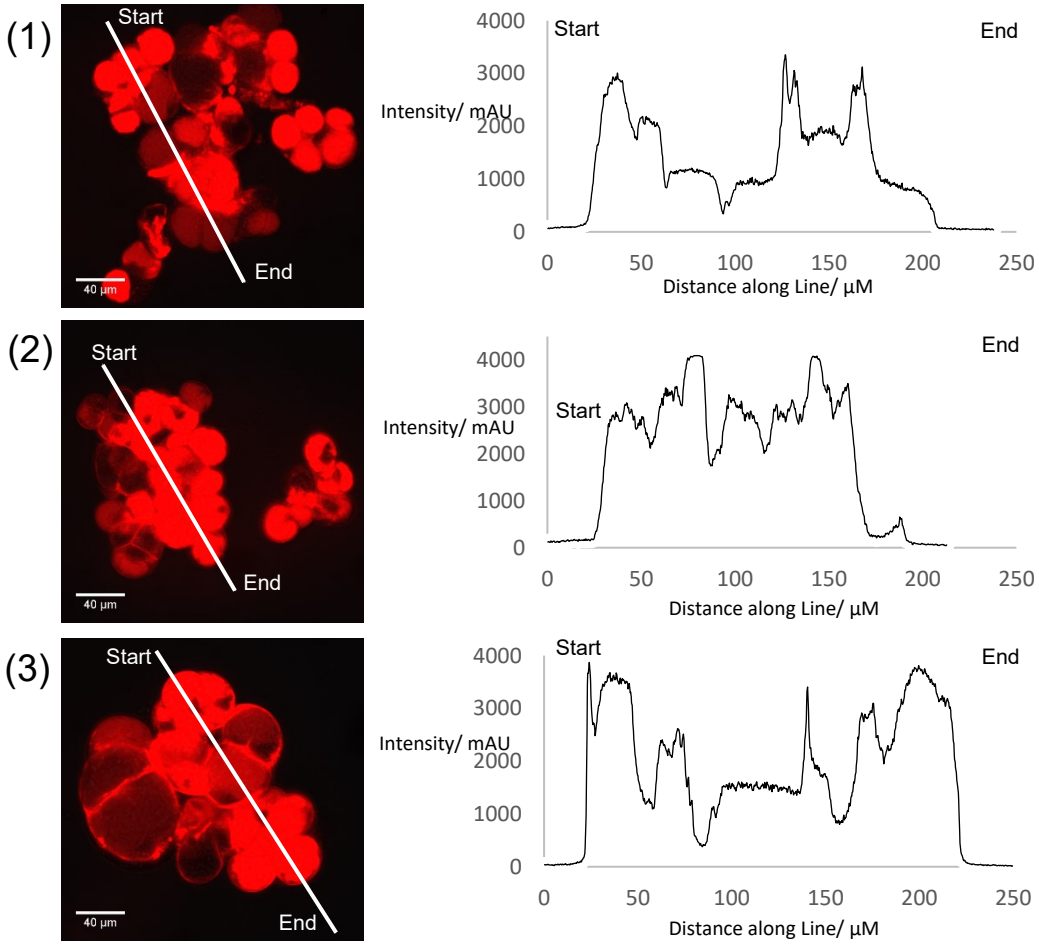


Figure 22 – **6-hour incubation of R9 with cell culture – line intensity assessment.** Line intensity assessments showed peptide location for 6-hour incubations. Images were recorded under the same confocal and post processing settings to allow direct quantitative comparisons between the images and with the 20-minute incubations.

Broader profiles were observed for the 6-hour incubation corresponding to intracellular R9. Higher absorption integrals for the 6-hour incubation showed that peptide absorption was not limiting as it continued to penetrate inside the cell during the incubation. The profile is strikingly different from the 20-minute incubation and clearly showed the effective action of R9 penetrating leaf cell culture tissue.

3.3.3.2 – R9 Incubation with Protoplasts

The cell wall can be artificially removed to create protoplasts, which are turgid membranous spheres provided that the media has the appropriate osmotica. A cellulase enzyme solution was applied to excised leaf tissue to digest the cell walls, yielding protoplasts. In this experiment, protoplasts were formed and incubated with R9 to try and determine whether the peptide was located around the phospholipid bilayer when compared with the cell culture images. Protoplast formation was successful but after incubation with R9, the protoplasts were no longer viable and did not appear as the characteristic spheres. Instead small membranous vesicles formed, smaller than the original protoplast, containing TAMRA-R9 fluorescence. It appeared that the high surface tension created by the positively charged guanidinium groups in the R9 peptide, caused the protoplast cell membrane to rupture, consequently destroying the protoplasts.

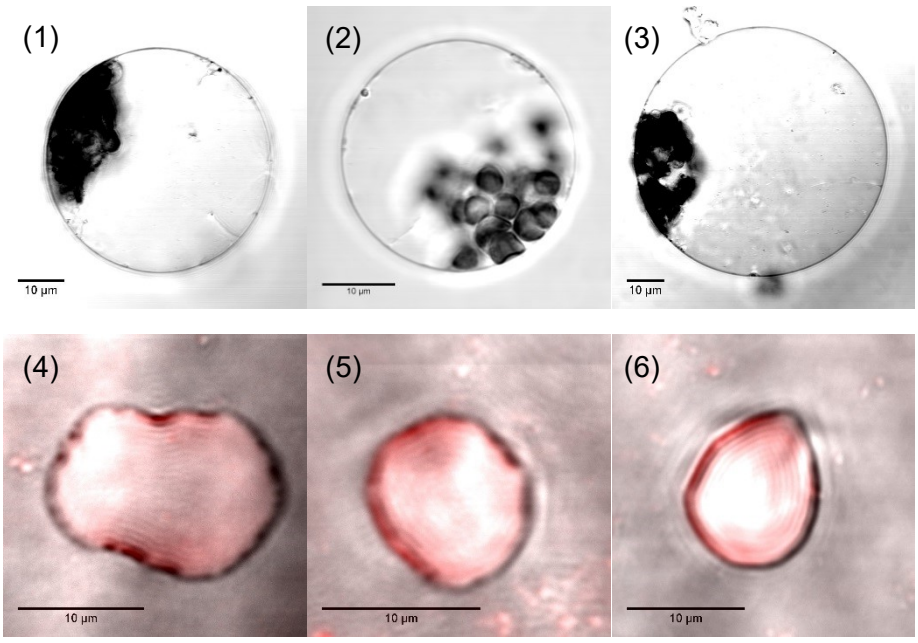


Figure 23 – Confocal Images of protoplasts before and after R9 uptake. Viable protoplasts are displayed in the top three brightfield confocal images ***(1)-(3)***. After incubation with peptide they collapsed and small vesicles containing peptide fluorescence are displayed in the bottom three images ***(4)-(6)*** (overlaid TAMRA and BF channels).

3.3.3.3 – R9 Quantitative Uptake Assessment

Confocal microscopy is an important technique used to reveal spatial information about fluorophores in a system. Images display a 2-dimensional map of pixel intensity and quantitative information as well as qualitative profiling of fluorophores.

In this experiment, pUBQ10::WAVE131:YFP mutant (herein called WAVE131) was used; it has YFP attached to SNARE proteins which are trafficked to the plasma membrane and resides in the phospholipid bilayer [153]. This acted as a membrane marker showing root tip fluorescence at the cellular boundaries under the correct excitation. In the same way as before, R9 was incubated with root tips following the experimental conditions laid out previously for *Figures 11* and *12* and R9 uptake was recorded after 6 hours. Confocal microscopy acquisitions recorded dual channel images: the YFP acted as a plasma membrane marker and R9-TAMRA fluorescence was observed.

A MatLab computation performed by collaborator Anne-Mieke Reijne used the YFP channel to assign cellular boundaries and also calculated the fluorescence intensity inside the cells per unit area. 10 WAVE131 control roots were imaged to ascertain background fluorescence levels as were 10 roots subjected to a 6-hour R9 incubation. The MatLab computation assigned the cells and they were numbered allowing manual sorting into the different cell types that are present in the root tip; these include, the lateral root cap, columella, epidermis, cortex, endodermis, quiescent centre, pericycle and stele cells [161]. The latter two were recorded together as it was hard to differentiate between the pericycle and stele from the confocal images, as such, these were collectively recorded as the *stele*. Intensity values for in excess of one hundred cells in each cell type were recorded over the 10 roots in both control and R9 incubation conditions, allowing for representative averages and comparison. The quiescent centre stem cell niche and stem cell initials for the adjoining cell types were collectively called the *quiescent centre* as it was hard to reliably categorise them in the computational

assignment. They were assigned a purple colour and, in this analysis, collectively termed the *quiescent centre*. They were removed from the quantitative part of the analysis as they only account for a small number of the total cells and their main purpose is in determining the median longitudinal plane of the root tip, to standardise confocal acquisitions.

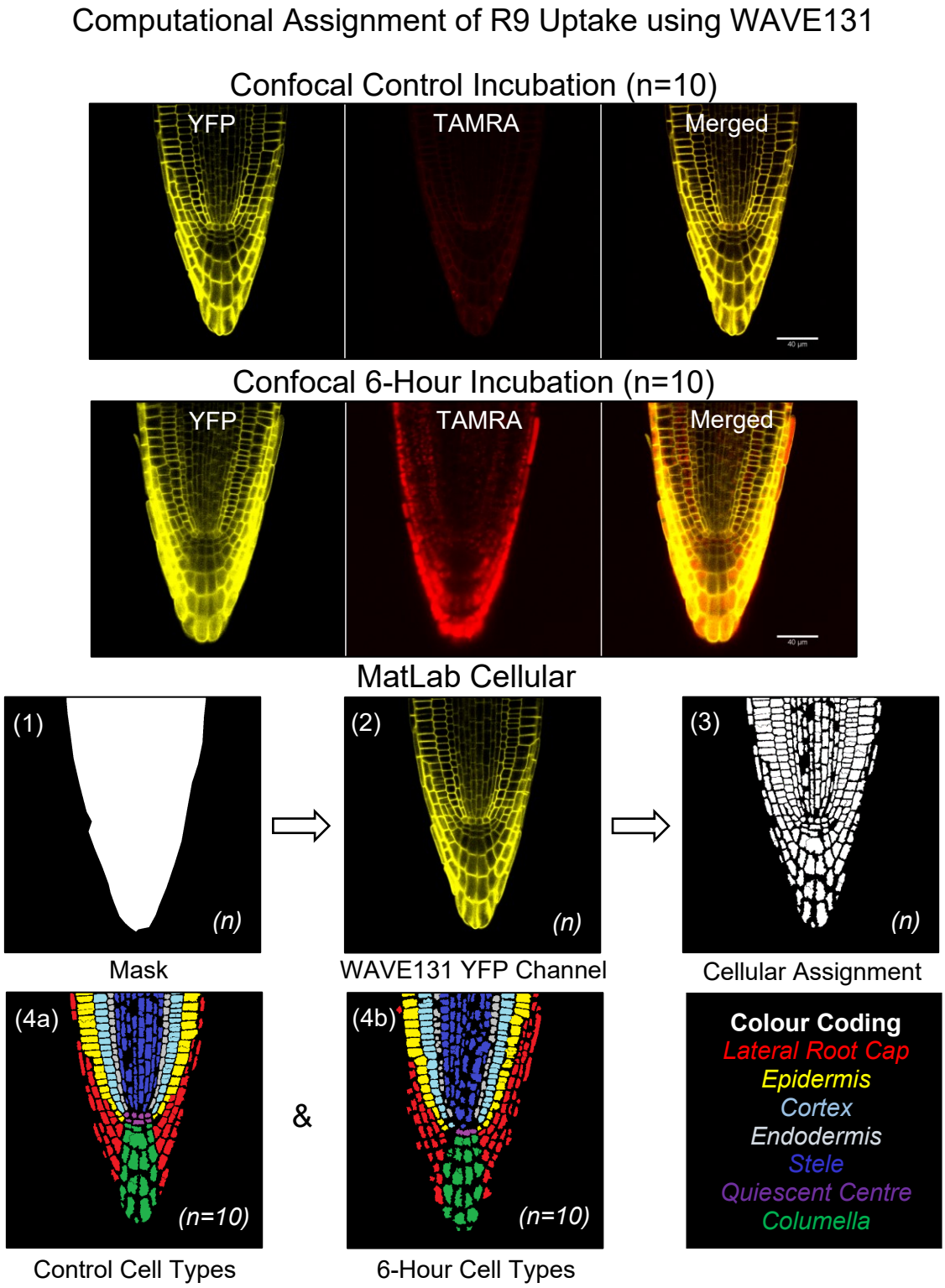


Figure 24 – **A representation of the computational assessment of R9 uptake in root tips.** 10 control incubations and 10 6-hour R9 incubations were recorded using confocal microscopy. A mask was drawn around the root tip shell **(1)**, the YFP channel **(2)** was used to assign cell boundaries **(3)**. **(1) - (3)** were conducted by collaborator Anne-Mieke Reijne on 10 control and 10 6-hour root tip incubation acquisitions. Cell types were manually assigned for the control incubations **(4a)** and 6-hour incubations **(4b)**.

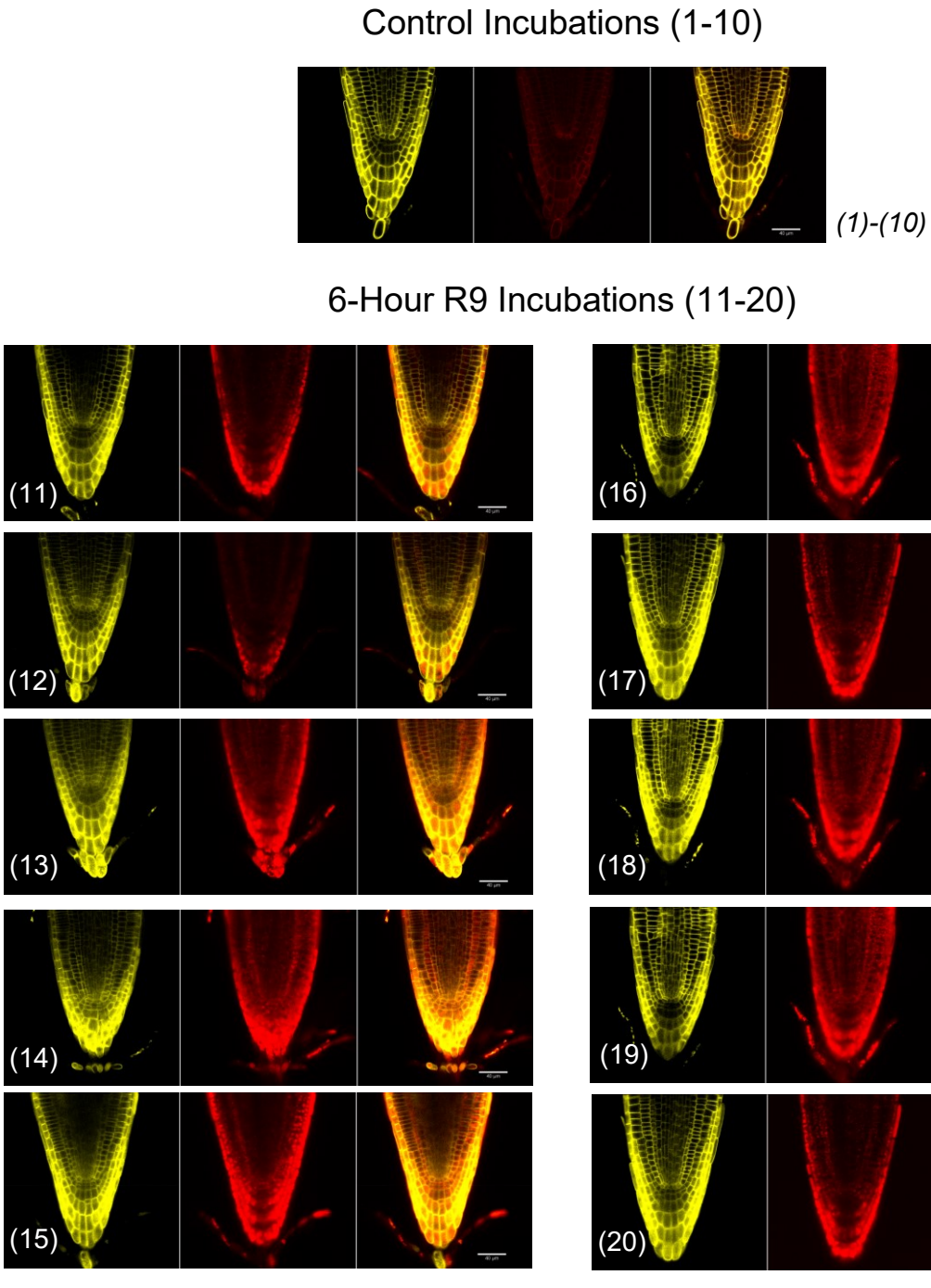


Figure 25 – Control and 6-hour uptake acquisitions for R9 into Wave131 root tips. A representation of the computational assessment of R9 uptake in root tips. 10 control incubations and 10 6-hour R9 incubations were recorded using confocal microscopy.

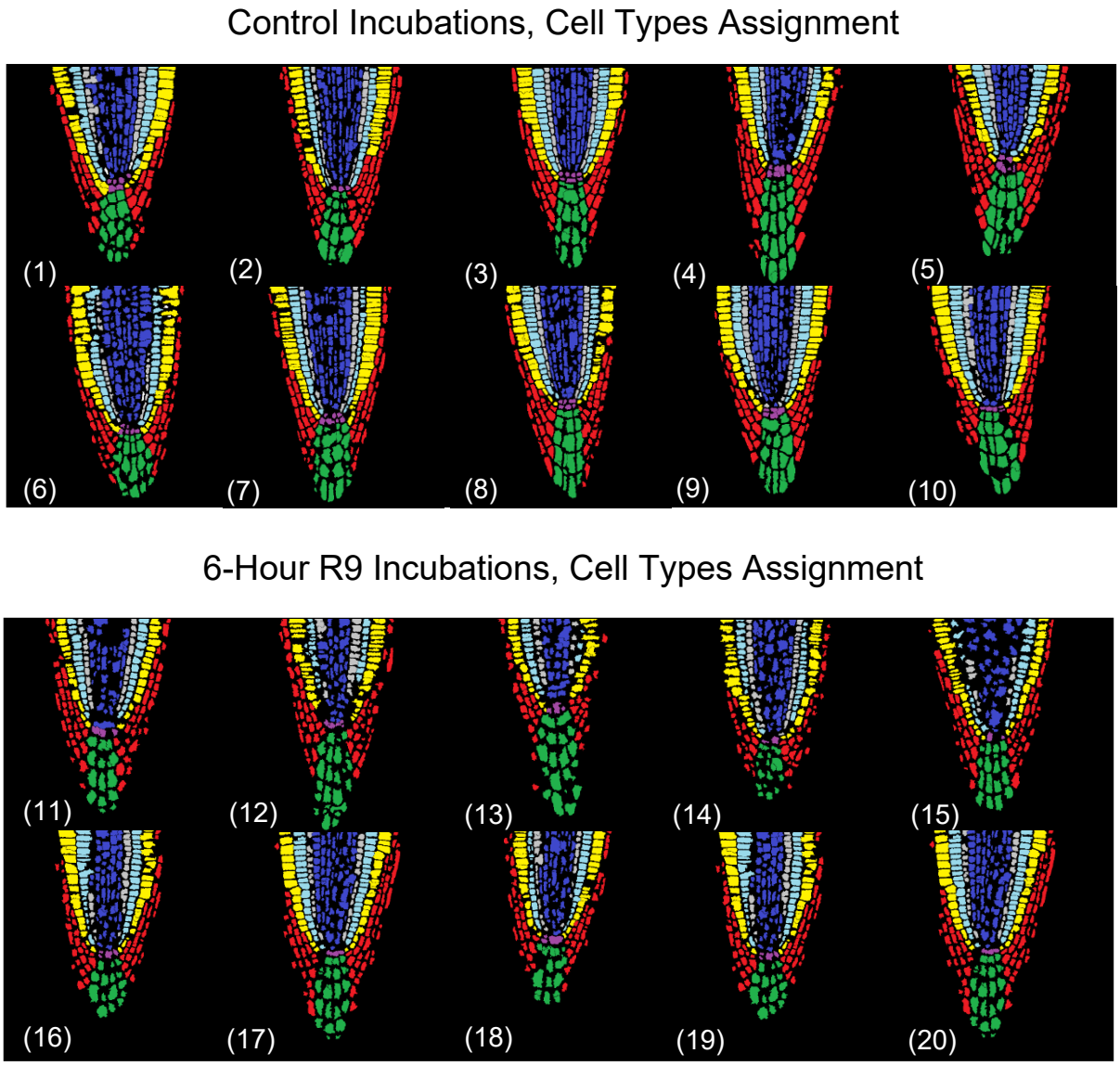


Figure 26 – Computational cell type assignment for control and 6-hour uptake incubations for R9 into WAVE131 root tips. Images from the control incubations and the R9 6-hour incubations. Images **1-10** are the computational representations from the control incubations whereas images **11-20** correspond to 6-hour incubations presented in *Figure 20* above. The original cell assignment was conducted by Anne-Mieke Reijne, the cellular types assignment was conducted manually afterwards.

Control Incubations – Cumulative Cellular Uptake Assessment

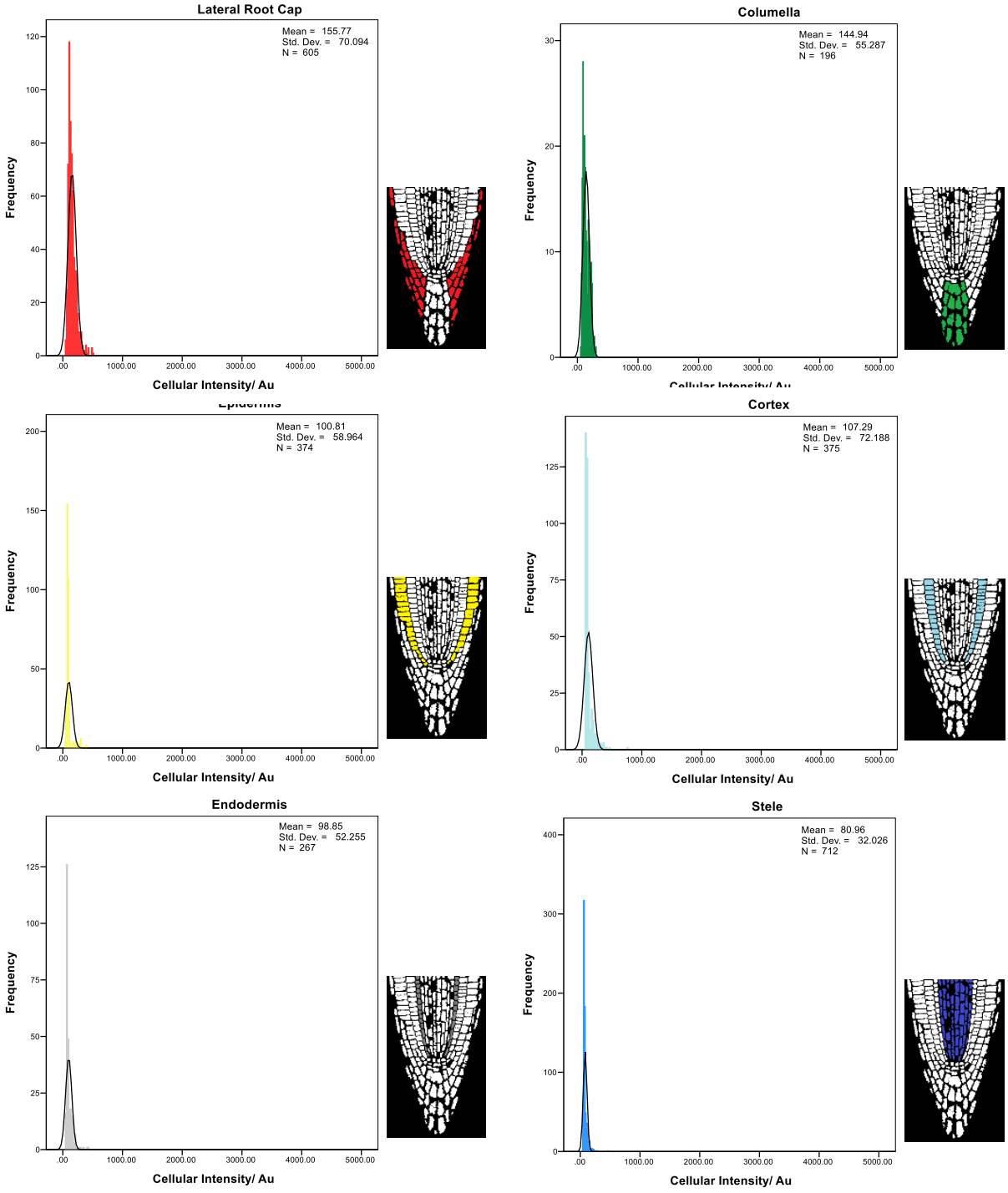


Figure 27 – Control incubations – cumulative cellular uptake assessment. This depicts the fluorescence intensity recorded in control incubations within cells from different cell types within the root. The small fluorescence intensities recorded in the above charts were due to a minimum amount of background channel overlap from YFP into the TAMRA collection window. Normal distributions are given for the fitted curves.

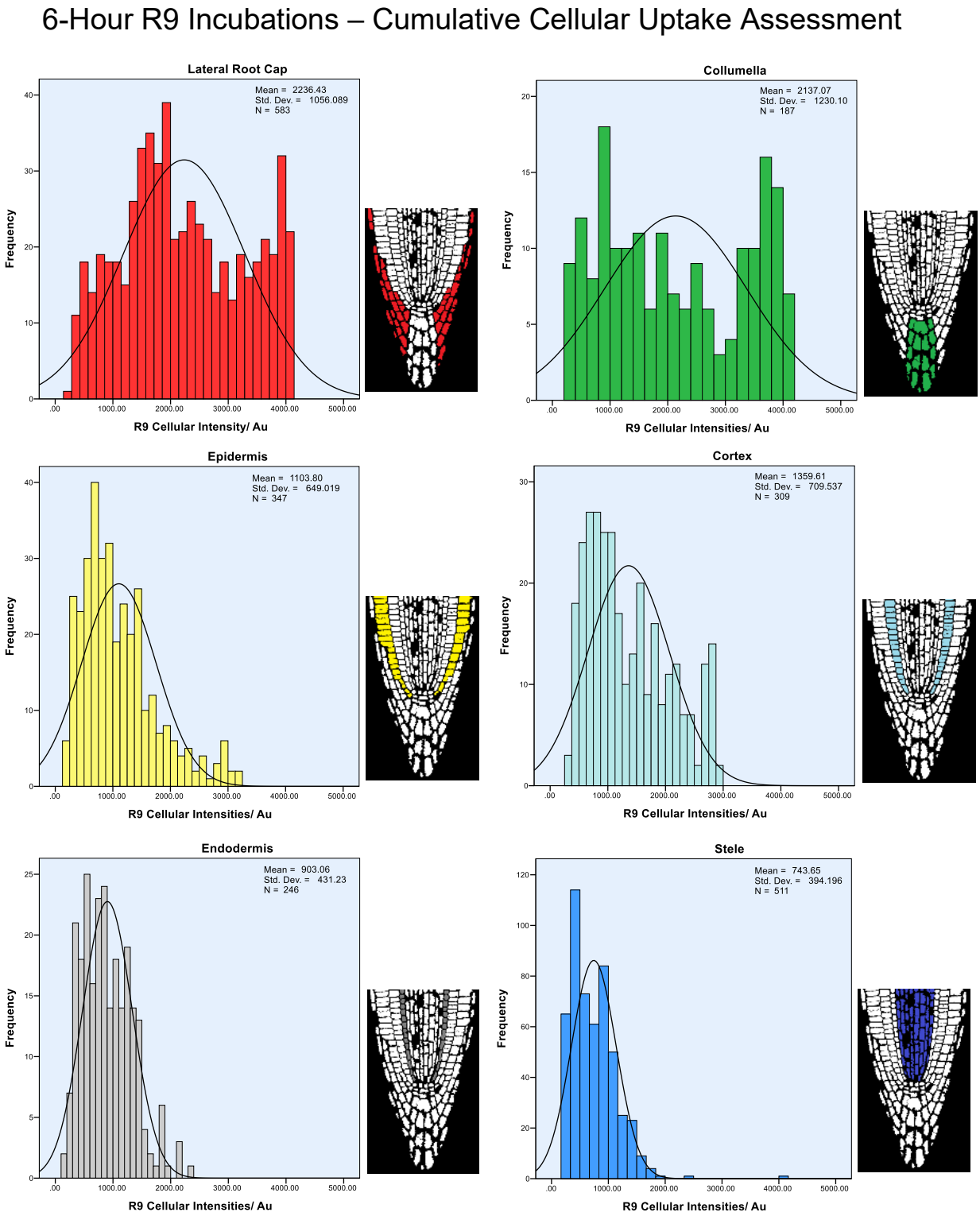


Figure 28 – 6-hour R9 incubations – cumulative cellular uptake assessment. This depicts the fluorescence intensity recorded in the cell types after the 6-hour incubation of R9 with the root tips 11-20. Uptake is recorded for the lateral root cap, columella, epidermis, cortex, endodermis, and stele (which includes the pericycle measurements). The graphs depict the total absorbance intensities for the cell types from all 10 root tips. Fitted curves are for a normal distribution.

A dramatic difference was clear between all the control incubations and their corresponding 6-hour incubations in *Figures 22* and *23*; the small fluorescence intensity recorded for the control incubations was attributed to a slight channel overlap due to a small amount of YFP detected in the TAMRA channel. This was not significant and it is clear to state that the fluorescence recorded from inside the root cells was attributed to the TAMRA-R9 peptide. This was also clear from a qualitative assessment of the confocal images in *Figure 20*. The mean values along with the standard deviations and total number of cells for the different cell types are detailed below in *Table 15*.

Table 16 – Cellular uptake assessment summary. Summary of the uptake fluorescence values for both the control and 6-hour R9 incubations, giving the mean, standard deviation and number of cells recorded for each cell type.

	Uptake Fluorescence Intensity					
	Control Incubation			R9 6-Hour Incubation		
Cell Type	**Mean/ mAu**	**St. Dev./ mAu**	**№ Cells**	**Mean/ mAu**	**St. Dev./ mAu**	**№ Cells**
Lateral Root Cap	155.77	70.09	605	2236.43	1056.09	583
Columella	144.94	55.29	196	2137.07	1230.10	187
Epidermis	100.81	58.96	374	1103.80	649.02	347
Cortex	107.29	72.19	375	1359.61	709.54	309
Endodermis	98.85	52.26	267	903.06	431.23	246
Stele	80.96	32.03	712	743.65	394.17	511

Averages and standard deviations were recorded for each cell type. The highest average intensities were for the lateral root cap (2236.43 mAu) and columella (2137.07 mAu) followed by the cortex, epidermis, endodermis and stele in that order. It is interesting to note that the cortex recorded a higher average intensity that the epidermis (1359.61 mAu vs 1103.80 mAu), perhaps because this cell type is deeper inside the root tip. Another important observation was that the standard deviations were higher for the lateral root cap (1056.089) and columella

(1230.10) and uptake intensities span the full range of intensities. This can be explained quite simply: first; these cell types are layered and the outer cells were likely to absorb more peptide than the inner cells and secondly, whilst the average cellular uptake intensity is calculated in this work, the lateral root cap and columella cells are all different sizes meaning that they have different surface area to volume ratios, a larger surface area to volume ratio allowed more peptide to enter the cells as uptake was not limiting. On the other hand, cells within the epidermis, cortex and endodermis, as layers of cells, reside the same distance from the edge of the root and were consistent in size and therefore surface area to volume ratio. For these two reasons, respective standard deviations (649.019, 709.537 & 431.23) were smaller for the epidermis cortex and endodermis *c.f.* the columella and lateral root cap (1230.10 & 1056.09 respectively).

3.3.3.4 – R9 Uptake into the Shoot Apical Meristem

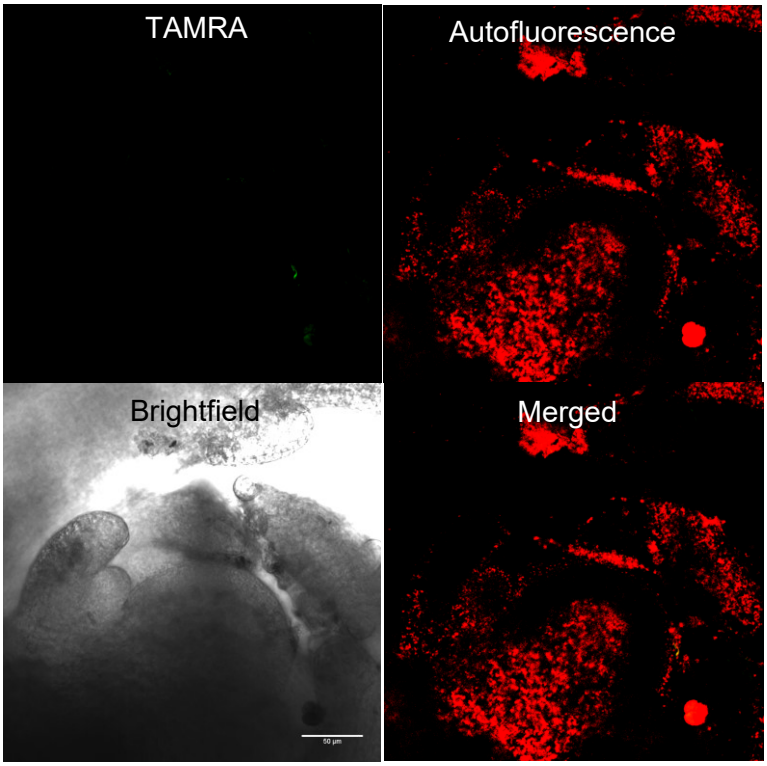
R9 Peptide was delivered to the shoot apical meristem of Arabidopsis and successful uptake of the peptide into both the apical tissue and the leaf primordia was observed. The shoot apical meristem is hidden deep in the centre of the growing tip of the plant and it remains vegetative, retaining a shallow dome-like structure before the response from floral stimulus is detected [82].

In this study, the meristem was exposed by gentle dissection and R9-TAMRA was applied to the apical tissue using a pipette and aided by a dissecting microscope; incubation occurred for 20 minutes. The leaves were then removed from the plant, the meristem was extracted from the tissue by dissection and the cross-section washed and mounted ready for imaging by confocal microscopy; the results are presented in *Figure 24* below. The 63X objective revealed greater cellular detail especially in *Tile 4* below depicting the leaf primordia. R9 is clearly inside the apical cells and the cells of the leaf primordia. Importantly, this represents the first example of cell penetrating peptide uptake into the apical meristem and presents an

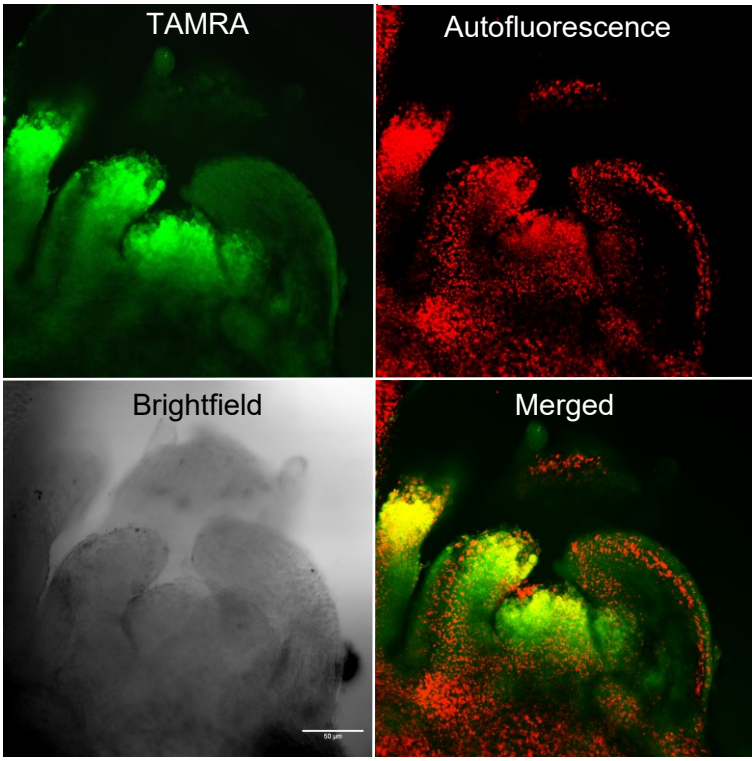
exciting opportunity to target this organ with CPPs and the potential uptake facilitation of their cargos. The z-stack also showed R9 deep inside the tissue of the apical meristem and a three-dimensional projection is presented below. Autofluorescence channels (presented in red) included in the images both confirmed that the fluorescence observed is from TAMRA-R9 and also this helped to visualise the meristem structure. The combination of confocal images and z-stacks, clearly showed R9 present in the apical cells of the plant's stem cell niche.

Apical Meristem Incubations with TAMRA-R9: *(1)-(5)*

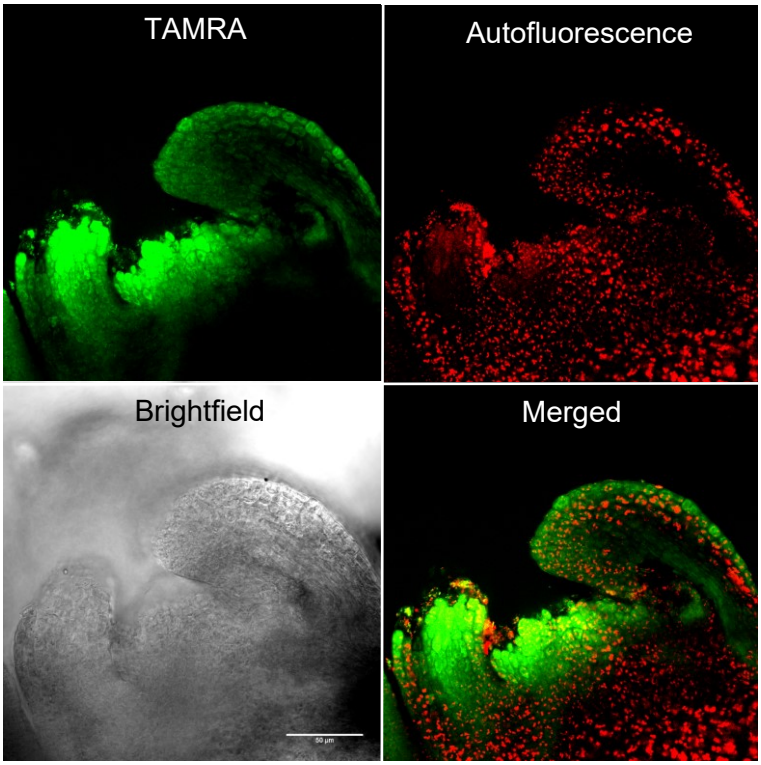
(1) Negative Control Incubation (10X Objective)



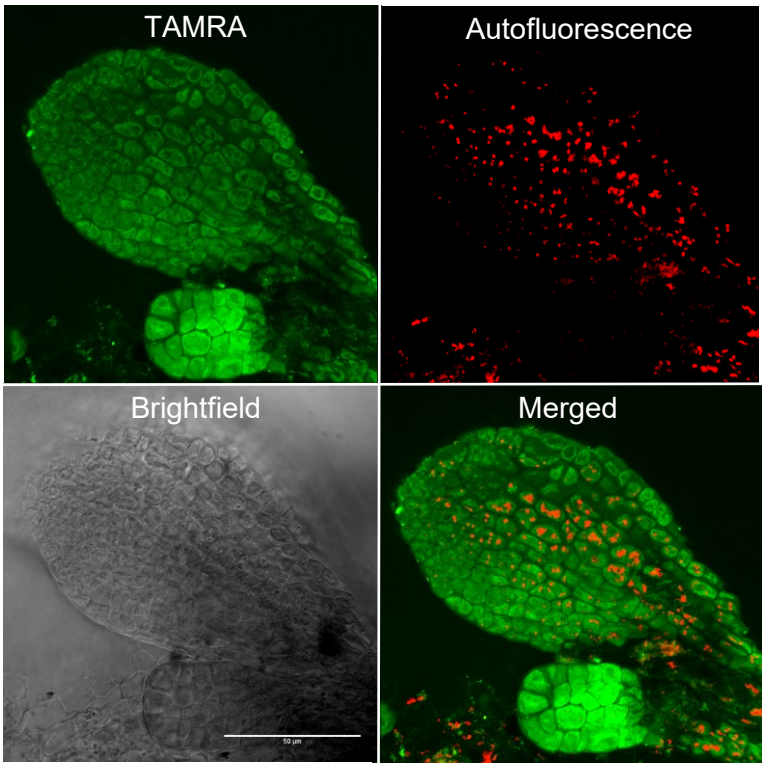
(2) R9 Incubation (10X Objective)



(3) R9 Incubation (63X Objective)



(4) R9 Incubation (63X Objective - Zoom)



(5) R9 Incubation (z-Stack)

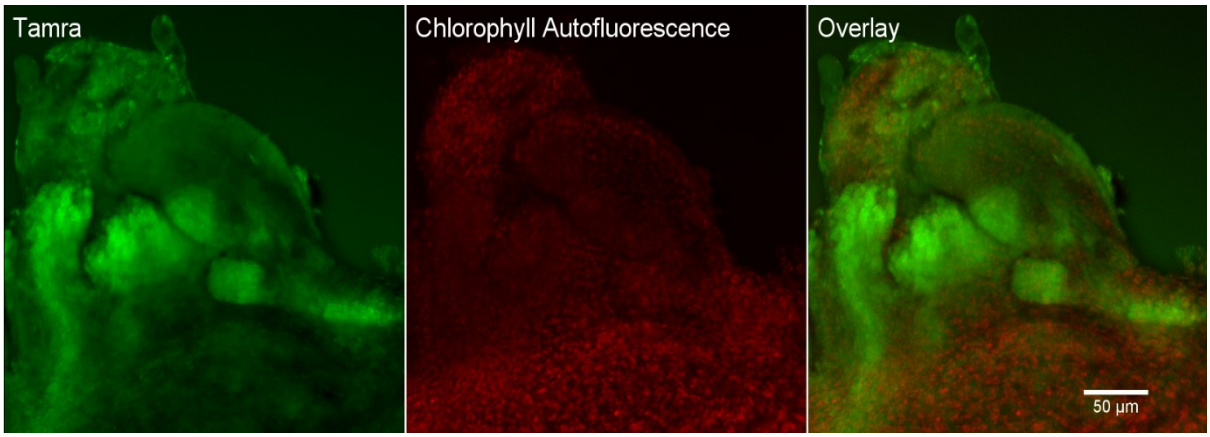


Figure 29 – Apical meristem incubations with TAMRA-R9. **(1)** Negative control incubation with water using a 10X objective, **(2)** R9 incubation recorded with a 10X objective, **(3)** R9 incubation recorded with a 63X oil objective (same meristem as presented in ***(2)***). Apical Meristems presented as a cross section mounted on the imaging slide. **(4)** R9 incubation with the leaf primordia recorded with a 63X objective, **(5)** R9-TAMRA incubation with the apical meristem presented as a z-stack. In the above images peptide is presented in green and the chlorophyll autofluorescence in the red channel.

3.4 – Discussion

This chapter investigated the uptake properties of 4 cell penetrating peptides, Tat, R9, pVEC and TP10 and in particular, an in-depth analysis was conducted into R9 uptake. There are only a small number of examples showing the uptake of cell penetrating peptides in the plant literature - the field is narrow and largely incomplete [138-143]. A mechanistic understanding, taking into account the additional structural features of plant systems, notably the cell wall's influence on uptake, is not properly understood [138-143]. There are isolated examples of Tat, pVEC and TP10 uptake in the plant literature, however an investigation into R9 uptake is missing and this represents a significant area of novelty reported in the results presented in this chapter [138-140]. Moreover, the uptake of R9 into the apical meristem in this thesis, is the first recorded example of CPP uptake into this type of tissue.

The principal technique used to investigate CPP uptake in the literature is fluorescent microscopy, and it is invalid to compare imaging conducted under different acquisition settings. The breadth of literature is small for plant CPPs and is presented in full in *Tables 2* & *3* (*Sections 1.5.3.1 & 1.5.3.2*) indicate that the CPPs and cellular hierarchy examples have been studied primarily in isolation and the depth of research into a particular system is limited. It is important to note that each experiment in a published study has tailored settings which have been determined as a result of the local conditions of the microscope and optimised for collection of a specific sample. In this way, it is not reliable to critically compare confocal imaging results from different literature studies. This study enabled the direct comparison of Tat, R9, pVEC and TP10 under the same settings with a model system, namely root tips which were standardised from the quiescent cells in the centre of the root.

3.4.1 – Analysis of R9 Uptake

R9 and Tat are the most commonly reported CPPs in the plant literature for covalent and non-covalent delivery of protein cargos [133, 140, 144, 148, 150]. The independent uptake of Tat has been investigated however the independent uptake of R9 has not been studied in plant systems [133, 140, 144, 148, 150]. This is surprising as it is essential to understand the uptake behaviour of the CPP before it is tested as a facilitation tool for the transport of protein cargos. For this reason, particular attention is given to the uptake action of R9 in this work.

Previously reported examples of R9 mediated protein delivery have reported the location of the cargo, through intrinsic protein fluorescence [133, 146]. Chang *et al.* showed that the non-covalent delivery of GFP and RFP by R9 into onion root tips and empirical evidence showed the uptake of GFP and RFP inside the cells [133]. The uptake action of R9 is however omitted from the discussion and its influence on protein cargo uptake is unclear without fluorescent CPP labelling [133].

In this study, R9 coupled to TAMRA, was used to assess R9 uptake characteristics in experiments showing the location of peptide in experiments and its uptake over a time course. The uptake of R9 is reported with an analogous behaviour to Tat; uptake is dependent upon a time course and required 6 hours to enter inside cells. Initial incubation after 20 minutes showed R9 attached to the cellular boundaries; R9 was then shown inside the cell after 6 hours, and this was confirmed using PI and a dual channel image. Chang *et al.* hypothesise a macropinocytosis mechanism for R9 and the cargo which becomes evident after only a 10-minute incubation with root tips. In contrast, in this study, R9 is not penetrating after 20 minutes and is likely to be interacting with the negatively charged components within the cellulosic cell wall [133, 141, 159]. In other examples, R9 is covalently linked by cloning attachment to the cargo proteins and in the experiments it has been shown to enter onion root tips, tomato root tips and onion epidermal cells (Chang *et al.*), wheat microspores (Bilichak *et al.*) and

again, onion root tips (Lu *et al.*) [146, 148, 150]. The covalent attachment of CPPs to FT protein cargo is reported and analysed in depth in *Chapter 4*.

3.4.1.1 – Quantitative Assessment of R9 Uptake

In this work, the quantitative assessment of R9 uptake into the root tip cells is the first reported computational analysis of CPP uptake into the root tip (performed by collaborator Anne Mieke-Reijne). It showed the uptake profiles into different cell layers within the root. The quantitative assessment outlined the consistency of R9 uptake from the corresponding confocal images (*Figure 20*). Intuitively, the highest recorded mean uptake per area of the cell was for the lateral root cap, seconded by the columella as these are positioned on the outside of the root. Indeed, standard deviations for the lateral root cap and columella are higher than the epidermis, cortex and endodermis due to differences in their structural alignments and surface area to volume ratios.

WAVE131 was chosen in this experiment to highlight cell boundaries instead of using a propidium iodide stain for 3 reasons [153]. The system was simplified because the fluorescence is inherent to the root tip and a stain does not have to be applied after the incubation. The fluorescence intensity was consistently comparable between root tips whereas a propidium iodide stain intensity depended on the time for applying the stain. Moreover, the fluorescence intensity of WAVE131 was more consistent across the root, this was not the case for a propidium iodide stain as the intensity is higher for the outer cells than the inner most cells of the stele; in effect WAVE131 allowed better visualisation of the inner cells within the root tip [153].

3.4.1.2 – R9 Shoot Apical Meristem Delivery

This study presented the first recorded example of CPP (R9) delivery to the apical meristem. External delivery of CPPs to the meristem offers an exciting opportunity to deliver cargos to this growing centre of the plant. This result indicated that it is possible to dose this structure with CPP and as is discussed later in the thesis - the delivery of recombinant FT coupled with CPP. It is interesting to note that R9 was able to enter directly into the apical meristem cells and CPP was not observed attached to cellular boundaries after 20 minutes. Perhaps these cells were more supple than the root tip and leaf culture cells.

3.4.2 – The Effect of the Cell Wall on Uptake

Whilst protoplast experiments are a useful model to study the fundamental uptake properties of CPPs across a plant cell membrane, they are misleading when assessing the uptake in plant systems as a whole due to their lack of a cell wall. The advantage of using protoplasts, is as a comparative tool to draw comparisons with the wider and more expansive mammalian CPP literature [139]. The cell wall is the most significant difference between plant and mammalian systems when considering CPP uptake. Whilst the structure is porous, the ability of molecules to pass through the matrix is subject to size and charge [141, 162]. The effect of the cell wall was first addressed in tobacco suspension cell culture with a group of poly-arginine peptides - R4, R8 and R12 [141]. The best uptake in this study was reported for R8, the localisation was reported in the cell walls of tobacco suspension cells and the authors hypothesised that guanidinium groups might interact with the negative charges of the carboxylate groups in the cell wall matrix [141]. In this thesis, a parallel finding was observed; peptide was reported attached to the cell wall after an initial 20-minute incubation for both root tips and leaf cell culture and as such a direct penetration mechanism was hypothesised including the effect of the cell wall.

3.4.3 – Poly-Arginine Uptake Mechanism in Plants

Direct penetration is the preferred explanation for cellular entry of arginine rich CPPs - Herce *et al.* proposed a mechanism for mammalian systems based on the interaction of guanidinium groups of the arginine residues with membrane fatty acids such as oleic acid and linoleic acid; and the pH gradient that exists across the cell membrane from a higher extracellular pH to a protonating environment on the inside of the cell [132]. Importantly the pKa of fatty acids in a bilayer is around the neutral mark allowing for both deprotonation and protonation across a cell membrane enabling poly-arginine interaction; importantly guanidinium groups maintain a positive charge across this pH range [132, 163, 164].

In short, Herce *et al.* proposed that deprotonated fatty acids allow guanidinium groups to bind on the extracellular side, a cavity is then created in the membrane and after direct infusion through the bilayer [132]. This maintains a configuration and orientation that shields the charged molecule from the hydrophobic interface [132]. Fatty acids are then protonated when in contact with the cytosol allowing release of the peptide inside the cell; the cavity then closes [132]. This mechanism explains the ubiquitous action of arginine rich CPPs across mammalian cell lines [132].

In particular, in plants the proposed mechanism below in *Figure 25* includes the cell wall, hypothesising that a high concentration of arginine-rich CPP around the membrane is created by CPP interaction with the negatively charged components in the cell wall [141, 159]. This interaction helps to bring the peptide close to the cell membrane creating a gradient enabling the peptide to enter the cell via direct penetration. The mechanism, proposed in this thesis, is depicted in *Figure 30* below.

In plants however, the effect of the cell wall poses an additional requirement to the entry mechanism as the extracellular pH is also acidic and as such the pH gradient across the

membrane does not occur [165]. Acid growth is the specific term detailing the cell wall's ability to expand under acidic conditions caused by auxin secretion leading to protons being pumped into the cell wall cavity [165]. This expansion is due to a protein called expansin which elongates the networks of structural microfibrils in the cell wall under acidic conditions, the internal cell volume increases due to an influx of osmotic turgor [165]. The acid growth phenomenon maintains the primary cell wall at pH 4.5 and this is lower than the physiological acid pH of the cytosol [165].

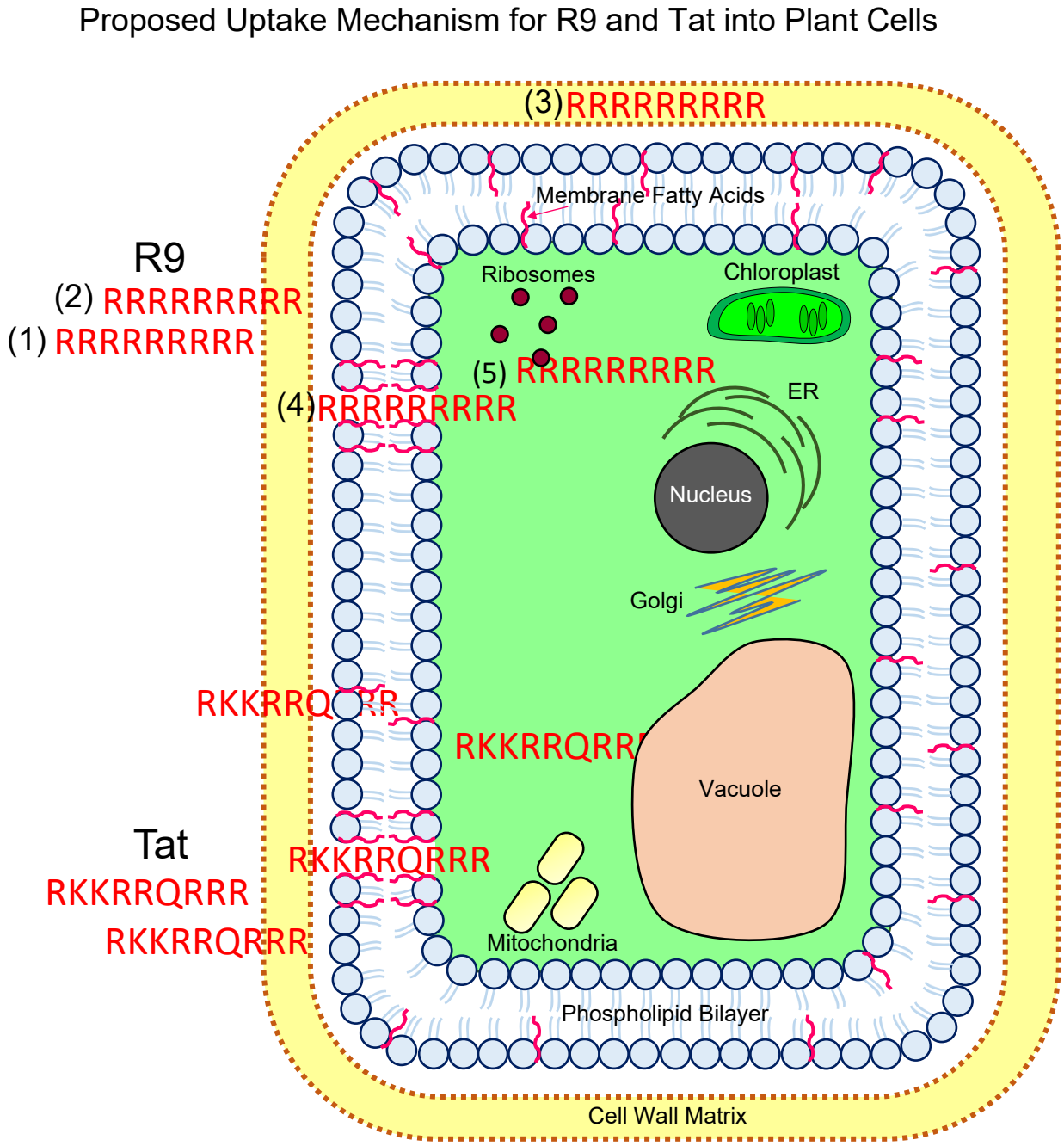
Another difference between plant and animal cells is the composition of the membrane. In particular the fatty acid composition which Herce *et al.* evoke as the key facilitator in the transduction mechanism [132]. Phytosterols take the place of cholesterol and the main lipid constituents of plant cell membrane are glycerolipids. A much higher percentage of the plant cell membrane is comprised of fatty acids compared with mammalian cells. Around 30% of the plant cell membrane is comprised of fatty acids compared to 1% in mammalian cells [166] [132].

The universal mechanism proposed by Herce *et al.* needs to be modified for plant specific entry, and a revised version is proposed based on the experimental evidence collected within this study [132]. Arginine rich peptides clearly attach to the cell wall and this is observed in the results for root tips and leaf cell culture.

The opposite gradient exists whereby the extracellular pH of the acidic cell wall is lower than the cytosolic pH. This means that fatty acids are deprotonated on both sides of the membrane. Fatty acids are cited in a flip-flop mechanism and with a 30-fold higher concentration of fatty acids this 'flip-flop' could incorporate CPP delivery facilitating the passage of peptide through the hydrophobic core [167] . CPP is already in a high concentration and in close proximity to the membrane through cell wall interaction observed in the experimental evidence from this chapter. The high availability of CPP might could enable incorporation within the 'flip-flop' of

fatty acids [167] . Membrane association is not important as CPP is already readily abundant and in high concentration in close proximity to the membrane within the cell wall cavity.

The proposed mechanism is non-invasive, energy independent, and involves spontaneous infusion of peptides through the bilayer in a non-endocytic manner [132]. Whilst previous hypotheses have stated the role of phospholipids (and their polar charged heads) in an internalisation mechanism they only explain how a peptide interacts with the membrane surface and not how the charged molecule passes through the hydrophobic barrier, Herce *et al.* proposed that phospholipids are only important in membrane association of arginine rich CPPs and do not form part of the internalisation mechanism [132]. This was tested *in vitro* and also using Molecular Dynamics simulations in a stochastic computational system [132]. Other suggested entry mechanisms have proposed inverted micelle formation, whilst this could explain entry inside the cell, it does not account for cytosolic release of the peptide [168]. Herce *et al.* showed, using molecular dynamics, the formation of a water channel enabling the entry of arginine rich peptides through these transient pores [132].



(1) The guanidinium rich CPPs associate with the negatively charged components within the cell wall matrix [159].
(2) CPPs are small and are able to traverse through the porous cell wall matrix.
(3) Tat and R9 surround the cell membrane, and associate with the cell wall, this creates a high concentration of peptide around the membrane.
(4) A direct penetration mechanism involving the flip-flop fatty acid internalisation mechanism and spontaneous insertion into the bilayer [132], [167].
(5) The CPP is released on the cytosolic side and peptide entry into the cell is non-saturable [132].

Figure 30 – Proposed uptake mechanism for R9 and Tat into plant cells. This mechanism accounts for the cell wall matrix on the outer boundary of the membrane. The figure combines observations reported in this chapter for arginine rich CPP interaction with plant cells and the explanations from Herce *et al.* set out both by experiment and with molecular dynamics simulations [132].

3.4.4 – Bespoke Plant CPPs

Eggenberger *et al.* questioned the universality of CPPs suggesting that sequences will need to be reconfigured and optimised to successfully penetrate the cell membrane, due to the differing membrane compositions of plant cells and their mammalian counterparts [142]. Indeed Mäe *et al.* showed reduced uptake of pVEC, TP10, Transportan and Penetratin in triticale protoplasts compared to Bowes human melanoma cells [139]. This opens up the possibility of newly refined CPPs specifically designed for plant cell uptake [142]. The sequence BP100 was tested by Eggenberger *et al.* which is an important agent against Gram-negative plant pathogens [169]. BP100 was developed through rational re-design of Pep3 which was established as a valuable plant-antifungal and bactericidal peptide [169-172].

Lifeact Peptide was discovered from a domain in yeast protein Abp140p and was shown to universally bind to actin in higher eukaryotes [173]. Lifeact can be used in tandem as a GFP fusion for binding and labelling of native actin filaments in a system, and this approach has been shown in plants with the transgenic expression of a fluorescent protein fused to Lifeact [173, 174]. Eggenberger *et al.* presented the first example of extracellular delivery of Lifeact using the BP100 cell penetrating peptide, presenting an elegant solution for actin labelling in tobacco suspension cells without the need for large fusion constructs and laborious genetic transformation methods [142]. The fast uptake rate of BP100 when compared to an FD-4 (fluorescent dextran classically used to show endocytic uptake) control for endocytosis suggested that another mechanism was present in this case [142, 175].

Whilst time limitations prevented the assessment of BP100 uptake in this thesis, an interesting study would be to assess the properties of bespoke plant CPPs with the arginine rich sequences, Tat and R9, which are proven to work successfully within this chapter. BP100 is lysine rich and previous reports have stated arginine rich sequences as superior to lysine rich

sequences in model membranes as such in this study, Tat and R9 were prioritised for investigation [132].

3.5 - Conclusion

This chapter assessed the independent uptake action of R9, Tat, pVEC and TP10. In the root tip uptake model, a clear difference was observed between the cellular penetrating capacity of the cationic R9 and Tat sequences and the hydrophobic pVEC and TP10 sequences. R9 and Tat clearly enter cells after a 6-hour incubation whilst pVEC and TP10 remained trapped in the outer lateral root cap and this was confirmed using a propidium iodide cell wall indicator. The cell wall forms an important part of the uptake mechanism and R9 and Tat were clearly shown attached to this cellular component after a 20-minute incubation, this enabled to peptide to reside in close proximity to the cell membrane for affective penetration. This observation was also corroborated in cell culture and quantitative ImageJ analysis showed R9 attached to the cell wall at 20 minutes before internalisation after a 6-hour incubation.

An in-depth assessment of R9 uptake into plant tissue was recorded and in total this included root tips, leaf mesophyll cell culture, protoplasts, and apical meristems. Successful uptake was recorded except for protoplasts. In this case the turgidity of the cell membrane was compromised by the highly charged R9 peptide, and the protoplasts collapsed into cytoplasts as small membranous spheres containing fluorescence. The uptake of R9 into the apical tissue is the first reported targeting of this organ with CPPs. This opens up exciting opportunities to target the apical tissue with the CPP mediated delivery of macromolecular cargo.

A novel method was developed to quantitatively assess the uptake of R9 into the Arabidopsis root tip. This enabled segmentation of uptake into the different cell types within the root tip. The lateral root cap and the columella recorded the highest peptide penetration but large standard deviations were linked with different cell sizes in these cell types. More

consistent uptake was recorded for the cortex, epidermis and endodermis with lower uptake standard deviation due to consistent cell sizes across the cell type.

The main aim of this chapter was to test out the independent action of CPPs, before they are assessed for their ability to facilitate the transduction of FT inside of cells. In light of this, the successful cationic R9 and Tat CPPs can be pooled and used in further investigation for the delivery of FT into cells which is reported in *Chapter 4* and *Chapter 5*.

4. Results 2 – Tools to Assess Cellular Delivery of FT using Tat and R9

4.1 – Introduction

This chapter reports the development of recombinant FT protein tools using the CPP technology. In addition to technical results, this chapter assessed both covalent and non-covalent protein transduction using the R9 and Tat CPPs which were reported with successful uptake properties into Arabidopsis tissue in *Chapter 3*. Consideration was given to whether R9 and Tat can facilitate the delivery of FT inside cells as this is an essential requirement before artificial floral activation can be assessed.

A small number of examples exist in the plant literature, citing the use of CPPs as a delivery tool for recombinant proteins and both covalent and non-covalent technologies have been successfully tested in plant systems, albeit overwhelmingly with cargo lacking endogenous function such as the fluorescent GFP and RFP proteins [133, 146, 149, 150]. This is in contrast to the wide range of examples cited in the mammalian literature; as such, it is possible to detail a complete list - given in *Table 3* in *Section 1.5.3.2* [176, 177]. In this chapter, tools were designed to incorporate the CPP technology into the recombinant FT sequence and this is significantly novel as it is the first reported example of an endogenous and functional plant protein cargo attached to a CPP tested in a biological system.

Literature examples are reported for R9 and Tat CPPs as delivery vehicles for protein cargo in plant systems including the fluorescent proteins GFP and RFP and also GUS enzyme for histochemical staining [133, 140, 144, 146, 149, 150]. Moreover, examples are recorded for both covalent and non-covalent delivery in different tissues, including root tips, microspores, immature embryos and epidermal cells; and these include different organisms such as tomato,

corn, onion and triticale [133, 140, 144, 146, 149, 150]. This is a brief and succinct summary of the literature which is critically assessed in the discussion section in this chapter.

4.2 – Experimental Aims for the Chapter

1) Build a set of tools that covalently link Tat and R9 cell penetrating peptides with recombinant FT protein. In this way build the set of modified Florigen proteins, FT, FT-Tat and FT-R9.
2) Design an approach to visualise FT, FT-Tat and FT-R9 *in vivo.* In this way, construct a recombinant GFP fusion with FT and use Sortagging to selectively label FT, FT-Tat and FT-R9 with a TAMRA fluorophore.
3) Assess delivery and uptake of FT-Tat and FT-R9 inside cells, compared with FT.
4) Assess non-covalent delivery of FT inside cells.
5) Critically assess the results and determine if the outcomes could be extrapolated and used to artificially activate AP1 in vivo.

4.3 – Results

4.3.1 – Purifications for FT, FT-Tat and FT-R9

The C-terminus of FT was modified with Tat and R9 insertions using site directed mutagenesis. FT in a pET-28b vector was gifted by David Charles and this contained the native FT sequence along with a His-tag and thrombin recognition motif at the N-terminus [41]. After thrombin cleavage, a G-S-H sequence was retained in front of the original start methionine of native FT. FT, FT-Tat and FT-R9 sequences along with their respective molecular weights and isoelectric points are presented below. The isoelectric points for FT-Tat and FT-R9 are higher due to the addition of arginine residues into the protein sequence.



FT

MGSSHHHHHHSSGLVPRGSHMSINIRDPLIVSRVVGDVLDPFNRSITLKVTYGQREVTNGLDLRPSQVQNKPRVEIGGEDLRN
FYTLVMVDPDVPSPSNPHLREYLHWLVTDIPATTGTTFGNEIVCYENPSPTAGIHRVVFILFRQLGRQTVYAPGWRQNFNTRE
FAEIYNLGLPVAAVFYNCQRESGCGGRRL

FT-TAT

MGSSHHHHHHSSGLVPRGSHMSINIRDPLIVSRVVGDVLDPFNRSITLKVTYGQREVTNGLDLRPSQVQNKPRVEIGGEDLRN
FYTLVMVDPDVPSPSNPHLREYLHWLVTDIPATTGTTFGNEIVCYENPSPTAGIHRVVFILFRQLGRQTVYAPGWRQNFNTRE
FAEIYNLGLPVAAVFYNCQRESGCGGRRL**RKKRRQRRR**

FT-R9

MGSSHHHHHHSSGLVPRGSHMSINIRDPLIVSRVVGDVLDPFNRSITLKVTYGQREVTNGLDLRPSQVQNKPRVEIGGEDLRN
FYTLVMVDPDVPSPSNPHLREYLHWLVTDIPATTGTTFGNEIVCYENPSPTAGIHRVVFILFRQLGRQTVYAPGWRQNFNTRE
FAEIYNLGLPVAAVFYNCQRESGCGGRRL**RRRRRRRRR**

Properties of FT, FT-Tat & FT-R9			
	FT	FT-Tat	FT-R9
MW (kDa)	21.97	23.29	23.38
Residues	195	204	204
pI*	8.53	10.07	10.44

M - Start methionine in construct
HHHHHH – His-tag
LVPRGS - Thrombin recognition motif
M - Start methionine of native FT protein
RRRRRRRRR - R9
RKKRRQRRR - Tat

*Theoretical pI determined by ExPASy ProtParam tool

Figure 31 – Introduction of Tat and R9 sequences at the C-terminus of FT. Protein sequences are given for FT, FT-Tat and FT-R9. The pET-28b vector included a His-tag, and thrombin cleavage site, the initial methionine of the native sequence is highlighted. The molecular weights, number of residues and isoelectric points are also given in the table.

4.3.1.1 – FT Purification

The original purification of FT was developed by David Charles, this was however 3 steps and did not include a His-tag cleavage step [41]. The first objective was to optimise this purification and the process was reduced to 2 steps with a nickel affinity stepped gradient, and a His-tag cleavage step. The main steps for the purification using an FPLC are outlined below (*Text Insert 1*) rather than in the *Materials and Methods* section, in this way they can be interpreted alongside the purification chromatograms in *Figure 27*. A robust, successful and reproducible FT purification was of central importance to the work presented in this thesis.

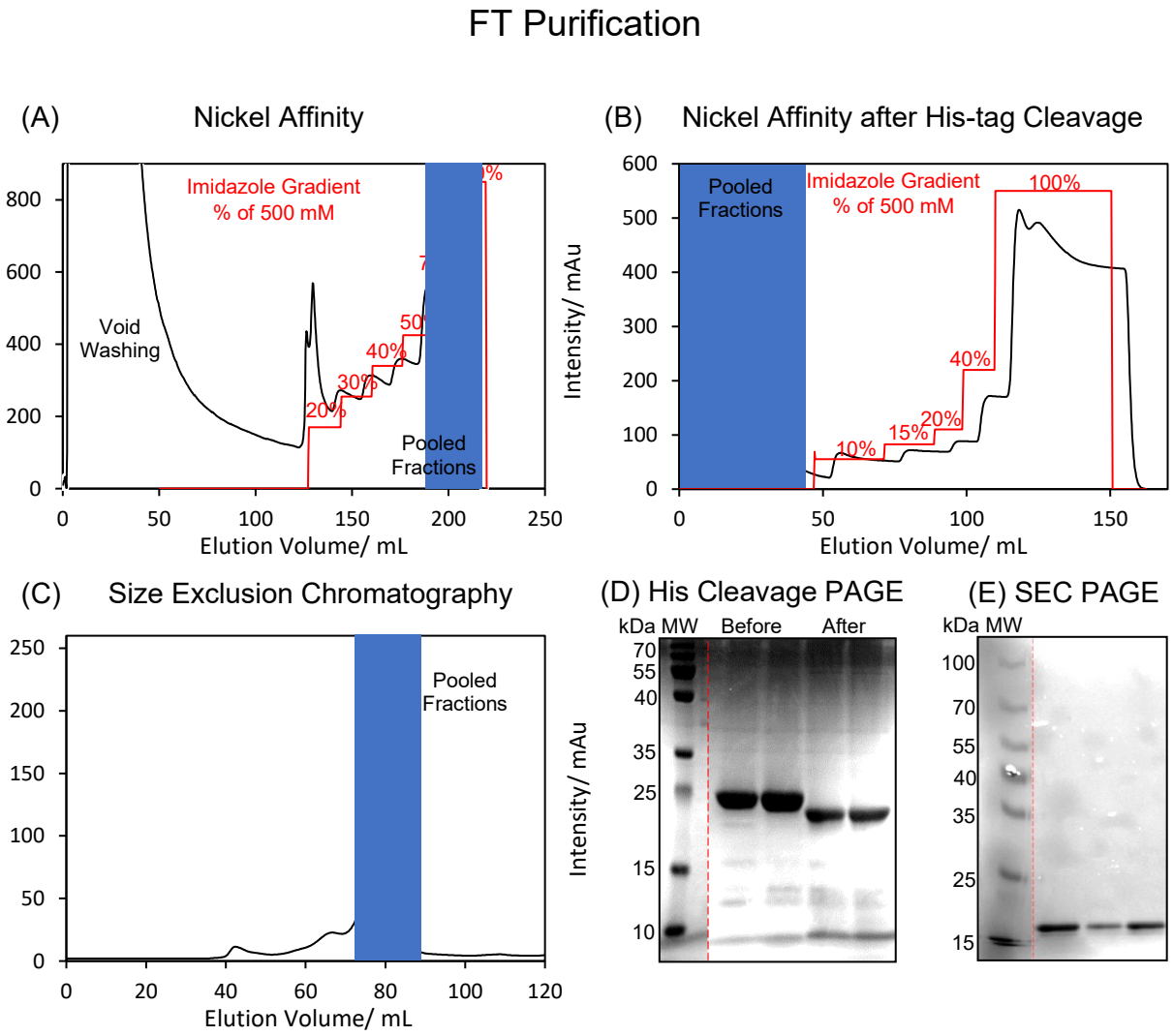


Figure 32 – FT purification with His-tag cleavage. (A) Nickel affinity chromatography stepped imidazole elution to remove impurities and FT eluted between 250-350 mM imidazole (between 50-70% step gradient). **(B)** Thrombin cleavage and removal of uncleaved protein and His-tag by re-passing the reaction through the nickel column – cleaved protein passed straight through the column. **(C)** Size exclusion chromatography of cleaved and pure FT. **(D)** SDS-PAGE showed His-tag cleavage. **(E)** SDS-PAGE of purified FT after size exclusion chromatography. This process was optimised and refined from a protocol from David Charles' thesis, by removing an ion exchange step and adding the His-tag cleavage step [41].

Stages of FT Purification – Key Points

(A) Nickel Affinity

- The nickel column was loaded with lysate and washed until the flow-through reached baseline UV output.
- Imidazole elution as a percentage of 500 mM imidazole concentration and FT eluted at between 50-70% gradient (250-350 mM imidazole).

(B) His-tag Cleavage

- 4 units of thrombin were used per mg of FT and the reaction performed under dialysis conditions for 4 hours at 4 ºC. Importantly, thrombin cleavage was not left for longer than 4 hours as non-specific digestion was observed for FT, *i.e. the reaction should not be left overnight*.
- Uncleaved protein was removed using a nickel column; cleaved protein passed straight through and fractions were pooled. SDS-PAGE 15% acrylamide gels depicted successful cleavage. 15% acrylamide (*c.f.* 10% acrylamide) was required to show clear gel separation and thus cleavage resolution.

(C) Size Exclusion Chromatography

- A Superdex 75 (SD75) column was used to ensure protein was properly folded and acted as a final separation for impurities. Fractions eluted at 80 mL and SDS-PAGE confirmed the protein purify.

Text Insert 1 – Attached to *Figure 32.* The key details are given for the FT purification reported in *Figure 27* above.

4.3.1.2 – FT-Tat and FT-R9 Purifications

Initially, nickel affinity chromatography was used to purify FT-Tat and FT-R9, with a stepped imidazole gradient - using the same protocol reported above for FT *(Figure 27)*. After nickel affinity chromatography, the size exclusion traces showed that both FT-Tat and FT-R9 were not properly folded - implying the presence of misfolded species in the collection fractions. This was possibly due to an interaction with the positive arginines and imidazole after elution from the nickel column resulting in distortion of the protein's tertiary structure. It is clear that the overlap of fractions and species was overriding and it was not possible to pool fractions for further purification (see *Figure 28*).

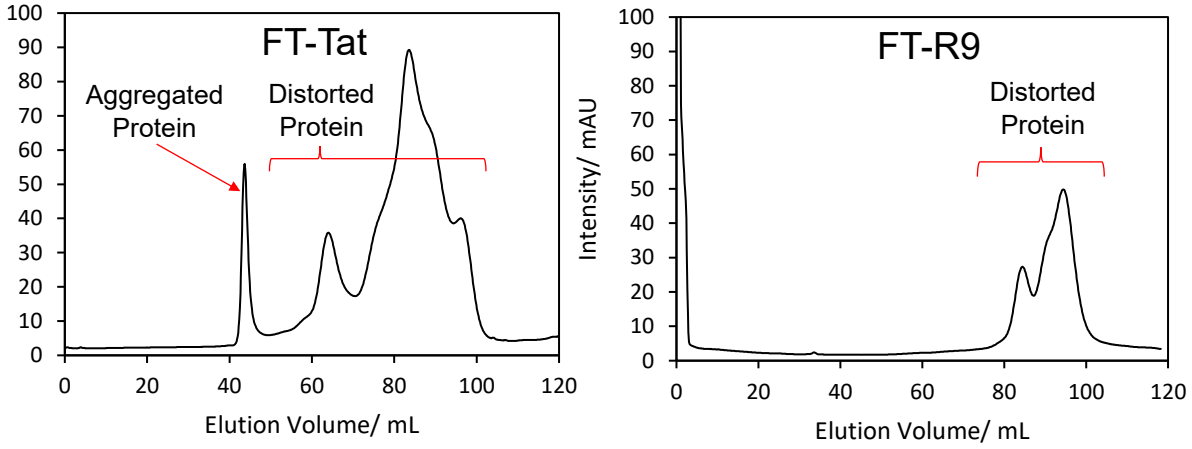
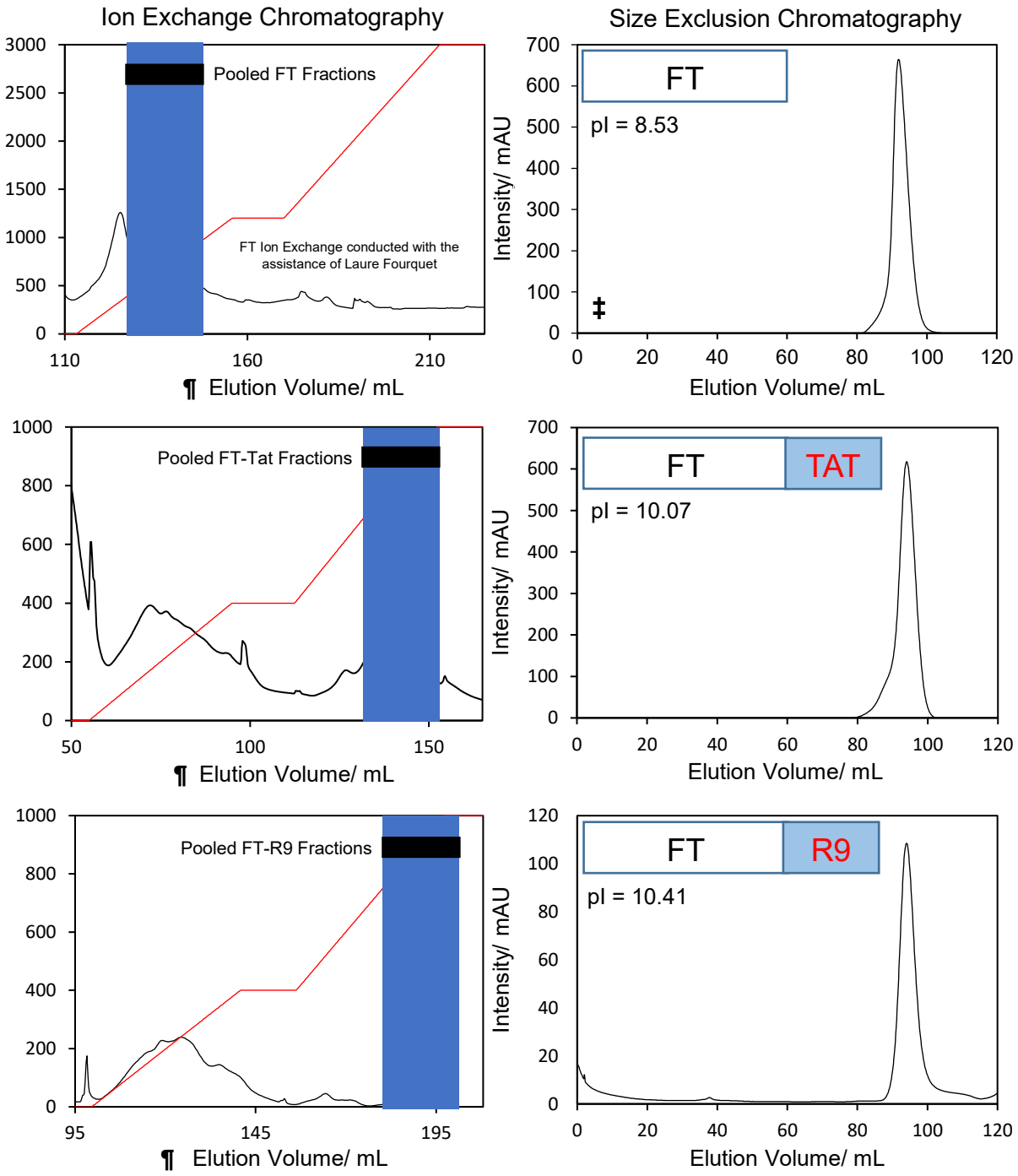
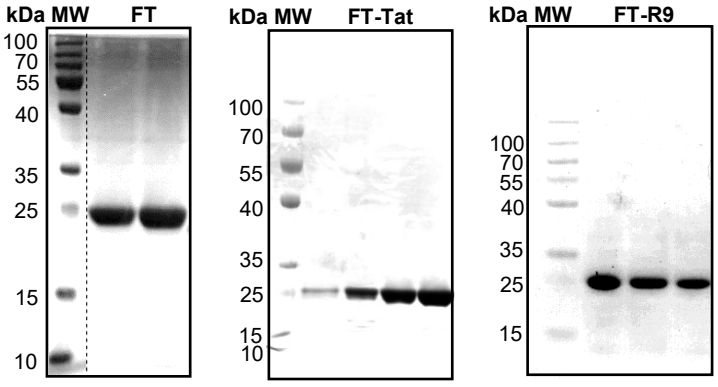


Figure 33 – FT-Tat and FT-R9 SEC traces following nickel affinity chromatography. The SEC traces for FT-Tat and FT-R9 after nickel affinity chromatography. Distorted folding of the protein is clear from both traces, moreover, the integral for FT-R9 is significantly less than for FT-Tat.

A new design for the protocol was required to purify FT-Tat and FT-R9 and as such, a cation exchange column was used in place of nickel resin for the first purification step; this enabled separation of proteins based on their charge. The extent of a highly cationic tail was noticeable as both FT-Tat and FT-R9 eluted around 1 M KCl concentration and a marked difference was observed when compared to FT elution under the same salt gradient, depicted below in *Figure 29*. Whilst the theoretical isoelectric points of FT-Tat (pI=10.07) and FT-R9 (pI=10.44) are moderately higher than for FT (pI=8.53), the real reason for this extreme difference in elution was attributed to the Tat and R9 tags exposed at the C-terminus and they effectively formed a purification tag for cation-exchange chromatography [178].





¶ *The elution volume presented above was from the start of the gradient elution to allow comparison. The different elution volumes corresponded to the different lengths of the void washing as columns were loaded directly from lysate and should be ignored.*

‡ *For FT, nickel affinity chromatography was used in between ion exchange chromatography and gel filtration to purify FT as ion exchange chromatography alone was insufficient to purify FT.*

Figure 34 – Purification properties for FT, FT-Tat and FT-R9. Ion exchange chromatography traces showed the significant difference between FT, and FT-Tat & FT-R9 in their elution volumes - highlighting the impact of the positively charged CPP tag on protein elution. Conversely, size exclusion chromatography showed near identical elution volumes implying the CPP tag has little influence on the hydrodynamic radius of the proteins. SDS-PAGE confirmed protein purity.

The theoretical pI for FT-R9 (10.41) is higher than for FT-Tat (10.07) and this manifested in a slightly later shift in elution for FT-R9 compared to FT-Tat in the cation exchange chromatogram. The extreme late elution of FT-Tat and FT-R9 was useful as contaminant *E. coli* proteins did not interact with the column at this high salt elution concentration and hence this avoided the need for a second purification step. The area under the FT-R9 peak is significantly lower than for FT-Tat (as deduced qualitatively), correlating with a lower overexpression for FT-R9 than for FT-Tat; conceivably this was down to the inability of the bacterial system to process an unnatural set of 9 contiguous arginines. In contrast, the 6 arginines present in the Tat sequence (RKKRRQRRR) are interspaced with two lysines and a glutamine and thus bacterial overexpression is more straightforward. In addition, the size exclusion chromatography traces for FT, FT-Tat and FT-R9 showed consistent elution volumes with a minute shift for FT-Tat and FT-R9 compared to FT. This was attributed to the slightly larger hydrodynamic radius created by the cationic tag. In light of this, the results showed that FT-Tat and FT-R9 are properly folded when assessed against FT (*c.f.* FT-Tat and FT-R9 size exclusion chromatography traces in *Figure 28*).

4.3.2 - Development of Fluorescent Protein Tools

4.3.2.1 – FT-GFP Cloning and Purification

The classical way of visualising a target protein in a living system is via a GFP fusion protein – fluorescent microscopy can track spatial location [179]. This transgenic approach is widely used and is important in providing spatial and temporal information *in planta*, moreover the transgenic expression (and overexpression) of FT-GFP has been reported to accelerate flowering with GFP but having little impact on observed endogenous FT function [179],[180],[181],[15]. An objective for this work was to track recombinant FT, introduced exogenously into biological samples; as such a purification for recombinant FT-GFP was developed. The Gibson Assembly technique was used to join the GFP with a short glycine/serine linker to the C-terminus of the FT sequence, as such removing the FT stop codon. Cloning details and purification are given below in *Figures 30* & *31*. The protocols for protein purification are described in the materials and methods chapter, however important considerations for the FT-GFP purification are outlined in *Text Insert 2*.

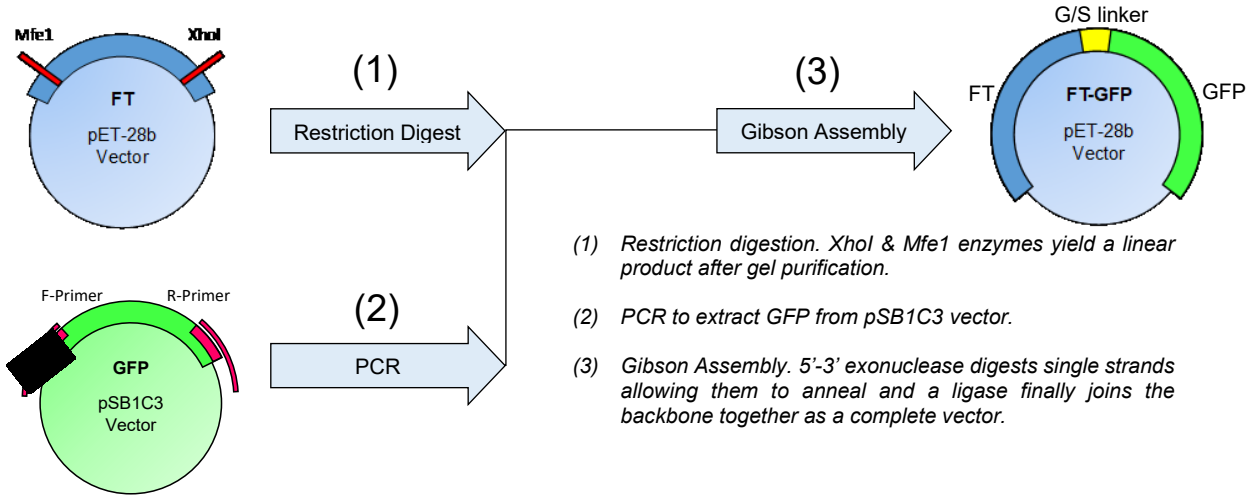


Figure 35 – FT-GFP construction using Gibson Assembly. A schematic is presented for the design and assembly of the FT-GFP fusion protein, including a short glycine/serine linker joining the FT and GFP constructs in the pET-28b vector. Forward and reverse primers were designed with the help of collaborator, Alex Nash.

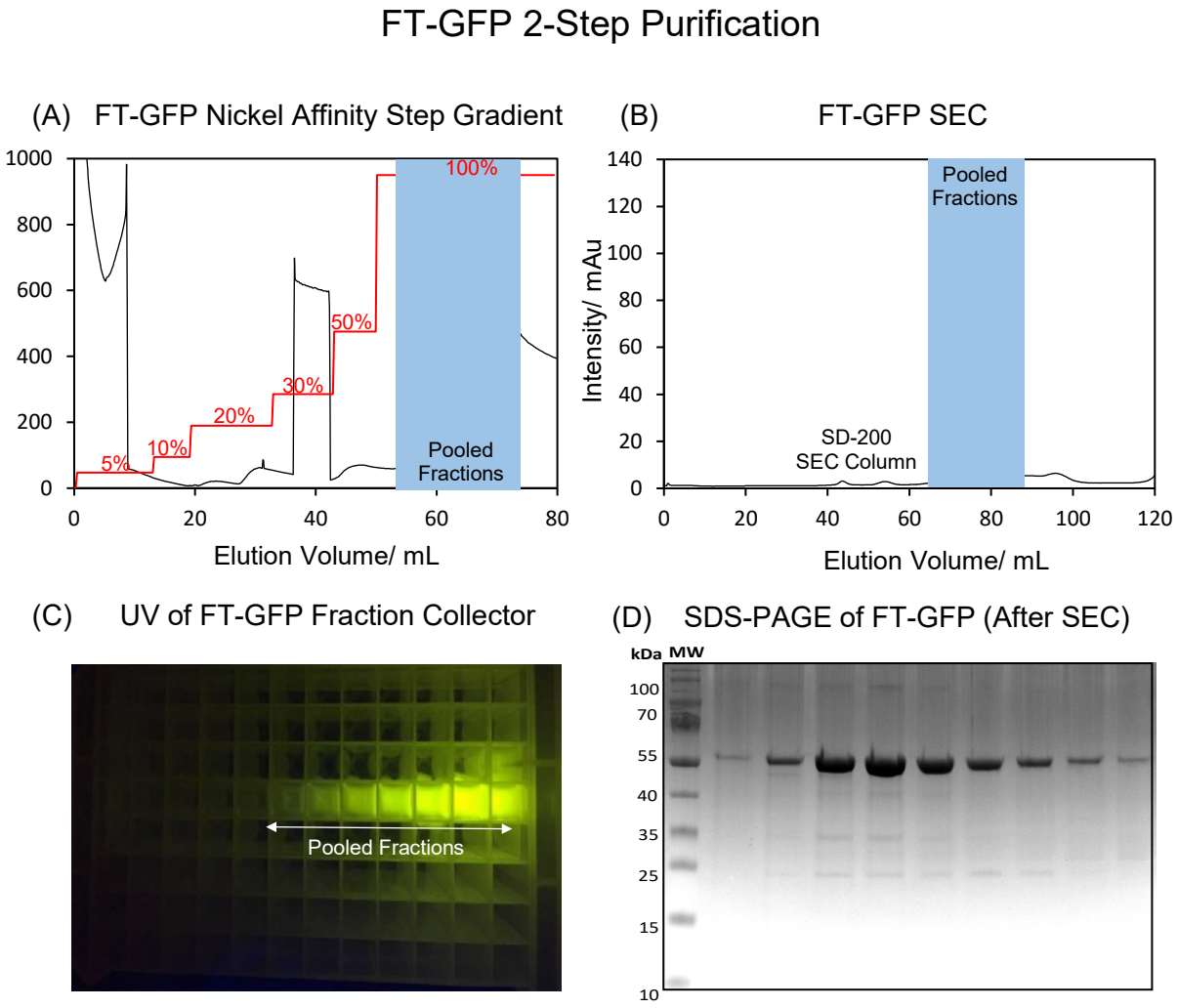


Figure 36 – 2-step purification of FT-GFP. (A) – Stepped gradient of imidazole during nickel affinity chromatography; a high concentration of imidazole was required and protein eluted at 500 mM imidazole. **(B)** – SEC trace with an SD 200 column, protein was properly folded, shown by the symmetrical SEC trace. **(C)** – the fraction collector from the SEC under UV light showed the position of fluorescent FT-GFP from the elution. **(D)** – SDS-PAGE after SEC confirmed protein purity and appeared at the correct molecular weight.

Stages of FT-GFP Purification – Key Points

(A) FT-GFP - Nickel Affinity

- FT-GFP elution required 500 mM imidazole (100% elution buffer), this high concentration required immediate dialysis to remove imidazole from pooled fractions.

(B) FT-GFP - Size Exclusion Chromatography

- Protein eluted according to its hydrodynamic radius index at approximately 77 mL. Pooled fractions were checked for functionality using a UV light source, and green fluorescence observed as shown in *(C)* in *Figure 31* above.

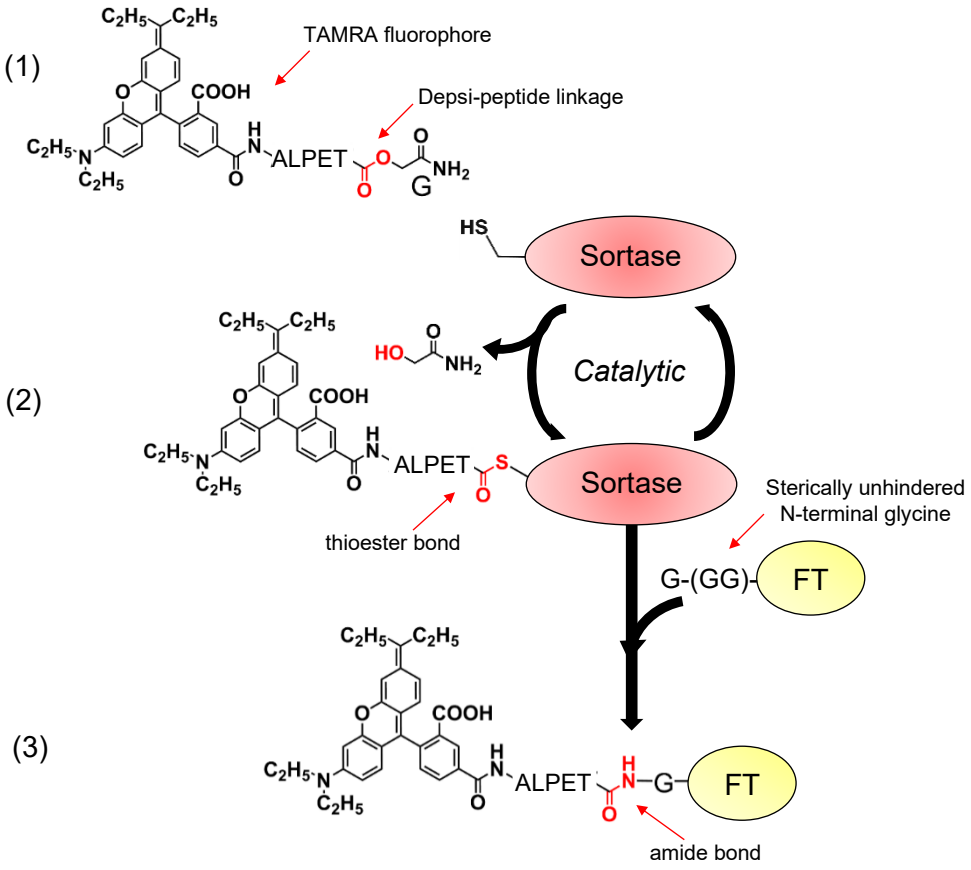
Text Insert 2 – Attached to *Figure 36.* Key points in the steps detailing the purification of FT-GFP.

4.3.2.2 – Fluorescent Labelling of FT by Sortase Trans-Peptidation Reactions

Sortagging was developed as another approach to fluorescently track recombinant FT after exogenous introduction into a biological system using confocal microscopy. GFP is a large and cumbersome addition to the native protein, GFP is larger than FT and therefore could distort FT uptake behaviour and create unrepresentative data on FT uptake action. Sortagging appears a superior approach to the recombinant FT-GFP fusion protein.

In the previous chapter, a TAMRA fluorophore was attached by chemical synthesis (carbonyl coupling) to the N-termini of the CPP sequences. Proteins however, have a tertiary structure which needs to be retained to maintain their functionality unlike the CPP sequences which only have primary structure – this means that the harsh reaction conditions used in chemical synthesis were not a viable option for chemical labelling of FT. TAMRA tracking proved successful for the CPPs as is a strong fluorophore and was straightforward to resolve against background autofluorescence and GFP. For these reasons Sortagging appeared a highly desirable option for investigation [152].

Sortase enzymes are important for catalysing transpeptidation reactions in gram positive bacteria where they attach proteins with a recognition motif onto a stretch of pentaglycines at the peptidoglycan cell wall [182, 183]. The *Staphylococcus aureus* strain recognises an LPXTG motif in substrates, to form a thioacyl intermediate [182, 183]. A nucleophilic glycine on the target protein then attacks this complex breaking the bond between the threonine and glycine and transferring the LPXT stretch onto the target protein [152, 182, 183]. This has become a valuable technique for recombinant protein engineering and in this work, the LPXTG-TAMRA peptide motif was covalently linked to FT and as such a TAMRA fluorophore was transferred onto the FT protein.



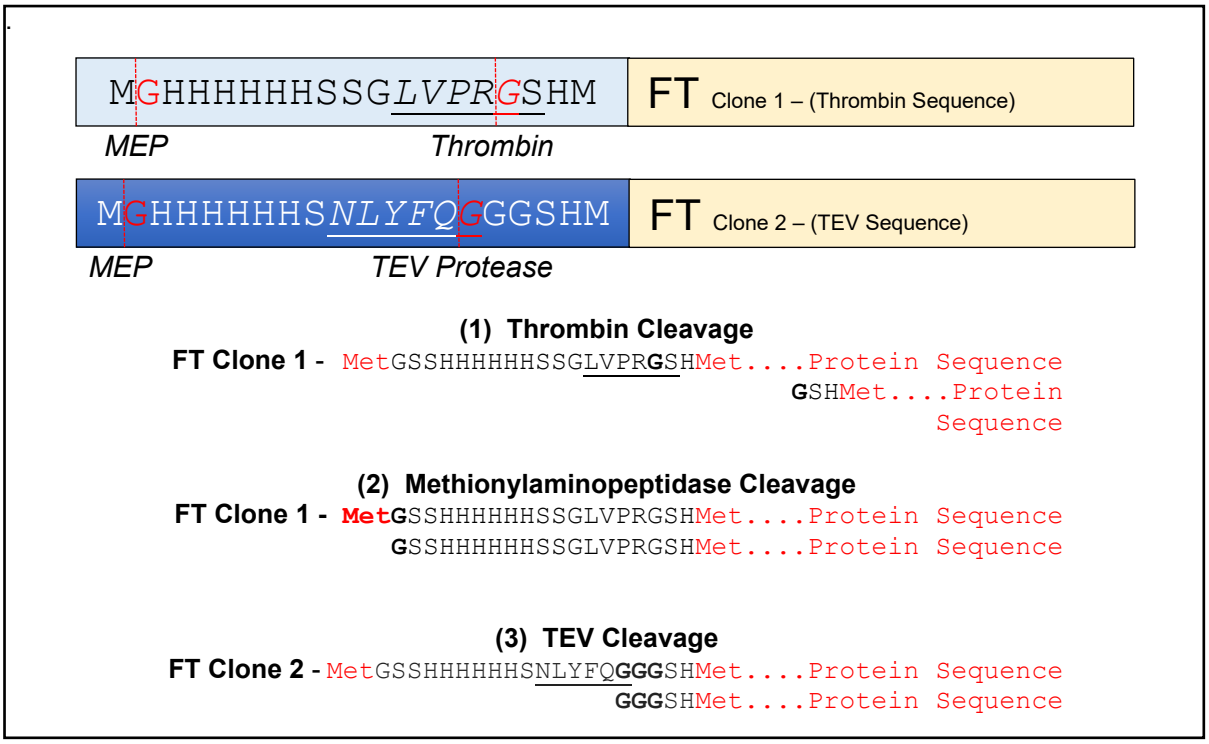
(1) The ALPETG probe contained a TAMRA fluorophore moiety and a depsi-peptide linkage between glycine and threonine, as an ester group leads to an irreversible reaction *c.f.* conventional peptide gives reaction equilibrium [184].
(2) The Sortase and probe form a complex via a thioester bond and a small by-product departs.
(3) The sterically unhindered N-terminal glycine attacks the Sortase-probe intermediate; the probe is then transferred onto the FT protein and the Sortase is catalytic for in transpeptidation reaction. The inclusion of the depsi-peptide linkage enables the reaction to reach completion and high labelling yields of FT were recorded [184].

Figure 37 – N-terminal Sortagging schematic for FT [152]**.** The Sortagging process is depicted above and is catalytic for the Sortase, requiring very small molar amounts of the enzyme in reactions [152]. Importantly, the probe has a TAMRA fluorophore attached and a depsi-peptide linkage makes the reaction irreversible and entropically favourable [184]. A sterically unhindered N-terminal glycine is required for nucleophilic attack on the probe-Sortase complex [183]. TAMRA labelled FT in high yield is the final product of the reaction and can be purified by dialysis. The TAMRA-depsi peptide used in this work was a gift from the Tate laboratory at Imperial College London.

The inclusion of a depsi-peptide meant that the Sortase formed a thiol-ester complex with the TAMRA labelled peptide [152]. This ester linkage allows the reaction to proceed to completion which would not be the case for the amide and this was an important modification to the protocol for Sortase mediated protein labelling reactions delivering a highly efficient labelling process [184]. Importantly, the Sortase is catalytic and the use of a depsi-peptide meant that an efficient reaction could be achieved with low quantities of the enzyme, whereas if the amide form had been used, stoichiometric quantities of Sortase would be required [152, 184].

Literature examples cite the need for a sterically exposed glycine in order to carry out effective nucleophilic attack at the Sortase-peptide complex [152]. This can be achieved by including a chain of glycine residues at the N-terminus and examples cited best conditions for this to happen are when three to five glycines are present, as this is most similar to the pentaglycine stretch at the peptidoglycan cell wall in *S. Aureus* [152, 182]. A single glycine might not yield sufficient exposure for the nucleophilic amine [152]. In other studies however, a single glycine is sufficient for attack and evidence is presented in a number of examples [185-187]. The best reaction conditions for FT had to be determined empirically.

In light of this, three available options were considered. Firstly, thrombin cleavage of the His-tag would yield a single glycine. Methionylaminopeptidase cleavage of the transcriptional start methionine would yield a single glycine [188]. In addition, a new clone was developed to expose three glycine residues and this included a TEV cleavage site. The opportunity was also afforded to change the cleavage site from a thrombin to a TEV recognition motif and this was because purification evidence, has shown that thrombin acts non-specifically to degrade FT during the His-tag cleavage, if the thrombin incubation is left in excess of 4 hours. These three options are presented in *Figure 33a*.



With the Assistance of Summer Student Laure Fourquet

Figure 38a – Introduction of sterically available N-terminal glycines for Sortagging. Exposure of an N-terminal glycine on FT by three available options including the introduction of a new clone (Clone 2) with a TEV cleavage site and a longer stretch of 3 glycines. For clarity this clone is referred to as FT_(TEV) in the text. The analogous FT_(TEV)-Tat clone was also developed.

Options for Exposure of Nucleophilic Glycine on FT for Sortagging

(1) Thrombin Cleavage
Thrombin cleavage in Clone 1 occurs between arginine and glycine in the LVPRGS recognition motif which was currently present in the pET-28b vector sequence.

(2) Methionylaminopeptidase Glycine Exposure
A glycine was present behind the start methionine in the sequence, and even whilst the protein is recombinant, native *E. coli* methionylaminopeptidase enzymes were able to remove this with adequate efficiency (complete removal was not observed) [188].

(3) TEV Cleavage
In Clone 2, TEV cleavage occurred between glutamine and glycine exposing three glycine residues. TEV cleavage is more specific than thrombin [189]. Primers were designed to build a longer glycine chain and also introduced the TEV site during the same mutagenesis reaction.

Text Insert 3 – Attached to *Figure 38a.* Details are given for the three options presented in *Figure 33a* for the exposure of an N-terminal glycine for Sortagging of FT.

In the previous part of this chapter nickel affinity chromatography was used to purify FT (*Figure 27*), and cation exchange chromatography was used to purify FT-Tat (*Figure 29*) before size exclusion chromatography and SDS-PAGE confirmed the presence of pure protein. Purifications for FT_(TEV) and FT_(TEV)-Tat were developed, however low expressions were recorded and this is particularly evident for FT-(TEV) in *Figure 33b* below as shown by the absolute intensity scale in mAu on the elution trace. FT_(TEV) peak maximum was 20 mAU, *c.f.* 160 mAu for FT-Tat_(TEV).

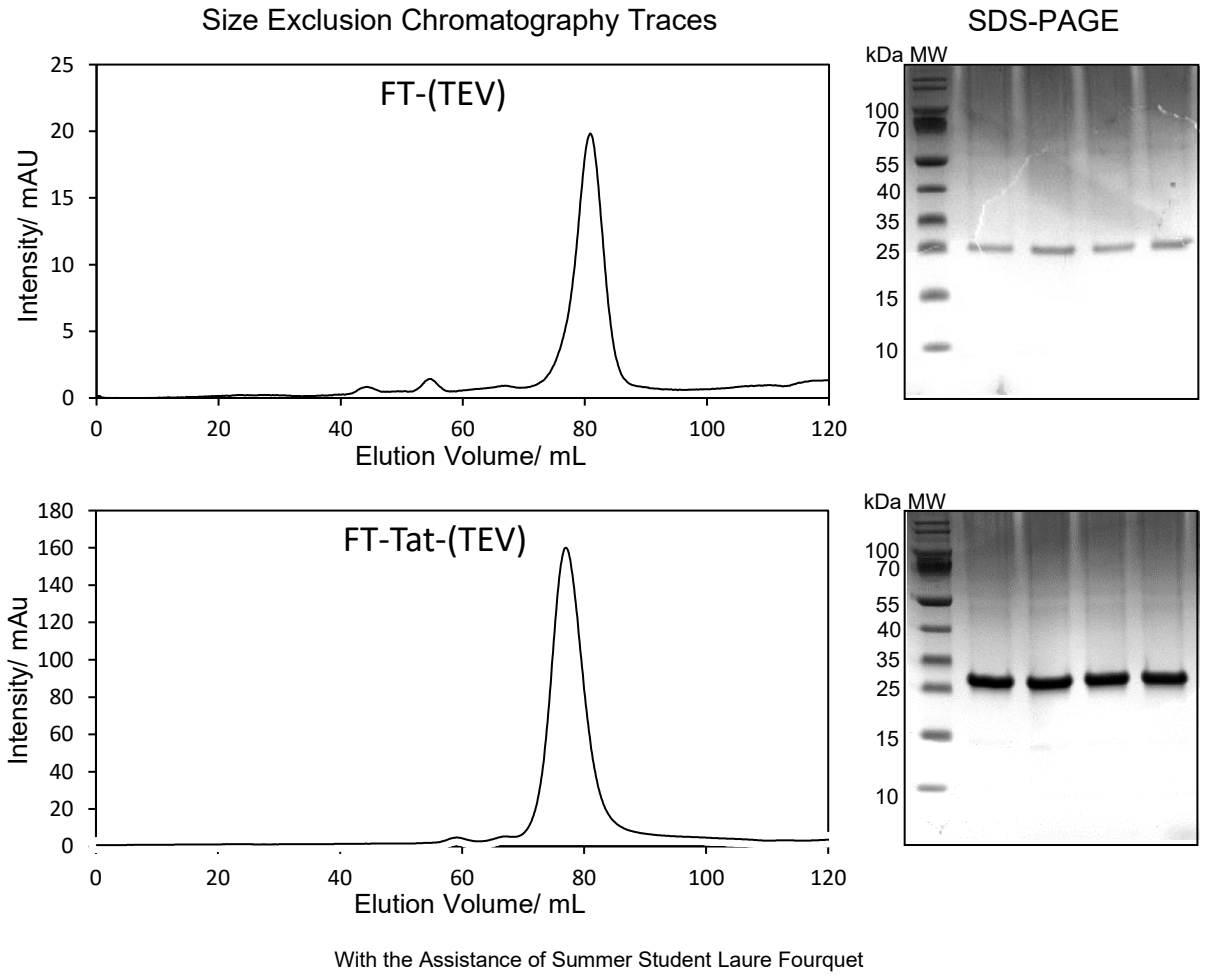
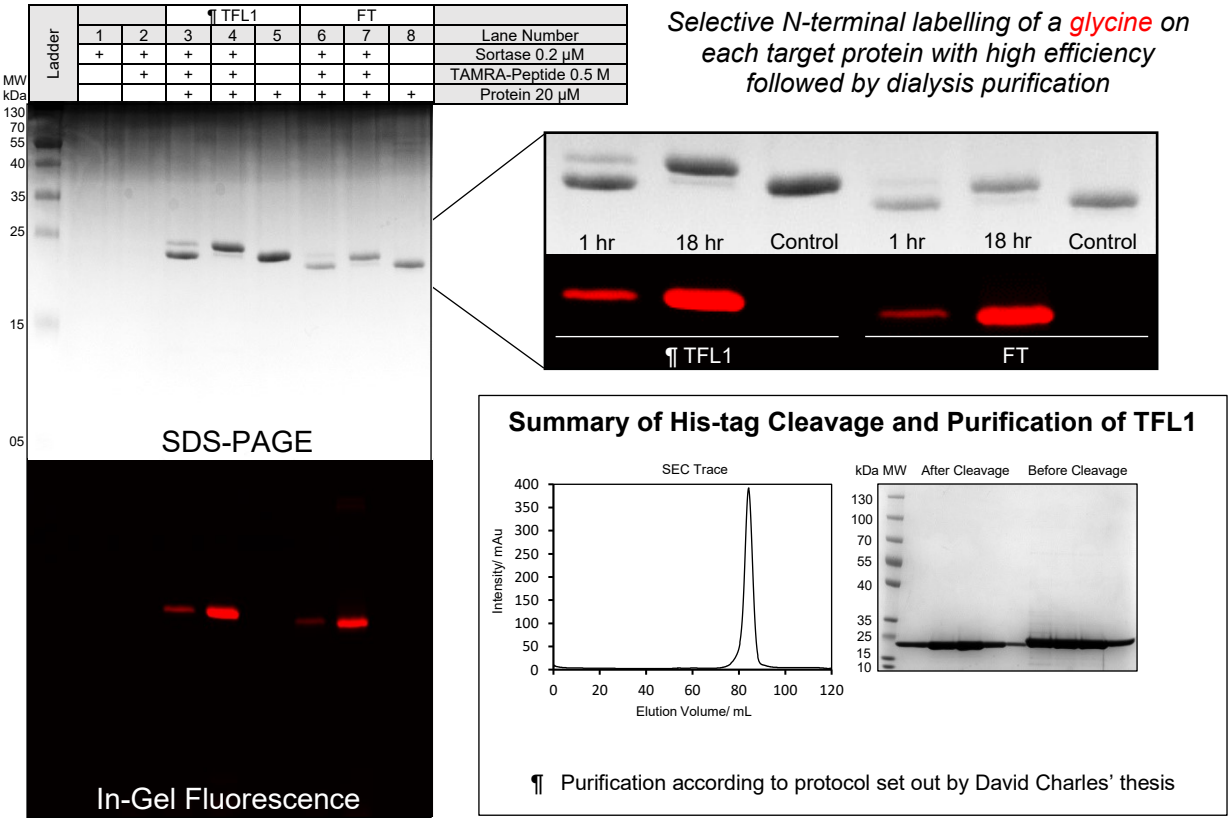
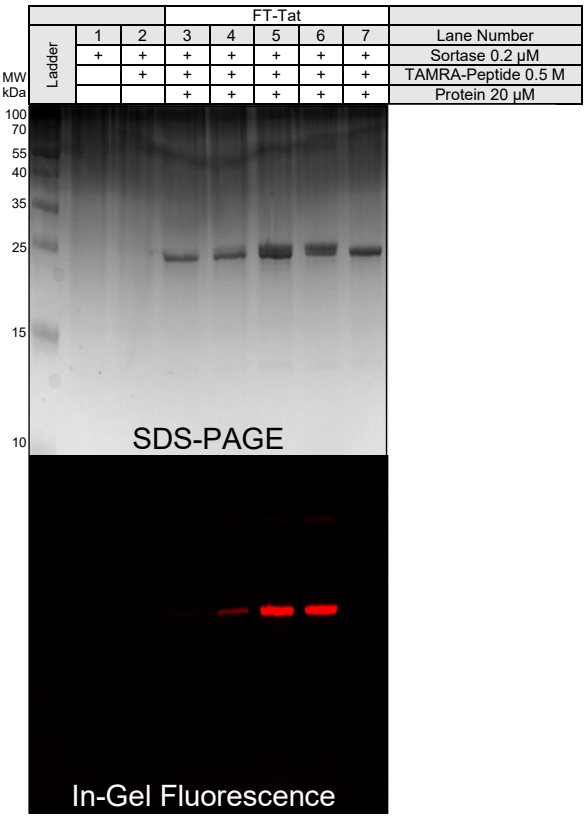


Figure 38b – Purification of protein constructs with introduced TEV sites. Size exclusion chromatography traces for FT and FT-Tat after ion exchange chromatography. These sequences contained a modified TEV cleavage site with the addition of 3 additional glycine residues at the N-termini. This was carried out with the help of summer student - Laure Fourquet.

Sortagging FT, FT-R9, FT-Tat and TFL1





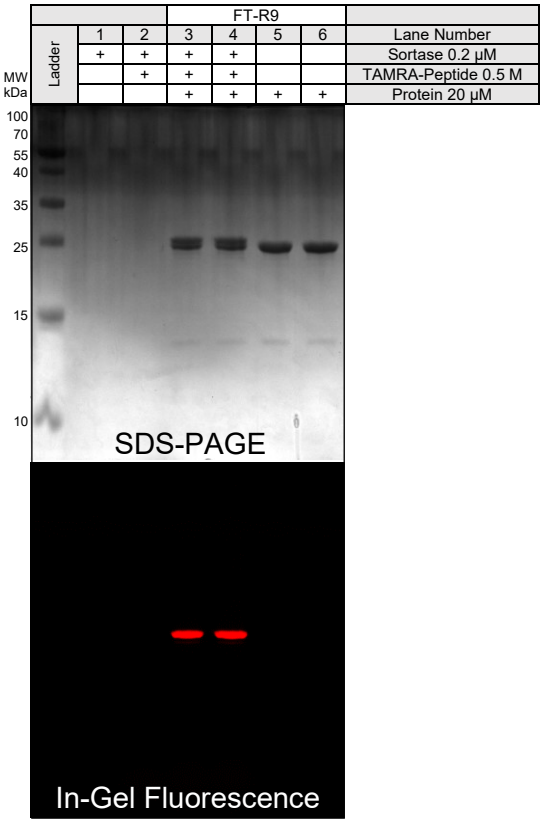


Figure 39 – Sortagging of FT, FT-Tat, FT-R9 and TFL1. Sortagging completion was shown via in-gel fluorescence and the presence of a TAMRA fluorophore. The purification of TFL1 is included as a symmetrical SEC trace and pure protein shown by SDS-PAGE. The TAMRA labelled depsi-peptide used in reactions was a gift form the Tate laboratory at Imperial College London.

SDS-PAGE and in-gel fluorescence were used to show Sortagging shifts via electrophoretic mobility. Whilst *Clone 2* (presented in *Figure 33a*) with the additional glycine residues and a TEV cleavage site was considered as an optimised version, the expression levels of these proteins were low. Therefore, Sortagging reactions were investigated with success on Clone 1 with the thrombin cleavage site and only a single available glycine. TFL1 is not mentioned in the text up to this point. Its sequence is cloned into a pET-28b vector (a gift from David Charles) and as such thrombin cleavage yields the same N-terminal sequence as for FT so Sortagging reactions are analogues [41].

Both cleaved FT and TFL1 underwent Sortagging reactions and after 1 hour, 2 bands in the SDS-PAGE were present, with the top band corresponding to labelled protein. After 18 hours, complete labelling was recorded, with an increase in intensity observed for in-gel fluorescence. The Sortagging reaction worked effectively for both FT and TFL1 after thrombin cleavage with a single nucleophilic glycine. In addition, successful Sortagging was also recorded for FT-Tat and FT-R9 with single pure bands observed in the in-gel fluorescence. The uptake properties of these proteins was now ready for testing in a biological system, and the Sortagging has enabled protein tracking using confocal microscopy.

4.3.3 - Assessment of FT, FT-Tat and FT-R9 Uptake in Cells

In *Chapter 3*, independent CPP action was tested in plant tissue and as such R9 and Tat were pooled as successful sequences, and potential candidates to test the delivery of FT cargo inside plant cells. In the first part of this chapter, biochemical tools were developed and R9 and Tat cloned into the C-terminus of FT creating FT-Tat and FT-R9. N-terminal Sortagging was used to label proteins with a single TAMRA fluorophore. This enabled the tracking of recombinant proteins, when introduced exogenously into a biological system and an assessment of the influence of Tat and R9 CPPs on the potential transduction of recombinant FT is reported in the following text.

4.3.3.1 – Covalent CPP Mediated Cellular Delivery with FT, FT-Tat & FT-R9

The action of Sortagged proteins was tested against leaf callus cells, and incubations were conducted at time points for 20 minutes, 6 hours and 24 hours. It is strikingly clear from the images, that the CPP tagged proteins interact with the outside of cells, whereas this is not the case for FT alone as shown in *Figures 35a-c*. After the initial 20-minute incubation FT-Tat and FT-R9 were held on the outside of the cells as shown in the TAMRA channel and this was confirmed with overlaid brightfield images. After 6 hours, a considerable fluorescence accumulation was observed for both FT-Tat and FT-R9 *c.f.* FT. After 24 hours, FT-Tat and FT-R9 fluorescence was observed inside the cells, importantly the integrity of cells after FT-Tat incubation was maintained whilst this was arguably not the case for FT-R9 (turgidity compromise indicated in the brightfield channel).

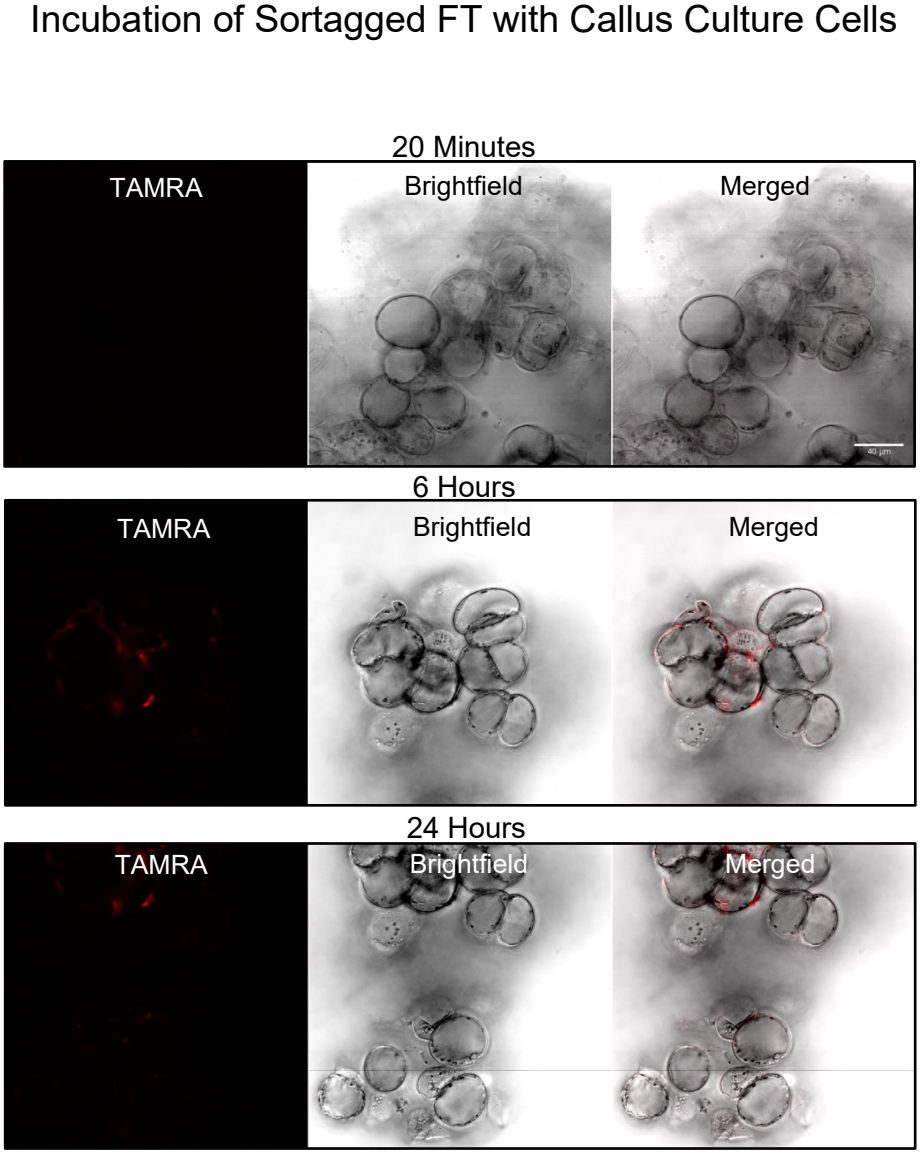


Figure 40a – Incubation of Sortagged FT with callus culture cells. Time points recorded at 20 minutes, 6 hours and 24 hours for the incubation of Sortagged FT with callus culture cells. After extensive washing, there was no observable fluorescence inside the cells.

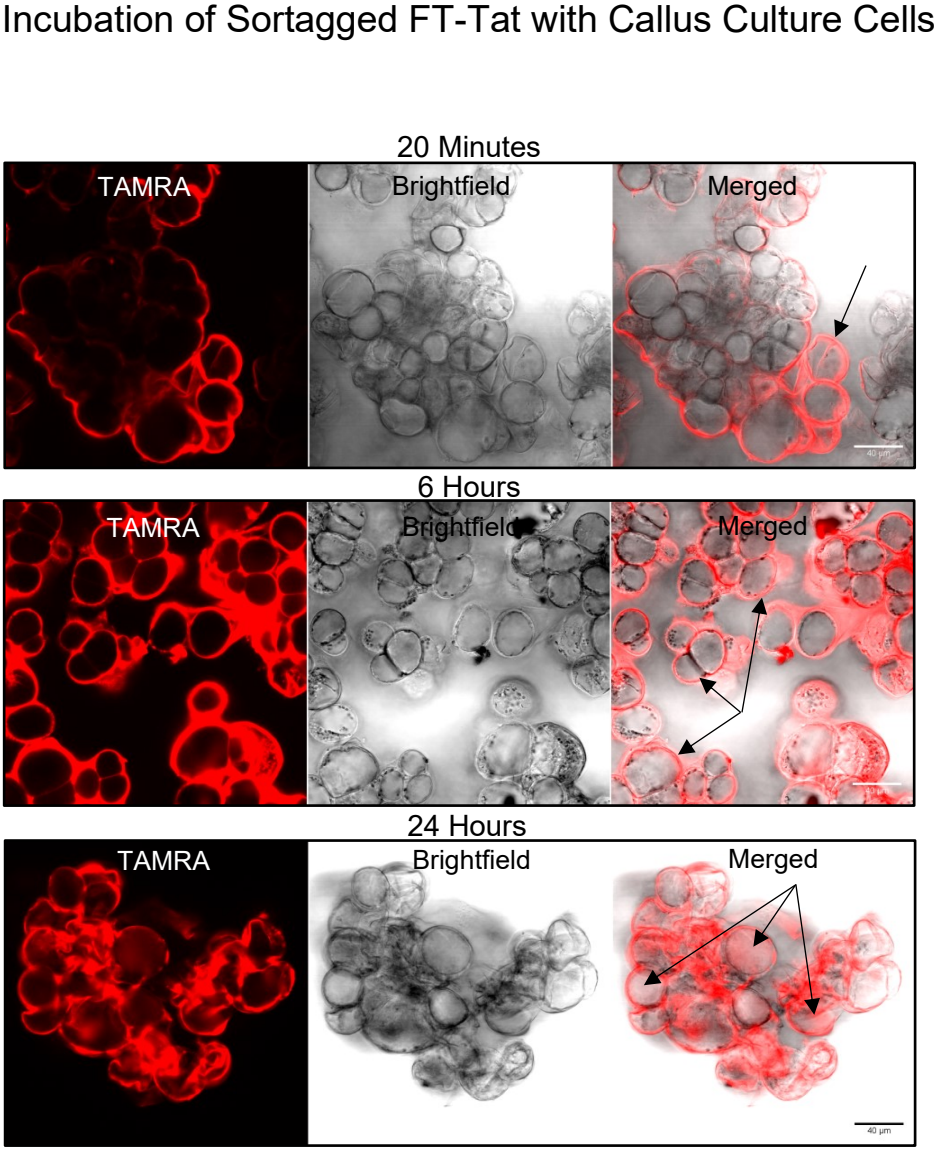


Figure 40b – **Incubation of Sortagged FT-Tat with callus culture cells.** Time points recorded for 20 minutes, 6 hours and 24 hours for the incubation of Sortagged FT-Tat with callus culture cells. Arrows indicate protein location and fluorescence was observed on the cell boundary at 20 minutes and 6 hours and was more pronounced inside the cells at 24 hours.

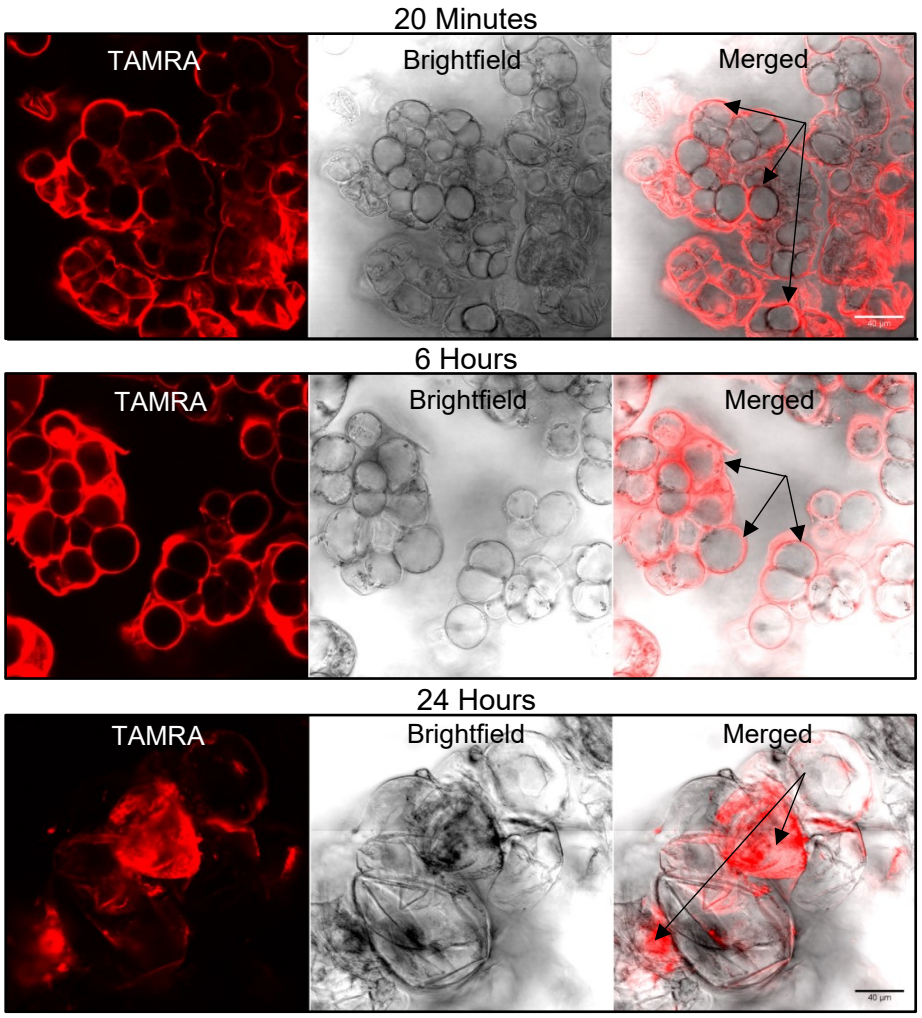


Figure 40c – **Incubation of Sortagged FT-R9 with callus culture cells.** Time points recorded for 20 minutes, 6 hours and 24 hours for the incubation of Sortagged FT-R9 with callus culture cells. Arrows indicate protein location and fluorescence was observed on the cell boundary at 20 minutes and 6 hours and was more pronounced inside the cells at 24 hours, however cells appear compromised.

4.3.3.2 - Assessment of Non-Covalent Protein Delivery of FT-GFP via R9

Covalent attachment of CPPs to cargo is the preferred delivery method in much of the literature for the facilitation of protein entry inside cells [190]. There is a small body of evidence that has shown non-covalent entry whereby a molar ratio mixture of CPP to protein enables protein uptake into cells and this has been demonstrated in the plant literature with success [133, 140, 144]. This option appears improbable for FT as conceivably, a transient complex must form between the CPP and cargo via electrostatic interaction within the protein's hydration sphere. This is not possible as both CPP (R9 & Tat) and FT (pI=7.80) are positively charged. It is inconceivable that the direct penetration of R9 and Tat across the membrane could somehow facilitate tandem FT entry when there is a repulsive interaction between FT and CPP. In the plant literature, the non-covalent delivery of GFP has been shown with cationic peptides and this is perhaps because GFP (pI=5.80) and CPP both have complementary charges enabling the formation of a transient complex [133].

For these reasons, the following trial experiment presented in *Figure 36* was conducted to investigate the possibility of non-covalent protein transduction for FT-GFP which has an isoelectric point below neutral (pI=6.58 *c.f.* pI=7.80 for FT). In addition, in FT-GFP there is de-coupling of FT and GFP into 2 separate entities since a glycine/serine linker joins the two distinctly folded proteins; as such, this might have enabled a transient complex to form between R9 and the GFP component of FT-GFP. This might enable entry inside the cell and this was touched up below in *Figure 36* for cell culture incubations of FT-GFP mixed with R9. Both the action of R9 (red channel) and FT-GFP (green channel) are depicted in the confocal images.

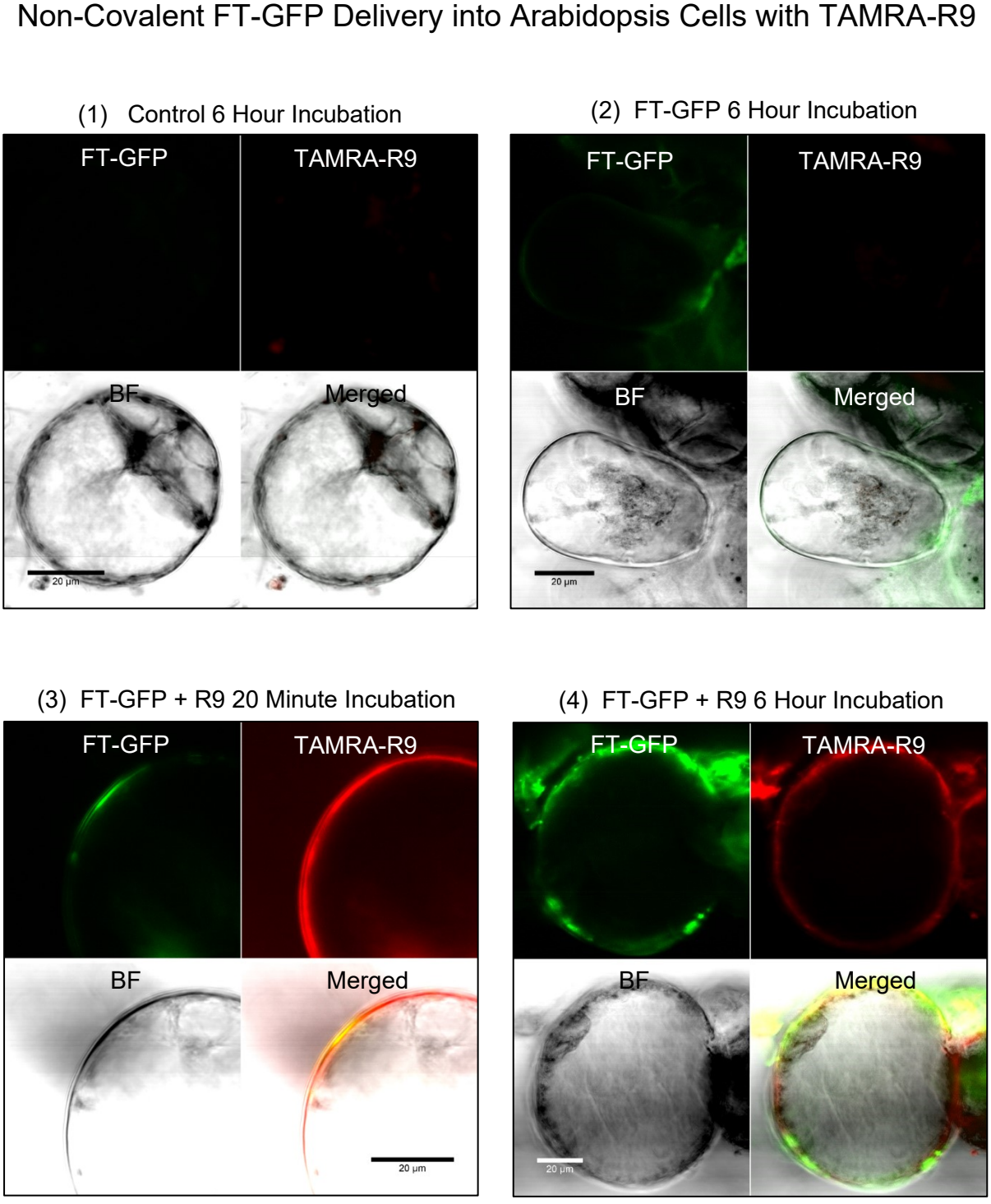


Figure 41 – Non-covalent FT-GFP delivery to Arabidopsis cells with TAMRA-R9. In the above, different incubations assessing non-covalent delivery of FT-GFP via R9 in callus culture. **(1)** Negative control incubation with buffer; **(2)** Incubation of FT-GFP alone for 6 hours, **(3)** 20-minute incubation of non-covalent FT-GFP with R9 suspension, **(4)** 6-hour incubation of FT-GFP and R9 suspension.

FT-GFP was used so that both the action of R9 and the cargo could be monitored enabling visualisation of GFP as well as TAMRA fluorescence. This would not have been possible had the Sortagged proteins been used as they both exhibit the same TAMRA fluorophore. In *Figure 36*, Incubation *(2)* above showed that FT-GFP alone is not sufficient to enter inside the cell and incubation *(1)* showed blank images for both the TAMRA channel and the GFP channel so all fluorescence can be attributed to protein and peptide associated fluorophores because background fluorescence is negligible at these settings. After 20 minutes in incubation *(3)*, R9 is attached to the cellular boundary and this is consistent with previous data reported in *Chapter 3*. A small amount of FT-GFP also appeared complexed to R9 and hence at the membrane.

Moreover, in *Figure 36*, after 6 hours in incubation *(4)*, R9 was attached to the outside of the cell along with FT-GFP and this suggests that a complex might have formed; as independently, R9 was able to enter cells within 6 hours as evidenced in *Chapter 3*. The evidence implies that FT-GFP was in proximity to the membrane but did not enter the cell. Further investigation is required to probe this situation in detail but from the scientific stance taken in this thesis, FT entry inside cells facilitated by non-covalent protein delivery is unlikely and as such is not explored further. In future experiments, different ratios of CPP to cargo could be tested in the non-covalent suspensions but in this work the non-covalent entry of FT inside cells cannot be satisfactorily explained using R9 mixtures.

4.4 - Discussion

This chapter reported the development of tools, incorporating the results from the previous chapter, and accordingly the covalent attachment of R9 and Tat to FT in order to facilitate FT cellular uptake was examined. A robust purification of FT was established incorporating the cleavage of the His-tag, moreover, the cloning of R9 and Tat peptides into the FT sequence by site directed insertion at the C-terminus formed FT-Tat and FT-R9. These new constructs were compared against FT in Arabidopsis cells to assess whether the CPP tag could facilitate FT cellular uptake. Confocal microscopy was an essential technique used to visualise the location of proteins once in the *in vivo* system; as such the covalent attachment of a TAMRA fluorophore was incorporated into FT, FT-Tat and FT-R9 through the novel Sortagging process. In this way, this chapter is essentially broken down into three facets, firstly establishing purifications for FT, FT-Tat and FT-R9, secondly developing ways to fluorescently label the proteins through Sortagging and an FT-GFP fusion protein. Lastly the delivery and uptake action of FT-Tat and FT-R9, assessed against FT using confocal microscopy; the non-covalent delivery of FT-GFP was also briefly considered.

4.4.1 – Fluorescent Labelling of FT

Fluorescent labelling is commonplace in transgenic systems, where the addition of GFP to the protein sequence enables tracking and localisation of the protein throughout the biological system [179]. This technique has advantages, primarily that it is a relatively simple and tested methodology [179]. In many cases the protein of interest is biologically functional after GFP-fusion, in certain examples this might however attenuate function as a large moiety like GFP can affect interaction with partners [191]. Transgenic FT-GFP overexpression has been shown to cause early flowering with the GFP attachment at the C-terminus of the protein; a precocious phenotype however was not recorded and whilst FT-GFP convincingly accelerates flowering it was not as effective as FT alone [15].

A purification for recombinant FT-GFP fusion protein was developed as a way to fluorescently track FT. GFP as a subunit of the FT-GFP fusion protein is larger than FT and whilst it is reasonable to use this as a model for action *in vivo*, FT-GFP is an unrepresentative comparison to model FT uptake into cells in these experiments as FT-GFP is more than twice the size of FT and could reasonably involve different uptake dynamics [15]. Moreover, two additional clones would have had to be created for FT-Tat-GFP and FT-R9-GFP.

Protein labelling kits are available for purchase, consisting of maleimide-fluorophore probes and N-hydroxyl-succinimide-fluorophore probes. Whilst these are useful for rapid labelling approaches, they are unspecific and label available backbone residues [192, 193]. This distorts the native surface of the protein and potentially the interaction with other protein partners. The efficiency of labelling is not always consistent and a range of labelling reaction completions are observed [194]. There are 2 lysine and 3 cysteine residues available in the FT sequence. In this work, the uptake of FT-Tat and FT-R9 was compared against FT. The Tat sequence itself contained 3 lysine residues which are highly exposed at the C-terminal tail, for this reason, lysine labelling was not a workable option. For example, if complete labelling was observed on all residues, FT and FT-R9 would have 2 fluorophores whereas the signal for FT-Tat would be 2.5 times as bright with 5 fluorophores per protein sequence cysteine labelling via maleimide probes is an option. FT contains 3 cysteines, TFL1 however does not contain any cysteines and in future work TFL1 delivery and cellular uptake could be assessed as a contra-tool to delay floral transition – cysteine labelling is impossible for TFL1. Schematics for maleimide and N-hydroxyl-succinimide labelling probe designs are detailed below.

Other labelling options were considered and Sortagging was investigated as a novel and as yet untested resource in plant sciences to label recombinant proteins. Sortagging is a reliable and robust procedure which can be used to label proteins and importantly, has little impact on the tertiary structure and surface of the protein [152].

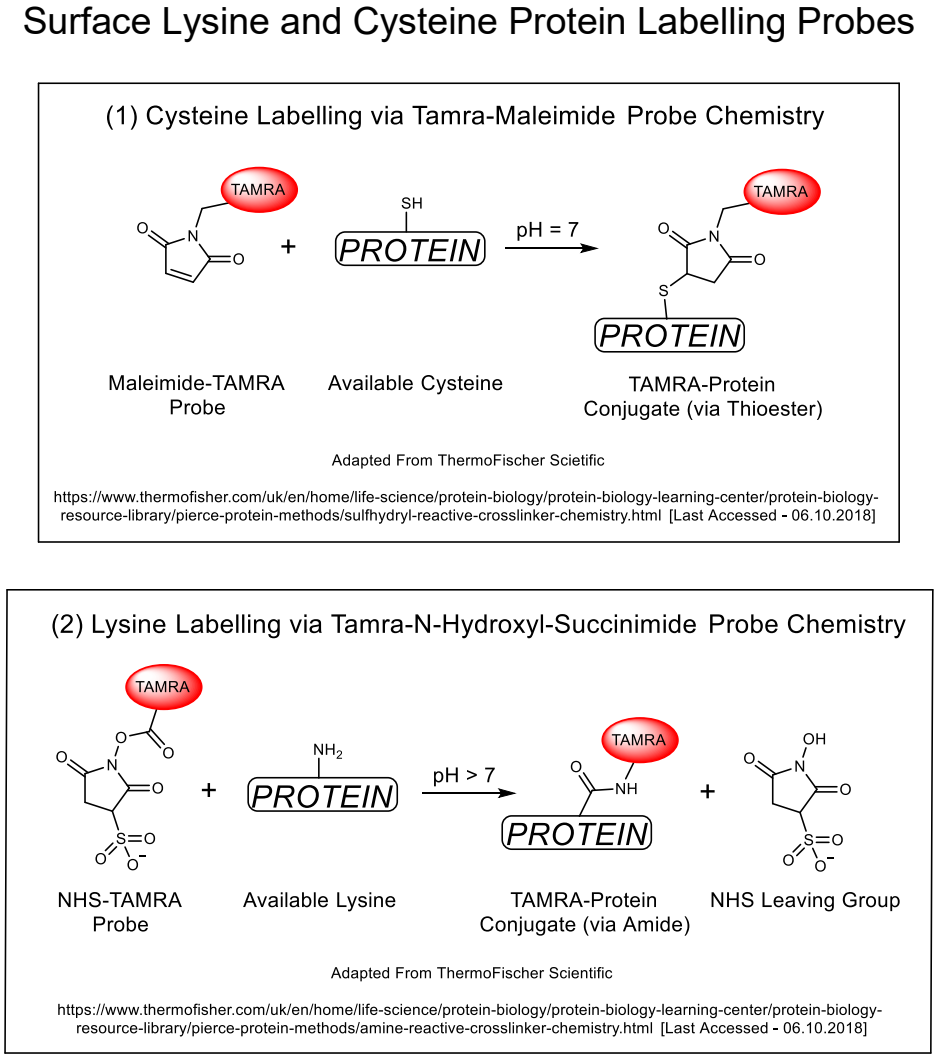


Figure 42 – Surface lysine and cysteine protein labelling probes. Labelling of surface cysteine and lysine residues via maleimide-TAMRA and NHS-TAMRA probes are respectively presented above. Probes are available from *ThermoFischer Scientific* and come as part of a commercial protein labelling package.

This work is the first reported example of Sortagging in plant sciences and selectively labels an N-terminal glycine by transferring a short peptidic sequence (with attached TAMRA fluorophore) and is mediated by a Sortase enzyme [152, 184]. This novel strategy has advantages over the FT-GFP fusion approach and also the use of maleimide and N-hydroxy-succinimide probe labelling [152, 184]. In particular, Sortagging is specific, the reaction efficiency consistently nears completion, transfers only a single fluorophore per protein (*c.f.* succinimide ester labelling kits), does not affect the tertiary structure and retains the protein at near native

size (*c.f.* GFP-fusion protein) [152, 184]. In conclusion, Sortagging offers a superior labelling approach for FT and as such was used to assess uptake of FT, FT-Tat and FT-R9 and the covalent CPP mediated protein transduction. FT-GFP is used to briefly assess non-covalent protein transduction as this allowed separation of the TAMRA labelled R9 CPP from GFP in the FT-GFP fusion construct.

4.4.2 - Covalent Delivery of Cargo

The action of R9 and Tat CPPs are assessed through the covalent attachment to FT, and their influence on FT uptake. Whilst FT-Tat and FT-R9 appear inside the cells after a 24-hour incubation reported in *Figure 35b* and *35c*, this was in contrast to the uptake of R9 and Tat peptides reported in isolation in *Chapter 3* (see *Figures 11 -13*). The same behaviour was observed at 20 minutes with R9 & Tat and FT-R9 & FT-Tat attached to the cell boundaries; the difference being that R9 can enter cells after 6 hours *c.f.* FT-R9 and FT-Tat. This suggested a different entry mechanism was at play in both situations [195, 196].

Direct penetration could be the entry mechanism for R9 and Tat in isolation, but when a protein is covalently attached, this might occur via endocytic cellular entry [195]. The results presented in *Figures 35a-c* suggested a different entry mechanism for FT-Tat and FT-R9 when compared to Tat and R9 peptides as uptake of the latter is within 6 hours whereas for FT-Tat and FT-R9, it is within 24 hours. Feasibly an endocytic entry mechanism is likely to occur for a protein due to its larger size than the peptide in isolation and as such a different uptake mechanisms appear to be at play for the entry of Tat and R9 alone, and then when coupled to FT protein [195, 196].

A consideration in this work was that the R9 and Tat CPPs might affect protein activity once inside the biological system. In the literature, efforts have been made to introduce temporary linkages between the peptide and protein sequences. An interesting result was reported by

Bilichak *et al.* whereby the delivery of mCherry by R9, was via a reversible intermolecular disulphide bond between peptide and cargo. This was then reduced upon exposure to the cytosol allowing the release of mCherry [150]. A cleavable linker (for example TEV or thrombin cleavage sites) between the protein and CPP would be an interesting strategy to circumvent cargo activity concerns, however this has not been investigated in plant literature and more broadly, in the wider CPP field [197]. Perhaps this is because of the need to introduce a recombinant protease into the system to conduct cleavage and this adds another level of complexity and potential disruption to the system. It appears that the broad assumption made across the literature is that the CPP will not greatly affect the intended endogenous protein function in the system however this should be assessed for individual examples. In the case of FT, FT-Tat and FT-R9, the CPP tag is exposed at the C-terminus with insignificant effect on the hydrodynamic radius as shown by the near identical size exclusion chromatography elution volumes *(Figure 29)*.

4.4.3 - Non-Covalent Delivery of Cargo

An interesting delivery option that does not require the covalent attachment of a CPP to the protein is non-covalent protein transduction [133]. In this way, a solution of CPP and cargo was mixed together and the combined effect is cargo delivery across a membrane and most probably occurs via macropinocytosis, reported by Chang *et al.* [133]. Although there is empirical evidence in support of this phenomenon, a mechanistic understanding is limited and it is assumed that the CPP and cargo form a transient complex [198]. This process is reported in the mammalian literature and also the plant literature with a handful of examples and with confocal evidence showing the transduction of fluorescent proteins [133, 140, 144, 147]. Classically, a protein is unable to pass through a hydrophobic barrier such as a plasma membrane, and the conventional entry of a protein inside a cell is receptor mediated [199]. This raised the question as to how a peptide operating under a direct penetration mechanism could co-

transport a large protein across a membrane? Macropinocytosis has been cited as the most likely operating mechanism to explain this [133].

A transient interaction exists between the peptide and the cargo requiring an oppositely charged interaction at the interface [145]. The isoelectric point and surface charge of GFP (pI=5.80) is such that it could form a transient complex with cationic peptides, facilitating cargo transduction and this perhaps explains why cationic peptides are the vehicles of choice, indeed Ng *et al.* cloned a stretch of cationic lysine residues onto the BP100 plant-based peptide to aid non-covalent interaction with the cargo [145, 200]. In addition, this also means that non-covalent protein transduction will not work in all scenarios as cargo and peptide of the same charge will logically not form a transient complex. FT is positively charged at neutral pH and in this way, it cannot form a transient complex with R9 therefore this delivery application is likely to be unsuccessful. There is however one major advantage to this technique, that the protein retains its complete native function after delivery and is not disrupted by the covalent inclusion of a CPP tag.

4.5 – Conclusion

This chapter reported the robust purification of FT using nickel affinity and size exclusion chromatography, a step was also introduced for the removal of the His-tag. The previous chapter reported the successful uptake of Tat and R9 CPP sequences as successful in plant tissue, were covalently linked to FT at the C-terminus. Modified purifications were developed for FT-Tat and FT-R9 taking into account the high positive localised charge at their C-termini. In this way, both FT-Tat and FT-R9 eluted at extraordinary high salt elution concentration (approximately 1 M KCl) within the cation exchange step, and as such further purification was not required. Misfolded FT-Tat and FT-R9 proteins were observed after nickel affinity purification and as such this method was not used *c.f.* the purification of FT. Whilst the Tat and R9 tags were clearly exposed at the C-terminus as evidenced by the ion exchange chromatography, they did not greatly affect the hydrodynamic radii as observed by size exclusion chromatography. The expression levels of FT-Tat are high and comparable with recombinant FT, this was not the case however for FT-R9. Lower expression of FT-R9 is attributed to the bacterial system's inability to process the unnatural set of 9 contiguous arginines.

Fluorescent labelling techniques were developed in this chapter and notably, Sortagging was used to attach a single TAMRA fluorophore selectively to the N-terminus of FT via a Sortase mediated transpeptidation reaction. Three different strategies were investigated to expose a sterically unhindered N-terminal glycine, including thrombin cleavage, methionylaminopeptidase cleavage to reveal single glycines and thirdly, the introduction of a new clone with a tri-glycine stretch at the N-terminus of FT and incorporating a TEV cleavage in order to avoid non-specific cleavage of FT protein during the His-tag removal. Empirical evidence determined that a single glycine was sufficient to enable successful Sortagging. An

FT-GFP protein was also constructed as a tool to track FT with spectral resolution away from TAMRA in preparation for uptake experiments.

The covalent protein transduction of FT was investigated with FT-R9 and FT-Tat in cell culture. After 20 minutes, proteins were attached to the cell boundaries in the same way as for the independent uptake of R9 and Tat. In contrast, after 6 hours the proteins still remained attached to the cellular boundaries and did not penetrate inside cells until 24 hours, this implies that a different mechanism occurs and is different from the independent uptake of R9 and Tat reported in *Chapter 3*. The uptake of FT-Tat was superior to uptake of FT-R9 in cell culture and fluorescence was clearly visible inside the cell after a 24-hour incubation. This is the first reported example of the covalent uptake of a functional protein mediated by CPPs in a plant system, whereas literature examples to date have focused on GFP and RFP and their derivatives, which have no endogenous function *in planta.*

The non-covalent delivery of FT-GFP was assessed using R9. FT-GFP was used in order to resolve the action of R9 as this would not have been possible with FT as it was Sortagged with a TAMRA fluorophore. This introductory study indicated that FT-GFP interacted with R9 at the cellular boundary however no fluorescence was observed inside the cells. The difficulty with non-covalent protein transduction is establishing a complimentary interaction between CPP and protein and this was not the case for FT and R9 and as such non-covalent protein transduction was not investigated further in this thesis.

This chapter successfully reported the uptake of FT-Tat inside cells which was superior to the penetrating ability of FT-R9. In addition, the recombinant expression levels of FT-Tat are higher than for FT-R9. In light of this, FT-Tat was pooled for further biological experimentation

in the following *Chapter 5* where it was used to assess whether AP1 can be artificially activated and whether reproductive development can be activated on demand in Arabidopsis.

5. Results 3 – Assessment of Exogenous FT Delivery and Biological Action *in Planta*

5.1 – Introduction

FT is a key component in the activation of the floral transition and essentially its absence holds the plant in the vegetative phase [22, 201]. A lack of FT stimulus prevents unwanted flowering at disadvantageous times of the year, such as during winter cold periods when light levels are low [22]. The action of FT as a florigen, propels the plant through this checkpoint by integrating the detection of positive floral signals within the leaf [201, 202]. Importantly, this has led to the hypothesis tested in this chapter - whether exogenously applied recombinant FT can replace and imitate the action of endogenous FT [201]. Homologues of FT exist within the PEBP gene clad in Arabidopsis; notably, TSF is a homologue and mobile florigen, however, its influence is secondary and inferior to FT meaning that the system is remarkably simple [15, 34, 35].

In this chapter, the delivery of recombinant FT into the plant by three access points are considered. These were explored by looking at the endogenous journey that FT takes from expression site within the companion cells, through phloem translocation, to action site in the shoot apical tissue [15]. The investigation focused on the following routes of application: infiltration through the stomata, microinjection into the stem and direct application onto the shoot apical meristem. Arabidopsis plants were treated with recombinant FT protein, and artificial floral activation was assessed through both phenotypic and molecular readouts - this chapter reports the most important part of the overall investigation.

Once in the apex, FT interacts with FD, facilitated by 14-3-3 proteins [46, 48, 49]. A heterohexameric protein complex forms comprising of two FT molecules bridged by a 14-3-3 protein dimer in which the FD dimer intercalates, binding at the phosphate pockets in the cleft of the 14-3-3 protein. This complex is called the ‘Florigen Activation Complex’ (FAC), a term

coined by Taoka *et al.*, and it interacts with the AP1 promoter at a C-box [48]. During the vegetative stages of development, the meristem apical dome is flat – at this point the influence of TFL1 delays the floral transition [203]. Whilst FT is predominantly discussed in this chapter, perhaps the potential exogenous application of TFL1 could be used as a parallel tool, in this case to delay flowering (this was briefly considered within the investigation) [203]. AP1 expression causes the cells in the apical meristem to differentiate and the structure becomes both pronounced and arched [39]. The apical meristem transitions through an inflorescence stage, a transition stage to the final floral meristem and is later marked by the appearance of buds as the final floral transition reaches completion [204]. The ABC model for floral development dictates how simple combinations of genes begin to form the floral organ structures, with AP1 accounting for development of sepals in the first whorl and then in combination with SEP3, PI, and AP3, petals, in the second whorl [205]. This molecular basis is the foundation for the concepts tested within this chapter.

5.2– Experimental Aims for the Chapter

(1) Investigate appropriate delivery routes for recombinant FT into plant tissue, where it could feasibly activate AP1 -

(1a) FT delivery inside the leaf via stomatal entry.

(1b) Microinjection as a technique to deliver FT inside the vasculature.

(1c) Direct delivery to the apex via microdissection.

(2) From 1a – 1c above, determine the most appropriate delivery route.

(3) Use the fluorescent protein tools from the previous chapter to track FT location and the accompanying delivery of FT-Tat and FT-R9. Whilst uptake ability is important, biological efficacy is essential and this should be considered.

(4) Develop an assay to assess the output of FT action *in vivo*, analysing a phenotypic readout through the macroscopic appearance of buds.

(5) Build an Arabidopsis reporter (pAP1::GFP in Col-0) which will provide a molecular readout for AP1 activation.

(6) Assess the outcomes of the chapter to critically determine whether recombinant FT can artificially turn on flowering – does a robust and reproducible floral activation tool exist?

(7) Consider the possibility of translating the experiments into other species – utilising the universality of FT across different species. Could recombinant FT be used as a universal floral activation tool?

5.3 – Results - Part 1

5.3.1 – Routes of Entry for Recombinant FT

In the previous chapter a toolkit was developed including recombinant FT, FT-R9 and FT-Tat proteins and fluorescent Sortagged derivatives – this chapter reports the use of these tools in biological experiments. The first consideration was uptake routes to deliver recombinant proteins *in planta* with a particular focus on the route taken by endogenous FT from site of expression through to site of action [15]. Three potential strategies were devised to investigate FT delivery and uptake, and they were then assessed to determine whether any were feasible as an exogenous delivery route. The strategies were to put FT into the plant via:

(1) Stomatal openings on the underside of the leaf.

(2) Microinjection into the vasculature.

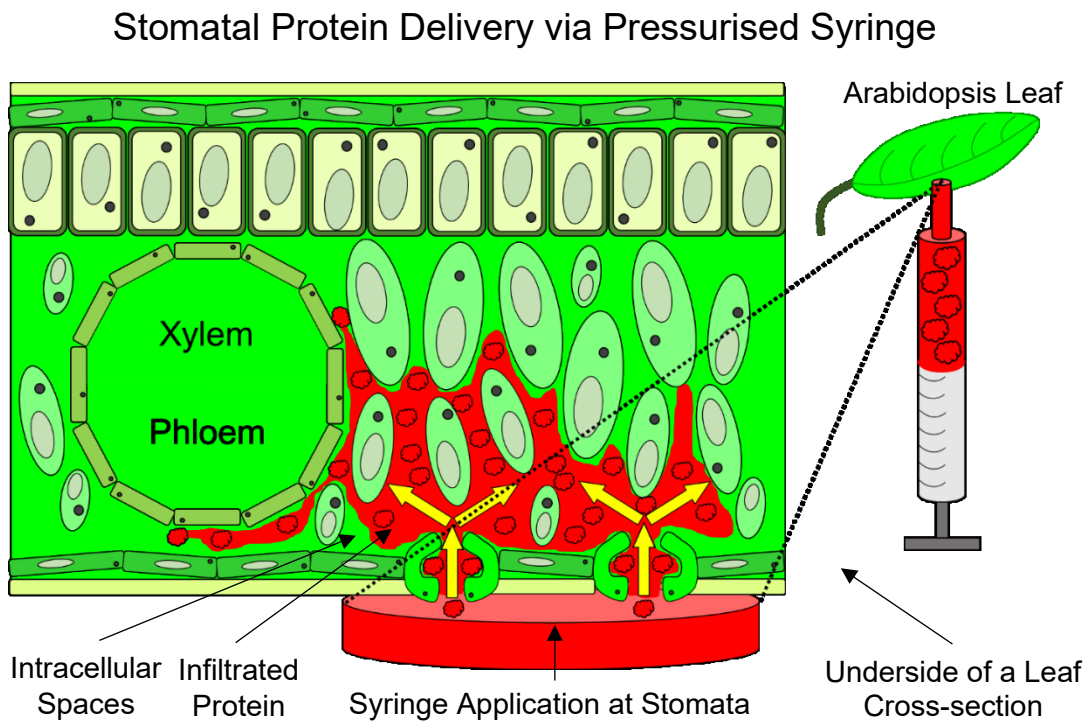
(3) Direct application onto the shoot apical meristem.

5.3.1.1 – Stomatal Openings on the Underside of the Leaf

On the underside of the leaf, the stomata form a porous network of openings for gaseous exchange, specifically, transpiration (O_2 and H_2O diffuse out) and photosynthesis (CO_2 diffuses in). Two guard cells stand sentry at the opening and whilst they are turgid, the stoma remains open [206]. Classically, plant transfection was via stomatal infiltration using a blunt ended syringe and resultant pressure, placed on the underside of the leaf, filled the intracellular spaces with liquid – this was evidenced by a darker colour being observed inside the leaf after successful infiltration. This method is still regarded as a robust method for transforming Nicotiana after leaf infiltration with agrobacterium [207]. In Arabidopsis, the floral dip procedure is most readily used; however, it is also possible to transfect Arabidopsis using leaf infiltration [208]. Recombinant FT delivery inside the leaf was investigated using this infiltration method. In this study, after successful infiltration, a solution of protein surrounded the cells via the intracellular spaces; cellular uptake investigations were also performed.

Initially, TFL1 was a straightforward sample to work with as it can withstand harsher working conditions and does not aggregate (no surface cysteines present); it also has a higher melting temperature than FT and as such was used to design and optimise the protein infiltration procedure. Infiltration of TFL1 was first tested in Tobacco as classically this was the easiest sample to infiltrate with 2 mL standard volumes. SDS-PAGE was used to analyse samples after protein extraction from the leaf (see *Figure 38*). On incubation, a band was observed for recombinant protein in the sample indicating successful infiltration. An activity assay was considered to check the function of TFL1 before infiltration, in addition to proper folding by size exclusion chromatography and centrifugal protein aggregation removal.

The interaction of 14-3-3 with TFL1 was studied by David Charles who recorded a dissociation constant of 10.3 μM ± 2.7 μM and this interaction was confirmed below [41]. However, when the assay was repeated for FT, the complex did not run on an electrophoretic gel and interaction was not observed by electrophoretic mobility shift assay (EMSA). A complex however did form, and this interaction has been studied by other techniques such as microscale thermophoresis [41]. Unfortunately, an activity assay was not available for FT in this work.



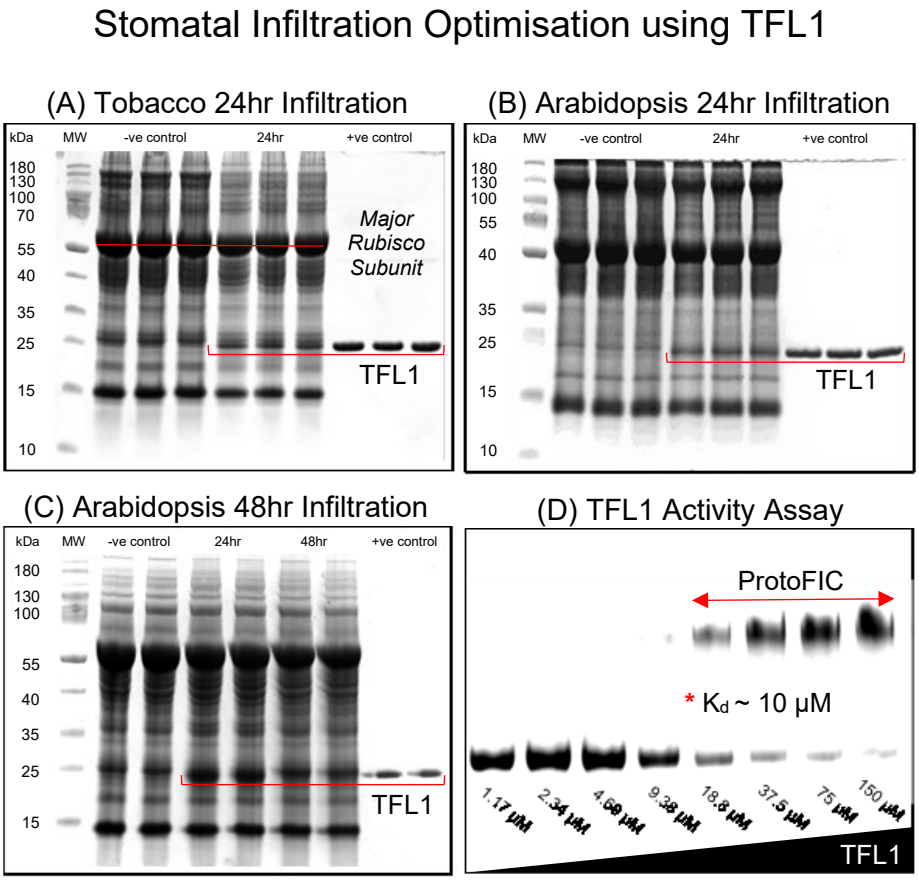


Figure 43 – Stomatal protein delivery via pressurised syringe. **(A)**-**(C)** Depicts stomatal infiltrations and protein recovery via cellular extraction, for **(A)** tobacco, **(B)** Arabidopsis and **(C)** Arabidopsis (both 24- and 48-hour incubations). **(D)** Activity assay showing functional TFL1 through 14-3-3 interaction, as shown by EMSA. Proto-14-3-3-TFL1 complex forms - shown by the gel shift.

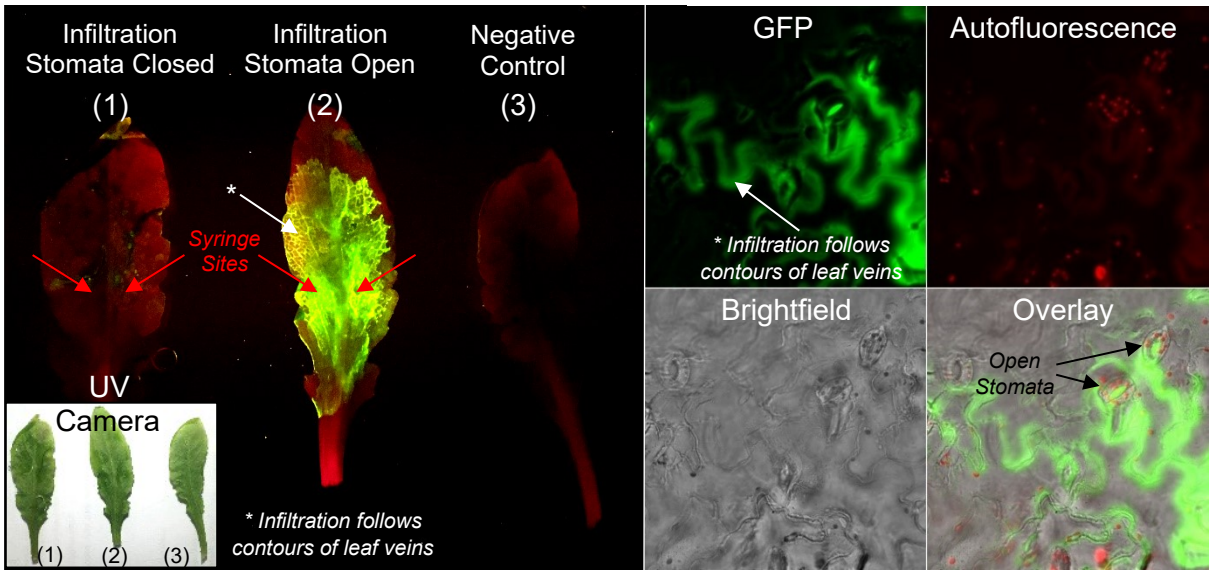


Figure 44 – FT-GFP Infiltration inside the leaf via stomatal entry. The left hand collection compares 3 leaves **(1)** unsuccessful infiltration through closed stomata, **(2)** succeessful infiltration through open stomata, **(3)** negative control comparison (no attempted infiltration). Brightfield camera images also shown for **(1), (2)** and **(3)**. The right hand collection shows a confocal microscopy tile of successul infiltration through the stomata and FT-GFP follows the contours around the cells.

Stomatal delivery of TFL1 and subsequent protein extraction showed that it was possible to recover the infiltrated sample after 24 hours inside the leaf in Tobacco and Arabidopsis. In the extracted plant sample, a plant protein band occurred at the same height as TFL1, therefore superior Western blot analysis was also employed in the further experiments as it is a method to detect protein presence.

FT-GFP purified in the previous chapter, was used to visualise protein after stomatal infiltration. In *Figure 40* below, the patterning of FT-GFP followed the contours of veins in the leaf. The time of day for infiltration was important; in order to ensure that the stomata were open; plants were also watered the previous evening [206]. Confocal microscopy imaging showed the FT-GFP entry through the stomata from whence the protein solution followed the intracellular apoplastic spaces inside the leaf. Initially, it was clear that stomatal entry was viable for delivery inside the leaf.

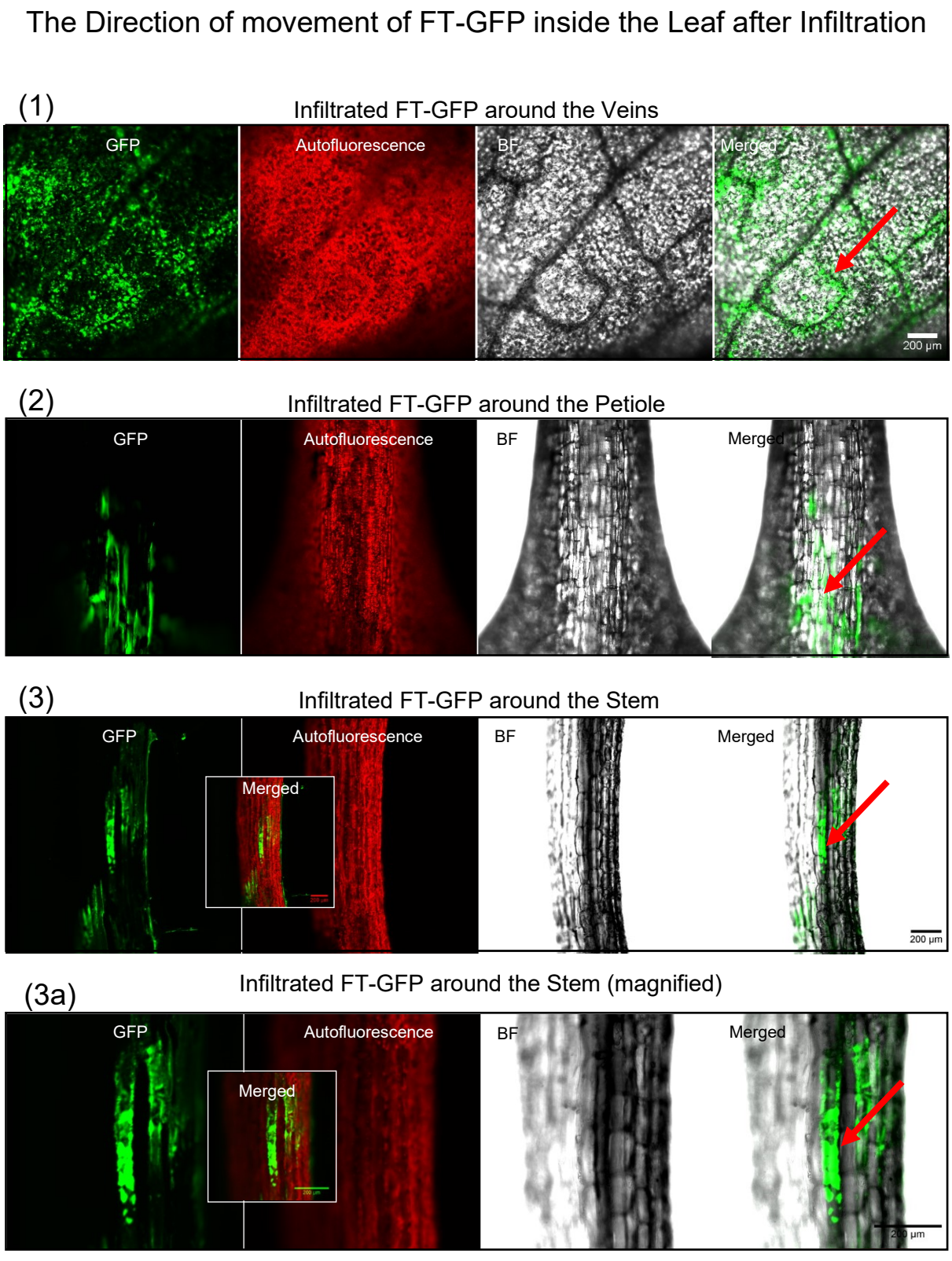


Figure 45 – The direction of movement of FT-GFP inside the leaf after infiltration. Confocal microscopy was used to investiate residing locations of FT-GFP after stomatal infiltration at the veins, petiole and inside the stem. **(1)** FT-GFP surrounded the veins after infiltration, **(2)** FT-GFP surrounded the petiole after infiltration, **(3)** FT-GFP in the stem and **(3a)** enlarged image. The red arrows highlight the residing location in each case.

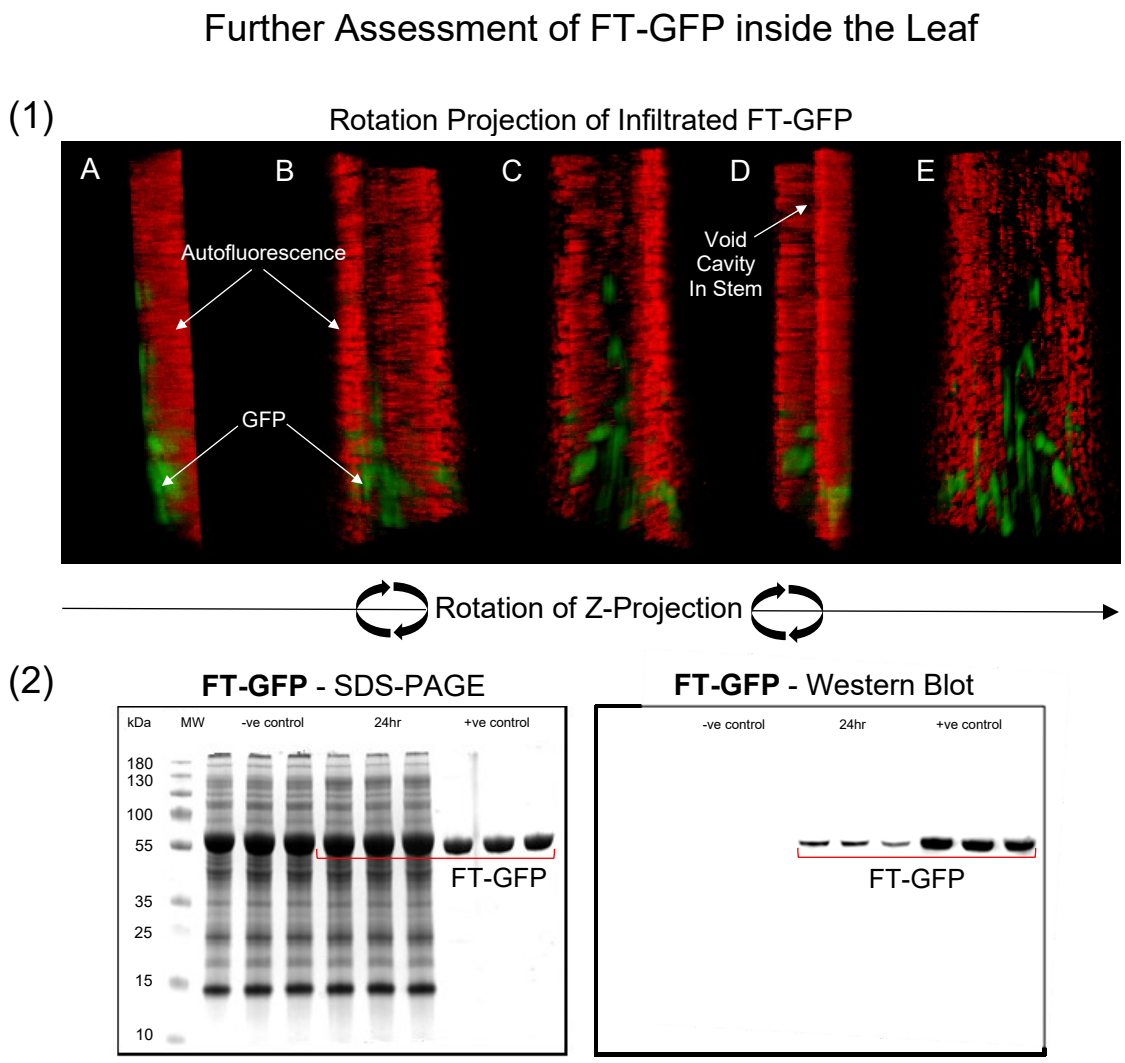


Figure 46 – Further assessment of FT-GFP inside the leaf. **(1)** Assessment of FT-GFP location inside the stem. The z-stack composite depth image is presented in the programme Velocity as a projection of rotations *(A)-(E)*. **(2)** SDS-PAGE and Western blot analysis of FT-GFP uptake inside the leaf.

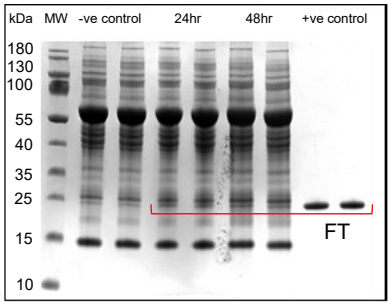
In *Figure 41* above, the programme Velocity was used to present the z-stack image of FT-GFP within the stem as a projection and was shown as a rotation about that projection in 5 time-lapse sections, *(A)-(E)*. A void cavity is present in the vasculature cells due to a minimal chlorophyll presence and this useful artefact was employed to determine FT-GFP position within the cavity. In addition, the recovery of FT-GFP by SDS-PAGE and Western blot showed that protein had not degraded and fluorescence was attributed to the complete fusion protein rather than a cleaved GFP component. The weaker band in the Western blot in *Figure 41* for

infiltrated protein was likely to be due to a technical constraint where protein was lost upon infiltration.

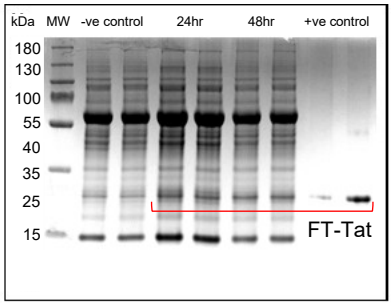
In the same way as before, recombinant FT, FT-Tat and FT-R9 were delivered via stomata and successful recovery assessed by SDS-PAGE and Western blot. In the previous chapter, CPP-tagged FT protein uptake was assessed in callus culture and further evidence presented below in *Figure 42*, indicated that R9 and Tat tagged proteins attached to the cellular boundaries yet were unable to penetrate inside the cells. Western blots were conducted with the help of undergraduate student, Laure Fourquet, and they showed the successful recovery of the protein up to 48 hours after infiltration. These results further reiterated that it is possible to deliver protein inside the leaf and that it remained stable and was not degraded. On account of this and the fact that any protein delivered inside the cells would subsequently have to move to the companion cells and translocate to the SAM, this mode of delivery was considered too complicated. Preliminary results showed protein inside the leaf, but fluorescence inside the cells was not observed.

FT, FT-Tat and FT-R9 Infiltration into Col-0 Leaves

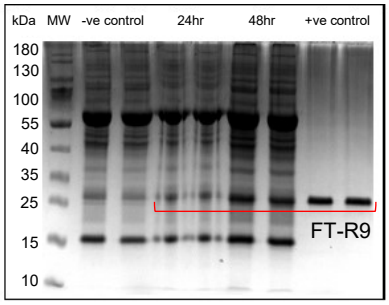
FT – SDS-PAGE



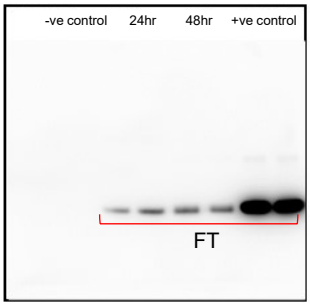
FT-Tat – SDS-PAGE



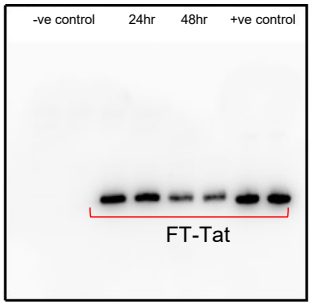
FT-R9 - SDS-PAGE



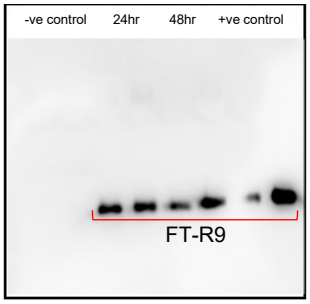
FT – Western Blot



FT-Tat – Western Blot

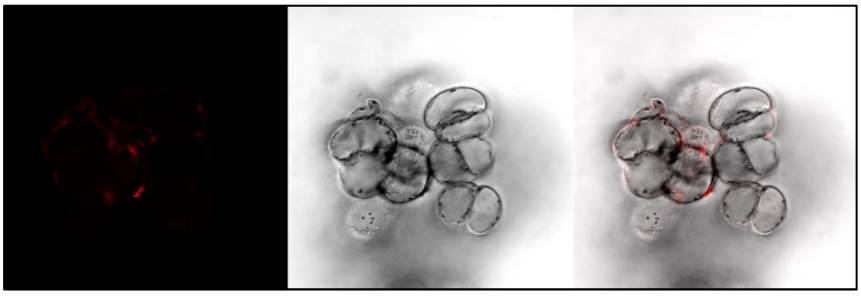


FT-R9 – Western Blot

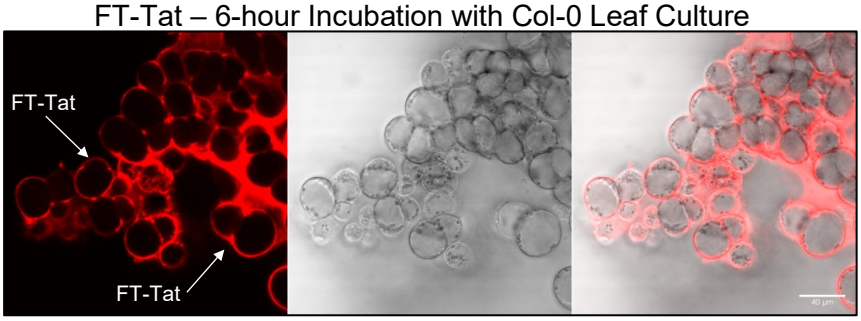


Western blots conducted with the assistance of Laure Fourquet.

FT – 6-hour Incubation with Col-0 Leaf Culture



FT-Tat – 6-hour Incubation with Col-0 Leaf Culture



FT-R9 – 6-hour Incubation with Col-0 Leaf Culture

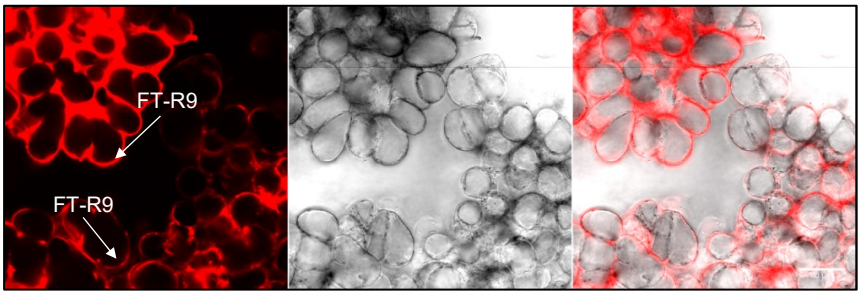


Figure 47 – FT, FT-Tat and FT-R9 infiltration into Col-0 leaves. The delivery of Recombinant FT, FT-Tat and FT-R9 inside the leaf is shown and then the recovery using SDS-PAGE and Western blot analysis. Confocal microscopy images are presented (complementing those presented in the *Chapter 4*) showing Sortagged FT, FT-Tat and FT-R9 and their interaction with the cellular boundaries in leaf callus culture. Western blots were carried out with the assistance of Laure Fourquet.

5.3.1.2 – Micro-injection

Inspiration for using this technique came from observing aphids and how they use their stylet to weave around the cells and selectively puncture sieve elements in the phloem [209]. This procedure is remarkably non-invasive and as such the cells are not compromised with callose formation, due to an aphid secretion sealing the insertion point, allowing *Myzus persicae* to successfully feed on Arabidopsis [210]. Aphid stylet mediated delivery has even been used to transport chemicals into the sieve elements [211]. Microinjection has been used effectively in plant sciences, albeit there is no recent work showing the application of microinjection technologies and literature reports are from the 1980s and 1990s [212, 213]. The aim in this investigation was to target the phloem cells with a microinjection needle and attempt to deliver recombinant protein directly into the sieve elements [213].

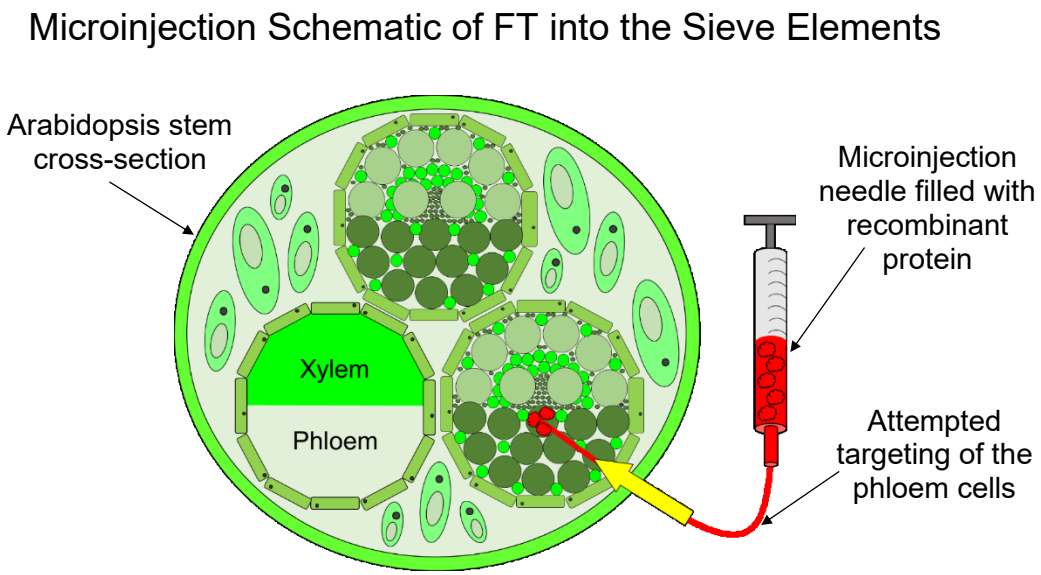


Figure 48 – Microinjection schematic of FT into the sieve elements. This diagram shows protein delivery through a pressurised syringe into the sieve elements through a cross section of the stem.

Initial optimisation experiments quickly demonstrated that it was not possible to perform precise cross-sectional microinjection on Arabidopsis with the tools available. Therefore, Sugar beet was tested as an alternative model [45]. The vasculature bundles in sugar beet are pronounced and it is possible to see them with the naked eye. The phloem is structured as a halo at the outer surface of the bundle, flanking the xylem (*Figure 44*).

Figure 44 below shows the sugar beet architecture and cross-sectional images as recorded by both confocal and widefield microscopy. The vasculature bundles and phloem halos are easily observed. The widefield cross-sectional sample displayed significant autofluorescence and this manifested strongly at the vasculature bundles which helped with detection. *Figure 44* shows the phloem in both cross-sectional and longitudinal samples and the site along the stem where the samples were taken, portraying extraordinary examples of imagery. In the subsequent *Figure 45*, microinjection targeting of the phloem was attempted and a microinjection needle and associated infrastructure assembled with FT-GFP loaded into the syringe. The phloem bundles were lined up using magnification and *Figure 45* below shows how they were successfully targetted with recombinant protein. The microinjection hole was visible through the tissue and FT-GFP deposited within the vasculature bundles.

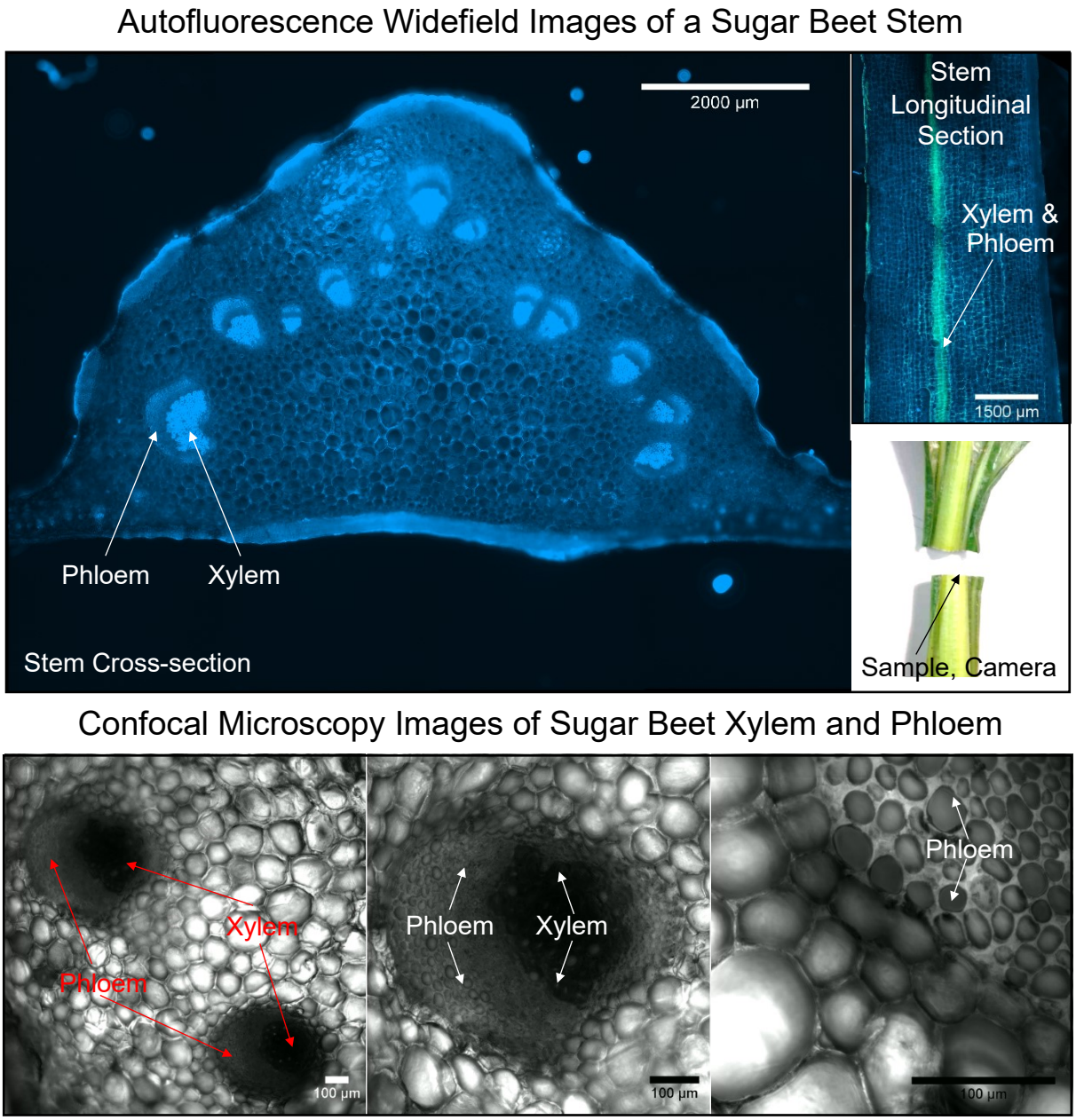


Figure 49 – Microscopy images of the phloem and xylem in sugar beet. The top section shows a cross-sectional slice through a sugar beet stem as recorded by widefield microscopy, a longitudinal section and a camera image of the sample. The bottom section shows three images of increasing magnification of sugar beet xylem and phloem when viewed from left to right as recorded by confocal microscopy brightfield imaging.

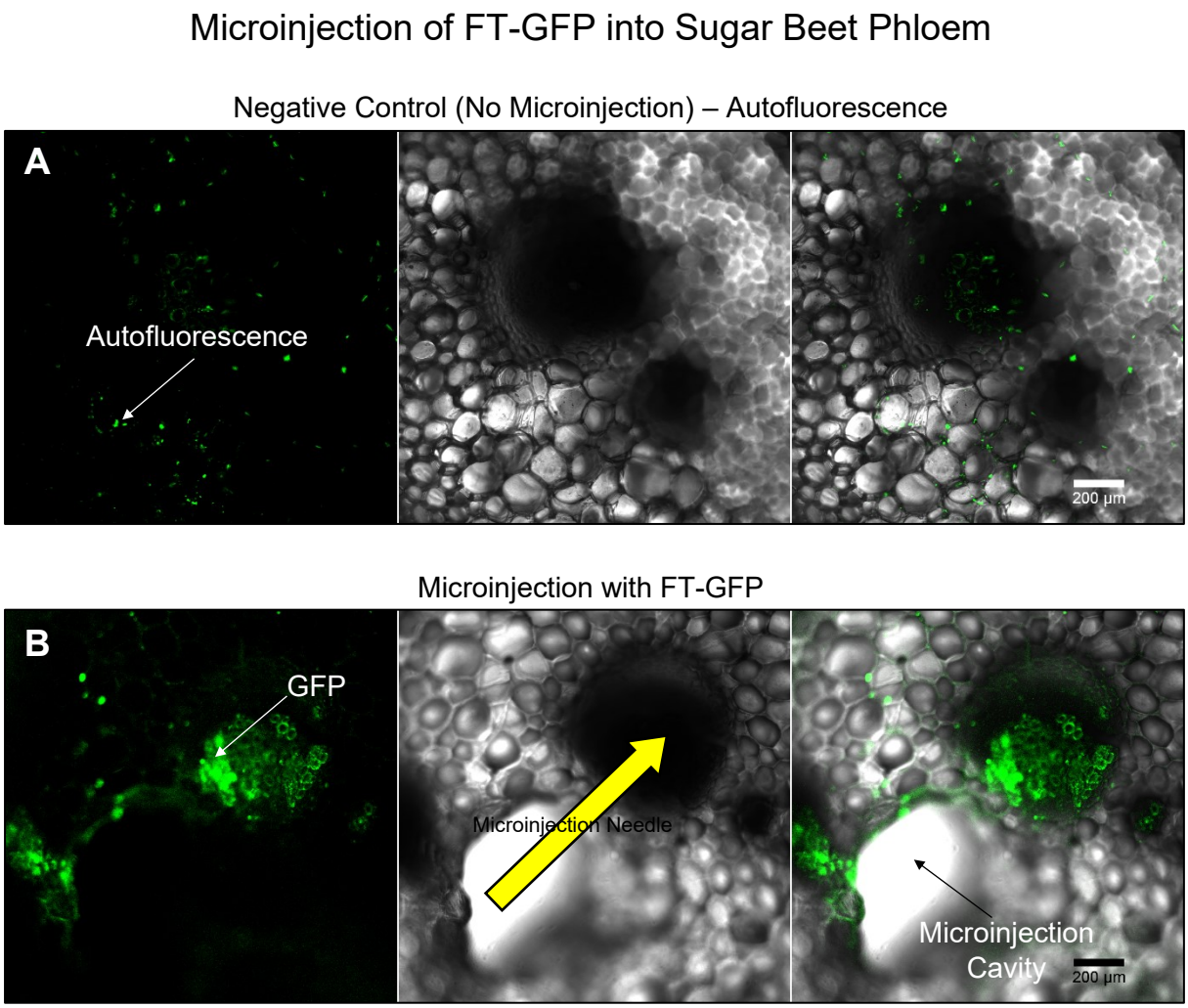


Figure 50 – Microinjection of FT-GFP into sugar beet phloem. **(A)** is a negative control confocal image, **(B)** is the attempted microinjection of FT-GFP into the phloem bundles of sugar beet and the remnant microinjection cavity was clearly seen in the tissue.

Microinjection as a technique was able to target the vasculature bundles, it was however invasive causing cellular damage and this prevented the recording of any FT-GFP movement along the bundles and indeed protein movement was not observed in confocal experiments. Whilst microinjection could be used to directly inject the shoot apical meristem cells in Arabidopsis, the technique was considered too challenging to use in the vasculature as a bird's eye view of the dissected meristem tissue was not possible to achieve using the available microinjection setup.

5.3.1.3 – Direct SAM Infiltration

Infiltration at the SAM was the most direct approach of delivering proteins to apical tissue. The SAM is hidden beneath layers of leaves and primordial leaves developing in whorls about the apex. Dissection was carried out in order to reach the apical dome however this area contained sensitive tissue and the procedure consequently was decided to be as non-invasive so as not to damage tissue and undifferentiated apical cells.

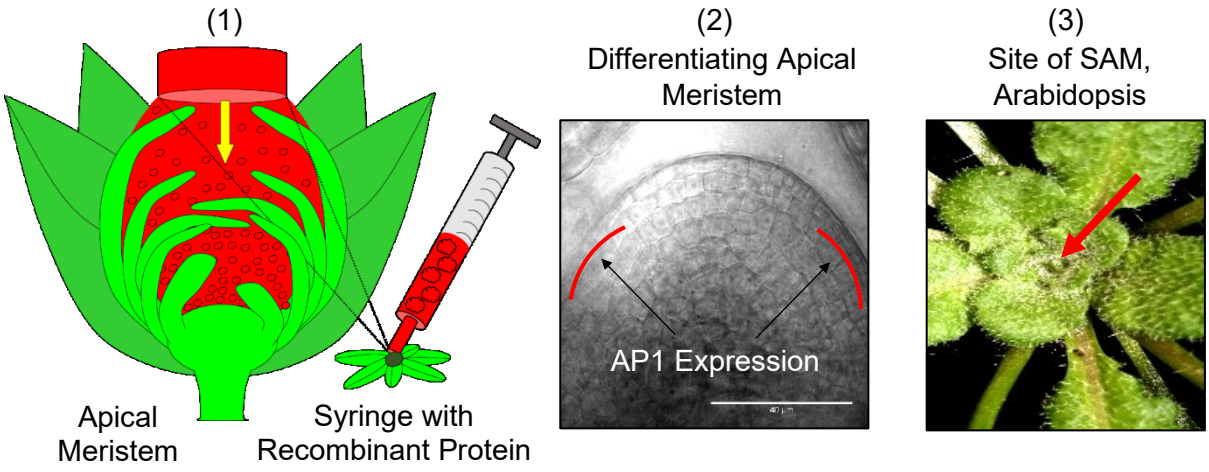
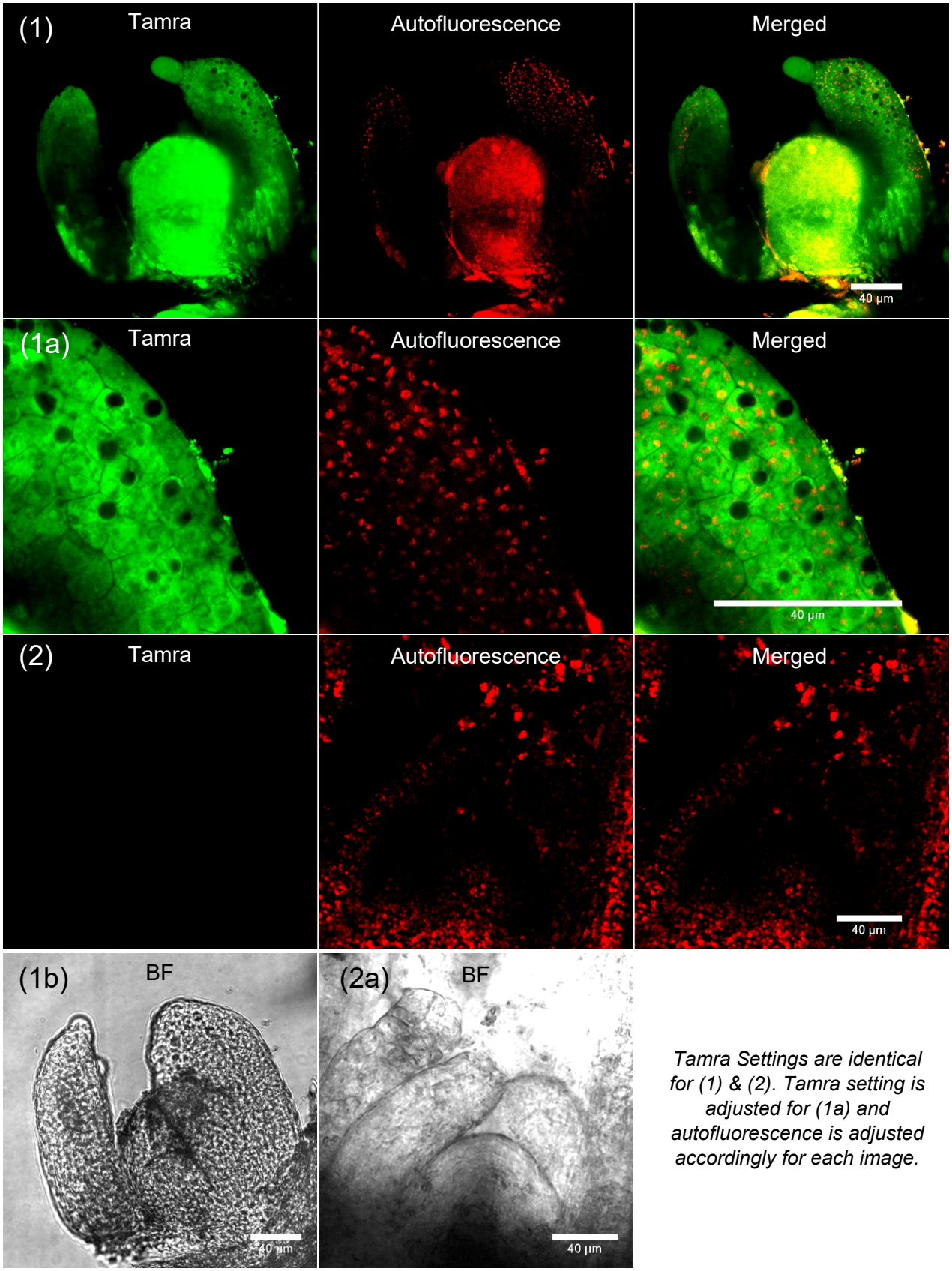


Figure 51 – Direct protein delivery to the SAM. **(1)** Infiltration at the apical meristem was via blunt ended syringe and dissection removed the outer leaves allowing access to the apical tissue. **(2)** The apical dome of a differentiating apical meristem, which was more pronounced after AP1 expression. **(3)** A 25-Day old Arabidopsis plant, the red arrow points to the site of dissection at the centre, with the SAM located beneath.

Early results showed that this technique had promise, whilst FT-Tat uptake in callus culture is limited by adhesion to the cell wall, the cells of the apical meristem appeared more supple and FT-Tat fluorescence was observed inside cells for the same incubation period. Whilst microdissection of the apical tissue did take time, the technique was an effective way of delivering protein to the apical meristem and the delivery and uptake of FT-Tat was presented in the following *Figure 47*.

FT-Tat Incubation with the SAM



Tamra Settings are identical for (1) & (2). Tamra setting is adjusted for (1a) and autofluorescence is adjusted accordingly for each image.

Figure 52 – FT-Tat incubation with the SAM. (1) Incubation of FT-Tat with SAM, **(1a)** zoomed image, **(2)** negative control water incubation. **(1b)** and **(2a)** are associated Brightfield images.

FT-Tat was clearly visible inside cells and the zoomed image showed its location inside the cell with the empty vacuole structures. The Sortagged TAMRA-FT-Tat was clearly distinguished against background autofluorescence and the negative control recorded sample acquisition settings for a water incubation and showed no fluorescence, deducing that all observed fluorescence was attributed to recombinant Sortagged protein. Whilst *Figure 47* reported a successful incubation, technical considerations meant that it was not possible to land the protein on the apical meristem each time. This was due to the structure being difficult to observe through the microscope, which meant that if the protein moved from the target area due to the water tension of the solution readjusting it was not always possible to correct the movement and the protein would be effectively misplaced. This is shown in *Figure 48*.

The slides below in *Figure 48* are for sample meristems which have begun differentiation. They were 3 weeks old and grown under long-day conditions. The incubations have been included merely as a model to show how recombinant protein uptake after infiltration was not consistent across a sample set. The brightfield images showed the integrity of the samples and TAMRA fluorescence was clearly distinguishable from background autofluorescence as shown in the merged images. It was also not clear how much infiltrated protein would have to be applied to cause a biological effect; whilst uptake was considerably lower than for *Figure 47* above, a small amount of endocytosed protein might be enough to activate AP1. This will form an important part of future work.

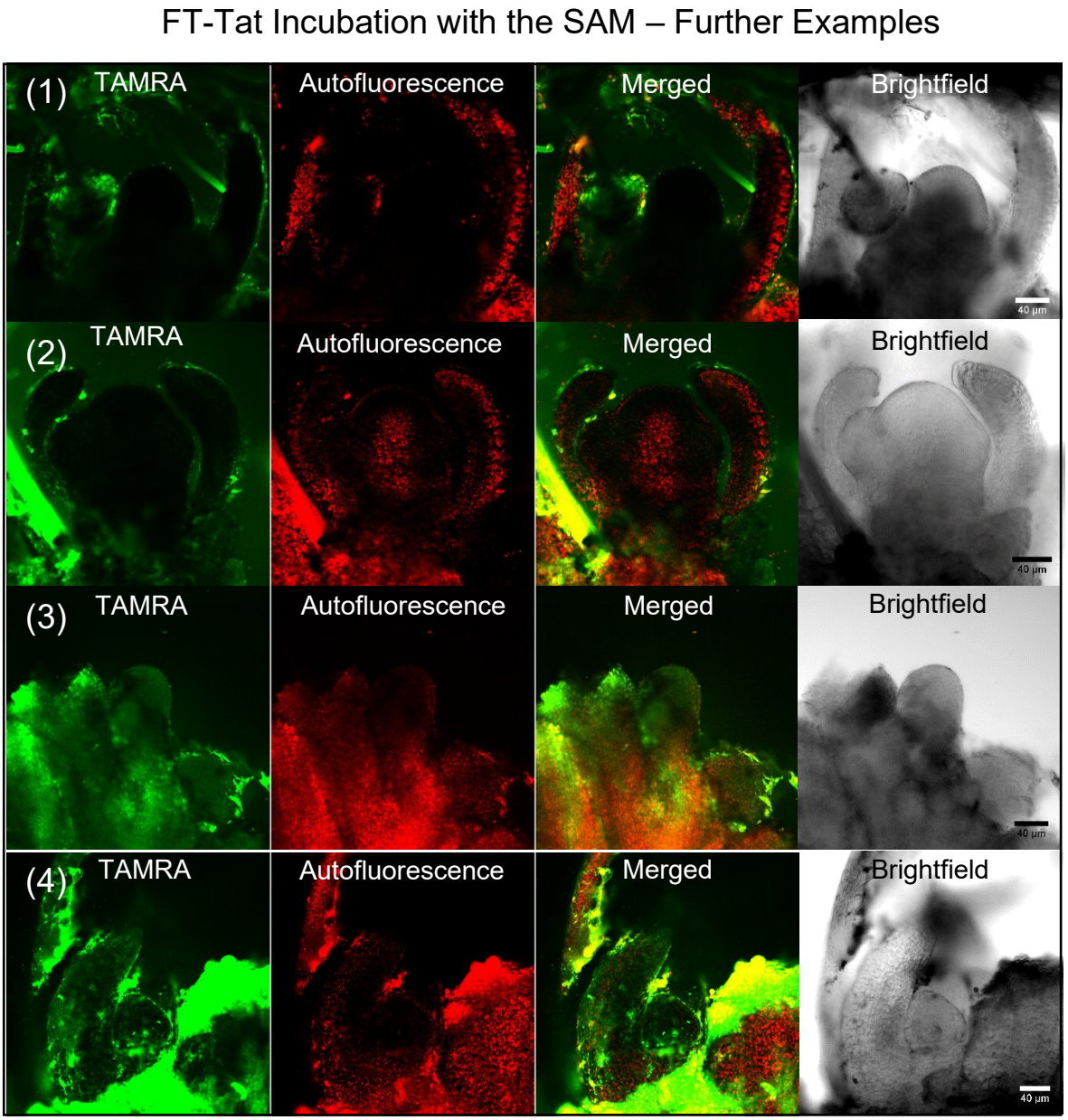


Figure 53 – FT-Tat incubation with the SAM – further examples. (1), (2), (3), (4) shows 4 examples of the FT-Tat delivery onto the apical meristem structure and the inconsistency in uptake as recorded by confocal microscopy.

5.3.1.4– Review of Available Delivery Routes

Advantages and Disadvantages of Protein Delivery Strategies

(1) Stomatal Openings on the Underside of the Leaf

Advantages

- Easily accessible and non-invasive procedure.
- High throughput.

Disadvantages

- Large infiltration volume required (50 µL *c.f.* 3 µL for SAM infiltration).
- This was the furthest delivery point from site of action. After successful infiltration. protein still had to enter cells and translocate to the phloem.

(2) Microinjection into the Vasculature

Advantages

- Can deliver protein directly to the native site of expression (sieve elements).

Disadvantages

- Invasive and can damage cells, causing callose formation which would prevent protein movement.
- Setup and technology not optimised for delivery into Arabidopsis phloem.
- Large application volume of protein required to fill microinjection needle (50 µL).
- Low throughput.

(3) Direct Application to the Shoot Apical Meristem

Advantages

- The most direct method, and not requiring protein to travel to site of action.
- Small infiltration volume required (3 µL).

Disadvantages

- Medium to low throughput.
- Risk of damaging the tissue (including apical tissue) during dissection procedure.
- Inconsistency – application technique wasn't always spatially accurate.

Conclusion

From the 3 potential uptake routes, the most viable was direct infiltration onto the SAM as this required a small incubation volume (3 µL) and was the most direct method, avoiding the added complication of tracking recombinant protein movement in the sample. Whilst leaf infiltration was higher throughput than direct infiltration, it required larger volumes to fill the apoplastic space and also was the farthest application entry point from the site of action. Microinjection did not offer any advantages over SAM direct infiltration. Therefore, it was concluded that the best route to deliver recombinant FT protein was directly at the SAM and this was taken into account in the following experiments in the second part of the chapter.

Text Insert 4 – A summary of exogenous protein delivery routes. The advantages and disadvantages are presented by the three delivery routes which were assessed within the first part of this chapter.

5.4 – Results – Part 2

5.4.1 – Phenotypic Assessment

The first part of this chapter investigated three potential methods for applying the recombinant protein treatment and concluded that direct application at the SAM was the most optimal. In Part 2, the biological effect of exogenous recombinant protein treatment was tested and assessed using two approaches. These were: firstly, plants were given the recombinant protein treatment and a phenotypic readout marked the macroscopic appearance of buds; secondly, a molecular reporter constructed with the AP1 promoter with the aim of assessing GFP expression through artificial AP1 activation was developed. A number of plants were treated with FT and FT-Tat (FT-R9 treatments were not conducted). FT-R9 had a significantly lower recombinant expression level in *E. coli* and as large quantities of protein were required for experiments, it was more appropriate to use FT and FT-Tat. A number of different conditions were trialled and optimised for both FT and FT-Tat and these results are presented with the following evidence.

5.4.1.1 - Flowering Time Results - Treatment at 45 Days Old

After initial piloting experiments, an advanced study was conducted on plants which were 45 days old at the point of treatment. The experimental design is presented below in *Figure 50*, and includes both a single treatment and triple treatment (three single treatments over 3 days) for FT and FT-Tat at both 5 and 50 μM concentrations (3 μL application volumes). BSA was used as a control treatment and the untreated control included as reference for the expected normal flowering time under short-day conditions (approximately 70-day old untreated plants began to flower).

The macroscopic appearance of buds was recorded at daily intervals. At 21 days after initial protein treatment (66-day old plants), the number of bolted plants was recorded and this was defined as a stem elevation of at least 1 cm. A 5 μM (3 μL volume) single treatment of FT,

remarkably caused half the plants to flower (12 out of 24 data points) and this was the most successful treatment recorded for the experiment (*Figure 50a*). The second most successful was recorded for a 50 μM FT triple treatment where 10 out of 24 samples displayed early flowering - the results are presented in *Figure 50a*.

In addition to these encouraging results, the observed phenotypes for a small number of treated plants were particularly interesting revealing a curious partial inductive phenotype (in *Figure 50a*). In these examples, plants have displayed early buds but have then returned to a vegetative state with final flower formation not observed. 6 examples overall were recorded and the images in *Figure 50a* below showed that the phenotype was very different from the complete inductive phenotype. *Image 2* in *Figure 50a* is particularly striking showing the stem having bolted after the development of buds, and has then returned to a vegetative state and floral buds are no longer visible at the vegetative apex. This phenotype is also very pronounced in the repeat treatment (*Image 1* in *Figure 50b*).

It was important to observe the partial inductive phenotype in the repeat treatment for FT (*Figure 50b*), which was further supporting evidence that flowering was artificially activated with recombinant FT [214, 215]. Naturally, once light levels have reached a photoperiod threshold, FT is expressed endogenously and this occurs continuously [216]. In these experiments, either a single or a triple treatment of FT was applied to the plant whereas endogenously, an induced plant would continue to express FT during floral activation, with an abundant presence inside the plant after photoperiod induction [216]. This could help to explain the partially induced phenotype (floral reversion) - enough FT is delivered to apical cells to cause the developmental changes and even induce bolting; however, the plant returned to a vegetative meristem once FT availability stopped and this gave rise to the unique partially bolted and potentially vegetative phenotype following induction.

Experimental Design for FT and FT-Tat Treatment for 45-Day Old Plants

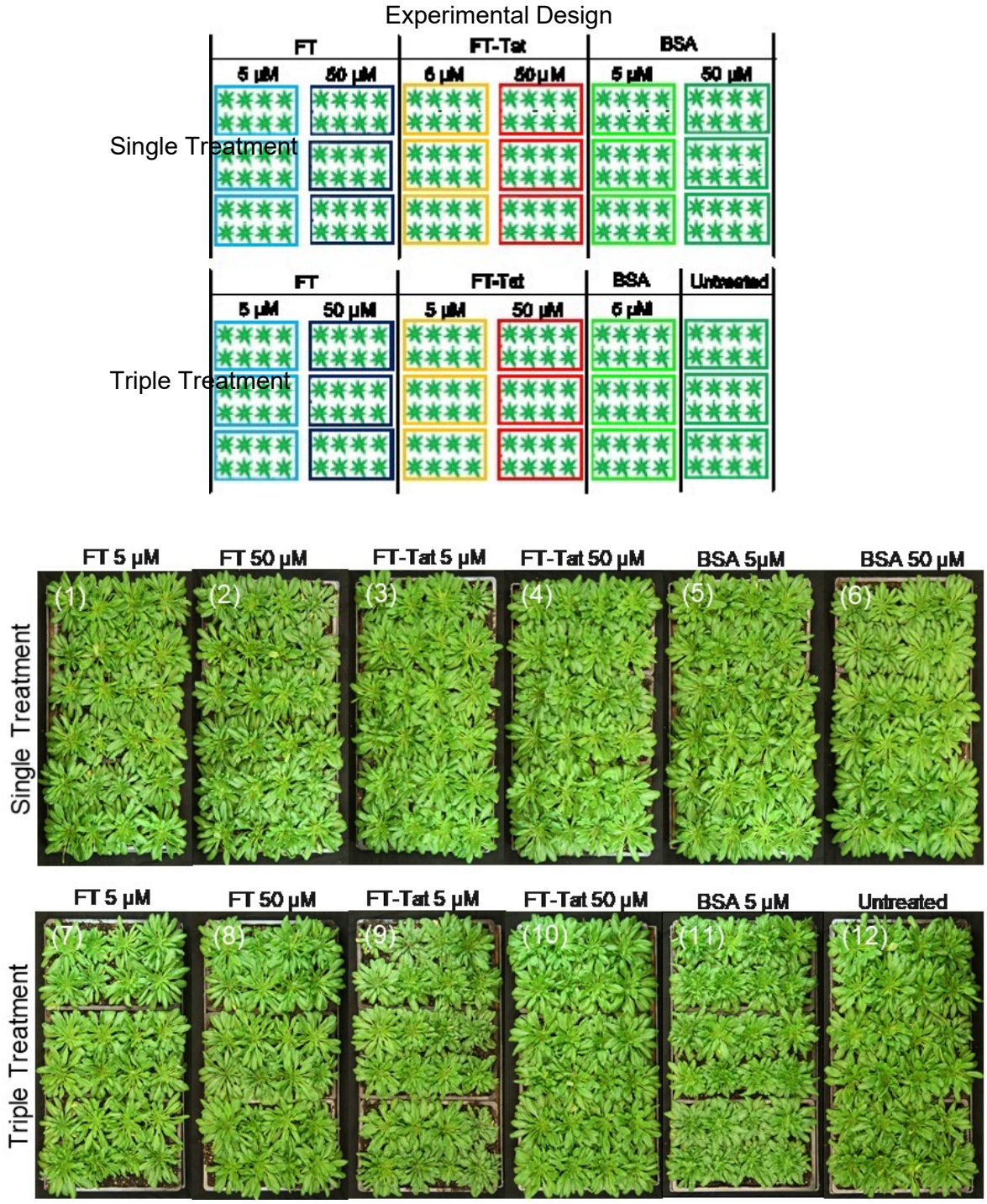
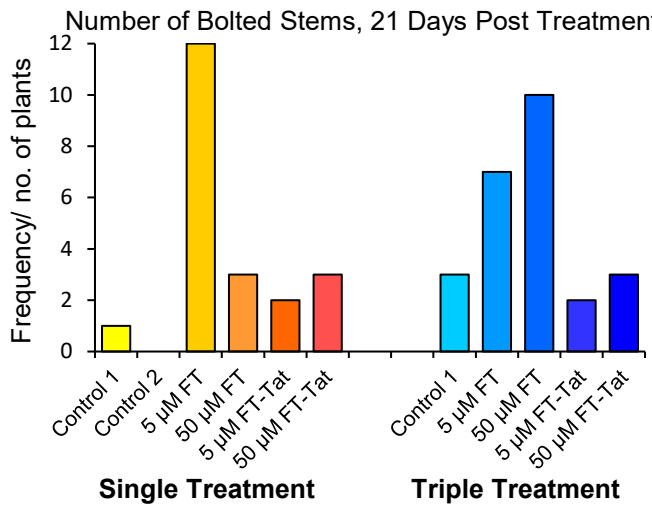
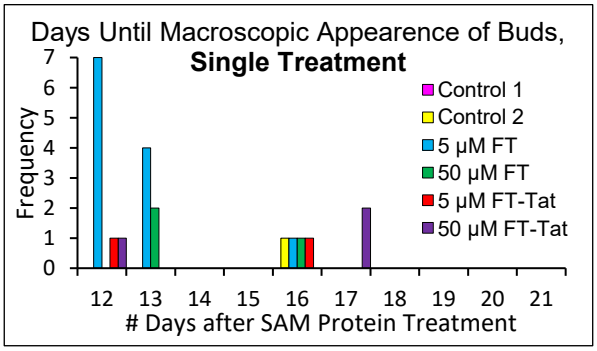


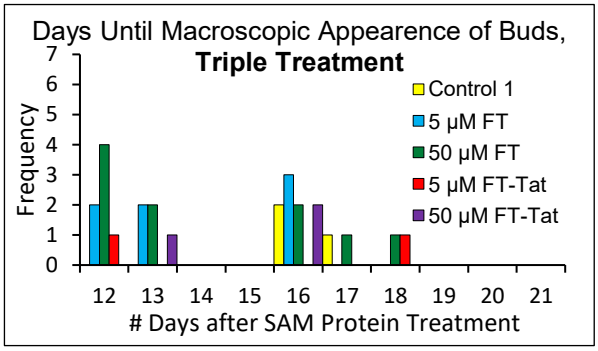
Figure 54 – Experimental design for FT and FT-Tat treatment for 45-day old plants. Shows the experimental design for treatment of short-day grown plants at 45 days old, and also shows the size and scale of the experiments with healthy plants. The data recorded from these plants is summarised in *Figure 50a* below.

45-Day Old Treatment & Unique Partial Induction Phenotype (***Fig 50a***)

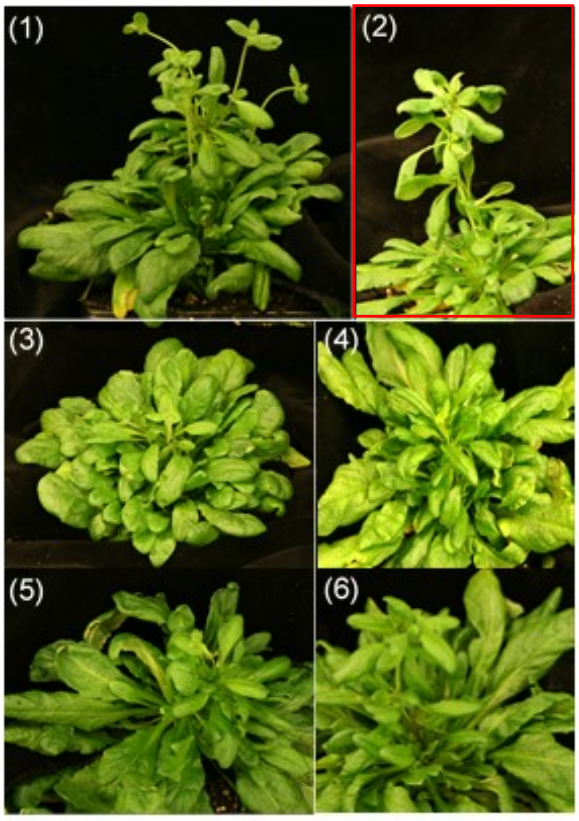


Single Treatment/ 24 plants		
Condition	# Bolted	% Bolted
Control 1	1	4%
Control 2	0	0
5 µM FT	12	50%
50 µM FT	3	12%
5 µM FT-Tat	2	8%
50 µM FT-Tat	3	12%
Triple Treatment/ 24 plants		
Control 1	3	12%
-	-	-
5 µM FT	7	28%
50 µM FT	10	42%
5 µM FT-Tat	2	8%
50 µM FT-Tat	3	12%

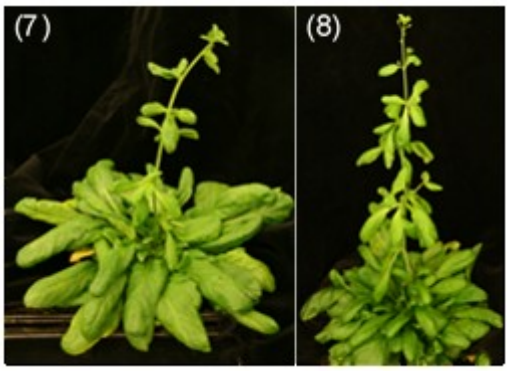




Partial Induction Phenotype



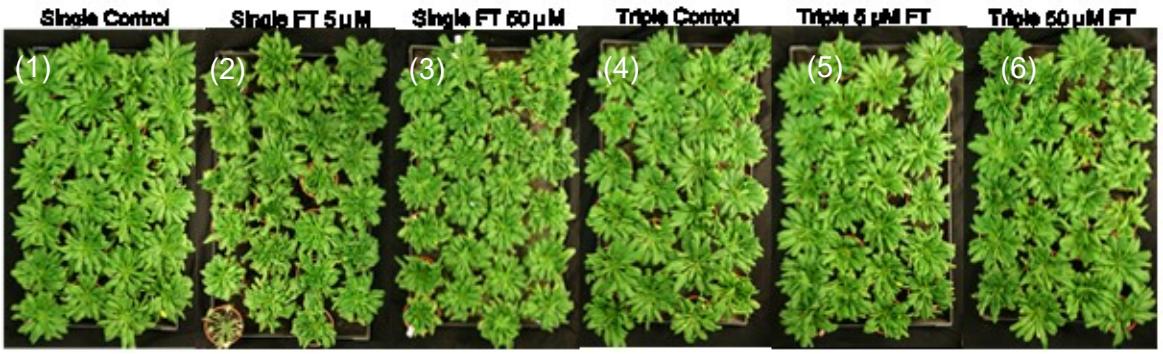
Typical Complete Induction

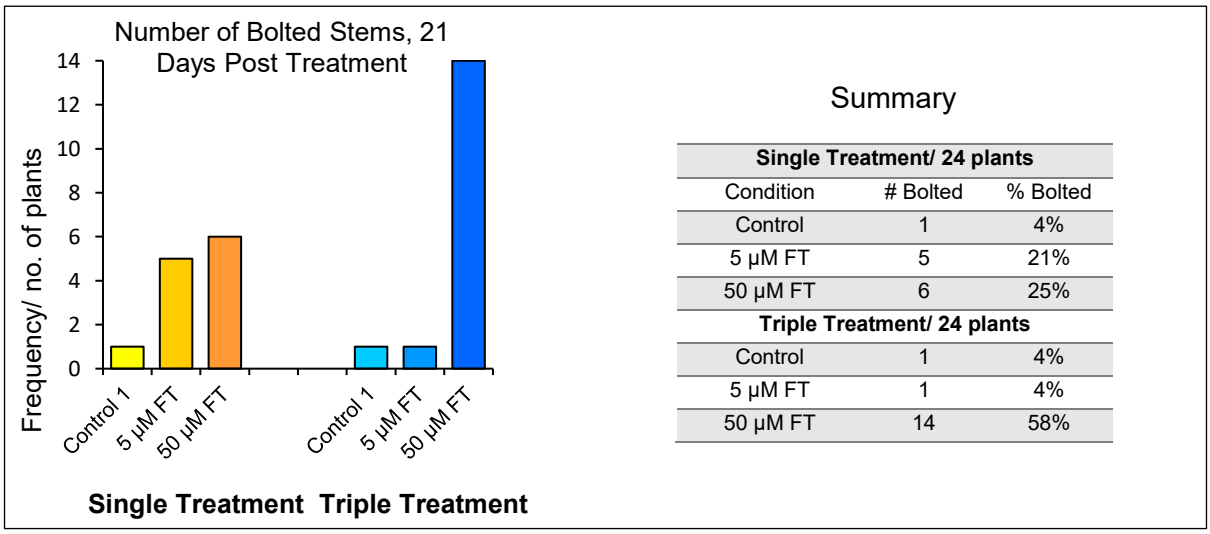


Partial vs Complete Induction



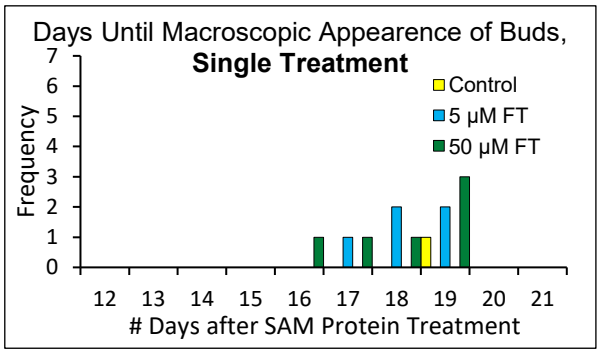
Repeat of 45-Day Old FT Treatment & Unique Phenotype ***(Fig 50b)***

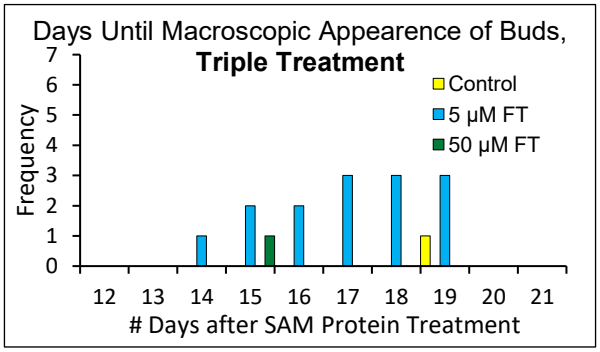




Summary

Single Treatment/ 24 plants		
Condition	# Bolted	% Bolted
Control	1	4%
5 µM FT	5	21%
50 µM FT	6	25%
Triple Treatment/ 24 plants		
Control	1	4%
5 µM FT	1	4%
50 µM FT	14	58%





Partial Induction Phenotype

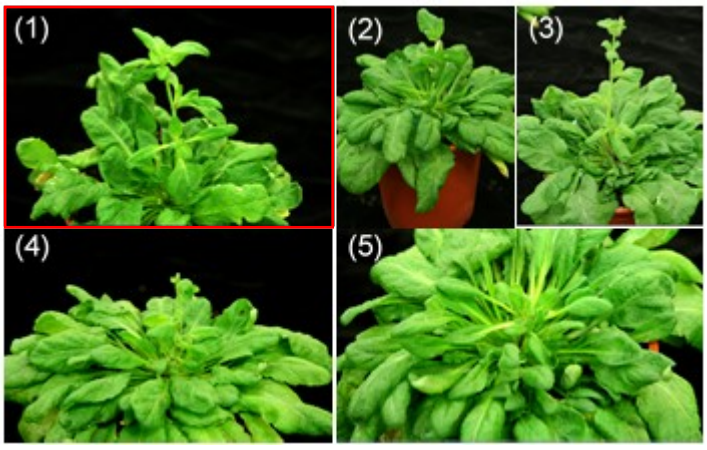


Figure 55a – 45-day old treatment, summary & unique partial induction phenotype. The quantitative assessment showed the macroscopic appearance of buds recorded as a function of days after treatment and the number of bolted stems recorded at 21 days post treatment of 45 days old Arabidopsis with 5 and 50 μM FT and FT-Tat. The images showed unique partially inductive phenotype recorded for 6 plants when compared to a full inductive phenotype.

Figure 55b - Repeat of 45-day old FT treatment, summary and unique partial induction phenotype. Results were repeated for the single and triple FT treatment at both 5 & 50 μM. Quantitative results summary is shown and also images recorded for the partial inductive phenotype.

In the repeated flowering time experiment in *Figure 50b*, the best treatment was a single 50 μM FT treatment, and 14 out of 24 plants were recorded with bolted stems at 21 days. This was interesting because it differs from the previous experiment in *Figure 50a* as the best treatment (5 μM FT single treatment), significantly it showed strong induction, compared to 1 control plant which had bolted at 21 days. The reason why a different treatment is showing the best phenotypic results might be because, as stated previously, it was not always possible to ensure that the protein landed directly on the apical meristem and in such cases, the protein may not have entered the cells as shown by the confocal microscopy images above in *Figure 48*. 5 and 6 out of 24 plants (in *Figure 50b*) for a single treatment of FT 5 μM and 50 μM were also recorded as bolted after 21-day post treatment and whilst this number was not as high as 14 plants, it was still noteworthy.

5.4.1.2 - Additional FT Treatments, 25 Days, 32 Days, Summary

In the previous experiments, the approach detailing FT delivery was via a delicate dissection of the surrounding leaves and primordial tissue and gentle application of the protein solution. It is not clear at this point if a threshold amount of FT is required for gene activations; inconsistent optimum treatment results were recorded for 5 μM and 50 μM protein solutions and single and triples dosages in *Figure 50a* and *Figure 50b*. It does appear that treatment with FT is superior to FT-Tat, and this might be an activity complication caused by the poly-arginine tag. Whilst the Tat tag may be able to assist in protein delivery, it might affect protein activity and as such the efficacy of the treatment may have been hampered. Whilst the

delivery of FT-Tat is assessed in previous chapters, an activity assessment was not made and this would form a useful component of future work.

In the following treatments presented in *Figure 51*, FT delivery was assessed for plants treated at 25 and 35 days and also for different concentrations of FT. It was clear that an FT treatment was able to accelerate flowering but it was not clear what the optimal amount and concentration of protein might be along with potential saturation effects. The dissection procedure was also important for exposing the meristem, but this work investigated whether it was actually necessary to perform this dissection. Instead, Tween-20 surfactant was added to protein treatments to minimise the coefficient of friction on surrounding leaf bases and with the aim of enabling the protein to leach into apical tissue, removing the need for mechanical dissection.

It is likely that the older the plant is the more effective the treatment will be, but it was important to investigate this as there might be an age threshold for when treatment efficacy becomes more effective. It is clear that there is a substantial difference between the response of 25-day old plants and 45-day old plants and this was also confirmed by Corbesier *et al.* [217]. No acceleration of flowering was observed in the experiments using Tween-20. This was an unexpected result and further experiments should be employed to test which treatment (concentration and molar amount) of FT is effective at a particular plant age for artificial activation of flowering [216, 217]. It is feasible that the older the plants are, the more responsive they are to treatment as they are biologically closer to flowering through autonomous progression due to the accumulation of higher levels of endogenous T-6-P [72, 73]. The scale of the experiment and the different treatments tested with 25 and 32-day old plants are presented below in *Figure 51*.

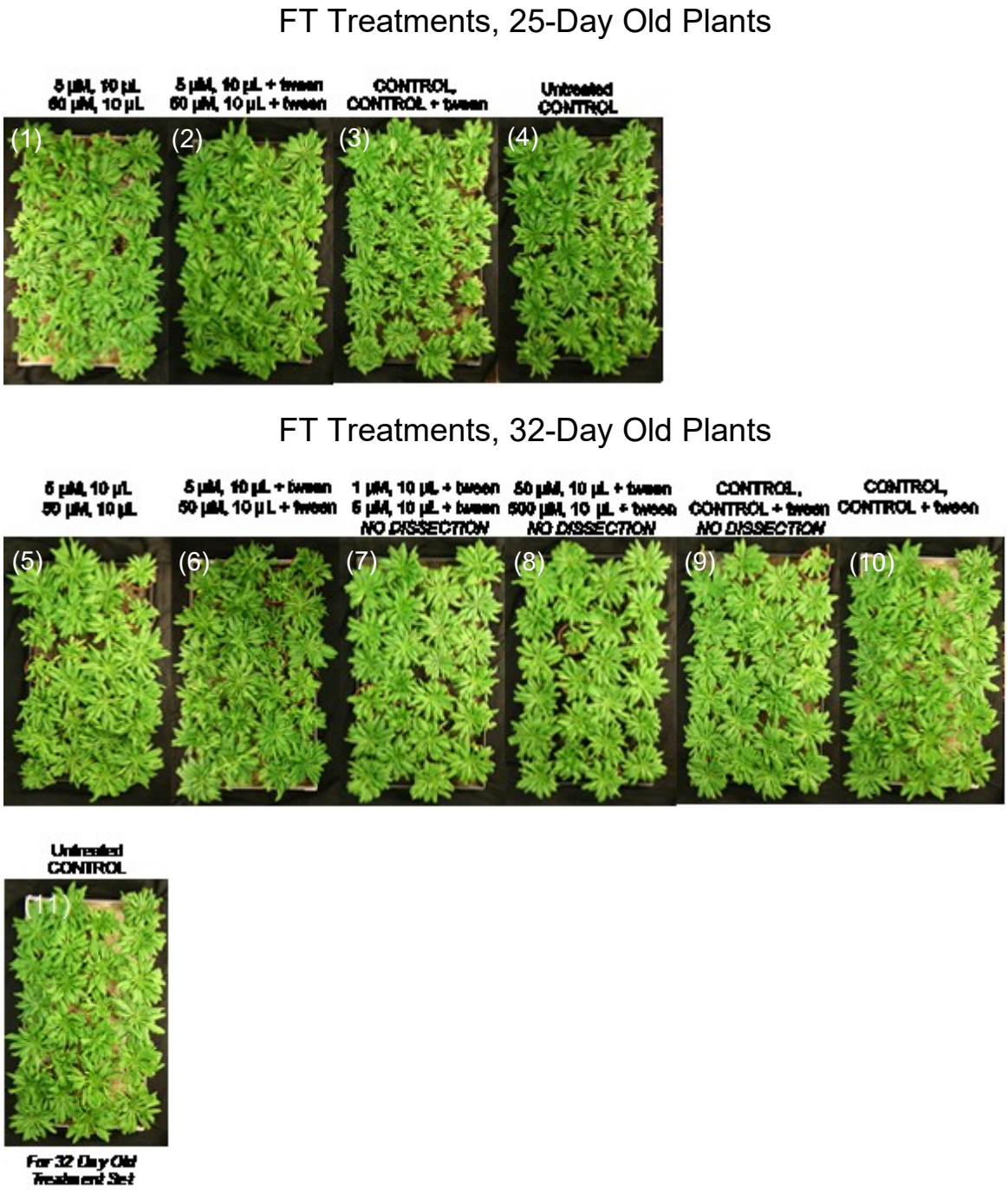


Figure 56 – Additional exogenous FT protein treatments. These include Tween-20 surfactant for plants at 25 and 32 days old. The scale of the experiment is depicted above, however the acceleration of flowering was not observed in experimental results.

5.4.2 – Molecular Readout

The phenotyping experiments yielded promising results, including examples of partial induction, demonstrating a floral reversion phenotype. This section reports the development of a transgenic reporter, designed to prove floral activation (via AP1 activation) at the molecular level through the activation of GFP. The reporter was designed comprising a 2000 base pair AP1 promoter sequence, known to include a C-box and a short-extended region which is the binding site of bZIP transcription factor, FD, in FAC [48]. The sequence for the 2000 base pair promoter DNA section is given in *Figure 53* below, including the highlighted C-box.

Previous data recorded in the Turnbull laboratory reported that the TFL1 binding sites in the ProtoFIC complex reside in an extended region around the C-box comprising of approximately 40 base pairs either side [7, 41]. Microscale thermophoresis and *in vitro* assays were used to show that TFL1 binds (whilst in a proto-complex with 14-3-3) to this region of sequence [7, 41]. The exact molecular mechanism underlying the molecular action of both FT and TFL1 is not fully understood [218]. The proto-complex of FT-14-3-3 does not bind to this truncated region and a proposed explanation is that FT binds to outer regions of the promoter within a 2000 base pair sequence to activate transcription of the AP1 gene (*Figure 52b*) [41]. For this reason, this 2000 base pair promoter sequence was used in the construction of the transgenic reporter.

In the pAP1::GFP in Col-0 transgenic reporter, a pGWB4 vector from the Gateway Series™ was used for plant transformation and this included the 2000 base pair promoter sequence given in *Figure 52b*. This was introduced by LR reaction and resided in front of the GFP sequence in the pGWB4 vector. In this way, in theory, binding of FAC to the 2000 base pair sequence would cause GFP expression in the transgenic plant which was observed using confocal microscopy. In addition, a plant line transformed with the pGWB4 vector without the promoter

DNA insert was created as a negative control and this is referred to as the *Empty Vector* (*c.f. Insert Vector*) in the text. It affirmed that GFP fluorescence is dependent upon FAC interaction with the 2000 base pair promoter sequence under photoperiod activation.

The reporter was tested for GFP expression and this was observed by growing the plants for 45 days under a short-day photoperiod and then transferring them to a long-day photoperiod for 7 days; the meristems were then dissected. Fluorescence was observed with the transformed insert vector whilst the empty vector displayed no GFP fluorescence even though the meristem had begun differentiation and was captured as an inflorescence meristem. This confirmed a functional reporter ready for experimental studies. The following *Figures 53* and *54* show the reporter working and the observed fluorescence. *Figure 52* below shows how the reporter was generated through cloning and the stages of selection in order to generate a homozygous line with a single insertion for both the insert and empty vector transformed plant lines. Finding constraints mean the dataset was incomplete, but an important part of future work will be to screen reporter plants after exogenous recombinant protein application.

Design of pAP1::GFP in Col-0 Reporter Line

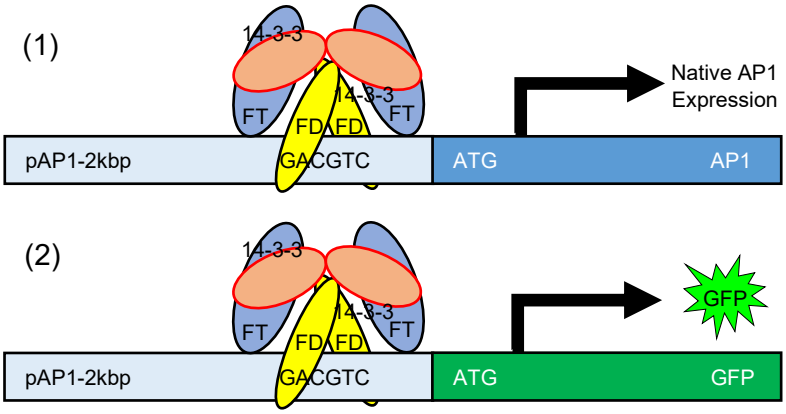


Figure 52a - Activation of AP1 via FT in complex with the 14-3-3 dimer and FD dimer (FAC). **(1)** Native FT expression as is the case in Col-0. **(2)** pAP1::GFP in Col-0 reporter – after FAC has bound to pAP1-2kbp, GFP is expressed showing activation of AP1.

pAP1 Promoter Sequence (2kbp)

```
aaaagggatatttaatgggaagaaaagaagggtggagatgtaacaaaggcgaagataatggatattcttgggatgttgtcttcaaggccacgagcttagattcttttagtttgctcaatt
tgttaagtttctacttttccttttgttgcttactacttttgctcatgatctccatatacatatcatacatatatatagtatactatctttagactgatttctctatacactatcttttaac
ttatgtatcgtttcaaaactcaggacgtacatgtttaaatttggttatataaccacgaccatttcaagtatatatgtcataccataccagatttaatataacttctatgaagaaaatacat
aaagttggattaaaatgcaagtgacatctttttagcataggttcatttggcatagaagaaatatataactaaaaatgaacttttaacttaaatagattttactatattacaatttttttctttt
ttacatggtctaatttatttttctaaaattagtataattgttgttttgatgaaacaataatacccgtaagcaatagttgctaaaagatgtccaaatatttataaattacaaagtaaatcaaa
taaggaagaagacacgtggaaaacaccaaatagagaagaaatggaaaaaacagaaagaaatttttttaacaagaaaaatcaattagtcctcaaacctgagatatttaaagtaatcaactaa
aacaggaacacttgactaacaaagaaatttgaaacgtggtccaactttcacttaattatattgttttctctaaggcttatgcaatatatgccttaagcaaatgccgaatctgttttttttt
tttttgttattggatattgactgaaaataaggggttttttcacacttgaagatctcaaaagagaaaactattacaacggaaattcattgtaaaagaagtgattaagcaaattgagcaaagg
tttttatgtggtttatttcattatatgattgacatcaaattgtatatatatggttgttttatttaacaatatatatggatataacgtacaaactaaatatgtttgattgacgaaaaaaaat
atatgtatgtttgattaacaacatagcacatattcaactgatttttgtcctgatcatctacaacttaataagaacacacaacattgaacaaatctttgacaaaatactatttttgggtttg
aaattttgaatacttacaattattcttctcgatcttcctctctttccttaaatcctgcgtacaaatccgtcgacgcaatacattacacagttgtcaattggttctcagctctaccaaaaac
atctattgccaaaagaaaggtctatttgtacttcactgttacagctgagaacattaaatataataagcaaatttgataaaacaaagggttctcaccttattccaaaagaatagtgtaaaat
agggtaatagagaaatgttaataaaaggaaattaaaaatagatatttttggttggttcagattttgtttcgtagatctacagggaaatctccgccgtcaatgcaaagcgaaggtgacacttg
gggaaggaccagtggtccgtacaatgttacttacccatttctcttcacgagacgtcgataatcaaattgtttattttcatatttttaagtccgcagttttattaaaaaatcatggacccga
cattagtacgagatatacccaatgagaagtcgacacgcaaatcctaaagaaaccactgtggtttttgcaaacaagagaaaccagctttagcttttccctaaaaccactcttacccaaatctc
tccataaataaagatcccgagactcaaacacaagtcttttttataaaggaaagaaagaaaaactttcctaattggttcataccaaagtctgagctcttctttatatctctcttgtagtttct
tattgggggtctttgttttgtttggttcttttagagtaagaagtttcttaaaaaaggatcaaaa----------GFP----------
```

Figure 52b - AP1 Sequence, 2000 base pairs used in the pAP1::GFP in Col-0 design. The C-box (gacgtc) is highlighted in yellow and an additional extended region around the C-box is highlighted in red. GFP is in place at the end of promoter and the start of the coding region.

pAP1::GFP in Col-0 Reporter Construction

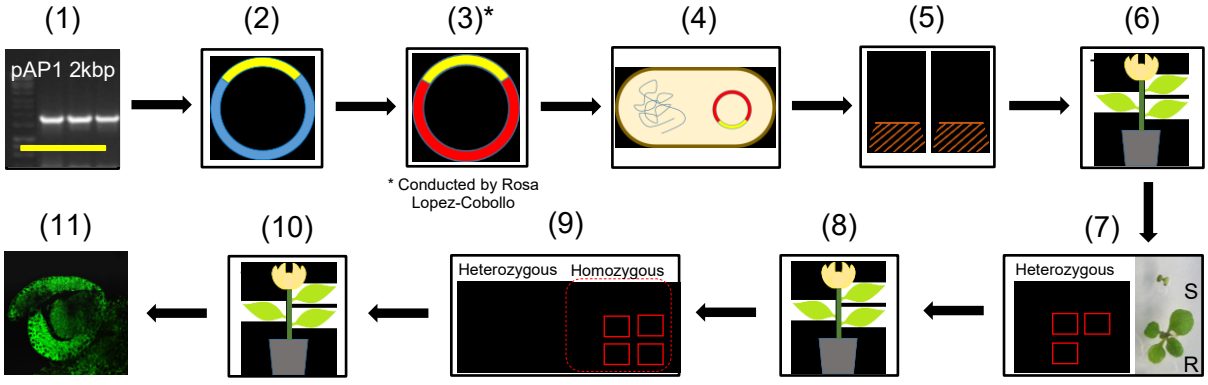
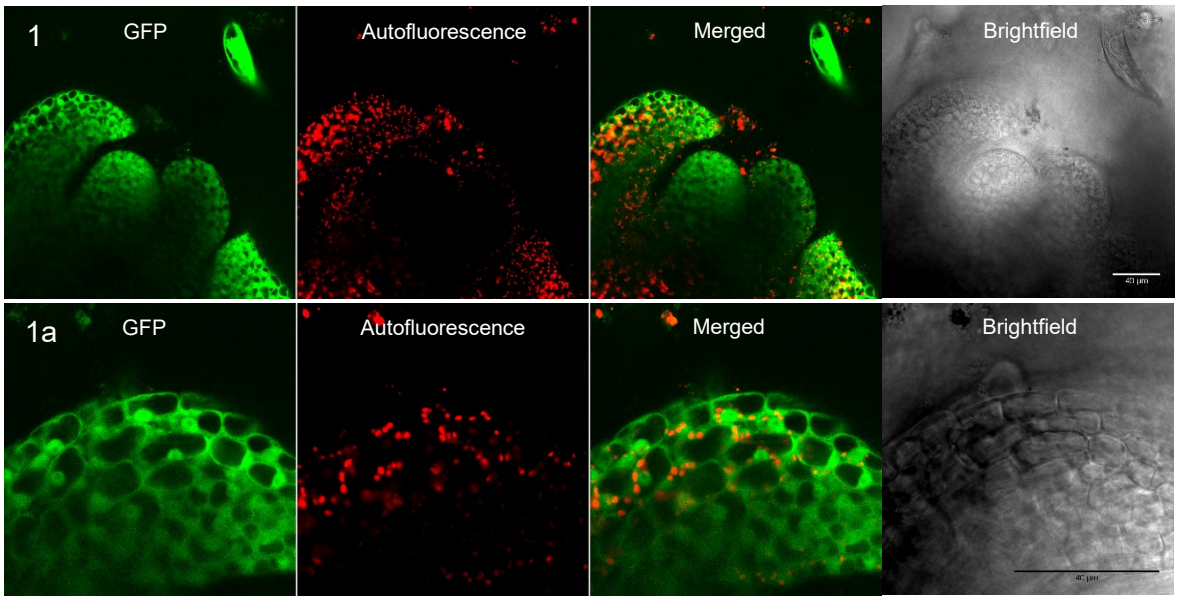


Figure 57c – pAP1::GFP in Col-0 molecular reporter design. **(1)** PCR of pAP1-2kbp, **(2)** TOPO cloning into pCR8 vector, **(3)** LR Reaction into pGWB4 vector *(conducted by Rosa Lopez-Cobollo)*, **(4)** transformation into *Agl1* agrobacterium, **(5)** growth of agrobacterium to confluence, **(6)** transformation of T_0 Col-0 and seed harvest, **(7)** antibiotic selection for single insertion via heterozygous ratio, **(8)** Growth of T_1 and seed harvest, **(9)** homozygous selection, **(10)** Growth of T_2 and seed harvest, **(11)** Assessment of GFP expression.

Assessment of GFP Expression for Differentiating pAP1::GFP in Col-0 Apical Meristem

Positive Control - Insert Vector Transferred to Long-Day Photoperiod



Negative Control - Empty Vector transferred to Long-Day Photoperiod

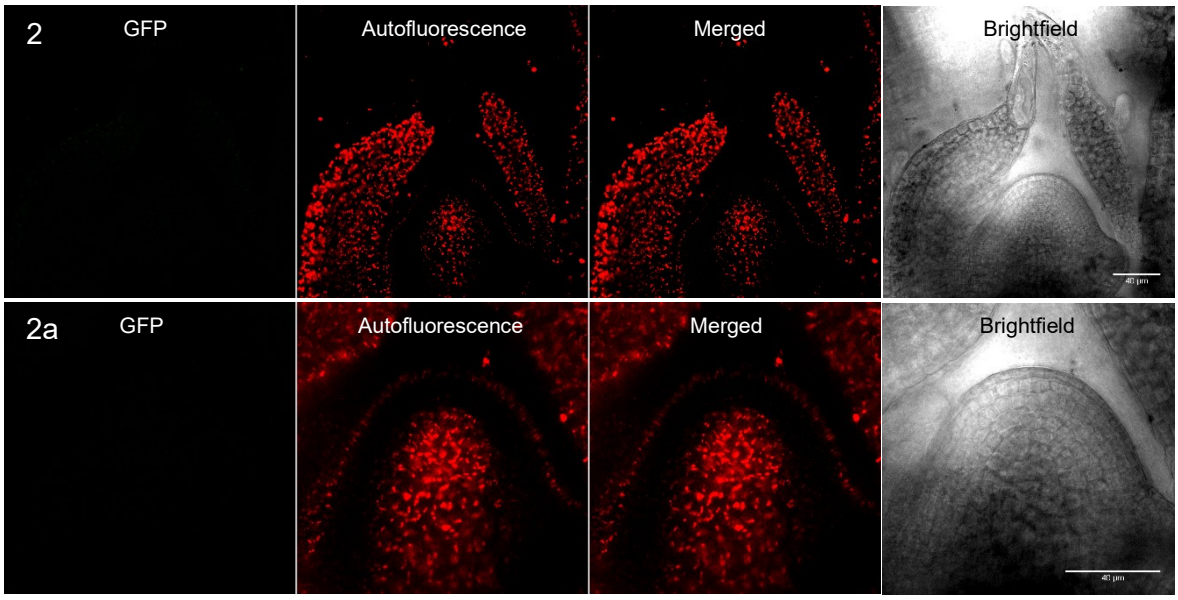
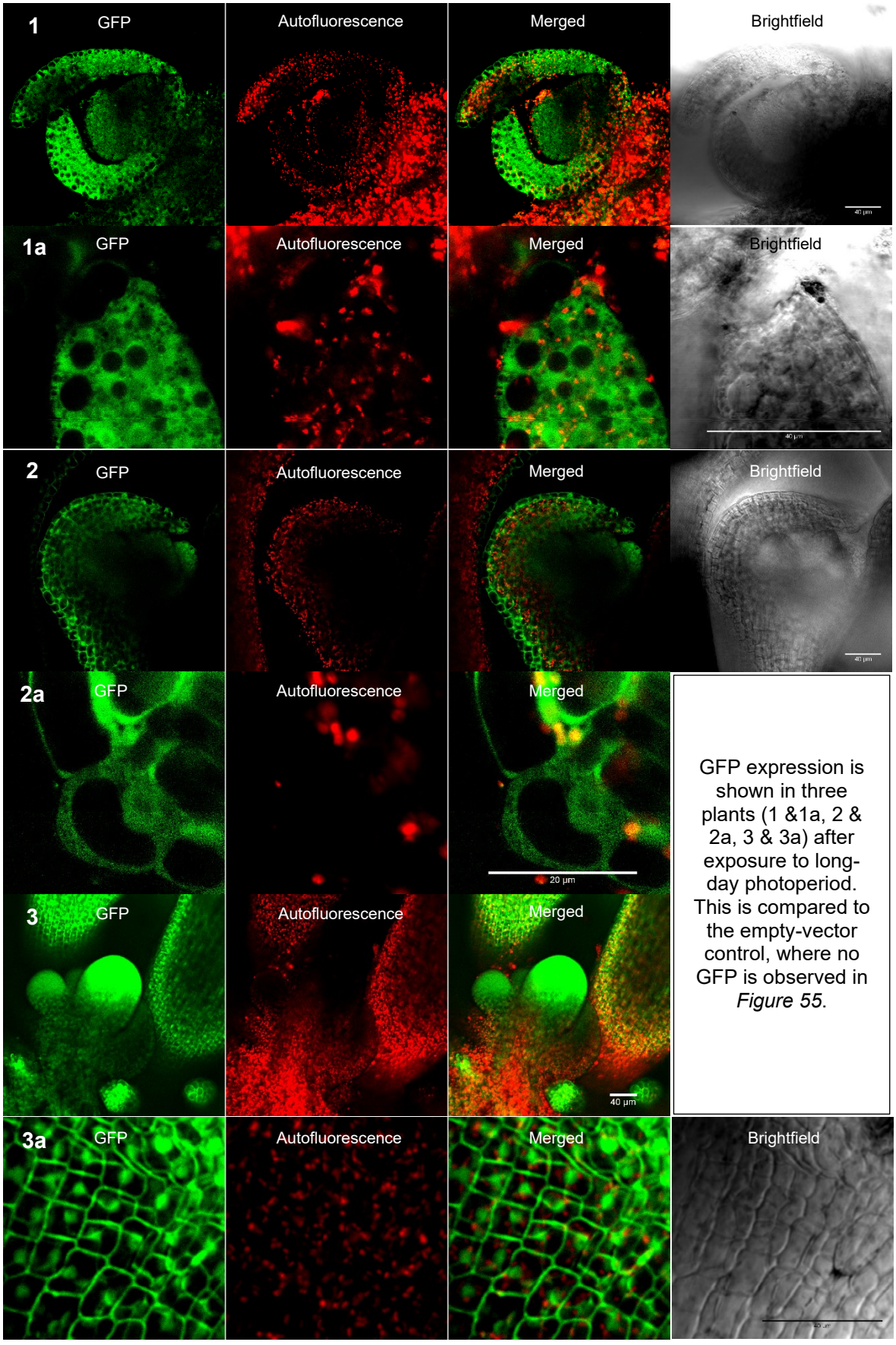


Figure 58 – Assessment of pAP1::GFP in Col-0 function in the apical tissue. (1) GFP fluorescence displayed under positive control conditions - induction by photoperiod and then confocal imaging of the SAM **(2)** No GFP fluorescence was observed for the negative control empty vector, under inductive conditions, as GFP fluorescence was not observed.

Additional Positive Control Images for Three Plant Replicates



GFP expression is shown in three plants (1 &1a, 2 & 2a, 3 & 3a) after exposure to long-day photoperiod. This is compared to the empty-vector control, where no GFP is observed in *Figure 55*.

Figure 59 – Additional assessment of pAP1::GFP in Col-0 GFP expression. Images for the insert vector and GFP expression in the apical tissue for three additional plants are displayed, including three corresponding zoomed images. They can be compared against the negative control empty vector for the same settings in *Figure 53*.

5.5– Discussion

5.5.1 – Examples of Recombinant Protein Use as a Therapeutic

Proteins are used for therapeutic applications in medicine, for examples, the first certified use of Etanercept was approved in 1998 for treatment of conditions in autoimmune disease patients including rheumatoid arthritis [219]. Further examples include, insulin used to control blood sugar levels as a treatment for diabetes, Epoetin beta used to treat anaemia and Interferon beta-1b to treat multiple sclerosis [220]. A large global market exists for biological therapeutics (including protein treatments) with recorded sales exceeding 100 billion US dollars in 2010 [220]. Whilst the biologicals market is relatively new in clinical science, the niche is significant, and proteins have been shown as effective therapeutics with good efficacy, acting with specificity on targets; moreover, new targets are also a continual source of investigation for new potential biological therapies [220]. Currently, the field has not been explored as extensively in plant sciences and only small molecule chemical solutions to agricultural problems exist - due to their high throughput application requirement, ease of uptake by the plant and appropriate lipophilicities of the small molecule [221].

At present, this study is the first reported investigation of protein therapeutics for plant sciences. Whilst a number of model proteins have been delivered in singular context using cell penetrating peptides, this work is the first reported attempt to enable an innate biological function inside the plant with recombinant protein therapy. Exciting results showed that an accelerated flowering phenotype was achieved using recombinant FT, paving the way for other delivery options and manipulations. It could even be possible for example to deliver the

CRISPR Cas9, state-of-the-art gene editing apparatus internally, to either whole plants or using microfluidic protoplast manipulation technologies [222].

5.5.2 – Apical Meristem Development

In this work, the first macroscopic appearance of buds was recorded at 12 days after protein treatment. The dividing inflorescence meristem is sectioned into three regions, the central, rib and peripheral zones [223]. AP1 expression is in this peripheral zone as the floral meristem forms on the outside of the inflorescence meristem and the central zone provides undifferentiated cells to this region [223]. The rib zone accounts for dividing cells constituting the stem and is particularly active as the floral meristem bolts; similarly, the central zone acts as a source of undifferentiated cells to supply this region [223].

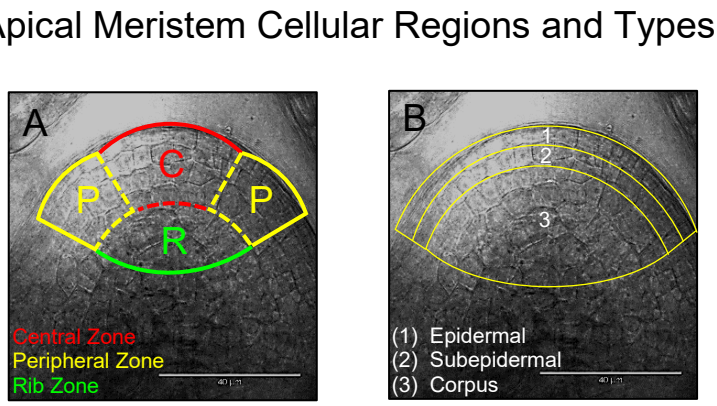


Figure 60 – Regions and cellular layers in the differentiating apical meristem. **(A)** The 3 regions of the meristem are shown – *Central*, *Rib* and *Peripheral zones,* **(B)** The cellular layers are shown – *Epidermal, Sub-epidermal* and *Corpus layers* [223]. Together the epidermal and sub-epidermal layers are called the *Tunica* [223]. **(A)** & **(B)** are adapted brightfield images for a dividing inflorescence meristem.

The export and movement of endogenous FT into the apex has not been well studied however in conjunction with FD it activates AP1 in the peripheral regions, as such recombinant FT uptake needs to target the cells of the periphery [224, 225]. Recombinant FT uptake into the SAM was assessed by confocal microscopy and Sortagged FT-Tat fluorescence was recorded in

the peripheral zones in the results presented in *Figure 47*. Differentiation of the apical cells occurs at a peripheral region, and after approximately 7 days, the floral primordia are fully formed on the meristem periphery; 13.25 days later, the macroscopic appearance of buds in the Landsberg ecotype grown under long-day growth conditions are recorded as benchmark literature values [226, 227].

The application of FT yielded better results for floral induction than FT-Tat (presented in *Figure 50a*). Whilst the Tat tag might help in protein uptake, the high terminal positive charge may have affected biological action and the likely interactions with molecular partners including those in FAC. In addition, the meristematic tissue may be more suppler than leaf tissue and as such FT alone is able to enter the cells – this was not tested and should form part of the future work on this topic.

5.5.3 – Floral Reversion Phenotype

In this study, a curious result is the partial floral induction (floral reversion phenotype) recorded after FT protein treatments [228]. The macroscopic appearance of buds was recorded along with a bolted stem of at least 1 cm, and what appears to be development en route to determinate flowering, yet the apex returned to a vegetative state [214, 215]. This was recorded for 6 applications in *Figure 50a* and then again for 5 applications in *Figure 50b*; particularly striking phenotypes were recorded in *Image 2* and *1* in both experiments respectively.

Floral reversion is defined by a switch to vegetative growth on a forming floral shoot [214, 215]. The irregular expression of SOC1, AGL24 and SVP is cited as a reason for floral reversion in the literature; SOC1 and AGL24 cause floral meristems to return to inflorescence, regaining indeterminacy, and SVP completes this by capping off the return to vegetative meristem formation [229, 230], . Importantly AP1 directly represses *SOC1*, *AGL24* and *SVP* by binding to cis-regulatory regions in their promoter sequences, and preventing the reversion phenotype [229]. Additionally, positive feedback loops involving *AP1* and other meristem identity genes

including *LFY* ensure typical floral progression [39, 230, 231]. For example, an explanation is that when the exogenous FT treatment was stopped, AP1 activation also ceased causing a sudden change in the normal balance of *SOC1*, *AGL24* and *SVP* – resulting in floral reversion [214, 215, 229].

Different quantities of AP1 (originating from the artificial FT treatments) in the apical tissue can alter the meristem fate by differentially repressing *SVP*, *SOC1* and *AGL24*, as lower levels of AP1 have been show to repress *SVP* and *SOC1* but not *AGL24* [229]. Naturally in the plant, AP1 plays an important role in preventing the reversion of the floral meristem by suppressing AGL24 [214]. In the event of floral reversal, a curious bolted phenotype is observed without floral buds, occurring after floral initiation as the developing inflorescence assembly reverts back to a leafy structure [232]. In this work, the partial induction and floral reversion phenotype is further proof that *AP1* is artificially activated, however the level of expression is halted when artificial recombinant FT treatment ended, causing this change in developmental architecture and the partially induced phenotype [215, 232].

5.5.4 - Exogenous Control of Flowering Time

For long-day plants like Arabidopsis, short-day growing conditions enable an extended period of vegetative growth before the plant commits to flowering - as photoperiod activation is not possible due to the short daylengths. Notably, the work by Corbesier *et al.* influenced the experimental designs in this work. Corbesier *et al.* reported specific conditions for a plant to commit to flowering: after growth under short-day conditions and then transfer for a single day to long-day conditions [217]. The paper reported how irradiance light level, vernalisation, and plant age all affected flowering time in a classical photoperiod induced system [217].

In summary, Corbesier *et al.* recorded how plant age affected suseptibility to floral transition upon transfer to an inductive photoperiod [217]. Plants were assessed at 30, 45 and 60 days

for their floral fate as a result of consecutive long-day cycles (1 treatment is defined as 24 hours of light in addition to the following 8-hour short-day) [217]. Corbesier *et al.* reported results for the complete flowering of a data set of 12 plants; at 30 days old, 7 long day cycles were required, at 45 days, 4 cycles and at 60 days, 2 cycles were required in order to induce flowering for the complete dataset [217]. By comparison, for 45-day old plants treated in this study, the best treatments were recorded as 14 out of 24 plants for a triple treatment of 50 µM FT, followed by 12 out of 24 plants for a single treatment of 5 µM FT. A particular variable was the application of treatments onto the apical tissue, and whist the procedure was performed consistently, it was technically challenging. In addition, the appearance of buds for the untreated control under short-day growth conditions was from 70 days and this is compared to 85 days reported by Corbesier *et al.* [217]. Both Krzymuski *et al.* and Corbesier *et al.* confirm that younger plants grown under short-day conditions require more than a single long-day inductive cycle to accelerate flowering with 4 and 3 long-day treatments for plants aged 25 and 30 days old respectively in the two independent studies [216, 217].

In addition to plant age, a number of other factors affect the sensitivity to floral induction, including, vernalisation treatment, temperature and light intensity. A higher level of irradiance accelerates flowering, the modern convention is to use a light intensity of 120 $\mu mol.m^{-2}.s^{-1}$ and for non-vernalised plants, buds are reported at 85 days [217]. In contrast, at a light intensity of 48 $\mu mol.m^{-2}.s^{-1}$, buds are recorded at 135 days [217]. In addition, the reliability of the results also decreases as light intensity is dropped yielding more erratic flowering time results [217]. Consequently light intensity was monitored in these experiments and was crucially maintained at 120 $\mu mol.m^{-2}.s^{-1}$.

From the current understanding of flowering, it is not clear what molar quantity of FT is required for floral transition and at what quantitative level saturation effects might occur. For instance, in the plant, FT is expressed upon exposure to a single long-day through CO transcriptional

activation; however depending on the plant age, this might not accelerate flowering – with the plant requiring further long-day exposure for full floral activation [16, 216, 217]. The endogenous FT signal must accumulate over more than 1 day in order to achieve the required sensitivity to activate flowering and it is this duration, rather than maximum intensity, which is important [216]. Moreover, the FT signal is likely to be short-lived and internally degraded. In particular, reports by Krzymuski *et al.* showed that for 25-day old plants, a single long-day did not yield measurable changes in AP1 expression whereas this was apparent when exposed to 6 long-days and with full floral transition reported [216]. It is not clear what the molar endogenous expression level of FT is inside the plant and what threshold is required to activate the floral transition – in this way, 5 µM and 50 µM of 3 µL protein treatments (15 and 150 pmol of FT respectively) were only presumed to fall within the biologically active threshold in this work. Further experiments can refine the treatment to deduce an optimised quantity per dosage. Further questions need consideration for example, would a prolonged exposure with recurrent FT treatment might be more effective to activate flowering.

From the results presented in this study, it is clear that flowering can be artificially activated by using recombinant FT but further work is required to find the optimal dosage (single 5 µM treatment, [12/24 plants] *c.f.* triple 50 µM treatment [14/24 plants]). Sensitivity and saturation are important conditions to consider when refining the treatment on top of the actual technical challenges related to cellular uptake of recombinant protein [216]. Additionally, the technical challenges of the SAM dissection technique might be overcome by development of an automated procedure which would remove this factor in the variability recorded for optimal treatments and dosages.

5.5.5 – Further Studies in Different Organisms

In this chapter, promising results are recorded for the phenotyping experiments and as such, consideration was given to extending this work into other plants within the Brassicaceae family. This brief section is presented as a topic for future work. The delivery of FT as a potential plant therapeutic for flowering time control is an exciting prospect and as the FT sequence is well conserved across species then it may be possible to use it as a wide-ranging inter-species treatment [233, 234].

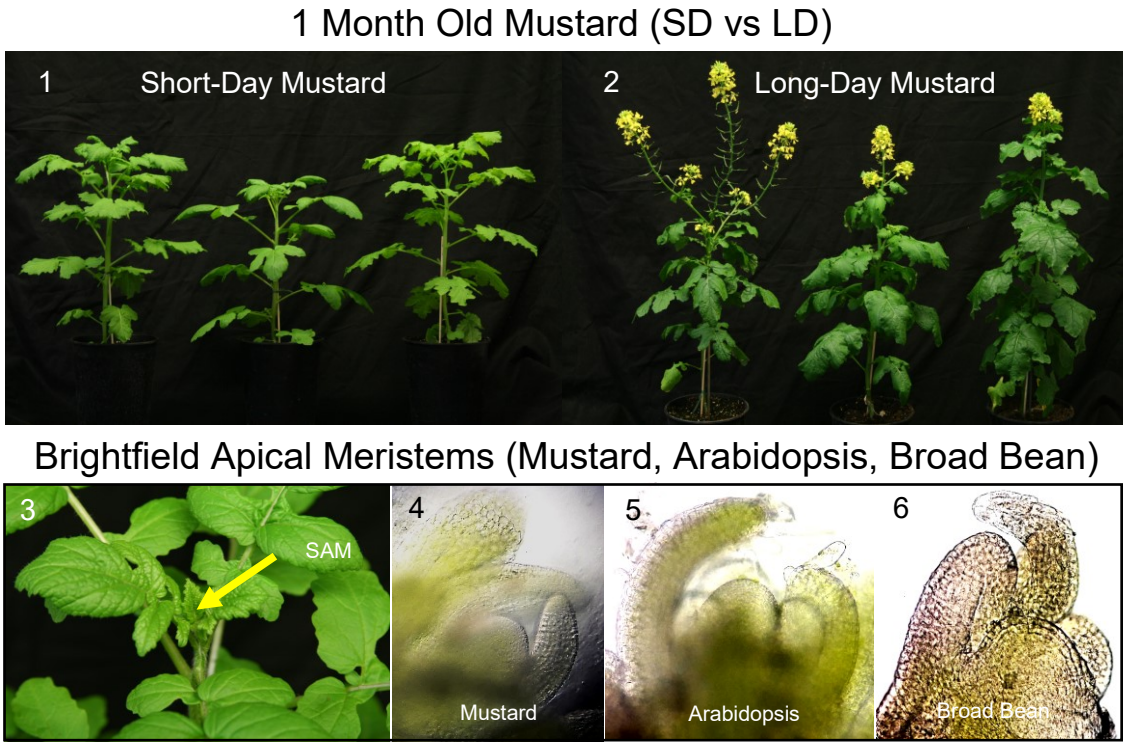


Figure 61 – Example of other species for exogenous protein treatment. **(1)** Mustard grown under short day conditions for 1 month and vegetative, **(2)** mustard grown under long day conditions for 1 month and floral, **(3)** the apical meristem at the apex of the plant, **(4), (5) & (6)** brightfield apex for mustard, Arabidopsis and broad bean respectively.

Figure 56, is illustrative and shows Mustard grown under short-day remaining vegetative and under long-day, with three floral phenotypes for 4 weeks of growth in respective conditions. The apical meristem is easily reachable by dissection and exogenous treatment of

recombinant protein might be possible to target this structure and activate a flowering time phenotype. This can form an important part of future work, to see if the recombinant FT treatment can be replicated in other species.

5.6– Conclusion

The results in this chapter assessed whether it was possible to artificially control flowering. This was carried out using a phenotype screen to determine whether the exogenous treatment of FT resulted in the macroscopic appearance of buds for plants grown under short-day conditions. Large phenotyping assessments were conducted in order to determine the optimal amounts and duration of FT treatment. A single 5 μM treatment of FT caused half the plants in the dataset to flower (12/24), a triple 50 μM FT treatment caused 10/24 plants to flower early and a repeat reading showed that 14/24 plants flowered early with a single 50 μM treatment of FT. Whilst it was noteworthy that the exogenous FT treatment caused early flowering, the inconsistency in the different treatment results was attributed to the ability to successfully land the recombinant FT protein solution on the apical tissue during the technical experimental setup.

A reporter plant was constructed to determine whether AP1 can be artificially activated after the exogenous treatment with FT. This included the 2000 base pair sequence of the AP1 promoter before the start codon, which contains a C-box which is the reported FD binding site in FAC. A homozygous line with a single insertion was created along with a line containing an empty vector which did not contain the AP1 promoter insert. Experiments showed that the AP1 reporter was functional and GFP expression was observed compared against a negative control and the empty vector line. Immediate future experiments will determine whether GFP can be artificially activated after exogenous FT delivery.

Three delivery routes were assessed for their merits to determine which would be the best for exogenous delivery of FT. They were chosen taking into consideration the endogenous journey that FT takes from the leaf to the shoot apical meristem. The delivery routes included targeting the leaf via stomatal delivery, into the phloem via microinjection and directly onto the apical tissue using a pipette. The advantage of direct delivery to the apical

cells was clear as smaller application volumes could be used – 3 µL instead of the 50 µL used for stomatal delivery and also the procedure was non-invasive. Another key advantage was that the recombinant FT was not required to travel to the site of action *c.f.* stomatal or direct phloem delivery.

The work in this chapter formed the most important part of the thesis and determined whether it is possible to artificially activate reproductive development in Arabidopsis. The exogenous FT application technique was refined however technical inconsistencies meant that the optimal treatment strength and time course were not achieved and further work could develop an automated procedure for application of protein onto the apical meristem to increase the throughput of the procedure. Immediate future work will also confirm the molecular activation of AP1 with the pAP1 transgenic reporter.

6. Concluding Remarks

6.1 - Summary

The action of cell penetrating peptides are reported in *Chapter 3* in this thesis and the uptake of 4 sequences were investigated (Tat, R9, pVEC and TP10). The cationic R9 and Tat sequences were superior and recorded promising uptake properties. A current understanding of cell penetrating peptide uptake in the plant literature in general, reports unconvincing conclusions, this work however earmarks cationic R9 and Tat sequences with useful uptake properties. Furthermore, the uptake of R9 was reported in other Arabidopsis tissues including leaf culture cells and the shoot apical meristem showing their widespread uptake into different tissues. The aim of this chapter was to investigate the properties of cell penetrating peptides in isolation; however, their usefulness is further characterised by their ability to transport cargo into tissues.

The flowering time experiments in this study reported remarkable evidence that flowering can be accelerated after the exogenous treatment of recombinant FT protein. Further evidence was also reported with a floral reversion phenotype showing that some plants were only partially induced and consequently returned to a vegetative phenotype after displaying a bolted stem. Tracking of recombinant protein *in planta* was enabled with the sortagging technology which transferred a TAMRA fluorophore onto the N-terminus of FT. This technology is an excellent way of labelling recombinant protein and this was critiqued in *Chapter 4*.

Covalent delivery of FT inside cells was investigated using Tat and R9 peptides. The results suggested that a different mechanism existed for the delivery of R9 and Tat independently and then when covalently attached to FT. Tat and R9 facilitated the delivery of FT to the cellular boundary and protein was observed attached to the outsides of the cells; it did however

take longer for protein to be delivered inside the cells when compared to isolated peptide action. This suggested a different entry mechanism for both scenarios. In addition, whilst the covalently attached CPP tag enabled cellular delivery, the flowering time experiments did not show considerable floral acceleration. The cationic tag might affect the *in vivo* action of FT and as such the efficacy of FT-Tat treatment was attenuated compared with FT. In addition, it was assumed that FT was able to enter the apical cells without the need for CPP attachment which was an interesting development.

6.2 - Future Perspectives

6.2.1 - R9 Uptake Could Guide Electrotrophic Response in Plant Growth

The cationic R9 peptide could be used to drive electrotrophic growth responses after uptake into tissue. In particular, directional growth responses to an applied electric field within the Arabidopsis root could be defined using R9 as a direct application and translation of the results presented for R9 uptake into root tips within this thesis. Electrotrophism is phenomenon reported whereby plants display a trophic directional growth response to an electric field [235]. Indeed, Arabidopsis roots tips have been shown to grow in a particular direction in response to an artificially applied electric field where the direction of growth can be changed depending of the alignment of the electric field [236]. Whilst Arabidopsis is a model organism, it is proposed that the technique could be applied to other plants whereby directional growth is important for defining the aesthetics of the organism for sales in horticultural markets. It could be possible to guide electrotrophism in Arabidopsis roots, after the uptake of cationic guanidinium rich peptide as surely in an applied electric field, the root tip after R9 uptake will move towards a negative electrode. This is something further to test and could be a useful and as yet untested application of cationic cell penetrating peptides.

6.2.2 – Further Flowering Time Experiments.

A natural progression of further experimentation follows from the results conducted in *Chapter 5* and this includes further measurements to determine the optimum molar amounts and dosages of FT required to accelerate flowering. In addition, experiments should be conducted to determine how plant age affects susceptibility to exogenous FT treatments and at what threshold age plants respond to treatments.

In addition to this, recombinant TFL1 could be investigated as a tool to delay flowering. This would require a different experimental set-up. It is likely to be more complicated to investigate because plants would have to be grown under long-day growth conditions with more variables

that can affect flowering time, namely the expression of endogenous FT will be a competing factor. Treatments could be conducted to test whether recombinant TFL1 protein could be used to either delay flowering or reverse flowering once the developmental transition has begun.

6.2.3 – Optimising the Exogenous Treatment Technology

The application of recombinant FT as a protein therapy for plants is presented with success in *Chapter 5* of this thesis. Literature evidence cites the importance of particular features within the FT protein sequence which differentiates it from the close homologue, TFL1, in particular residues at the ligand binding site and the external loop display stark variation between the two closely related FT and TFL1 proteins [33, 38, 237]. The external loop is also likely to play an important part in the interaction of both FT and TFL1 to promoter DNA in the FAC and FIC complexes [45]. Once a complete understanding of the molecular mechanism detailing FT and TFL1 exists, perhaps the protein sequences could be truncated into peptidic motifs which might be able to activate flowering. The work in this thesis shows that it is possible to activate flowering artificially using a non-transgenic approach. Perhaps the treatment could be simplified into a peptidic form and then as such, created in higher throughput which might enable large scale application of a treatment to accelerate flowering in agriculture.

6.2.4 – A Universal Treatment across Species

In *Chapter 5*, the concept of a universal tool to activate flowering across species is touched upon. The reason why Arabidopsis is a good model to study flowering, is that many of the pathways are conserved across species, and FT shares much similarity across species with many homologues present [233]. This opens up the possibility for testing out the exogenous application of recombinant FT in other species, or perhaps even cloning and purifying species specific florigen for exogenous treatments. Whilst it is recognised that the high throughput

application of recombinant FT on a crop of brassicas such as oil seed rape or mustard might not be viable, it might be useful for lower throughput application - for example speeding up the growth cycles of fruit trees.

6.2.5 – Commercial Possibilities for FT Protein Therapy

The only current reliable option for speeding up flowering time is using GM approaches and overexpression studies. Transgenic resources are used widely in academic laboratories for investigation into a particular system. In contrast, GM plants are banned from use in European commercial agriculture, as such, the work in this thesis presents a non-GM approach to modifying flowering. A tool to accelerate flowering could be a useful commercial option to accelerate plant breeding. In light of this an exogenous FT protein tool could form a useful component of an industrial toolkit to accelerate breeding of agronomically important cropping species.

References

1. A. Enghiad, D. Ufer, A. M. Countryman and D. D. Thilmany, *An Overview of Global Wheat Market Fundamentals in an Era of Climate Concerns.* International Journal of Agronomy, 2017. **2017**: p. 15.
2. N. Hanley, T. D. Breeze, C. Ellis and D. Goulson, *Measuring the economic value of pollination services: Principles, evidence and knowledge gaps.* Ecosystem Services, 2015. **14**: p. 124-132.
3. T. R. Wheeler and P. Q. Craufurd, *Climate change and the flowering time of annual crops.* Journal of Experimental Botany, 2009. **60**(9): p. 2529-2539.
4. M. Gammans, P. Mérel and A. Ortiz-Bobea, *Negative impacts of climate change on cereal yields: statistical evidence from France.* Environmental Research Letters, 2017. **12**(5): p. 054007.
5. C. Zhao, B. Liu, S. Piao, X. Wang, D. B. Lobell, Y. Huang, M. Huang, Y. Yao, S. Bassu, P. Ciais, J.-L. Durand, J. Elliott, F. Ewert, I. A. Janssens, T. Li, E. Lin, Q. Liu, P. Martre, C. Müller, S. Peng, J. Peñuelas, A. C. Ruane, D. Wallach, T. Wang, D. Wu, Z. Liu, Y. Zhu, Z. Zhu and S. Asseng, *Temperature increase reduces global yields of major crops in four independent estimates.* Proceedings of the National Academy of Sciences, 2017. **114**(35): p. 9326-9331.
6. D. B. Lobell and S. M. Gourdji, *The influence of climate change on global crop productivity.* Plant physiology, 2012. **160**(4): p. 1686-1697.
7. W. Joyce, *MRes Thesis, Imperial College London.* 2015.
8. The Arabidopsis Genome, I., *Analysis of the genome sequence of the flowering plant Arabidopsis thaliana.* Nature, 2000. **408**: p. 796.
9. W. Leijten, R. Koes, I. Roobeek and G. Frugis, *Translating Flowering Time from Arabidopsis thaliana to Brassicaceae and Asteraceae Crop Species.* Plants, 2018. **7**(4).
10. D. C. Boyes, A. M. Zayed, R. Ascenzi, A. J. McCaskill, N. E. Hoffman, K. R. Davis and J. Gorlach, *Growth stage-based phenotypic analysis of Arabidopsis: a model for high throughput functional genomics in plants.* Plant Cell, 2001. **13**(7): p. 1499-510.
11. Koornneef, M. and D. Meinke, *The development of Arabidopsis as a model plant.* The Plant Journal, 2010. **61**(6): p. 909-921.
12. R. Lemoine, S. La Camera, R. Atanassova, F. Dédaldéchamp, T. Allario, N. Pourtau, J.-L. Bonnemain, M. Laloi, P. Coutos-Thévenot, L. Maurousset, M. Faucher, C. Girousse, P. Lemonnier, J. Parrilla and M. Durand, *Source-to-sink transport of sugar and regulation by environmental factors.* Frontiers in plant science, 2013. **4**: p. 272-272.
13. P. Huijser and M. Schmid, *The control of developmental phase transitions in plants.* Development, 2011. **138**(19): p. 4117.
14. A. Mouradov, F. Cremer, and G. Coupland, *Control of flowering time: interacting pathways as a basis for diversity.* Plant Cell, 2002. **14 Suppl**: p. S111-30.
15. L. Corbesier, C. Vincent, S. Jang, F. Fornara, Q. Fan, I. Searle, A. Giakountis, S. Farrona, L. Gissot, C. Turnbull and G. Coupland, *FT protein movement contributes to long-distance signaling in floral induction of Arabidopsis.* Science, 2007. **316**(5827): p. 1030-3.
16. M. Yanovsky, and S Kay, *Molecular basis of seasonal time measurement in Arabidopsis.* Nature, 2002. **419**(6904): p. 308-12.
17. S. Kim, X. Yu, and S.D. Michaels, *Regulation of CONSTANS and FLOWERING LOCUS T expression in response to changing light quality.* Plant physiology, 2008. **148**(1): p. 269-279.
18. P. Suárez-López, K. Wheatley, F. Robson, H. Onouchi, F. Valverde and G. Coupland, *CONSTANS mediates between the circadian clock and the control of flowering in Arabidopsis.* Nature, 2001. **410**: p. 1116.
19. S. Tiwari, Y. Shen, H. Chang, Y. Hou, A. Harris, S. Ma, M. McPartland, G. Hymus, L. Adam, C. Marion, A. Belachew, P. Repetti, *The flowering time regulator CONSTANS is recruited to the FLOWERING LOCUS T promoter via a unique cis-element.* New Phytol, 2010. **187**(1): p. 57-66.

20. F. Valverde, A. Mouradov, W. Soppe, D. Ravenscroft, A. Samach and G. Coupland, *Photoreceptor regulation of CONSTANS protein in photoperiodic flowering.* Science, 2004. **303**(5660): p. 1003-6.
21. M. Endo, Y. Tanigawa, T. Murakami, T. Araki and A. Nagatani, *PHYTOCHROME-DEPENDENT LATE-FLOWERING accelerates flowering through physical interactions with phytochrome B and CONSTANS.* Proceedings of the National Academy of Sciences, 2013. **110**(44): p. 18017-18022.
22. C. Turnbull, *Long-distance regulation of flowering time.* J Exp Bot, 2011. **62**(13): p. 4399-413.
23. F. Turck, F. Fornara, and G. Coupland, *Regulation and identity of florigen: FLOWERING LOCUS T moves center stage.* Annu Rev Plant Biol, 2008. **59**: p. 573-94.
24. T. Huang, H. Bohlenius, S. Eriksson, F. Parcy and O. Nilsson, *The mRNA of the Arabidopsis gene FT moves from leaf to shoot apex and induces flowering.* Science, 2005. **309**(5741): p. 1694-6.
25. S. Tamaki, S. Matsuo, H. L. Wong, S. Yokoi and K. Shimamoto, *Hd3a protein is a mobile flowering signal in rice.* Science, 2007. **316**(5827): p. 1033-6.
26. H. Liu, X. Yu, K. Li, J. Klejnot, H. Yang, D. Lisiero and C. Lin, *Photoexcited CRY2 interacts with CIB1 to regulate transcription and floral initiation in Arabidopsis.* Science, 2008. **322**(5907): p. 1535-9.
27. S. V. Kumar, D. Lucyshyn, K. Jaeger, E. Alos, E. Alvey, N. Harberd and P. Wigge, *Transcription factor PIF4 controls the thermosensory activation of flowering.* Nature, 2012. **484**(7393): p. 242-245.
28. M. Sawa and S. Kay, *GIGANTEA directly activates Flowering Locus T in Arabidopsis thaliana.* Proceedings of the National Academy of Sciences, 2011. **108**(28): p. 11698-11703.
29. P. Pin and O. Nilsson, *The multifaceted roles of FLOWERING LOCUS T in plant development.* Plant Cell Environ, 2012. **35**(10): p. 1742-55.
30. J. Mathieu, L. Yant, F. Murdter, F. Kuttner and M. Schmid, *Repression of flowering by the miR172 target SMZ.* PLoS Biol, 2009. **7**(7): p. e1000148.
31. D. Li, C. Liu, L. Shen, Y. Wu, H. Chen, M. Robertson, C. Helliwell, T. Ito, E. Meyerowitz and H. Yu, *A repressor complex governs the integration of flowering signals in Arabidopsis.* Dev Cell, 2008. **15**(1): p. 110-20.
32. C. Castillejo, and S. Pelaz, *The balance between CONSTANS and TEMPRANILLO activities determines FT expression to trigger flowering.* Curr Biol, 2008. **18**(17): p. 1338-43.
33. J. Ahn, D. Miller, V. Winter, M. Banfield, J. Lee, S. Yoo, S. Henz, R. Brady and D. Weigel, *A divergent external loop confers antagonistic activity on floral regulators FT and TFL1.* EMBO J, 2006. **25**(3): p. 605-14.
34. A. Yamaguchi, Y. Kobayashi, K. Goto, M. Abe and T. Araki, *TWIN SISTER OF FT (TSF) acts as a floral pathway integrator redundantly with FT.* Plant Cell Physiol, 2005. **46**(8): p. 1175-89.
35. S. Jin, H. Jung, K. Chung, J. Lee and J. Ahn, *FLOWERING LOCUS T has higher protein mobility than TWIN SISTER OF FT.* J Exp Bot, 2015. **66**(20): p. 6109-17.
36. S. Yoo, I. Kardailsky, J. Lee, D. Weigel and J. Ahn, *Acceleration of flowering by overexpression of MFT (MOTHER OF FT AND TFL1).* Mol Cells, 2004. **17**(1): p. 95-101.
37. W. Xi, C. Liu, X. Hou and H. Yu, *MOTHER OF FT AND TFL1 regulates seed germination through a negative feedback loop modulating ABA signaling in Arabidopsis.* Plant Cell, 2010. **22**(6): p. 1733-48.
38. Y. Hanzawa, T. Money, and D. Bradley, *A single amino acid converts a repressor to an activator of flowering.* Proc Natl Acad Sci U S A, 2005. **102**(21): p. 7748-53.
39. S. Liljegren, C. Gustafson-Brown, A. Pinyopich, G. Ditta and M. Yanofsky, *Interactions among APETALA1, LEAFY, and TERMINAL FLOWER1 specify meristem fate.* Plant Cell, 1999. **11**(6): p. 1007-18.
40. J. Moon, H. Lee, M. Kim and I. Lee, *Analysis of flowering pathway integrators in Arabidopsis.* Plant Cell Physiol, 2005. **46**(2): p. 292-9.

41. D. Charles, *PhD Thesis Imperial College London.* 2014.
42. D. Wickland and Y. Hanzawa, *The FLOWERING LOCUS T/TERMINAL FLOWER 1 Gene Family: Functional Evolution and Molecular Mechanisms.* Mol Plant, 2015. **8**(7): p. 983-97.
43. S. Yoo, K. Chung, S. Jung, S. Yoo, J. Lee and J. Ahn, *BROTHER OF FT AND TFL1 (BFT) has TFL1-like activity and functions redundantly with TFL1 in inflorescence meristem development in Arabidopsis.* Plant J, 2010. **63**(2): p. 241-53.
44. N. Huang, W. Jane, J. Chen and T. Yu, *Arabidopsis thaliana CENTRORADIALIS homologue (ATC) acts systemically to inhibit floral initiation in Arabidopsis.* Plant J, 2012. **72**(2): p. 175-84.
45. P. Pin, R. Benlloch, D. Bonnet, E. Wremerth-Weich, T. Kraft, J. Gielen and O. Nilsson, *An antagonistic pair of FT homologs mediates the control of flowering time in sugar beet.* Science, 2010. **330**(6009): p. 1397-400.
46. M. Abe, Y. Kobayashi, S. Yamamoto, Y. Daimon, A. Yamaguchi, Y. Ikeda, H. Ichinoki, M. Notaguchi, K. Goto and T. Araki, *FD, a bZIP protein mediating signals from the floral pathway integrator FT at the shoot apex.* Science, 2005. **309**(5737): p. 1052-6.
47. J. Lee and I. Lee, *Regulation and function of SOC1, a flowering pathway integrator.* J Exp Bot, 2010. **61**(9): p. 2247-54.
48. K. Taoka, I. Ohki, H. Tsuji, K. Furuita, K. Hayashi, T. Yanase, M. Yamaguchi, C. Nakashima, Y. Purwestri, S. Tamaki, Y. Ogaki, C. Shimada, A. Nakagawa, C. Kojima and K. Shimamoto, *14-3-3 proteins act as intracellular receptors for rice Hd3a florigen.* Nature, 2011. **476**(7360): p. 332-5.
49. P. Wigge, M. Kim, K. Jaeger, W. Busch, M. Schmid, J. Lohmann and D. Weigel, *Integration of spatial and temporal information during floral induction in Arabidopsis.* Science, 2005. **309**(5737): p. 1056-9.
50. H. Tsuji, *Molecular function of florigen.* Breeding science, 2017. **67**(4): p. 327-332.
51. S. Tylewicz, H. Tsuji, P. Miskolczi, A. Petterle, A. Azeez, K. Jonsson, K. Shimamoto and R. Bhalerao, *Dual role of tree florigen activation complex component FD in photoperiodic growth control and adaptive response pathways.* Proc Natl Acad Sci U S A, 2015. **112**(10): p. 3140-5.
52. H. Tsuji, K.-i. Taoka, and K. Shimamoto, *Florigen in rice: complex gene network for florigen transcription, florigen activation complex, and multiple functions.* Current Opinion in Plant Biology, 2013. **16**(2): p. 228-235.
53. N. Jaspert, C. Throm, and C. Oecking, *Arabidopsis 14-3-3 proteins: fascinating and less fascinating aspects.* Front Plant Sci, 2011. **2**: p. 96.
54. N. Kawamoto, M. Sasabe, M. Endo, Y. Machida and T. Araki, *Sci Rep*, 2015, **5**, 8341.
55. J. Mylne and P. Wigge, *Calcium-dependent protein kinases responsible for the phosphorylation of a bZIP transcription factor FD crucial for the florigen complex formation.* Sci Rep, 2015. **5**: p. 8341.
55. J. Mylne, and P. Wigge, *Plant chemical biology: Florigen takes two to tango.* Nat Chem Biol, 2011. **7**(10): p. 665-6.
56. E. Bihn, A. Paul, S. Wang, G. Erdos and R. Ferl, *Localization of 14-3-3 proteins in the nuclei of arabidopsis and maize.* Plant J, 1997. **12**(6): p. 1439-45.
57. W. Deng, H. Ying, C. Helliwell, J. Taylor, W. Peacock and E. Dennis, *FLOWERING LOCUS C (FLC) regulates development pathways throughout the life cycle of Arabidopsis.* Proceedings of the National Academy of Sciences of the United States of America, 2011. **108**(16): p. 6680-6685.
58. S. Michaels and R. Amasino, *Memories of winter: vernalization and the competence to flower.* Plant, Cell & Environment, 2000. **23**(11): p. 1145-1153.
59. D. Jiang, W. Yang, Y. He and R. M. Amasino, *Arabidopsis relatives of the human lysine-specific Demethylase1 repress the expression of FWA and FLOWERING LOCUS C and thus promote the floral transition.* Plant Cell, 2007. **19**(10): p. 2975-87.

60. J. Risk, R. Laurie, R. Macknight and C. Day, *FRIGIDA and related proteins have a conserved central domain and family specific N- and C- terminal regions that are functionally important.* Plant Mol Biol, 2010. **73**(4-5): p. 493-505.
61. I. Searle, Y. He, F. Turck, C. Vincent, F. Fornara, S. Krober, R. Amasino and G. Coupland, *The transcription factor FLC confers a flowering response to vernalization by repressing meristem competence and systemic signaling in Arabidopsis.* Genes Dev, 2006. **20**(7): p. 898-912.
62. C. Sheldon, D. Rouse, E. Finnegan, W. Peacock and E. Dennis, *The molecular basis of vernalization: the central role of FLOWERING LOCUS C (FLC).* Proc Natl Acad Sci U S A, 2000. **97**(7): p. 3753-8.
63. D. Bond, E. Dennis, B. Pogson and E. Finnegan, *Histone Acetylation, VERNALIZATION INSENSITIVE 3, FLOWERING LOCUS C, and the Vernalization Response.* Molecular Plant, 2009. **2**(4): p. 724-737.
64. Z. Chen and L. Tian, *Roles of dynamic and reversible histone acetylation in plant development and polyploidy.* Biochimica et biophysica acta, 2007. **1769**(5-6): p. 295-307.
65. C. Sheldon, E. Jean Finnegan, W. James Peacock and E. Dennis, *Mechanisms of gene repression by vernalization in Arabidopsis.* The Plant Journal, 2009. **59**(3): p. 488-498.
66. R. Amasino and S. Michaels, *The timing of flowering.* Plant Physiol, 2010. **154**(2): p. 516-20.
67. J.-Z. Cheng, Y.-P. Zhou, T.-X. Lv, C.-P. Xie and C.-E. Tian, *Research progress on the autonomous flowering time pathway in Arabidopsis.* Physiology and Molecular Biology of Plants, 2017. **23**(3): p. 477-485.
68. J. Mulekar, Q. Bu, F. Chen and E. Huq, *Casein kinase II alpha subunits affect multiple developmental and stress-responsive pathways in Arabidopsis.* Plant J, 2012. **69**(2): p. 343-54.
69. J. Mulekar and E. Huq, *Arabidopsis casein kinase 2 alpha4 subunit regulates various developmental pathways in a functionally overlapping manner.* Plant Sci, 2015. **236**: p. 295-303.
70. M. Luo, R. Tai, C. W. Yu, S. Yang, C. Y. Chen, W. D. Lin, W. Schmidt and K. Wu, *Regulation of flowering time by the histone deacetylase HDA5 in Arabidopsis.* Plant J, 2015. **82**(6): p. 925-36.
71. F. Liu, V. Quesada, P. Crevillen, I. Baurle, S. Swiezewski and C. Dean, *The Arabidopsis RNA-binding protein FCA requires a lysine-specific demethylase 1 homolog to downregulate FLC.* Mol Cell, 2007. **28**(3): p. 398-407.
72. V. Wahl, J. Ponnu, A. Schlereth, S. Arrivault, T. Langenecker, A. Franke, R. Feil, J. E. Lunn, M. Stitt and M. Schmid, *Regulation of flowering by trehalose-6-phosphate signaling in Arabidopsis thaliana.* Science, 2013. **339**(6120): p. 704-7.
73. J. Ponnu, V. Wahl, and M. Schmid, *Trehalose-6-phosphate: connecting plant metabolism and development.* Front Plant Sci, 2011. **2**: p. 70.
74. J. Wang, B. Czech, and D. Weigel, *miR156-regulated SPL transcription factors define an endogenous flowering pathway in Arabidopsis thaliana.* Cell, 2009. **138**(4): p. 738-49.
75. E. Spanudakis and S. Jackson, *The role of microRNAs in the control of flowering time.* J Exp Bot, 2014. **65**(2): p. 365-80.
76. A. Yamaguchi and M. Abe, *Regulation of reproductive development by non-coding RNA in Arabidopsis: to flower or not to flower.* J Plant Res, 2012. **125**(6): p. 693-704.
77. G. Wu, M. Park, S. Conway, J. Wang, D. Weigel and R. Poethig, *The sequential action of miR156 and miR172 regulates developmental timing in Arabidopsis.* Cell, 2009. **138**(4): p. 750-9.
78. L. Yang, M. Xu, Y. Koo, J. He and R. Poethig, *Sugar promotes vegetative phase change in Arabidopsis thaliana by repressing the expression of MIR156A and MIR156C.* Elife, 2013. **2**: p. e00260.
79. T. Jack, *Relearning our ABCs: new twists on an old model.* Trends Plant Sci, 2001. **6**(7): p. 310-6.

80. V. Irish, *The ABC model of floral development.* Current Biology, 2017. **27**(17): p. R887-R890.
81. X. Liu, Y. J. Kim, R. Muller, R. Yumul, C. Liu, Y. Pan, X. Cao, J. Goodrich and X. Chen, *AGAMOUS terminates floral stem cell maintenance in Arabidopsis by directly repressing WUSCHEL through recruitment of Polycomb Group proteins.* Plant Cell, 2011. **23**(10): p. 3654-70.
82. J. Bowman, J. Alvarez, D. Weigel, E. Meyerowitz and D. Smyth, *Control of flower development in Arabidopsis thaliana by APETALA1 and interacting genes.* Development, 1993. **119**(3): p. 721-743.
83. M. Alejandra Mandel, C. Gustafson-Brown, B. Savidge and M. F. Yanofsky, *Molecular characterization of the Arabidopsis floral homeotic gene APETALA1.* Nature, 1992. **360**: p. 273.
84. S. Urbanus, S. de Folter, A. Shchennikova, K. Kaufmann, R. Immink and G. Angenent, *In planta localisation patterns of MADS domain proteins during floral development in Arabidopsis thaliana.* BMC Plant Biol, 2009. **9**: p. 5.
85. V. Irish and I. Sussex, *Function of the apetala-1 gene during Arabidopsis floral development.* The Plant cell, 1990. **2**(8): p. 741-753.
86. C. Ferrandiz, Q. Gu, R. Martienssen and M. Yanofsky, *Redundant regulation of meristem identity and plant architecture by FRUITFULL, APETALA1 and CAULIFLOWER.* Development, 2000. **127**(4): p. 725.
87. K. Kaufmann, F. Wellmer, J. M. Muino, T. Ferrier, S. Wuest, V. Kumar, A. Serrano-Mislata, F. Madueno, P. Krajewski, E. Meyerowitz, G. Angenent and J. Riechmann, *Orchestration of floral initiation by APETALA1.* Science, 2010. **328**(5974): p. 85-9.
88. S. Bemis and K. Torii, *Autonomy of cell proliferation and developmental programs during Arabidopsis aboveground organ morphogenesis.* Developmental Biology, 2007. **304**(1): p. 367-381.
89. C. Carles and J. Fletcher, *Shoot apical meristem maintenance: the art of a dynamic balance.* Trends in Plant Science, 2003. **8**(8): p. 394-401.
90. P. Laufs, O. Grandjean, C. Jonak, K. Kiêu and J. Traas, *Cellular Parameters of the Shoot Apical Meristem in Arabidopsis.* The Plant Cell, 1998. **10**(8): p. 1375.
91. S. Dodsworth, *A diverse and intricate signalling network regulates stem cell fate in the shoot apical meristem.* Dev Biol, 2009. **336**(1): p. 1-9.
92. K. Mayer, H. Schoof, A. Haecker, M. Lenhard, G. Jurgens and T. Laux, *Role of WUSCHEL in regulating stem cell fate in the Arabidopsis shoot meristem.* Cell, 1998. **95**(6): p. 805-15.
93. A. Haecker, R. Gross-Hardt, B. Geiges, A. Sarkar, H. Breuninger, M. Herrmann and T. Laux, *Expression dynamics of WOX genes mark cell fate decisions during early embryonic patterning in Arabidopsis thaliana.* Development, 2004. **131**(3): p. 657-68.
94. R. Yadav, M. Tavakkoli, and G. Reddy, *WUSCHEL mediates stem cell homeostasis by regulating stem cell number and patterns of cell division and differentiation of stem cell progenitors.* Development, 2010. **137**(21): p. 3581-9.
95. S. Hamada, H. Onouchi, H. Tanaka, M. Kudo, Y.-G. Liu, D. Shibata, C. Machida and Y. Machida, *Mutations in the WUSCHEL gene of Arabidopsis thaliana result in the development of shoots without juvenile leaves.* The Plant Journal, 2000. **24**(1): p. 91-101.
96. H. Schoof, M. Lenhard, A. Haecker, K. F. X. Mayer, G. Jürgens and T. Laux, *The Stem Cell Population of Arabidopsis Shoot Meristems Is Maintained by a Regulatory Loop between the CLAVATA and WUSCHEL Genes.* Cell, 2000. **100**(6): p. 635-644.
97. M. Somssich, B. I. Je, R. Simon and D. Jackson, *CLAVATA-WUSCHEL signaling in the shoot meristem.* Development, 2016. **143**(18): p. 3238-48.
98. Kwiatkowska, D., *Flowering and apical meristem growth dynamics.* J Exp Bot, 2008. **59**(2): p. 187-201.
99. R. Benlloch, A. Berbel, A. Serrano-Mislata and F. Madueño, *Floral initiation and inflorescence architecture: a comparative view.* Ann Bot, 2007. **100**(3): p. 659-76.

100. S. Kempin, B. Savidge, and M. Yanofsky, *Molecular basis of the cauliflower phenotype in Arabidopsis.* 1995. **267**(5197): p. 522-525.
101. D. Weigel and O. Nilsson, *A developmental switch sufficient for flower initiation in diverse plants.* Nature, 1995. **377**(6549): p. 495-500.
102. D. Weigel, J. Alvarez, D. Smyth, M. Yanofsky and E. M. Meyerowitz, *LEAFY controls floral meristem identity in Arabidopsis.* Cell, 1992. **69**(5): p. 843-59.
103. S. Singer and G. Nicolson, *The Fluid Mosaic Model of the Structure of Cell Membranes.* 1972. **175**(4023): p. 720-731.
104. E. Steudle, U. Zimmermann, and U. Lüttge, *Effect of Turgor Pressure and Cell Size on the Wall Elasticity of Plant Cells.* Plant Physiology, 1977. **59**(2): p. 285.
105. C. Somerville, *Cellulose synthesis in higher plants.* Annu Rev Cell Dev Biol, 2006. **22**: p. 53-78.
106. M. Tepfer and I. Taylor, *The permeability of plant cell walls as measured by gel filtration chromatography.* Science, 1981. **213**(4509): p. 761-3.
107. L. Braidwood, C. Breuer, and K. Sugimoto, *My body is a cage: mechanisms and modulation of plant cell growth.* New Phytol, 2014. **201**(2): p. 388-402.
108. M. Dick-Perez, Y. Zhang, J. Hayes, A. Salazar, O. Zabotina and M. Hong, *Structure and interactions of plant cell-wall polysaccharides by two- and three-dimensional magic-angle-spinning solid-state NMR.* Biochemistry, 2011. **50**(6): p. 989-1000.
109. S. Marcus, Y. Verhertbruggen, C. Herve, J. Ordaz-Ortiz, V. Farkas, H. Pedersen, W. Willats and J. Knox, *Pectic homogalacturonan masks abundant sets of xyloglucan epitopes in plant cell walls.* BMC Plant Biol, 2008. **8**: p. 60.
110. K. Caffall and D. Mohnen, *The structure, function, and biosynthesis of plant cell wall pectic polysaccharides.* Carbohydr Res, 2009. **344**(14): p. 1879-900.
111. M. Sticklen, *Plant genetic engineering for biofuel production: towards affordable cellulosic ethanol.* Nat Rev Genet, 2008. **9**(6): p. 433-43.
112. N. Yang and M. Hinner, *Getting across the cell membrane: an overview for small molecules, peptides, and proteins.* Methods in molecular biology (Clifton, N.J.), 2015. **1266**: p. 29-53.
113. H. McMahon and E. Boucrot, *Molecular mechanism and physiological functions of clathrin-mediated endocytosis.* Nat Rev Mol Cell Biol, 2011. **12**(8): p. 517-33.
114. S. Conner and S. Schmid, *Regulated portals of entry into the cell.* Nature, 2003. **422**(6927): p. 37-44.
115. X. Chen, N. Irani, and J. Friml, *Clathrin-mediated endocytosis: the gateway into plant cells.* Curr Opin Plant Biol, 2011. **14**(6): p. 674-82.
116. S. Falcone, E. Cocucci, P. Podini, T. Kirchhausen, E. Clementi and J. Meldolesi, *Macropinocytosis: regulated coordination of endocytic and exocytic membrane traffic events.* J Cell Sci, 2006. **119**(Pt 22): p. 4758-69.
117. S. Gordon, *Phagocytosis: An Immunobiologic Process.* Immunity, 2016. **44**(3): p. 463-475.
118. P. Cosson and T. Soldati, *Eat, kill or die: when amoeba meets bacteria.* Curr Opin Microbiol, 2008. **11**(3): p. 271-6.
119. R. Parton and K. Simons, *The multiple faces of caveolae.* Nature Reviews Molecular Cell Biology, 2007. **8**: p. 185.
120. C. Mineo and R. Anderson, *Potocytosis.* Histochemistry and Cell Biology, 2001. **116**(2): p. 109-118.
121. A. Frankel and C. Pabo, *Cellular uptake of the tat protein from human immunodeficiency virus.* Cell, 1988. **55**(6): p. 1189-93.
122. M. Green and P. Loewenstein, *Autonomous functional domains of chemically synthesized human immunodeficiency virus tat trans-activator protein.* Cell, 1988. **55**(6): p. 1179-88.
123. E. Vives, P. Brodin, and B. Lebleu, *A truncated HIV-1 Tat protein basic domain rapidly translocates through the plasma membrane and accumulates in the cell nucleus.* J Biol Chem, 1997. **272**(25): p. 16010-7.

124. J. Park, J. Ryu, K. Kim, H. Lee, J. Bahn, K. Han, E. Choi, K. Lee, H. Kwon and S. Choi, *Mutational analysis of a human immunodeficiency virus type 1 Tat protein transduction domain which is required for delivery of an exogenous protein into mammalian cells.* J Gen Virol, 2002. **83**(Pt 5): p. 1173-81.
125. G. Guidotti, L. Brambilla, and D. Rossi, *Cell-Penetrating Peptides: From Basic Research to Clinics.* Trends Pharmacol Sci, 2017. **38**(4): p. 406-424.
126. D. Kalafatovic and E. Giralt, *Cell-Penetrating Peptides: Design Strategies beyond Primary Structure and Amphipathicity.* Molecules, 2017. **22**(11).
127. F. Milletti, *Cell-penetrating peptides: classes, origin, and current landscape.* Drug Discov Today, 2012. **17**(15-16): p. 850-60.
128. B. Liu, J. Liou, Y. Chen, Y. Huang and H. Lee, *Delivery of nucleic acids, proteins, and nanoparticles by arginine-rich cell-penetrating peptides in rotifers.* Mar Biotechnol (NY), 2013. **15**(5): p. 584-95.
129. A. Elmquist, M. Lindgren, T. Bartfai and U. Langel, *VE-cadherin-derived cell-penetrating peptide, pVEC, with carrier functions.* Exp Cell Res, 2001. **269**(2): p. 237-44.
130. U. Soomets, M. Lindgren, X. Gallet, M. Hallbrink, A. Elmquist, L. Balaspiri, M. Zorko, M. Pooga, R. Brasseur and U. Langel, *Deletion analogues of transportan.* Biochim Biophys Acta, 2000. **1467**(1): p. 165-76.
131. F. Madani, S. Lindberg, U. Langel, S. Futaki and A. Graslund, *Mechanisms of cellular uptake of cell-penetrating peptides.* J Biophys, 2011. **2011**: p. 414729.
132. H. Herce, A. Garcia, and M. Cardoso, *Fundamental molecular mechanism for the cellular uptake of guanidinium-rich molecules.* J Am Chem Soc, 2014. **136**(50): p. 17459-67.
133. M. Chang, J. Chou, C. Chen, B. Liu and H. Lee, *Noncovalent protein transduction in plant cells by macropinocytosis.* New Phytol, 2007. **174**(1): p. 46-56.
134. P. Wender, D. Mitchell, K. Pattabiraman, E. Pelkey, L. Steinman and J. Rothbard, *The design, synthesis, and evaluation of molecules that enable or enhance cellular uptake: peptoid molecular transporters.* Proc Natl Acad Sci U S A, 2000. **97**(24): p. 13003-8.
135. N. Unnamalai, B. Kang, and W. Lee, *Cationic oligopeptide-mediated delivery of dsRNA for post-transcriptional gene silencing in plant cells.* FEBS Lett, 2004. **566**(1-3): p. 307-10.
136. K. Numata, Y. Horii, K. Oikawa, Y. Miyagi, T. Demura and M. Ohtani, *Library screening of cell-penetrating peptide for BY-2 cells, leaves of Arabidopsis, tobacco, tomato, poplar, and rice callus.* Sci Rep, 2018. **8**(1): p. 10966.
137. A. Chugh and F. Eudes, *Cellular uptake of cell-penetrating peptides pVEC and transportan in plants.* J Pept Sci, 2008. **14**(4): p. 477-81.
138. A. Chugh and F. Eudes, *Translocation and nuclear accumulation of monomer and dimer of HIV-1 Tat basic domain in triticale mesophyll protoplasts.* Biochimica et biophysica acta, 2007. **1768**(3): p. 419-426.
139. M. Mäe, H. Myrberg, Y. Jiang, H. Paves, A. Valkna and U. Langel, *Internalisation of cell-penetrating peptides into tobacco protoplasts.* Biochimica et biophysica acta, 2005. **1669**(2): p. 101-107.
140. A. Chugh and F. Eudes, *Study of uptake of cell penetrating peptides and their cargoes in permeabilized wheat immature embryos.* Febs j, 2008. **275**(10): p. 2403-14.
141. T. Mizuno, M. Miyashita, and H. Miyagawa, *Cellular internalization of arginine-rich peptides into tobacco suspension cells: a structure–activity relationship study.* 2009. **15**(4): p. 259-263.
142. K. Eggenberger, C. Mink, P. Wadhwani, A. S. Ulrich and P. Nick, *Using the peptide BP100 as a cell-penetrating tool for the chemical engineering of actin filaments within living plant cells.* Chembiochem, 2011. **12**(1): p. 132-7.
143. K. Eggenberger, P. Sanyal, S. Hundt, P. Wadhwani, A. S. Ulrich and P. Nick, *Challenge Integrity: The Cell-Penetrating Peptide BP100 Interferes with the Auxin-Actin Oscillator.* Plant Cell Physiol, 2017. **58**(1): p. 71-85.

144. A. Chugh, E. Amundsen, and F. Eudes, *Translocation of cell-penetrating peptides and delivery of their cargoes in triticale microspores.* Plant Cell Rep, 2009. **28**(5): p. 801-10.
145. K. Ng, Y. Motoda, S. Watanabe, A. Sofiman Othman, T. Kigawa, Y. Kodama and K. Numata, *Intracellular Delivery of Proteins via Fusion Peptides in Intact Plants.* PLOS ONE, 2016. **11**(4): p. e0154081.
146. M. Chang, J. Chou, and H. Lee, *Cellular internalization of fluorescent proteins via arginine-rich intracellular delivery peptide in plant cells.* Plant Cell Physiol, 2005. **46**(3): p. 482-8.
147. Y.-H. Wang, C.-P. Chen, M.-H. Chan, M. Chang, Y.-W. Hou, H.-H. Chen, H.-R. Hsu, K. Liu and H.-J. Lee, *Arginine-rich intracellular delivery peptides noncovalently transport protein into living cells.* Biochemical and Biophysical Research Communications, 2006. **346**(3): p. 758-767.
148. S. Lu, J. W. Hu, B. Liu, C. Lee, J. F. Li, J. Chou and H. Lee, *Arginine-rich intracellular delivery peptides synchronously deliver covalently and noncovalently linked proteins into plant cells.* J Agric Food Chem, 2010. **58**(4): p. 2288-94.
149. X. Qi, T. Droste, and C. Kao, *Cell-penetrating peptides derived from viral capsid proteins.* Mol Plant Microbe Interact, 2011. **24**(1): p. 25-36.
150. A. Bilichak, J. Luu, and F. Eudes, *Intracellular delivery of fluorescent protein into viable wheat microspores using cationic peptides.* Front Plant Sci, 2015. **6**: p. 666.
151. *SDS-PAGE Gel.* Cold Spring Harbor Protocols, 2015. **2015**(7): p. pdb.rec087908.
152. C. Theile, M. Witte, A. Blom, L. Kundrat, H. Ploegh and C. Guimaraes, *Site-specific N-terminal labeling of proteins using sortase-mediated reactions.* Nat Protoc, 2013. **8**(9): p. 1800-7.
153. N. Geldner, V. Denervaud-Tendon, D. Hyman, U. Mayer, Y. Stierhof and J. Chory, *Rapid, combinatorial analysis of membrane compartments in intact plants with a multicolor marker set.* Plant J, 2009. **59**(1): p. 169-78.
154. C. Lelivelt, K. van Dun, C. de Snoo, M. McCabe, B. Hogg and J. Nugent, *Plastid transformation in lettuce (Lactuca sativa L.) by polyethylene glycol treatment of protoplasts.* Methods Mol Biol, 2014. **1132**: p. 317-30.
155. J. Doyle, *A rapid total DNA preparation procedure for fresh plant tissue.* Focus, 1990. **12**: p. 13-15.
156. H. Lagassé, A. Alexaki, V. Simhadri, N. Katagiri, W. Jankowski, Z. Sauna and C. Kimchi-Sarfaty, *Recent advances in (therapeutic protein) drug development.* F1000Res, 2017. **6**: p. 113.
157. C. Bechara and S. Sagan, *Cell-penetrating peptides: 20 years later, where do we stand?* FEBS Lett, 2013. **587**(12): p. 1693-702.
158. H. Herce, A. Garcia, J. Litt, R. Kane, P. Martin, N. Enrique, A. Rebolledo and V. Milesi, *Arginine-rich peptides destabilize the plasma membrane, consistent with a pore formation translocation mechanism of cell-penetrating peptides.* Biophys J, 2009. **97**(7): p. 1917-25.
159. I. Shomer, A. Novacky, S. Pike, U. Yermiyahu and T. Kinraide, *Electrical potentials of plant cell walls in response to the ionic environment.* Plant Physiol, 2003. **133**(1): p. 411-22.
160. A. Bidhendi and A. Geitmann, *Relating the mechanics of the primary plant cell wall to morphogenesis.* Journal of Experimental Botany, 2015. **67**(2): p. 449-461.
161. J. Van Norman, W. Xuan, T. Beeckman and P. Benfey, *To branch or not to branch: The role of pre-patterning in lateral root formation*. Vol. 140. 2013. 4301-4310.
162. A. Bidhendi and A. Geitmann, *Relating the mechanics of the primary plant cell wall to morphogenesis.* J Exp Bot, 2016. **67**(2): p. 449-61.
163. S. Salentinig, L. Sagalowicz, and O. Glatter, *Self-Assembled Structures and pKa Value of Oleic Acid in Systems of Biological Relevance.* Langmuir, 2010. **26**(14): p. 11670-11679.
164. M. Harms, J. Schlessman, G. Sue and B. García-Moreno E., *Arginine residues at internal positions in a protein are always charged.* 2011. **108**(47): p. 18954-18959.
165. M. Majda and S. Robert, *The Role of Auxin in Cell Wall Expansion.* Int J Mol Sci, 2018. **19**(4).
166. J-L. Cacas, *Revisiting Plant Plasma Membrane Lipids in Tobacco: A Focus on Sphingolipids.* 2016. **170**(1): p. 367-384.

167. C. Wei, and A. Pohorille, *Flip-Flop of Oleic Acid in a Phospholipid Membrane: Rate and Mechanism.* The Journal of Physical Chemistry B, 2014. **118**(45): p. 12919-12926.
168. D. Derossi, A. Joliot, G. Chassaing and A. Prochiantz, *The third helix of the Antennapedia homeodomain translocates through biological membranes.* J Biol Chem, 1994. **269**(14): p. 10444-50.
169. R. Ferre, M. Melo, A. Correia, L. Feliu, E. Bardají, M. Planas and M. Castanho, *Synergistic effects of the membrane actions of cecropin-melittin antimicrobial hybrid peptide BP100.* Biophys J, 2009. **96**(5): p. 1815-27.
170. L. Cavallarin, D. Andreu, and B. San Segundo, *Cecropin A-derived peptides are potent inhibitors of fungal plant pathogens.* Mol Plant Microbe Interact, 1998. **11**(3): p. 218-27.
171. E. Badosa, R. Ferre, M. Planas, L. Feliu, E. Besalu, J. Cabrefiga, E. Bardaji and E. Montesinos, *A library of linear undecapeptides with bactericidal activity against phytopathogenic bacteria.* Peptides, 2007. **28**(12): p. 2276-85.
172. P. Wadhwani, E. Strandberg, J. van den Berg, C. Mink, J. Bürck, R. Ciriello and A. Ulrich, *Dynamical structure of the short multifunctional peptide BP100 in membranes.* Biochimica et biophysica acta, 2014. **1838**(3): p. 940-949.
173. J. Riedl, A. Crevenna, K. Kessenbrock, J. H. Yu, D. Neukirchen, M. Bista, F. Bradke, D. Jenne, T. A. Holak, Z. Werb, M. Sixt and R. Wedlich-Soldner, *Lifeact: a versatile marker to visualize F-actin.* Nat Methods, 2008. **5**(7): p. 605-7.
174. A. Era, M. Tominaga, K. Ebine, C. Awai, C. Saito, K. Ishizaki, K. Yamato, T. Kohchi, A. Nakano and T. Ueda, *Application of Lifeact reveals F-actin dynamics in Arabidopsis thaliana and the liverwort, Marchantia polymorpha.* Plant Cell Physiol, 2009. **50**(6): p. 1041-8.
175. L. Cole, J. Coleman, D. Evans and C. Hawesl, *Internalisation of fluorescein isothiocyanate and fluorescein isothiocyanatedextran by suspension-cultured plant cells.* 1990. **96**(4): p. 721-730.
176. S. Deshayes, M. C. Morris, G. Divita and F. Heitz, *Cell-penetrating peptides: tools for intracellular delivery of therapeutics.* Cell Mol Life Sci, 2005. **62**(16): p. 1839-49.
177. F. Eudes and A. Chugh, *Cell-penetrating peptides: From mammalian to plant cells.* Plant Signal Behav, 2008. **3**(8): p. 549-50.
178. S. Fuchs and R. Raines, *Polyarginine as a multifunctional fusion tag.* Protein Sci, 2005. **14**(6): p. 1538-44.
179. S. DeBlasio, A. Sylvester, and D. Jackson, *Illuminating plant biology: using fluorescent proteins for high-throughput analysis of protein localization and function in plants.* Brief Funct Genomics, 2010. **9**(2): p. 129-38.
180. M. Notaguchi, M. Abe, T. Kimura, Y. Daimon, T. Kobayashi, A. Yamaguchi, Y. Tomita, K. Dohi, M. Mori and T. Araki, *Long-distance, graft-transmissible action of Arabidopsis FLOWERING LOCUS T protein to promote flowering.* Plant Cell Physiol, 2008. **49**(11): p. 1645-58.
181. J. Mathieu, N. Warthmann, F. Kuttner and M. Schmid, *Export of FT protein from phloem companion cells is sufficient for floral induction in Arabidopsis.* Curr Biol, 2007. **17**(12): p. 1055-60.
182. H. Ton-That and O. Schneewind, *Anchor structure of staphylococcal surface proteins. IV. Inhibitors of the cell wall sorting reaction.* J Biol Chem, 1999. **274**(34): p. 24316-20.
183. M. Popp and H. Ploegh, *Making and breaking peptide bonds: protein engineering using sortase.* Angew Chem Int Ed Engl, 2011. **50**(22): p. 5024-32.
184. D. Williamson, M. Fascione, M. Webb and W. Turnbull, *Efficient N-terminal labeling of proteins by use of sortase.* Angew Chem Int Ed Engl, 2012. **51**(37): p. 9377-80.
185. K. Alt, B. Paterson, E. Westein, S. Rudd, S. Poniger, S. Jagdale, K. Ardipradja, T. Connell, G. Krippner, A. Nair, X. Wang, H. Tochon-Danguy, P. Donnelly, K. Peter and C. Hagemeyer, *A versatile approach for the site-specific modification of recombinant antibodies using a combination of enzyme-mediated bioconjugation and click chemistry.* Angew Chem Int Ed Engl, 2015. **54**(26): p. 7515-9.

186. S. Baer, J. Nigro, M. Madej, R. Nisbet, R. Suryadinata, G. Coia, L. Hong, T. Adams, C. Williams and S. D. Nuttall, *Comparison of alternative nucleophiles for Sortase A-mediated bioconjugation and application in neuronal cell labelling.* Org Biomol Chem, 2014. **12**(17): p. 2675-85.
187. R. David Row, T. Roark, M. Philip, L. Perkins and J. Antos, *Enhancing the efficiency of sortase-mediated ligations through nickel-peptide complex formation.* Chem Commun (Camb), 2015. **51**(63): p. 12548-51.
188. P. Wingfield, *N-Terminal Methionine Processing.* Curr Protoc Protein Sci, 2017. **88**: p. 6 14 1-6 14 3.
189. R. Kapust, J. Tozser, T. Copeland and D. Waugh, *The P1' specificity of tobacco etch virus protease.* Biochem Biophys Res Commun, 2002. **294**(5): p. 949-55.
190. D. Copolovici, K. Langel, E. Eriste and U. Langel, *Cell-penetrating peptides: design, synthesis, and applications.* ACS Nano, 2014. **8**(3): p. 1972-94.
191. E. Snapp, *Design and use of fluorescent fusion proteins in cell biology.* Curr Protoc Cell Biol, 2005. **Chapter 21**: p. 21 4 1-21 4 13.
192. C. Toseland, *Fluorescent labeling and modification of proteins.* J Chem Biol, 2013. **6**(3): p. 85-95.
193. C. Spicer and B. Davis, *Selective chemical protein modification.* Nat Commun, 2014. **5**: p. 4740.
194. J. Nanda and J. Lorsch, *Labeling a protein with fluorophores using NHS ester derivitization.* Methods Enzymol, 2014. **536**: p. 87-94.
195. J. Maiolo, M. Ferrer, and E. Ottinger, *Effects of cargo molecules on the cellular uptake of arginine-rich cell-penetrating peptides.* Biochim Biophys Acta, 2005. **1712**(2): p. 161-72.
196. C. Jiao, D. Delaroche, F. Burlina, I. Alves, G. Chassaing and S. Sagan, *Translocation and endocytosis for cell-penetrating peptide internalization.* J Biol Chem, 2009. **284**(49): p. 33957-65.
197. A. Dinca, W. Chien, and M. Chin, *Intracellular Delivery of Proteins with Cell-Penetrating Peptides for Therapeutic Uses in Human Disease.* Int J Mol Sci, 2016. **17**(2): p. 263.
198. M. Chang, Y. Huang, R. Aronstam and H. Lee, *Cellular delivery of noncovalently-associated macromolecules by cell-penetrating peptides.* Curr Pharm Biotechnol, 2014. **15**(3): p. 267-75.
199. J. Wadia, R. Stan, and S. Dowdy, *Transducible TAT-HA fusogenic peptide enhances escape of TAT-fusion proteins after lipid raft macropinocytosis.* Nat Med, 2004. **10**(3): p. 310-5.
200. E. Gasteiger, C. Hoogland, A. Gattiker, S. Duvaud, M. Wilkins, R. Appel and A. Bairoch, *Protein Identification and Analysis Tools on the ExPASy Server*, in *The Proteomics Protocols Handbook*, J.M. Walker, Editor. 2005, Humana Press: Totowa, NJ. p. 571-607.
201. P. Wigge, *FT, a mobile developmental signal in plants.* Curr Biol, 2011. **21**(9): p. R374-8.
202. J. Lee, S. Hong, S. Yoo, O. Park, J. Lee and J. Ahn, *Integration of floral inductive signals by flowering locus T and suppressor of overexpression of Constans 1.* Physiologia Plantarum, 2006. **126**(4): p. 475-483.
203. S. Hanano and K. Goto, *TERMINAL FLOWER1 Is Involved in the Regulation of Flowering Time and Inflorescence Development through Transcriptional Repression.* The Plant Cell, 2011. **23**(9): p. 3172-3184.
204. C. Périlleux, G. Lobet, and P. Tocquin, *Inflorescence development in tomato: gene functions within a zigzag model.* Frontiers in Plant Science, 2014. **5**(121).
205. J. Lohmann, R. Hong, M. Hobe, M. Busch, F. Parcy, R. Simon and D. Weigel, *A molecular link between stem cell regulation and floral patterning in Arabidopsis.* Cell, 2001. **105**(6): p. 793-803.
206. M. Hassidim, Y. Dakhiya, A. Turjeman, D. Hussien, E. Shor, A. Anidjar, K. Goldberg and R. M. Green, *CIRCADIAN CLOCK ASSOCIATED1 (CCA1) and the Circadian Control of Stomatal Aperture.* Plant Physiol, 2017. **175**(4): p. 1864-1877.

207. M. Wydro, E. Kozubek, and P. Lehmann, *Optimization of transient Agrobacterium-mediated gene expression system in leaves of Nicotiana benthamiana.* Acta Biochim Pol, 2006. **53**(2): p. 289-98.
208. S. Clough and A. Bent, *Floral dip: a simplified method for Agrobacterium-mediated transformation of Arabidopsis thaliana.* Plant J, 1998. **16**(6): p. 735-43.
209. J. Louis and J. Shah, *Arabidopsis thaliana-Myzus persicae interaction: shaping the understanding of plant defense against phloem-feeding aphids.* Front Plant Sci, 2013. **4**: p. 213.
210. T. Will, A. Furch, and M. Zimmermann, *How phloem-feeding insects face the challenge of phloem-located defenses.* Front Plant Sci, 2013. **4**: p. 336.
211. S. Fujimaki, T. Fujiwara, and H. Hayashi, *A new method for direct introduction of chemicals into a single sieve tube of intact rice plants.* Plant Cell Physiol, 2000. **41**(1): p. 124-8.
212. I. Brust-Mascher and J. Scholey, *Microinjection techniques for studying mitosis in the Drosophila melanogaster syncytial embryo.* J Vis Exp, 2009(31).
213. G. Neuhaus and G. Spangenberg, *Plant transformation by microinjection techniques.* Physiologia Plantarum, 1990. **79**(1): p. 213-217.
214. H. Yu, T. Ito, F. Wellmer and E. M. Meyerowitz, *Repression of AGAMOUS-LIKE 24 is a crucial step in promoting flower development.* Nat Genet, 2004. **36**(2): p. 157-61.
215. F. Tooke, M. Ordidge, T. Chiurugwi and N. Battey, *Mechanisms and function of flower and inflorescence reversion.* J Exp Bot, 2005. **56**(420): p. 2587-99.
216. M. Krzymuski, F. Andres, J. I. Cagnola, S. Jang, M. J. Yanovsky, G. Coupland and J. J. Casal, *The dynamics of FLOWERING LOCUS T expression encodes long-day information.* Plant J, 2015. **83**(6): p. 952-61.
217. L. Corbesier, I. Gadisseur, G. Silvestre, A. Jacqmard and G. Bernier, *Design in Arabidopsis thaliana of a synchronous system of floral induction by one long day.* Plant J, 1996. **9**(6): p. 947-52.
218. M. Kaneko-Suzuki, R. Kurihara-Ishikawa, C. Okushita-Terakawa, C. Kojima, M. Nagano-Fujiwara, I. Ohki, H. Tsuji, K. Shimamoto and K. Taoka, *TFL1-Like Proteins in Rice Antagonize Rice FT-Like Protein in Inflorescence Development by Competition for Complex Formation with 14-3-3 and FD.* Plant Cell Physiol, 2018. **59**(3): p. 458-468.
219. M. Feldmann and R. Maini, *Lasker Clinical Medical Research Award. TNF defined as a therapeutic target for rheumatoid arthritis and other autoimmune diseases.* Nat Med, 2003. **9**(10): p. 1245-50.
220. V. Voynov and J.A. Caravella, *Therapeutic Proteins: Methods and Protocols*, Editors. 2012, Humana Press: Totowa, NJ. p. 1-26.
221. K. Smith, D. Evans, and G. El-Hiti, *Role of modern chemistry in sustainable arable crop protection.* Philos Trans R Soc Lond B Biol Sci, 2008. **363**(1491): p. 623-37.
222. L. Bortesi and R. Fischer, *The CRISPR/Cas9 system for plant genome editing and beyond.* Biotechnology Advances, 2015. **33**(1): p. 41-52.
223. V. Sharma and J. Fletcher, *Maintenance of shoot and floral meristem cell proliferation and fate.* Plant Physiol, 2002. **129**(1): p. 31-9.
224. E. Alvarez-Buylla, M. Benítez, A. Corvera-Poiré, A. Chaos Cador, S. de Folter, A. Gamboa de Buen, A. Garay-Arroyo, B. García-Ponce, F. Jaimes-Miranda, R. Pérez-Ruiz, A. Piñeyro-Nelson and Y. Sánchez-Corrales, *Flower development.* Arabidopsis Book, 2010. **8**: p. e0127.
225. F. Hempel, D. Welch, and L. Feldman, *Floral induction and determination: where is flowering controlled?* Trends Plant Sci, 2000. **5**(1): p. 17-21.
226. D. Smyth, J. Bowman, and E. Meyerowitz, *Early flower development in Arabidopsis.* Plant Cell, 1990. **2**(8): p. 755-67.
227. G. Denay, H. Chahtane, G. Tichtinsky and F. Parcy, *A flower is born: an update on Arabidopsis floral meristem formation.* Curr Opin Plant Biol, 2017. **35**: p. 15-22.

228. J. Adrian, S. Torti, and F. Turck, *From Decision to Commitment: The Molecular Memory of Flowering.* Molecular Plant, 2009. **2**(4): p. 628-642.
229. C. Liu, J. Zhou, K. Bracha-Drori, S. Yalovsky, T. Ito and H. Yu, *Specification of Arabidopsis floral meristem identity by repression of flowering time genes.* Development, 2007. **134**(10): p. 1901-10.
230. N. Siriwardana and R.S. Lamb, *The poetry of reproduction: the role of LEAFY in Arabidopsis thaliana flower formation.* Int J Dev Biol, 2012. **56**(4): p. 207-21.
231. K. Goslin, B. Zheng, A. Serrano-Mislata, L. Rae, P. T. Ryan, K. Kwasniewska, B. Thomson, D. O'Maoileidigh, F. Madueno, F. Wellmer and E. Graciet, *Transcription Factor Interplay between LEAFY and APETALA1/CAULIFLOWER during Floral Initiation.* Plant Physiol, 2017. **174**(2): p. 1097-1109.
232. R. Muller-Xing, O. Clarenz, L. Pokorny, J. Goodrich and D. Schubert, *Polycomb-Group Proteins and FLOWERING LOCUS T Maintain Commitment to Flowering in Arabidopsis thaliana.* Plant Cell, 2014. **26**(6): p. 2457-2471.
233. E. Ballerini and E. Kramer, *In the Light of Evolution: A Reevaluation of Conservation in the CO-FT Regulon and Its Role in Photoperiodic Regulation of Flowering Time.* Front Plant Sci, 2011. **2**: p. 81.
234. F. Kong, B. Liu, Z. Xia, S. Sato, B. M. Kim, S. Watanabe, T. Yamada, S. Tabata, A. Kanazawa, K. Harada and J. Abe, *Two coordinately regulated homologs of FLOWERING LOCUS T are involved in the control of photoperiodic flowering in soybean.* Plant physiology, 2010. **154**(3): p. 1220-1231.
235. C. Wolverton, J. Mullen, H. Ishikawa and M. Evans, *Two distinct regions of response drive differential growth in Vigna root electrotropism.* Plant Cell Environ, 2000. **23**(11): p. 1275-80.
236. N. Kral, *PhD Thesis Imperial College London.* 2018.
237. W. Ho and D. Weigel, *Structural features determining flower-promoting activity of Arabidopsis FLOWERING LOCUS T.* The Plant cell, 2014. **26**(2): p. 552-564.